

Scalable multi-enzyme platforms for the *in vitro* glycoengineering of therapeutic proteins & synthesis of human milk oligosaccharides

Dissertation
zur Erlangung des akademischen Grades
Doktoringenieur
(Dr.-Ing.)

von

Reza Mahour

geboren am

19. September 1990 in Sary, Iran

genehmigt durch die Fakultät für Verfahrens- und Systemtechnik der
Otto-von-Guericke-Universität Magdeburg

Promotionskommission:

Prof. Dr.-Ing. Andreas Seidel-Morgenstern	(Vorsitz)
Prof. Dr.-Ing. Udo Reichl	(Gutachter)
Prof. Sabine Flitsch	(Gutachter)
Prof. Dr. rer. nat. Lothar Elling	(Gutachter)

eingereicht am: 16.12.2021

Promotionskolloquium am: 13.05.2022

To My Family

“I began to realize how important it was to be an enthusiast in life. He taught me that if you are interested in something, no matter what it is, go at it at full speed ahead. Embrace it with both arms, hug it, love it, and above all become passionate about it. Lukewarm is no good. Hot is no good either. White hot and passionate is the only thing to be.”

— Roald Dahl, My Uncle Oswald

This page intentionally left blank

Abstract

Sugars in their free form or conjugated to biomolecules like proteins, lipids, and small molecules have significant functional roles in different biological processes. The importance of free sugars is very pronounced in human milk — through human milk oligosaccharides (HMOs) — by directly and indirectly contributing to the cognitive and physical development of infants. In their attached form, for instance, it has been shown that certain sugar (glycan) structures significantly contribute to therapeutic properties of glycoproteins such as efficacy and half-life. However, difficulties in synthesis of free glycans in large quantities, or modification of glycans on biomolecules to different structures have limited their biotechnological application as well as fundamental understanding of their biological roles.

This work proposes enzymatic synthesis and modification of oligosaccharides as a suitable approach to unlock the potential of glycosylation for various field of applications. In the principal step of this work, novel multi-enzyme cascades were developed to synthesize sugar nucleotides as glycosylation substrates.

For synthesis of uridine diphosphate (UDP) sugars, uridine (Uri) and the corresponding monosaccharides were used as the major precursors. In a cascade of six enzymes and seven reactions, uridine diphosphate *N*-acetylglucosamine (UDP-GlcNAc) was produced to a concentration of 66.2 mM (40.2 g/L), a synthesis yield of 97.4%, and a biocatalyst load of 0.01 g_{enzyme}/g_{product}. With the same cascade, uridine diphosphate *N*-acetylgalactosamine (UDP-GalNAc) was produced with a similar yield. In another multi-enzymatic cascade of six enzymes and seven reactions, uridine diphosphate galactose (UDP-Gal) was produced to a titer of 48 mM (27.2 g/L), a synthesis yield of 96%, and a biocatalyst load of 0.02 g_{enzyme}/g_{product}. For synthesis of uridine diphosphate glucose (UDP-Glc), a cascade of seven enzymes and eight reactions was developed. The cascade was able to deliver UDP-Glc to a final titer of 48.8 mM (27.6 g/L), a reaction yield of 81.3%, and a biocatalyst load of 0.04 g_{enzyme}/g_{product}.

For synthesis of guanosine diphosphate (GDP) sugars, three different cascades were designed and established — one for guanosine diphosphate mannose (GDP-Man) and two for guanosine diphosphate fucose (GDP-Fuc). Guanosine (Guo) — solubilized in dimethyl sulfoxide (DMSO) — was used as the guanosine-base of GDP-sugars. In a cascade of seven enzymes and eight reactions GDP-Man was produced to a titer of 6.7 mM (4 g/L). For initial synthesis of GDP-Fuc starting from fucose (Fuc), a cascade of five enzymes and seven reactions was established which resulted in a final concentration of 7 mM (4.1 g/L). To avoid usage of expensive Fuc, the GDP-Man cascade was extended to enable the synthesis of GDP-Fuc from Man. In the cascade of 10 enzymes and 11 reactions, GDP-Fuc was produced to a final concentration of 7.6 mM (4.5 g/L) and a reaction yield of 72% after 48 h with a biocatalyst load of 0.97 g_{enzyme}/g_{product}.

For synthesis of cytidine monophosphate *N*-acetylneuraminic acid (CMP-Neu5Ac), cytidine (Cyt) was used as one of the main precursors. At first, a cascade of five enzymes and six reactions was designed by using *N*-acetylneuraminic acid (Neu5Ac) as the source of monosaccharide which resulted in almost full conversion. A second cascade consisted of seven enzymes and eight reactions was developed to

enable the usage of GlcNAc and pyruvate (Pyr) instead of expensive Neu5Ac. By using this cascade, CMP-Neu5Ac was produced to a titer of 24.6 mM CMP-NeuAc (15.1 g/L) and synthesis yields of 77%, 34%, and 31% corresponding to Cyt, GlcNAc, and Pyr, respectively. Adenosine triphosphate (ATP) was used in catalytic amounts in all the developed cascades and was constantly regenerated by using polyphosphate (PolyP_n).

Upon successful establishment of multi-enzyme cascades for synthesis of sugar nucleotides, two strategies were proposed and demonstrated for synthesis of HMOs. In the first approach — the coupling approach — the sugar nucleotide synthesis cascade was coupled to a glycosyltransferase. The one-pot setting of this strategy offers the advantage of using nucleosides in catalytic amounts. To demonstrate the practicality of this strategy and as a proof-of-concept study, synthesis of two simple HMOs — e.g., 3-fucosyllactose (3-FL), and 6'-sialyllactose (6'-SL) — was demonstrated. In the second approach — the modular approach — the product of sugar nucleotide synthesis cascade was combined with an acceptor and a glycosyltransferase. This led to synthesis of 10 different HMOs — in a proof-of-concept study.

Two methods were proposed for glycoengineering of therapeutic proteins. In the first method, the addition of terminal Gal by using *E. coli*-derived human β -1,4-galactosyltransferase was demonstrated and enhancement of antibody-dependent cell-mediated cytotoxicity (ADCC) activity was shown with a chromatographic assay. In the second method, the concept of an *in vitro* microbial-based artificial Golgi was described by using mannosylated (high mannose) glycoproteins. For demonstration of this idea, the known inhibitor of mannosidase I — i.e., kifunensine — was added to Chinese hamster ovary (CHO) cells to produce mannosylated (Man9) immunoglobulin G (IgG) proteins. Afterwards, Man9 IgG was enzymatically trimmed to Man5 structures and further extended to Man5-G0 structure by using *E. coli* derived human α -1,3-mannosyl-glycoprotein 2- β -*N*-acetylglucosaminyltransferase (MGAT1). Despite successful expression of human α -1,6-mannosyl-glycoprotein 2- β -*N*-acetylglucosaminyltransferase (MGAT2) in *E. coli*, the concept was not further extended experimentally, due to inactive expression of mannosidase II in *E. coli*.

Finally, multiple process engineering strategies are presented to demonstrate the scalability of multi-enzyme synthesis of sugar nucleotides. UDP-Gal and UDP-GlcNAc were scaled to 1 L and 4 L (directly from 200 μ L), respectively, by using centrifugally clarified cell lysate. In the second strategy, six enzymes were simultaneously produced in a single *E. coli* strain through co-expression of their corresponding genes in order to minimize the number of independent fermentations. The combination of six enzymes enabled the synthesis of UDP-GlcNAc and UDP-Gal at 150 mL and 3 L scale, respectively. This approach was also used for synthesis of CMP-Neu5Ac at 100 mL scale. Lastly, six enzymes were co-immobilized on commercially available resins for synthesis of UDP-GlcNAc. The activity of co-immobilized enzymes was demonstrated for 20 cycles.

The results presented in this work have the potential to be used for production of functional oligosaccharides (e.g., HMOs) at industrial scales as well as development of glycoengineered therapeutic proteins. Overall, I hope that the presented work can serve as a contribution to the

glycobiotechnology field in the development of superior nutritious and therapeutic products to better the quality of human life.

Kurzfassung

Zucker oder Saccharide spielen in ihrer freien Form oder konjugiert an Biomoleküle (Proteine, Lipide oder andere Moleküle) bei verschiedenen biologischen Prozessen eine wichtige Rolle. In der humanen Muttermilch ist die Bedeutung von freien Zuckern durch „human milk oligosaccharides“ (HMOs) — sehr ausgeprägt, da diese sowohl direkt als auch indirekt zur kognitiven und körperlichen Entwicklung von Säuglingen beitragen. Es hat sich auch gezeigt, dass bestimmte Zuckerstrukturen (Glykane), in ihrer gebundenen Form, wesentlich zu therapeutischen Eigenschaften von Glykoproteinen wie Wirksamkeit und Halbwertszeit beitragen. Probleme bei der Schwierigkeiten oder bei der Übertragung und Modifikation von Glykanen auf Biomoleküle beschränken jedoch nicht nur ihre Anwendung in größerem Maßstab sondern erschweren auch die Durchführung grundlegender Studien bezüglich ihrer biologischen Rolle.

Diese Arbeit schlägt die enzymatische Synthese und Modifizierung von Oligosacchariden als vielversprechenden Ansatz vor, um die Glykosylierung für verschiedene Anwendungsfelder zu erschließen. Im Hauptteil dieser Arbeit wurden neuartige Multienzymkaskaden zur Synthese von Zuckernukleotiden als Glykosylierungssubstrate entwickelt.

Für die Synthese von Uridindiphosphat (UDP)-Zuckern wurden Uridin (Uri) und die entsprechenden Monosaccharide als Hauptvorläufer verwendet. In einer Kaskade von sechs Enzymen und sieben Reaktionen wurde Uridindiphosphat-*N*-Acetylglucosamin (UDP-GlcNAc) mit einem Titer von 66,2 mM (40,2 g/L), einer Syntheseausbeute von 97,4% und einer Biokatalysatorlast von 0,01 $\text{g}_{\text{enzym}}/\text{g}_{\text{produkt}}$ hergestellt. Mit der gleichen Enzymkaskade wurde Uridindiphosphat-*N*-Acetylgalactosamin (UDP-GalNAc) mit einer ähnlichen Ausbeute hergestellt. In einer anderen multi-enzymatischen Kaskade mit sechs Enzymen und sieben Reaktionen wurde Uridindiphosphat-Galaktose (UDP-Gal) mit einer Konzentration von 48 mM (27,2 g/L), einer Syntheseausbeute von 96% und einer Biokatalysatorlast von 0,02 $\text{g}_{\text{enzym}}/\text{g}_{\text{produkt}}$ hergestellt. Für die Synthese von Uridindiphosphat-Glukose (UDP-Glc) wurde eine Kaskade aus sieben Enzymen und acht Reaktionen entwickelt. Die Kaskade war in der Lage, UDP-Glc mit einer Konzentration von 48,8 mM (27,6 g/L), einer Reaktionsausbeute von 81,3% und einer Biokatalysatorlast von 0,04 $\text{g}_{\text{enzym}}/\text{g}_{\text{produkt}}$ herzustellen.

Für die Synthese von Guanosindiphosphat-Zuckern (GDP) wurden drei verschiedene Kaskaden entwickelt und etabliert — eine für Guanosindiphosphat-Mannose (GDP-Man) und zwei für Guanosindiphosphat-Fucose (GDP-Fuc). Guanosin (Guo) — gelöst in Dimethylsulfoxid (DMSO) — wurde als Guanosin-Base der GDP-Zucker verwendet. In einer Kaskade von sieben Enzymen und acht Reaktionen wurde GDP-Man bis zu einer Konzentration von 6,7 mM (4 g/L) hergestellt. Für die Erstsynthese von GDP-Fuc ausgehend von Fucose (Fuc) wurde eine Kaskade von fünf Enzymen und sieben Reaktionen etabliert, die zu einer Endkonzentration von 7 mM (4,1 g/L) führte. Um die Verwendung von teurem Fuc zu vermeiden, wurde die GDP-Man-Kaskade erweitert, um die Synthese von GDP-Fuc aus Man zu ermöglichen. In der Kaskade mit 10 Enzymen und 11 Reaktionen wurde

GDP-Fuc bis zu einer Konzentration von 7,6 mM (4,5 g/L) und einer Reaktionsausbeute von 72% nach 48 Stunden mit einer Biokatalysatorlast von 0,97 g_{enzym}/g_{produkt} hergestellt.

Für die Synthese von Cytidinmonophosphat-*N*-Acetylneuraminsäure (CMP-Neu5Ac) wurde Cytidin (Cyt) als einer der wichtigsten Ausgangsstoffe verwendet. Zunächst wurde eine Kaskade aus fünf Enzymen und sechs Reaktionen unter Verwendung von *N*-Acetylneuraminsäure (Neu5Ac) als Monosaccharidquelle entwickelt, die zu einer fast vollständigen Umsetzung führte. Eine zweite Kaskade, bestehend aus sieben Enzymen und acht Reaktionen, wurde entwickelt, um die Verwendung von *N*-Acetylglucosamin (GlcNAc) und Pyruvat (Pyr) anstelle des teuren Neu5Ac zu ermöglichen. Mit dieser Kaskade wurde CMP-Neu5Ac mit einer Konzentration von 24,6 mM CMP-NeuAc (15,1 g/L) und Syntheseausbeuten von 77%, 34% und 31% entsprechend Cyt, GlcNAc bzw. Pyr hergestellt. Adenosintriphosphat (ATP) wurde in allen entwickelten Kaskaden in katalytischen Mengen verwendet und durch die Verwendung von Polyphosphat (PolyP_n) ständig regeneriert.

Nach erfolgreicher Etablierung der Multienzymkaskaden für die Synthese von Zuckernukleotiden wurden zwei Strategien für die Synthese von HMOs demonstriert. In einem Kopplungsansatz wurde die Zuckernukleotid-Synthesekaskade an eine Glykosyltransferase gekoppelt. Diese Strategie bietet den Vorteil, dass Nukleoside in katalytischen Mengen verwendet werden können. Um die Realisierung dieser Strategie zu demonstrieren, wurde die Synthese von zwei einfachen HMOs — z.B. 3-Fucosyllactose (3-FL) und 6'-Sialyllactose (6'-SL) — als Proof-of-Concept-Studie durchgeführt. In einem modularen Ansatz wird das Produkt der Zuckernukleotidsynthesekaskade mit einem Akzeptor und einer Glykosyltransferase kombiniert. Dies führte zur Synthese von 10 verschiedenen HMOs.

Für das Glyco-Engineering von therapeutischen Proteinen wurden zwei Methoden vorgeschlagen. Bei der ersten Methode wurde die Verbindung von endständigem Gal mit einem Antikörper unter Verwendung der aus *E. coli* stammenden humanen β -1,4-Galaktosyltransferase demonstriert und eine Erhöhung der Aktivität der antikörperabhängigen zellvermittelten Zytotoxizität (ADCC) mittels einem chromatographischen Assay nachgewiesen. Bei der zweiten Methode wurde das Konzept eines künstlichen Golgi Kompartments auf mikrobieller Basis *in vitro* unter Verwendung mannosylierter (mannosereicher) Glykoproteine beschrieben. Zur Demonstration dieser Idee wurde ein bekannter Inhibitor der Mannosidase I (Kifunensin) zu Ovarialzellen des chinesischen Hamsters (CHO) gegeben, um mannosylierte (Man9) Immunglobulin G (IgG)-Proteine zu produzieren. Anschließend wurde das Man9-IgG enzymatisch auf Man5-Strukturen getrimmt und mit Hilfe der aus *E. coli* stammenden humanen α -1,3-Mannosyl-Glykoprotein 2- β -*N*-Acetylglucosaminyltransferase (MGAT1) weiter zur Man5-G0-Struktur verlängert. Trotz erfolgreicher Expression des humanen α -1,6-Mannosyl-Glykoprotein 2- β -*N*-Acetylglucosaminyltransferase (MGAT2) in *E. coli* wurde das Konzept aufgrund der inaktiven Expression von Mannosidase II in *E. coli* experimentell nicht weiter ausgebaut.

Schließlich wurden mehrere verfahrenstechnische Strategien vorgestellt, um die Skalierbarkeit von Multi-Enzym-Synthese von Zuckernukleotiden zu demonstrieren. UDP-Gal und UDP-GlcNAc wurden unter Verwendung von abzentrifugiertem Zelllysate auf 1 L bzw. 4 L (direkt aus 200 μ L) skaliert. Um die Anzahl der unabhängigen Fermentationen zu minimieren, wurden bei der zweiten Strategie sechs

Enzyme gleichzeitig in einem einzigen *E. coli*-Stamm durch Koexpression der entsprechenden Gene hergestellt. Die Kombination von sechs Enzymen ermöglichte die Synthese von UDP-GlcNAc und UDP-Gal im Maßstab von 150 mL bzw. 3 L. Dieser Ansatz wurde auch für die Synthese von CMP-Neu5Ac im 100-mL-Maßstab verwendet. Schließlich wurden sechs Enzyme auf handelsüblichen Chromatographieharzen für die Synthese von UDP-GlcNAc co-immobilisiert. Die Aktivität der co-immobilisierten Enzyme wurde für 20 Zyklen nachgewiesen.

Die in dieser Arbeit vorgestellten Ergebnisse haben das Potenzial, für die Produktion funktioneller Oligosaccharide (z. B. HMOs) in industriellem Maßstab sowie für das Glykoengineering von Therapeutika mit besserer klinischer Wirksamkeit genutzt zu werden. Insgesamt ist zu hoffen, dass die vorgestellte Arbeit als Beitrag zur Glykobiotechnologie bei der Entwicklung von hochwertigen Nährstoffen und therapeutischen Produkten zur Verbesserung der menschlichen Lebensqualität dienen kann.

Contents

Abstract	IV
Kurzfassung	VII
List of Abbreviations	XII
1 Introduction	1
2 Theoretical Background	4
2.1 Glycosylation	4
2.1.1 Therapeutic glycoproteins	5
2.1.2 Human milk oligosaccharides	8
2.2 Sugar nucleotides	12
2.3 Multi-enzyme systems	13
3 Materials and Methods	16
3.1 Multi-enzyme cascade design for synthesis of sugar nucleotides	16
3.2 Recombinant enzyme production	16
3.2.1 Plasmid design	16
3.2.2 Transformation	18
3.2.3 Fermentation	18
3.2.4 Cell lysis	18
3.2.5 Purification	19
3.3 Enzyme activity and cascade reactions	19
3.3.1 Synthesis of sugar nucleotides	20
3.3.2 Synthesis of HMOs	22
3.3.3 <i>In vitro</i> glycoengineering	25
3.4 Process development	26
3.4.1 Scale-up of UDP-Gal synthesis cascade	26
3.4.2 Scale-up of UDP-GlcNAc synthesis cascade	26
3.4.3 Co-expression of enzymes	27
3.5 Immobilization	29
3.6 Cell culture methods for antibody production	29
3.7 Analytics	30
3.7.1 Protein quantification	30
3.7.2 SDS-PAGE	30
3.7.3 HPAEC-UV/PAD	30
3.7.4 MALDI-TOF-MS	33
3.7.5 xCGE-LIF	34
3.7.6 ADCC assay	35
4 Results and Discussion	36
4.1 Multi-enzyme cascades for synthesis of sugar nucleotides	37

4.1.1	Synthesis of UDP-sugars	37
4.1.2	Synthesis of GDP-sugars	46
4.1.3	Synthesis of CMP-Neu5Ac.....	53
4.1.4	Discussion on synthesis of sugar nucleotides	60
4.2	Synthesis of HMOs	74
4.2.1	Coupling strategy for synthesis of HMOs.....	74
4.2.2	Modular strategy for synthesis of HMOs	78
4.2.3	Discussion on synthesis of HMOs.....	87
4.3	Development of an artificial Golgi for protein glycoengineering.....	91
4.3.1	<i>In vitro</i> glycoengineering of therapeutic antibodies.....	91
4.3.2	Design and development of an artificial Golgi platform.....	96
4.3.3	Discussion of <i>in vitro</i> glycoengineering of therapeutic proteins	100
4.4	Process development and scale-up of multi-enzyme systems	104
4.4.1	Scale-up of multi-enzyme cascades	104
4.4.2	Co-expression of enzymes.....	107
4.4.3	Co-immobilization of a multi-enzyme cascade.....	111
4.4.4	Discussion on process engineering strategies.....	118
5	Conclusions and Outlook	124
	List of Figures.....	130
	List of Tables	138
	Author statement.....	139
	List of Scientific Contributions	140
	Bibliography	143
	Appendix A: List of Chemicals	159
	Appendix B: List of Plasmids.....	161
	Appendix C: Validation of HPAEC-UV-PAD measurements	162
	Appendix D: SDS-PAGE of purified enzymes.....	163
	Appendix E: MS of sugar nucleotides	165
	Appendix F: CHO-DP12 cultivation data.....	170

List of Abbreviations

(NH ₄) ₂ SO ₄	Ammonium sulfate
2'-FL	2'-Fucosyllactose
3/4-FT	α1-3/4-fucosyltransferase
3-FL	3-Fucosyllactose
3'-SL	3'-Sialyllactose
6'-SL	6'-Sialyllactose
6'-SLN	6'-Sialyl- <i>N</i> -acetyllactosamine
ACN	Acetonitrile
ADCC	Antibody-dependent cellular cytotoxicity
ADP	Adenosine diphosphate
AGE	<i>N</i> -acylglucosamine 2-epimerase
AKG	α-Ketoglutaric acid
AMP	Adenosine monophosphate
AP	Alkaline phosphatase
APTS	8-Aminopyrene-1,3,6-trisulfonic acid
Asn	Asparagine
ATP	Adenosine triphosphate
au	Arbitrary units
BLUSP	<i>B. longum</i> UDP-sugar pyrophosphorylase
BSA	Bovine serum albumin
C1q	Complement component 1q
CDC	Complement-dependent cytotoxicity
CDP	Cytidine diphosphate
CHO	Chinese hamster ovary
CMK	Cytidylate kinase
CMP	Cytidine monophosphate
CMP-Neu5Ac	Cytidine monophosphate <i>N</i> -acetylneuraminic acid
COVID-19	Coronavirus disease 2019
CQA	Critical quality attributes
CSS	<i>N</i> -acylneuramate cytidyltransferase
CTP	Cytidine triphosphate
Cvβ3GalT	<i>C. violaceum</i> β-1,3-galactosyltransferase
Cyt	Cytidine
Da	Dalton
DFL	Difucosyllactose
DF-LNH II	Difucosyllacto- <i>N</i> -hexaose II
DF-LNnT	Difucosyllacto- <i>N</i> -neotetraose
DSLNNt	Disialyllacto- <i>N</i> -neotetraose
DS-LNT	Disialyllacto- <i>N</i> -tetraose
DTT	Dithiothreitol
EGF	Epidermal growth factor
EndoS2	Endoglycosidase from <i>Streptococcus pyogenes</i>
ENGase	Endo-β- <i>N</i> -acetylglucosaminidase
EPO	Erythropoietin
ER	Endoplasmic reticulum
Fc	Fragment crystallizable
FcyRIIIa	Low affinity immunoglobulin gamma Fc region receptor III-A
FDA	Food and drug administration
FKP	Fucokinase/ fucose 1-phosphate guanylyltransferase
Fuc	Fucose
Fuc-1P	Fucose 1-phosphate
GAG	Glycosaminoglycans

Gal	Galactose
Gal-1P	Galactose 1-phosphate
GALK	Galactokinase
GalNAc	<i>N</i> -acetylgalactosamine
GalNAc-1P	<i>N</i> -acetylgalactosamine 1-phosphate
GALU	Glucose 1-phosphate uridylyltransferase
GDP	Guanosine diphosphate
GDP-4-dehydro-6-deoxy-Man	Guanosine diphosphate-4-keto-6-deoxy-mannose
GDP-Fuc	Guanosine diphosphate L-fucose
GDP-Man	Guanosine diphosphate mannose
Glc	Glucose
Glc-1P	Glucose 1-phosphate
Glc-6P	Glucose 6-phosphate
GlcA	Glucuronic acid
GlcN	Glucosamine
GlcNAc	<i>N</i> -acetylglucosamine
GlcNAc-1P	<i>N</i> -acetylglucosamine 1-phosphate
GLDH	Glutamate dehydrogenase
GLK	Glucokinase
GLMU	<i>N</i> -acetylglucosamine 1-phosphate uridyltransferase
GMD	Guanosine diphosphate mannose 4,6-dehydratase
GMP	Guanosine monophosphate
GMPK	Guanosine monophosphate kinase
GPI	Glycosylphosphatidylinositol
GSK	Guanosine kinase
GTP	Guanosine triphosphate
Guo	Guanosine
HEPES	4-(2-Hydroxyethyl)-1-piperazineethanesulfonic acid
HILIC-SPE	Hydrophilic interaction chromatography solid phase extraction
His tag	Histidine tag
HMOs	Human milk oligosaccharides
HPAEC	High-Performance Anion-Exchange Chromatography
IdoA	Iduronic acid
IGEPAL® CA-630	Octylphenoxy poly(ethyleneoxy)ethanol
IgG	Immunoglobulin G
IMAC	Immobilized metal affinity chromatography
K ₂ HPO ₄	Dipotassium phosphate
KCl	Potassium chloride
KH ₂ PO ₄	Monopotassium phosphate
KOH	Potassium hydroxide
Lac	Lactose
LacNAc	<i>N</i> -acetylglucosamine
LB	Lysogeny broth
L-Glu	L-Glutamic acid
LNFP III	Lacto- <i>N</i> -fucopentaose III
LNFP V	Fucosyllacto- <i>N</i> -neotetraose V
LNnH	Lacto- <i>N</i> -neohexaose
LNnT	Lacto- <i>N</i> -neotetraose
LNT	Lacto- <i>N</i> -tetraose
LNT II	Lacto- <i>N</i> -triose II
LOD	Limit of detection
LOQ	Limit of quantification
LSTc	Sialyllacto- <i>N</i> -tetraose c
m/z	Mass-to-charge ratio

mAbs	Monoclonal antibody
MALDI-TOF	Matrix-assisted laser desorption/ionization time of flight
Man	Mannose
Man I	α -1,2-Mannosidase
Man II	α -Mannosidase II
Man-1P	Mannose 1-phosphate
Man-6P	Mannose 6-phosphate
MANB	Phosphomannomutase
MANC	Mannose 1-phosphate guanylyltransferase
ManNAc	<i>N</i> -acetylmannosamine
mAU	Milli absorbance unit
MBP	Maltose binding protein
MES	2-(<i>N</i> -morpholino) ethane sulfonic acid
MGAT1	α -1,3-Mannosyl-glycoprotein 2-beta- <i>N</i> -acetylglucosaminyltransferase
MGAT2	α -1,6-Mannosyl-glycoprotein 2-beta- <i>N</i> -acetylglucosaminyltransferase
MGAT3	β -1,4-Mannosyl-glycoprotein 4- β - <i>N</i> -acetylglucosaminyltransferase
MgCl ₂	Magnesium chloride
MgSO ₄	Magnesium sulfate
MnCl ₂	Manganese (II) chloride
MOPS	3-(<i>N</i> -morpholino) propanesulfonic acid
MTU "	Migration time unit
NaCl	Sodium chloride
NADP	Nicotinamide adenine dinucleotide phosphate
NADPH	Reduced nicotinamide adenine dinucleotide phosphate
NAHK	<i>N</i> -acetylhexosamine 1-kinase
NANA	<i>N</i> -acetylneuraminic acid lyase
NaOAc	Sodium acetate
NaOH	Sodium hydroxide
nC	Nano-coulombs
Neu5Ac	<i>N</i> -acetylneuraminic acid
NH ₃	Ammonia
Ni-NTA	Nickel-nitrilotriacetic acid
NMK	Nucleoside monophosphate kinase
OPME	One-pot multi-enzyme
PAD	Pulsed amperometric detector
<i>para</i> -LNnH	<i>para</i> -Lacto- <i>N</i> -neohexaose
Pi	Phosphate
PK	Pyruvate kinase
PolyP _n	Polyphosphate
PPi	Diphosphate
PPK3	Polyphosphate kinase
RFU	Relative fluorescence units
SARS-CoV-2	Severe acute respiratory syndrome coronavirus 2
S-DHB	2, 5-Dihydroxybenzoic acid and 2-hydroxy-5-methoxybenzoic acid
SDS-PAGE	Sodium dodecyl sulphate–polyacrylamide gel electrophoresis
Ser	Serine
SOC	Super Optimal broth with Catabolite repression
SpGalk	<i>Streptococcus pneumoniae</i> TIGR4 galactokinase
ST2,6	α -2,6-Sialyltransferase
TB	Terrific broth
TFA	Trifluoroacetic acid
Thr	Threonine
TSR	Thrombospondin type 1 repeats
UDK	Uridine/cytidine kinase
UDP	Uridine diphosphate

UDP-Gal	Uridine diphosphate galactose
UDP-GalNAc	Uridine diphosphate <i>N</i> -acetylgalactosamine
UDP-Glc	Uridine diphosphate glucose
UDP-GlcNAc	Uridine diphosphate <i>N</i> -acetylglucosamine
UDP-Man	Uridine diphosphate mannose
UMP	Uridine monophosphate
UMPK	Uridine monophosphate and cytidine monophosphate kinase
URA6	Uridylate kinase
Uri	Uridine
UTP	Uridine triphosphate
UV	Ultraviolet
WCAG	Guanosine diphosphate L-fucose synthase
xCGE-LIF	Multiplexed capillary gel electrophoresis with laser-induced fluorescence
β 1,3GlcNAcT	β -1,3- <i>N</i> -acetylglucosaminyltransferase
β 1,4GalT	β -1,4-Galactosyltransferase
β 1,4GALT1	β -1,4-Galactosyltransferase 1

1 Introduction

The attachment of sugars to molecules such as proteins and lipids takes place in a process called glycosylation. Protein glycosylation is a co- and/or post-translational modification which is considered to be among the most complex biological processes [1]. The majority of glycosylation reactions *in vivo* are catalyzed by Leloir-glycosyltransferases by using sugar nucleotides as substrates [2]. The roles of glycosylation in different stages of life from infancy to adulthood as well as, in health and diseases are turning glycobiology to an incredibly attractive field to explore opportunities for better human health.

The glycosylation of therapeutic proteins is essential to their performance [3]. For instance, it has been demonstrated that intravenously administered erythropoietin (EPO) has a plasma half-life of 5 to 6 h, in contrast to desialylated EPO, which has a half-life of less than 2 min [4]. In the case of immunoglobulin G (IgG) antibodies, deglycosylated IgGs had an 85% lower affinity toward receptor proteins compared to glycosylated ones [5]. Furthermore, the glycosylation profile of IgGs is of significant importance in enhancing binding to receptor proteins as well as for their physical properties [6]. Therefore, the modification of glycosylation profiles of therapeutic proteins is considered as a relevant target in the glycoengineering field [7,8]. Tailoring the glycoforms is usually achieved through different strategies such as *in vivo* glycoengineering (e.g., genetic manipulation), cell culture additives (e.g., feeding glycosylation precursors), and *in vitro* glycoengineering (e.g., enzymatic) [9]. Amongst existing glycoengineering methods, enzymatic approaches have been demonstrated to be one of the most promising strategies for obtaining desired glycoforms [10]. Therefore, there is great interest in the advancement of enzymatic methods to modify the glycoforms of therapeutic proteins for development of superior or even novel drugs.

Functional roles of oligosaccharides in the human body (e.g., acting as prebiotics) have been described in various studies [11–13]. There are more than 200 different free oligosaccharides in human milk in a concentration range of ~5–20 g/L [13,14]. These oligosaccharides or so-called human milk oligosaccharides (HMOs) have substantial direct and indirect roles in an infant's cognitive and physical development [13]. Moreover, they can act as prebiotics and antivirals [15]. Research is ongoing to unravel their role in lives of infants [16,17] and adults [18,19]. Current infant formula is based on cow milk [20], which has an oligosaccharide content of ~1–2 g/L in colostrum and ~100 mg/L in mature milk [21] as well as significantly less complex structures compared to HMOs [22]. Therefore, there is significant interest in the addition of synthetic HMOs to infant formula [23]. So far, the addition of only two structures of 2'-fucosyllactose (2'-FL) and lacto-*N*-neotetraose (LNnT) has been achieved at a commercial scale thanks to fermentation-based production of HMOs [24]. Meanwhile, there is high demand for alternative, scalable synthesis technologies to enable commercial scale production of HMOs, ideally the complex structures which are challenging to produce through fermentation processes.

Leloir-glycosyltransferases have been described as a “game-changer” in synthesis of oligosaccharides [25]. Prudden *et al.* synthesized 60 different types of HMOs by employing 10 different Leloir-glycosyltransferases and four different sugar nucleotides [26]. Warnock *et al.* glycoengineered one kilogram of a therapeutic IgG by using a Leloir-glycosyltransferase and a sugar nucleotide [27]. Johnson *et al.* synthesized a few hundreds of grams of tri-, tetra-, and pentasaccharide HMOs by using Leloir-glycosyltransferases and sugar nucleotides [28]. Interestingly, the supply source of sugar nucleotides is not mentioned in the two latter studies.

As of 2021, the price of sugar nucleotides is in the range of ~1–30 €/mg with availability of milligram to a few gram quantities from known chemical suppliers. Evidently, both high price and limited availability of sugar nucleotides substantially hamper large-scale applications for production of HMOs and glycoengineering of therapeutic proteins.

In this work, it was hypothesized that developing scalable strategies for production of sugar nucleotides could significantly contribute to the glycoengineering and other glycotecnology fields. To bring this idea to practice, two main development categories were used: First, establishment of industrially applicable synthesis processes for production of glycosylation precursors — i.e., sugar nucleotides — and second, establishment of an artificial Golgi for large-scale synthesis and modification of glycans. In the following, the content of the dissertation is described.

This dissertation describes multi-enzyme methods for the scalable production of sugar nucleotides from industrially available precursors as well as platform technologies for synthesis of HMOs and glycoengineering of therapeutic proteins. In chapter 2, the theoretical background of the concepts used in this work is introduced and described. In chapter 3, the material and methods used are described in detail. In section 4.1 is described how eight novel multi-enzyme cascades were designed, established, and optimized for synthesis of sugar nucleotides in small scales. The obtained results are discussed and extensively compared to previous works regarding synthesis of sugar nucleotides. In section 4.2, two different strategies were proposed and demonstrated for synthesis of HMOs by using multi-enzyme cascade developed for synthesis of sugar nucleotides. In the first approach, sugar nucleotide synthesis cascades were coupled to relevant glycosyltransferases to synthesize three different HMOs by using catalytic amounts of nucleosides. In the second approach, products of multi-enzyme cascades for synthesis of sugar nucleotides were mixed with an acceptor and a glycosyltransferase to synthesize 12 different HMOs. Afterwards, the obtained results are discussed and developed approaches are compared to the state-of-the-art methods for enzymatic synthesis of HMOs. In section 4.3, two *E. coli*-based platforms were proposed and developed for glycoengineering of therapeutic proteins. In the first approach, therapeutic antibodies were engineered through addition of terminal galactose (Gal) to the existing glycans. The enhanced performance of glycoengineered antibodies was confirmed through evaluating antibody-dependent cellular cytotoxicity (ADCC) activity. In the second strategy, high mannose antibody was produced and furthered modified by using *E. coli*-derived enzymes. The obtained results were discussed and compared to the current methods used for glycoengineering of therapeutic proteins. In section 4.4, process development strategies were used for scale-up of the multi-enzyme cascades from microliter to litre scales. Moreover, multi-enzyme co-immobilization was

evaluated as a potential approach for large-scale production of sugar nucleotides. In chapter 5, conclusion of the work conducted in the context of this dissertation is described and some outlook for future advancement of the current work is presented.

2 Theoretical Background

2.1 Glycosylation

Glycosylation is one of the most common co- and/or post-translation modifications [29]. There are various forms of glycosylation in vertebrates, e.g., *N*-glycosylation and *O*-glycosylation [30]. *N*-glycosylation — the most studied form of glycosylation — starts in the endoplasmic reticulum (ER) through the addition of core structure from a lipid-linked oligosaccharide (donor) to the nitrogen atom of an asparagine (Asn) which is located in the Asn–X–serine (Ser)/threonine (Thr) consensus sequence, where X can be any amino acid except proline [30]. The glycan modifications take place in the Golgi apparatus. The details of various forms of glycosylation have been thoroughly reviewed in literature [30–32]. There are more than 7000 different glycans in mammals [30]. The large number of different glycans consist of different monosaccharides, e.g., *N*-acetylglucosamine (GlcNAc), mannose (Man), glucose (Glc), *N*-acetylgalactosamine (GalNAc), fucose (Fuc), and sialic acid [30]. However, there are two forms of sialic acid: *N*-glycolylneuraminic acid (Neu5Gc) which is only found in non-human mammals and *N*-acetylneuraminic acid (Neu5Ac) which is only found in human and a few other mammals [33]. Approximately, 200 out of the 700 proteins involved in glycosylation processes are glycosyltransferases that employ either lipid-linked oligosaccharides or nucleotide sugars [30]. An illustration of the *O*- and *N*-glycosylation processes is shown in Figure 2.1.

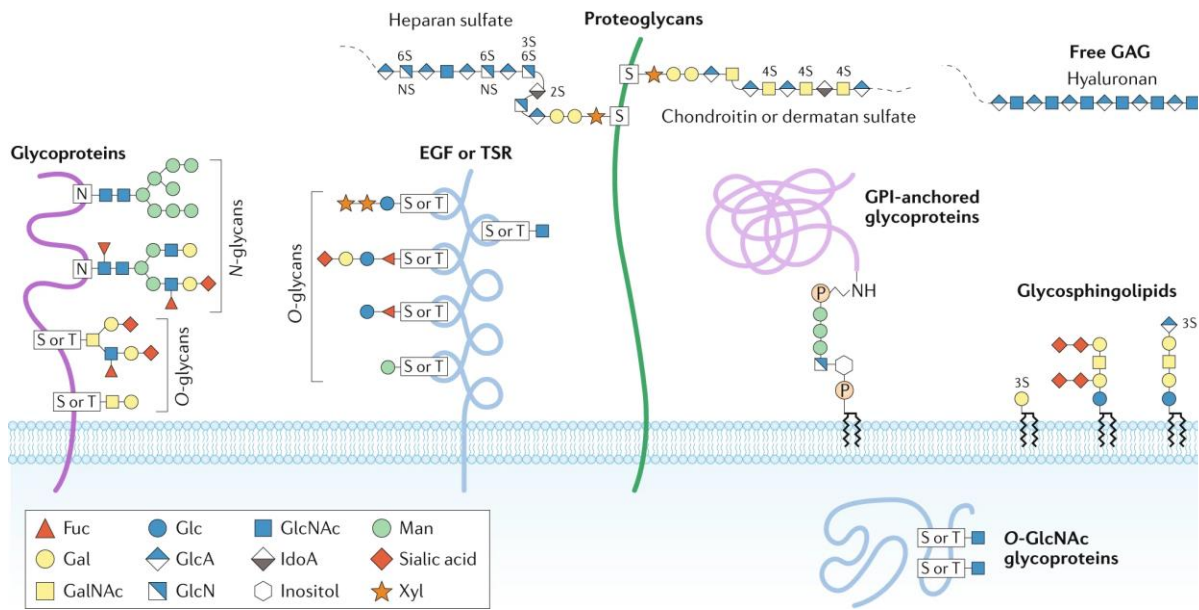


Figure 2.1. Schematic representation of major types of glycosylation in humans. Abbreviations are as follows: EGF, epidermal growth factor; TSR, thrombospondin type 1 repeats; GPI, glycosylphosphatidylinositol; GAG, glycosaminoglycans; N, Asn; S, Ser; T, Thr; 2S, sulfation at C-2 carbon; 3S, sulfation at C-3 carbon; 4S, sulfation at C-4; 6S, sulfation at C-6 carbon; NS, N-sulfation; GlcA, glucuronic acid; GlcN, glucosamine; IdoA, iduronic acid. Adapted with permission from Ref. [31].

Glycans either attached on glycoproteins or in their free form have crucial biological roles such as shaping physical structures (specifically glycans located on cell walls), water solubility of glycoproteins and glycolipids, protein folding, protection from proteases, modulation of membrane receptor signaling, antiadhesive actions, nutritional storage, intracellular trafficking, fertilization and reproduction, protection from immune recognition, triggering of endocytosis and phagocytosis, and many other functions which are thoroughly described and discussed elsewhere [32]. Therefore, glycans are involved in manifold biological phenomena which are directly and indirectly connected to human health and thus, one's well-being. The therapeutic roles of glycoproteins and functionality of free oligosaccharides are further described below.

2.1.1 Therapeutic glycoproteins

In 2017, 16 out of the 20 best-selling therapeutic proteins were glycoproteins, with 13 being monoclonal antibodies (mAbs) [34]. Therapeutic proteins are mainly produced in mammalian cell cultures [35]. The glycosylation of therapeutic proteins is important for their performance [9,36] to such an extent that it makes their glycosylation profile one of the most important critical quality attributes (CQAs) [37]. For example, in 2006, Genzyme received approval for alglucosidase alfa from the United States Food and Drug Administration (FDA) for treatment of Pompe disease. The approval was based on a 160 L scale cultivation. Under the same approval authorization, however, the application to produce alglucosidase alfa at the 2000 L scale was rejected due to a different glycosylation profile after scale-up [38].

Various studies have demonstrated that glycosylation has a significant effect on antibody-dependent cell-mediated cytotoxicity (ADCC) and complement-dependent cytotoxicity (CDC) activity of mAbs [39–41]. ADCC is a mechanism performed by different immune cells (leukocytes) carrying receptors for the fragment crystallizable region (Fc region) of IgG which are able to kill antibody-coated antigens [42,43].

CDC is a mechanism in which complement component 1q (C1q) binds to the Fc region of IgG to start the complement cascade as part of the immune system for lysis of antigens [6]. Improvements in ADCC and CDC activity through tailoring the glycosylation profile of IgGs have turned glycans into an important target for drug development purposes, an approach known as glycoengineering [6,9,44,45]. Currently, there are significant efforts in process towards the advancement of treatment options through modification of the glycan structure of therapeutic glycoproteins [8,9,46,47] and viral vaccines [48].

A protein can have multiple glycosylation sites, which results in heterogeneity in the site occupancy and glycan structure on the protein. Heterogeneity at glycosylation sites is referred to as macro-heterogeneity (completeness of glycosylation) and micro-heterogeneity refers to differences in glycan structures at a given glycosylation site [49,50]. Process parameters such as host cell line, dissolved oxygen [51], temperature [52], pH [53], and even scale-up [38] can contribute to heterogeneities in the glycosylation of proteins [54–58]. Therefore, due to such causes of heterogeneity, glycoproteins have several types of glycosylation. Both forms of heterogeneity can substantially affect protein properties and functionality [49,50,59]. The average relative distribution of glycans found on most therapeutic mAbs are shown in Figure 2.2.

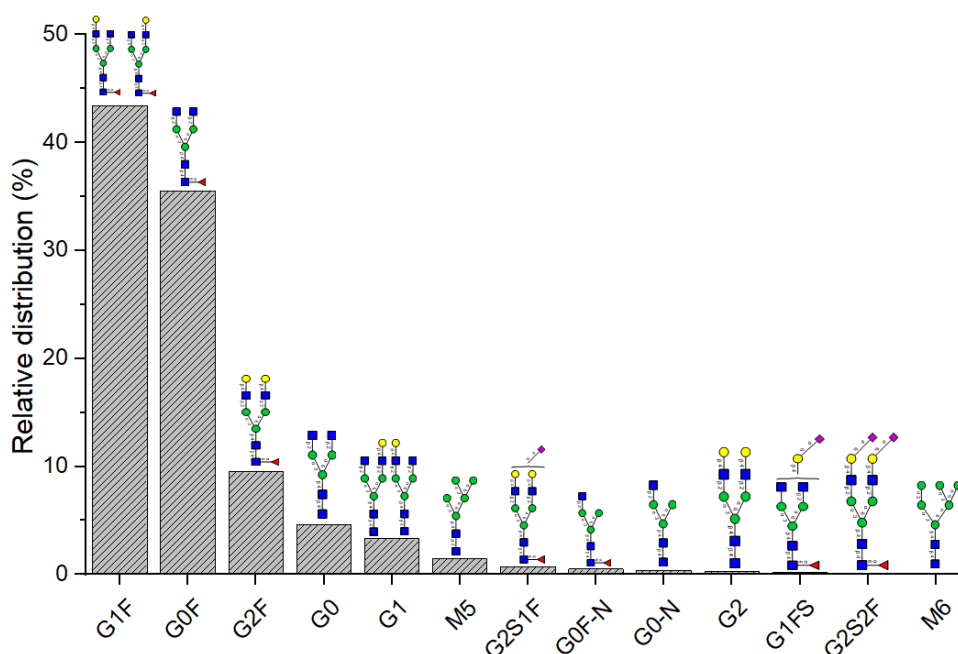


Figure 2.2. Most abundant glycans found on the Fc region of therapeutic mAbs. Values were obtained from Ref. [37]. Blue squares, N-acetylglucosamine; green circle, mannose; yellow circle, galactose; pink square, sialic acid; red triangles, fucose.

It has been shown that afucosylated (e.g., G0) and galactosylated (e.g., G2) mAbs have the highest ADCC activity, and thus, they are considered the main templates for mAb glycoengineering [41,45,60]. Obtaining such structures can be achieved by *in vivo* and/or *in vitro* glycoengineering [9].

There are currently substantial efforts underway to produce therapeutic glycoproteins with homogenous glycans through the feeding of glycosylation precursors [61], use of cell culture additives [62–64], and

especially through cell line glycoengineering (*in vivo* glycoengineering) [8,47,65]. Despite significant works on *in vivo* glycoengineering, obtaining homogenous glycoforms is still extremely challenging [47].

Enzymatic glycosylation has been demonstrated to be a very promising approach for obtaining homogenous glycoforms [10,66,67]. Enzymatic glycoengineering is typically performed using two strategies. In this first approach (the transglycosylation approach), endo- β -*N*-acetylglucosaminidase (ENGase) EndoS2 is used for glycan cleavage from the asparagine attached GlcNAc (Figure 2.3A) [6]. In this way, only a GlcNAc (either with or without Fuc) will remain. Afterwards, oxazoline oligosaccharides with defined structures are used as substrates in combination with engineered ENGase EndoS2-D184M [6]. This method was developed more than two decades ago and is still being used for synthesis of glycoproteins with homogenous glycoforms [8]. The enzymes used in transglycosylation reactions are readily produced in *E. coli* [6,68]. However, the reaction substrates have to be isolated from natural sources like egg yolk powder [69], which has its own challenges and disadvantages.

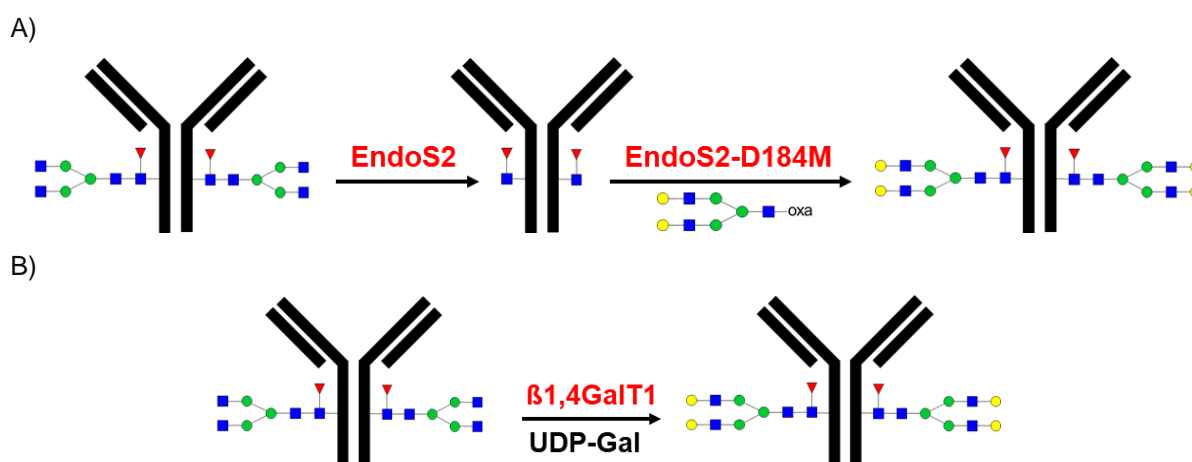


Figure 2.3. concepts used in *in vitro* or enzymatic glycoengineering. (A) Glycoengineering by using oxazoline glycans as the substrate and ENGase (EndoS2) and its engineered variants (EndoS2-D184M) as the biocatalyst [6]. (B) Glycoengineering by using sugar nucleotides and Leloir-glycosyltransferases. Abbreviations: β 1,4GALT1, β -1,4-Galactosyltransferase 1; UDP-Gal, uridine diphosphate galactose.

Another approach for enzymatic glycoengineering — the method that is used in this dissertation — is performed with Leloir-glycosyltransferases and sugar nucleotides as substrates (Figure 2.3B) [41,44,70]. This strategy is similar to what takes place *in vivo* [2]. Therefore, any glycan can be potentially synthesized with the suitable glycosyltransferase and sugar nucleotide precursors.

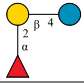
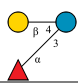
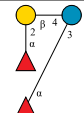
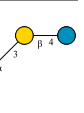
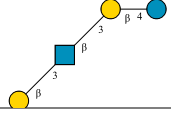
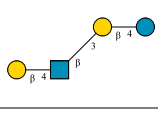
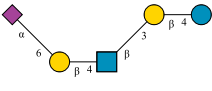
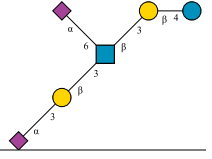
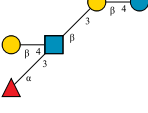
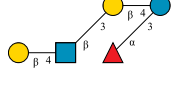
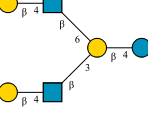
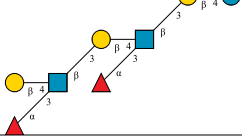
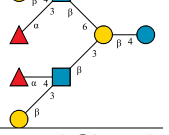
There are multiple reports on glycoengineering (e.g., galactosylation and sialylation) of different therapeutic proteins based on mammalian cell-derived Leloir-glycosyltransferases [41,44,71,72]. However, the cost of recombinant protein production is significantly higher in mammalian cells (compared to common microbial hosts e.g., *E. coli*) [73,74], which, through their usage for development of enzymatically glycoengineered drugs, substantially increase manufacturing cost. Additionally, high costs and unavailability of UDP-Gal and CMP-Neu5Ac (major sugar nucleotides used in glycoengineering) in large scales are among the main reasons that hamper process scale implementation of *in vitro* glycoengineering.

2.1.2 Human milk oligosaccharides

Free glycans are another important product of glycosylation. HMOs — sugars that are found in human milk — are one of the major components of functional free glycans [15]. The importance of HMOs in the infant's physical and cognitive development, together with their long term health benefits are currently being discovered [16,17,75]. In the following, the historical aspects of HMOs, their application, and synthesis strategies are described.

In the 1950s, there was clear evidence that breast-fed infants had higher physical and cognitive development as well as higher resistance to infections compared to formulae-fed infants [76,77]. There were two distinct differences between breast-fed and formulae-fed infants: 1) intestinal flora of breast-fed infants was found to be abundant with *Bifidobacterium* and 2) breast-fed infants had distinctly acidic feces, while formula-fed infants had neutral or even alkaline fecal pHs [78]. Experiments on human milk suggested that the presence of some active molecules — which were traditionally quantified as bifidus factor — promote the growth of *Bifidobacterium*, which does not exist (abundantly) in cow milk [78]. Interestingly, other body fluids, like tears and saliva, were also found to contain these active molecules (oligosaccharides) [78]. Richard Kuhn and Paul György demonstrated that these active molecules are a mixture of oligosaccharides which were later termed as HMOs [79–82]. So far, more than 200 different structures have been found in human milk. Due to the inherent complexity of HMOs, there are ongoing efforts for their identification and quantification [83,84]. Some example HMOs are shown in Table 2.1.

Table 2.1. Examples of human milk oligosaccharides (HMOs), their molecular structures, and reported concentrations in human milk. Concentrations are reported from Ref. [85].

Name	Conc. (mg/L)	Structure	Name	Conc. (mg/L)	Structure
2'-FL	2740		3-FL	420	
DFL	440		3'-SL	290	
LNT	790		LNnT	740	
LSTc	710		DS-LNT	770	
LNFP III	160		LNFP V	20	
LNnH	60		DF-para-LNnH	500	
			DF-LNH II	2700	

Abbreviations: 2'-FL, 2'-fucosyllactose; 3-FL, 3-fucosyllactose; DFL, difucosyllactose; 3'-SL, 3'-sialyllactose; LNnT, lacto-*N*-neotetraose; LNT, lacto-*N*-tetraose; LSTc, sialyl-lacto-*N*-neotetraose c; DS-LNT, disialyllacto-*N*-tetraose; LNFP V, fucosyllacto-*N*-neotetraose V; LNFP III, fucosyllacto-*N*-neotetraose III; LNnH, lacto-*N*-neohexaose; DF-LNH II, difucosyllacto-*N*-hexaose II.

Since the discovery of HMOs, there have been an increasing number of studies on their importance and functional roles [13,16,17]. Until the early 90s, HMOs were considered to have mainly prebiotic roles [13]. Prebiotics are defined as “a selectively fermented ingredient that allows specific changes, both in the composition and/or activity in the gastrointestinal microflora, that confers benefits upon host well-being and health” [13,86,87]. In order for prebiotics to promote growth of beneficial bacteria in the gut, they need to be resistant to the acidity of gastric juice, non-hydrolysable by host enzymes, and have low absorption affinity in the gastrointestinal tract [13]. The properties of HMOs meet all the requirements of prebiotic compounds [88,89]. Other roles of HMOs are antiadhesive antimicrobial agents as well as antivirals by acting as soluble decoys [90–93]. Such properties of HMOs make them potential candidates for antiviral applications [90]. Moreover, there is strong evidence regarding the regulatory role of HMOs in the maturation of the immune systems in infants both directly [94] and indirectly [95,96].

Necrotising enterocolitis was identified as one of the most common causes of death in preterm infants, for which there is yet no effective treatment [97]. Animal studies have proven that HMOs can significantly improve survival and reduce pathology [98,99]. Recently, the correlation of necrotising enterocolitis occurrence in infants and HMOs was reported [100]. Interestingly, there is a growing number of patent applications claiming the therapeutic application of HMOs [101–104].

The growth in head circumference — correlated with brain volume — is the fastest organ growth rate in human infants at a rate of 1.1 mm/day [105]. The role of sialic acid — i.e., Neu5Ac — and sialic acid-containing molecules in infant cognitive development has been supported by various studies [106,107]. Since Neu5Ac can only be found in human [108] (and a few other mammals e.g., New World monkeys [108] and ferrets [109]), there are not many sustainable resources for dietary supplementation of sialic acid. Therefore, sialylated HMOs are an important source of sialic acid for infants nutrition [13,106,107].

Patents titled “food compositions” [110] and “food products containing glucosides of *N*-acetyl-D-glucosamine” [111] by Paul György and Richard Kuhn — the scientists who discovered HMOs — demonstrate the first efforts to add HMOs to infant formulae. Further patents regarding processes for HMOs synthesis [112] (with Wyeth LLC, a well known company in infants nutrition at the time, as assignee) further illustrates the commercial interests in HMOs. Despite this, the addition of HMOs to infant formulae at commercial scales was not realized until 2016 [24]. However, among >200 different structures of HMOs, so far only 2'-FL and LNnT have been added to the formulae [24]. The main obstacle for launching HMOs at commercial scales is the lack of economically viable production processes [113,114].

Production strategies of HMOs and other oligosaccharides have been described in detail in various studies [115–119]. Fermentation of engineered *E. coli* is a promising strategy for the large scale production of simple HMOs such as 2'-FL [120] with successful commercial launches by various companies [24]. Fermentation-based production of HMOs has been thoroughly reviewed [121]. However, the production of complex and large HMOs is very challenging through fermentation due to known problems like high metabolic burden (e.g., high level of sugar nucleotides) and transport processes [119,122].

Utilizing Leloir glycosyltransferases is the only strategy which allows the synthesis of any type of HMOs, regardless of their complexity [26]. The main challenges for large scale application of Leloir glycosyltransferases are the high cost and unavailability of sugar nucleotides which serve as sugar donors (substrate) for this family of glycosyltransferases [123]. In addition, hurdles such as difficulties in recombinant production (mainly as inclusion bodies) and unfavorable process parameters (e.g., stability, activity) of Leloir-glycosyltransferases are among the challenges involved in the large scale application of this family of enzymes (thoroughly reviewed by Mestrom *et al.* [114]).

To avoid the direct usage of sugar nucleotides for the synthesis of oligosaccharides, the concept of one-pot multi-enzyme (OPME) systems has been developed to generate the desired sugar nucleotides

in situ [124]. In the OPME approach, sugar nucleotides are produced *in situ* from low cost precursors such as triphosphate nucleotides and monosaccharides. The concept of OPME is shown in Figure 2.4.

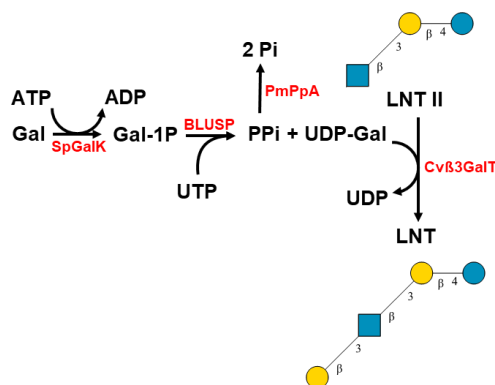


Figure 2.4. Concept of OPME for synthesis of lacto-*N*-tetraose (LNT) based on Ref. [125]. In this approach both syntheses of sugar nucleotide and HMO are carried out in one-pot. SpGalK, *Streptococcus pneumoniae* TIGR4 galactokinase; BLUSP, *Bifidobacterium longum* UDP-sugar pyrophosphorylase; PmPpA, *Pasteurella multocida* inorganic pyrophosphatase; Cvβ3GalT, *C. violaceum* β-1,3-galactosyltransferase; Gal, galactose, Gal-1P, galactose 1-phosphate; PPI, diphosphate; Pi, phosphate; ATP, adenosine triphosphate; ADP, adenosine diphosphate; UTP, uridine triphosphate; LNT II, lacto-*N*-triose II.

The concept of OPME is highly used for lab and preparative scale synthesis of various oligosaccharides [125–127]. However, there are multiple process-related aspects which significantly challenge OPME implementation in industry. For instance, stoichiometric usage of ATP and nucleotide triphosphates lead to high synthesis costs. Furthermore, direct application of low-abundance and costly sugars such as Fuc and Neu5Ac for synthesis of their nucleotide activated forms is another factor that challenges the scalability of OPME.

To avoid stoichiometric usage of nucleotide triphosphates, the concept of sugar nucleotide regeneration was developed in various studies [128–132]. In this strategy, named the coupling approach, released mono- or diphosphate nucleotides from a glycosyltransferase reaction enter a regeneration cycle in which they will convert to their triphosphate form and re-serve as substrates for sugar nucleotide synthesis — all in one pot. The concept of the coupling approach is shown in Figure 2.5. Based on this, mono-, di-, or triphosphate nucleotides are used in catalytic amounts in the excess presence of a phosphate donor compound e.g., phosphoenolpyruvate (PEP). This strategy is claimed to have been used in large scale synthesis of functional oligosaccharides in the form of carbohydrate vaccines [128]. However, using multiple purified enzymes for synthesis of one glycosidic bond is very costly and inefficient at large scales, specifically for applications like HMOs which are needed in multi-ton quantities.

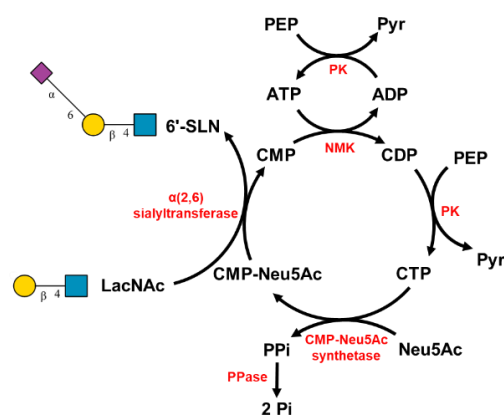


Figure 2.5. Illustration of coupling approach for synthesis of 6'-sialyl-N-acetyllactosamine (6'-SLN) from N-acetyllactosamine (LacNAc) as described in Ref. [133]. Neu5Ac, N-acetylneuraminic acid; ADP, adenosine diphosphate; ATP, adenosine triphosphate; CMP, cytidine monophosphate; CDP, cytidine diphosphate; CTP, cytidine triphosphate; CMP-NeuAc, cytidine monophosphate N-acetylneuraminic acid; PPi, inorganic pyrophosphate; Pi, inorganic phosphate; PEP, phosphoenolpyruvate; Pyr, pyruvate; PK, pyruvate kinase; NMK, nucleoside monophosphate kinase; PPase, inorganic pyrophosphorylase.

Either in the case of *in vitro* glycoengineering or synthesis of functional oligosaccharides, direct usage of sugar nucleotides and Lelior glycosyltransferases evidently offer significant advantages over any other synthesis strategies. However, the high cost of sugar nucleotides is the main bottleneck for large-scale purposes. Therefore, development of scalable processes for production of sugar nucleotides can enable the implementation of Lelior glycosyltransferases in large scales. In the following, previous approaches for synthesis of sugar nucleotides are described.

2.2 Sugar nucleotides

Sugar nucleotides are high energy molecules in the form of mono- or diphosphate nucleotide attached to a monosaccharide. Attachment of a high energy nucleotide through a phosphodiester bond to a monosaccharide significantly increases its thermodynamic energy level and makes it readily available to act as a sugar donor in glycosyltransferase reactions [134]. The main sugar nucleotides used in *in vitro* glycoengineering and HMOs synthesis are: guanosine diphosphate L-fucose (GDP-Fuc), which is the substrate for fucosyltransferases; uridine diphosphate N-acetylglucosamine (UDP-GlcNAc), which is the substrate for N-acetylglucosaminyltransferases; uridine diphosphate galactose (UDP-Gal), which is the substrate for galactosyltransferases; and cytidine monophosphate N-acetylneuraminic acid (CMP-Neu5Ac), which is the substrate for sialyltransferases.

Traditionally, sugar nucleotides were isolated from microbial sources like *E. coli* and yeast [135,136] but their low yield did not allow their application in large scales. There are some reports on fermentation-based production using metabolically engineered microorganisms, however, the reported titers are in the range of ~10 mg/L, which are too low for large-scale applications [137–139]. Chemical syntheses of sugar nucleotides consist of laborious and complex multi-step synthesis that has very low yield and productivity [140,141].

Using multi-enzyme systems for production of sugar nucleotides has proven to be the most viable option among the other synthesis methods (extensively reviewed in [116,134,142–144]). In 1988, Simon *et al.*

clearly stated that the high cost of CMP-Neu5Ac ($\sim 10^6$ \$/mol in 1988) was the reason behind the development of a multi-enzyme cascade for its synthesis [145]. The same reasoning applies to the synthesis of UDP-Gal reported by Liu *et al.* in 2002 [146]. Interestingly, despite the advances in various techniques associated with enzymatic synthesis, prices of sugar nucleotides in 2021 are still in the same range (except UDP-Glc which is still considerably expensive for large scale applications).

Despite many studies on the synthesis of sugar nucleotides, most syntheses, except for a few reports [147–149], were carried out from expensive and low-abundant precursors i.e., di- and triphosphate nucleotides [150–152]. Therefore, the lack of cost-efficient synthesis routes could be one of the reasons that sugar nucleotides are still scarce. The details of precursor choice and pathway design for synthesis of sugar nucleotides are thoroughly discussed in section 4.1.4. In the following, the concept of multi-enzyme synthesis and its utilization for process design and development is described.

2.3 Multi-enzyme systems

The first observation of enzymes being responsible for biochemical reactions took place in a multi-enzyme system by Eduard Buchner in 1897 [153], for which he was awarded the Noble Prize in Chemistry in 1907 for his work on “cell-free fermentation”. However, the high potential of multi-enzyme systems or multi-enzyme cascades for production of high value chemicals was not realized until recently [154–158]. The core concept of using multi-enzyme cascades for synthesis purposes is employing inexpensive precursors as raw materials [159–161]. There are multiple advantages of multi-enzyme synthesis over traditional synthesis methods such as: elimination of intermediates isolation, better handling of unstable intermediates, higher synthesis yield by shifting equilibrium reactions, and implementation of catalytic energy modules [156,158]. The significant decrease in DNA synthesis costs in the last decade has enabled accessibility to many types of enzymes [162]. Naturally, a majority of enzymes are active in physiological conditions, e.g., comparable pH and temperature activity ranges. Therefore, by bringing enzymes from different sources (i.e., organisms), efficient (and unnatural) multi-enzyme cascades can be designed and established based on thermodynamics and kinetic principles for synthesis of value-added chemicals [156,158]. Schrittwieser *et al.* provided an excellent review on multi-enzyme cascades for synthesis of organic molecules [163].

Availability of synthesis precursors has a crucial and often decisive role in the large-scale manufacturing of a product. Therefore, industrial availability of synthesis precursors at reasonable costs (reasonable value is defined based on the product value) is an important factor in designing large-scale processes. This issue is one of the main weak points of sugar nucleotide synthesis in literature which has significantly challenged its large-scale implementation despite of excellent reaction metrics such as yield and titer [150,164].

Scalability of a technology is a vital factor for its industrial implementation. For fermentation-based processes for product synthesis (e.g., small molecules), there is abundant literature from academia and industry for systematic analysis of process scale-up [165,166]. However, there is little information available regarding the scale-up of biocatalytic processes, specifically, for the case of multi-enzyme

processes. There are multiple reports on presenting the industrial enzymatic processes in various scales, however, the process scale-up details are not described [167,168].

Multi-enzyme systems are significantly more complex compared to common enzymatic processes involving one or two enzymes. For instance, fermentation scale-up is considered complex and costly [166,169]. Considering a six-enzyme cascade in which six separate fermentation units are required to produce the enzymes, the complexity of experimental work, development time, and consequently the scale-up cost is significantly higher (compared to, e.g., a single enzyme process) [170]. For instance, in the previous example of a six-fermentation unit, failure in one fermentation adversely affects the whole production process as well as process scheduling, and thus, product output. In stark contrast, using one large fermenter can be significantly cheaper than running multiple smaller fermenters (scale-up effect), considering process optimization, control, and logistics [171]. Furthermore, since fermentation is considered one of the costliest process steps (in terms of raw materials, utilities, and capital investment), reducing the number of required fermentation units will substantially decrease the scale-up cost [166]. Strategies such as simultaneous production of enzymes by co-expression in one fermentation unit can bring the concept of multi-enzyme synthesis closer to industrial applications. One strategy for co-expression of multiple enzymes is based on the gene fusion concept [172]. For example, for a cascade of two enzymes and two reactions, the corresponding two genes will be fused together and in the case of successful translation, a bifunctional enzyme will be produced which is capable of catalyzing the two reactions [172]. This strategy can be complicated for a cascade of more than two enzymes due to the complexity of protein structures.

Multiple Duet™ vectors capable of co-expressing two genes per vector with compatible antibiotic selection markers and origins of replication have been developed to enable co-expression of multiple genes in one strain [173]. This concept has been used in various metabolic engineering and biocatalysis studies [173–175]. In a successful application of Duet™ vectors or any other co-expression strategies of heterologous genes, only one fermentation unit is required for enzyme production. The application of co-expression of multiple genes in one strain for synthesis of sugar nucleotides is discussed in section 4.4.4.2.

The importance of biocatalyst formulation (e.g., purified, crude extract, immobilized) in development of enzymatic processes has been systematically analysed in reference [176]. Application of purified enzymes in a process is estimated to be ~5.5x more expensive compared to crude form enzymes (cell lysate) [176]. Due to the high cost of downstream processing, the use of purified enzymes in large scale processes is avoided [177]. As a rule of thumb, use of enzymes in their crudest form (i.e., cell lysate) is recommended in large-scale applications — without sacrificing product quality [177,178]. The usage of cell lysate for large-scale synthesis of sugar nucleotides is described in section 4.4.1.

Immobilization of enzymes on solid supports is another type of biocatalyst formulation for product synthesis. In this approach, enzymes are immobilized on a solid support through various mechanisms such as adsorption and covalent binding. The latter mechanism is the strongest form of binding, which is usually achieved through enzyme immobilization on epoxy-functionalized supports [179]. The details

of enzyme immobilization and the involved methods are thoroughly described in various studies [180–183]. Using immobilized enzymes allows for multiple usage of enzymes in different reaction cycles which can significantly decrease reaction costs [176]. Enzyme immobilization enables the application of co-solvents or higher synthesis temperature because of enzyme stability on solid supports [182]. Another advantage of immobilized enzymes is the opportunities in reactor design and operation mode such as using packed bed reactors for continuous synthesis [184]. Immobilized enzymes in product synthesis have been extensively used in industry [185]. However, because of changes in protein folding upon immobilization, enzyme activity can be reduced or even be completely lost.

In the case of multi-enzyme synthesis, co-immobilization (vs. separate immobilization) is considered during process development [186–188]. Since multi-enzyme cascades can be vastly different based on their pathway design, consequently, their co-immobilization might require different strategies. The details of multi-enzyme co-immobilization with respect to the design of the pathway are thoroughly described in [186].

There are only few reports on sugar nucleotides and Leloir glycosyltransferases-based synthesis by using immobilized enzymes [132,146,189]. The process for co-immobilization of multiple enzymes for synthesis of sugar nucleotides was designed and developed in this work (section 4.4.3) and thoroughly discussed in section 4.4.4.3.

3 Materials and Methods

Ultrapure water from a Milli-Q® Advantage A10 water purification system (Merck, Germany) for preparation of buffers and stock solutions was used for experiments except for preparation of *E. coli* cultivation media, where distilled water was used. The list of chemicals and suppliers are described in the Appendix A: List of Chemicals.

For the cost analysis of some compounds, all the prices were taken from the online catalogue of Carbosynth, Ltd (United Kingdom), during late 2020 and early 2021, except for PolyP_n, for which the list price was taken from Merck (Germany). The claims regarding availability of certain compounds, e.g., milligram, gram or kilogram amounts, were assumed based on the quantities available on the online catalogue of Merck and Carbosynth during late 2020 and early 2021.

3.1 Multi-enzyme cascade design for synthesis of sugar nucleotides

Ensuring the availability of the precursors was the major focus in designing pathways for synthesis of sugar nucleotides and HMOs. For synthesis of sugar nucleotides, the corresponding nucleosides i.e., Guo, Uri, and Cyt were chosen as precursor of the activated sugars. Monosaccharides were used as synthesis precursors, however, in the case of low-abundant monosaccharides i.e., Fuc and Neu5Ac, novel cascades were designed to avoid their direct usage. The details of each cascade are described in the Results and Discussion section.

3.2 Recombinant enzyme production

The selection of genes for recombinant production of enzymes in the developed cascades was based on database searches e.g., BRENDA [190,191] and available literature.

3.2.1 Plasmid design

The genes used in this work were purchased in the corresponding expression vectors from BioCat GmbH (Heidelberg, Germany) and GeneArt (Regensburg, Germany), unless stated otherwise. The plasmids for production of *N*-acetylhexosamine 1-kinase (NAHK), glucokinase (GLK), phosphomannomutase/mannose 1-phosphate guanylyltransferase (MANB/C), inorganic diphosphatase (PPA), glucose 1-phosphate uridylyltransferase (GALU), and guanosine kinase (GSK) were kind gifts of Prof. Dr. M. Pietzsch Chair of Downstream Processing at Martin Luther University Halle-Wittenberg. The list of the genes and plasmids used in this study is presented in Table 3.1. Glutamate dehydrogenase (GLDH from *Bos taurus*, Merck, Germany), and alkaline phosphatase (AP, FastAP Thermosensitive Alkaline Phosphatase, Thermo Fisher Scientific, USA) were purchased. More information on plasmids is described in the

Appendix B: List of Plasmids.

Table 3.1. List of genes used in this work for recombinant enzyme production.

Gene	Name	Uniprot acc. No.	Source	Plasmid	Ref.
Genes used for synthesis of sugar nucleotides					
udk	uridine/cytidine kinase (UDK)	P0A8F4	<i>E. coli</i>	pET-28a(+)	[192]
gsk	guanosine kinase (GSK)	O24767	<i>E. acetylicum</i>	pET-28a(+)	[193]
UMK3	UMP/CMP kinase (UMPK)	O04905	<i>A. thaliana</i>	pET-28a(+)	[194]
gmk	GMP kinase (GMPK)	P60546	<i>E. coli</i>	pET-28a(+)	[195]
SPO1727	PolyP _n kinase (PPK3)	Q5LSN8	<i>R. pomeroyi</i>	pET-28a(+)	[129]
nahk	<i>N</i> -acetylhexosamine 1-kinase (NAHK)	E8MF12	<i>B. longum</i>	pET-28a(+)	[196]
glk	glucokinase (GLK)	P0A6V8	<i>E. coli</i>	pET-28a(+)	[197]
galk	galactokinase (GALK)	B3DTF0	<i>B. longum</i>	pET100/D-TOPO	[198]
fkp	fucokinase/ L-Fuc1-phosphate guanylyltransferase (FKP)	Q58T34	<i>B. fragilis</i>	pET100/D-TOPO	[199]
galu	glucose 1-phosphate uridylyltransferase (GALU)	P0AEP3	<i>E. coli</i>	pET-28a(+)	[200]
glmu	GlcNAc 1-phosphate uridylyltransferase (GLMU)	Q9CK29	<i>P. multocida</i>	pET-15b	[201]
manC	mannose 1-phosphate guanylyltransferase (MANC)	P24174	<i>E. coli</i>	pET-28a(+)	[202]
manB	Phosphomannomutase (MANB)	P24175	<i>E. coli</i>	pET-28a(+)	[202]
EH233_206 15	<i>N</i> -acylglucosamine 2- epimerase (AGE)	A0A5Q0GK 66	<i>Anabaena sp.</i>	pET-28a(+)	[203]
nanA	<i>N</i> -acetylneuraminate lyase (NANA)	Q9CKB0	<i>P. multocida</i>	pET-22b(+)	[204]
neuA	<i>N</i> -acetylneuraminate cytidylyltransferase (CSS)	P0A0Z8	<i>N. meningitidis</i>	pET100/D-TOPO	[205]
wcaG	GDP-L-fucose synthase (WCAG)	P32055	<i>E. coli</i>	pET-28a(+)	[202]
gmd	GDP-mannose 4,6- dehydratase (GMD)	P0AC88	<i>E. coli</i>	pET-28a(+)	[202]
Genes used for synthesis of HMOs					
LgtA	β -1,3- <i>N</i> - acetylglucosaminyltransfer ase (β 1,3GlcNAcT)	Q8L2U7	<i>N. meningitidis</i>	pMAL-c4X	[206]
LgtB	β -1,4- galactosyltransferase (β 1,4GalT)	Q8L2V2	<i>N. meningitidis</i>	pET-15b	[207]
plst6	α -2,6-sialyltransferase (ST2,6)	D0VYB7	<i>P. leiognathi</i>	pColdII	[208]
fucTa	α 1-3/4-fucosyltransferase (3/4-FT)	Q9L8S4	<i>H. pylori</i>	pET22b(+)	[209]
Genes used for glycoengineering					
EF_2217	α -1,2-mannosidase (Man I)	Q832K9	<i>E. faecalis</i>	pET22b(+)	[210]
MGAT1	α -1,3-mannosyl- glycoprotein 2-beta- <i>N</i> - acetylglucosaminyltransfer ase (MGAT1)	P26572	<i>H. sapiens</i>	pET-28a(+)	[211]
MGAT2	α -1,6-mannosyl- glycoprotein 2-beta- <i>N</i> -	Q10469	<i>H. sapiens</i>	pET-28a(+)	This work

	acetylglucosaminyltransferase (MGAT2)				
β 1,4GalT1	β -1,4-galactosyltransferase (β 1,4GALT1)	P15291	<i>H. sapiens</i>	pET-28a(+)	[212]

Moreover, the pACYCDuet™ plasmid containing UMK3 and SPO1727 genes for co-expression of UMPK, and PPK3 was purchased from BioCat GmbH (Heidelberg, Germany). The produced enzyme mixture is shown as UMPK/PPK3.

3.2.2 Transformation

E. coli expression strain LOBSTR-BL21(DE3) (Kerafast Inc., USA) were used as a host for recombinant protein production, except for ST2,6, MGAT1, MGAT2, and β 1,4GALT1 where BL21(DE3) (NEB, USA) strain was used. The heat shock approach was used for transformation of the competent cells [213]. In brief, ~25 ng of plasmid was mixed with the competent cells and incubated on ice for 30 min. Afterwards, cells were heated at 42°C for 30–40 s, followed by 5 min incubation on ice. Super Optimal broth with Catabolite repression (SOC) media (NEB, USA) was added for cell growth for 1 h at 37°C. Afterwards, cells were cultivated on a selection plate by overnight incubation at 37°C.

3.2.3 Fermentation

The strains harboring the plasmids were incubated overnight at 37°C in Lysogeny broth (LB) medium consisted of 10 g/L tryptone (Carl Roth, Germany), 10 g/L sodium chloride (NaCl) (Carl Roth, Germany), 5 g/L yeast extract (Carl Roth, Germany), and their corresponding selection markers (antibiotics). The concentration of antibiotics was as follows: ampicillin (Carl Roth, Germany), 100 μ g/mL; kanamycin (Carl Roth, Germany), 50 μ g/mL; chloramphenicol (Carl Roth, Germany), 34 μ g/mL; spectinomycin (Merck, Germany), 50 μ g/mL. A seeding ratio of 1:100 was used to inoculate the main culture with overnight grown preculture. For the main cultivation, Terrific broth (TB) medium consisting of 20 g/L tryptone (for production of β 1,4GALT1 soybean peptone was used instead of tryptone), 24 g/L yeast extract, 4 mL/L glycerol (Carl Roth, Germany), 17 mM monopotassium phosphate (KH₂PO₄) (Carl Roth, Germany), 72 mM dipotassium phosphate (K₂HPO₄) (Carl Roth, Germany) with addition of 1.5 mM magnesium sulfate (MgSO₄) (Carl Roth, Germany), and a selection marker was used. The cultivation condition was as follows, unless stated otherwise: growth at 37°C up to an OD₆₀₀ of 0.8–1, induction with 0.4 mM isopropyl β -D-1-thiogalactopyranoside (IPTG) (Carbosynth Ltd, United Kingdom) followed by 20–24 h incubation at 16°C (for ST2,6 enzyme 15°C was used). Cell harvest was carried out through centrifugation (Eppendorf, Germany) at 7000xg for 20 min at 4°C. Cell pellets were stored at -20°C until cell lysis.

3.2.4 Cell lysis

The cell pellet was resuspended in lysis buffer up to a final concentration of ~20–30% w/v. The lysis buffer used in this work was 50 mM 3-(N-morpholino) propanesulfonic acid (MOPS) (Carl Roth, Germany) buffer, 300 mM NaCl, 10 mM magnesium chloride (MgCl₂) (Applichem, Germany), and 5% glycerol at pH 7.4, unless stated otherwise. Cell lysis was performed with a high-pressure homogenizer (Maximator, Switzerland) operated at a pressure of 800–1200 psi for three passages. Afterwards, the

cell extract was centrifuged at 12,000×g for 30 min (or 7,000×g for 45 min) at 4°C to collect the supernatant (cell lysate) and remove the cell debris.

3.2.5 Purification

Centrifugally clarified cell lysate was filtered with a 0.45 µm cellulose acetate filter (Sartorius, Germany). For purification of histidine tagged (His tag) enzymes, immobilized metal affinity chromatography (IMAC) was used. Amylose resin was used for purification of proteins tagged with maltose binding protein (MBP).

3.2.5.1 His-tag purification

Enzyme purification was carried out by employing an ÄKTA start instrument (Cytiva, Sweden) equipped with a 5 mL HisTrap FF column (Cytiva, Sweden). The binding buffer consisted of 50 mM MOPS, 300 mM NaCl, 10 mM MgCl₂, 10 mM imidazole (Carl Roth, Germany), and 5% glycerol at pH 7.4. The elution buffer consisted of 50 mM MOPS, 300 mM NaCl, 10 mM MgCl₂, 250 mM imidazole, and 5% glycerol at pH 7.4. Fractions containing the protein of interest were pooled and the buffer was exchanged using an Amicon® Ultra-15 centrifugal filter unit with a 3 KDa MW cutoff (Merck, Germany). The exchange buffer was 50 mM MOPS, 300 mM NaCl, and 10 mM MgCl₂ at pH 7.4. Afterwards, the retentate solution (concentrated enzyme) was mixed 1:1 with glycerol (50%). Enzyme stock solutions were stored at -20°C.

3.2.5.2 MBP-tag purification

Purification of MBP-tagged enzymes was performed based on the affinity of MBP toward amylose resin. The purification was performed with an ÄKTA start instrument (Cytiva, Sweden) equipped with a 1 mL MBPTrap HP column (Cytiva, Sweden). The binding buffer contained 50 mM MOPS, 300 mM NaCl, 10 mM MgCl₂, and 5% glycerol at pH 7.4. The elution buffer contained 50 mM MOPS, 300 mM NaCl, 10 mM MgCl₂, 10 mM maltose (Carl Roth, Germany), and 5% glycerol at pH 7.4. Fractions containing the protein of interest were pooled and the buffer was exchanged using an Amicon® Ultra-15 centrifugal filter unit with a 3 KDa MW cutoff (Merck, Germany). The exchange buffer was 50 mM MOPS, 300 mM NaCl, and 10 mM MgCl₂ at pH 7.4. Afterwards, the retentate solution was mixed 1:1 with glycerol. Enzyme stock solutions were stored at -20°C.

3.3 Enzyme activity and cascade reactions

All the cascade experiments were performed in 1.5 mL Eppendorf safe-lock tubes (Eppendorf, Germany) at 37°C, and 550 rpm with an Eppendorf Thermomixer comfort mixer (Eppendorf, Germany), unless stated otherwise. For reaction time course measurements, usually 1–2 µL aliquots were taken and quenched into 1000–2000 µL of water at 90°C for 3 min. For experiments including CMP-Neu5Ac, 2 µL of samples were quenched into 1000 µL of water at 4°C. The following buffers were used for performing the reactions: 2-(N-morpholino) ethanesulfonic acid (MES) buffer pH 5.5–6.5, MOPS buffer pH 7–7.5, Tris-HCl buffer pH 7–9, unless stated otherwise. The establishment and optimization of the cascades were done with purified enzymes. The details of each multi-enzyme experiment are described in the corresponding section.

3.3.1 Synthesis of sugar nucleotides

3.3.1.1 Synthesis of UDP-sugars

3.3.1.1.1 Synthesis of UDP-GlcNAc and UDP-GalNAc

The reaction conditions for synthesis of UDP-GlcNAc were as follows: Tris-HCl (pH, 8.5) 150 mM; MgCl₂ 75 mM; Uri 68 mM; GlcNAc 68 mM; ATP 2.1 mM; PolyP_n 21 mM; UDK 0.07 µg/µL; UMPK/PPK3 0.11 µg/µL; NAHK 0.18 µg/µL; GLMU 0.2 µg/µL, and PPA 0.05 µg/µL in a total volume of 200 µL. Results of this cascade are presented in section 4.1.1.1.

The reaction conditions for synthesis of UDP-GalNAc were as follows: Tris-HCl (pH, 8.5) 150 mM; MgCl₂ 75 mM; Uri 53 mM; GalNAc 53 mM; ATP 2.6 mM; PolyP_n 20 mM; UDK 0.07 µg/µL; UMPK/PPK3 0.11 µg/µL; NAHK 0.15 µg/µL; GLMU 0.27 µg/µL, and PPA 0.08 µg/µL in a total volume of 200 µL. Results are presented in section 4.1.1.1.

3.3.1.1.2 Synthesis of UDP-Gal

The reaction conditions were as follows: Tris-HCl (pH, 8.5) 150 mM; MgCl₂ 75 mM; Uri 50 mM; Gal 52 mM; ATP 0.6 mM, and PolyP_n 20 mM; UDK 0.07 µg/µL; UMPK/PPK3 0.11 µg/µL; GALK 0.16 µg/µL; GALU 0.12 µg/µL, and PPA 0.06 µg/µL in a total volume of 250 µL. Results of this cascade are presented in section 4.1.1.2.

3.3.1.1.3 Synthesis of UDP-Glc and UDP-Man

The reaction conditions for synthesis of UDP-Glc were as follows: 150 mM Tris-HCl (pH 8.5); 75 mM MgCl₂; 62.5 mM Glc; 60 mM Uri; 1.7 mM ATP; 19 mM PolyP_n; 0.86 µg/µL GLK; 0.06 µg/µL UDK; 0.1 µg/µL UMPK/PPK3; 0.14 µg/µL MANB/C; 0.15 µg/µL GALU, and 0.04 µg/µL PPA in a total volume of 200 µL. Results of this cascade are presented in section 4.1.1.3.

The reaction for synthesis of UDP-Man contained 200 mM Tris-HCl (pH 8.5); 26 mM Man; 25 mM Uri; 7.3 mM ATP; 9.7 mM PolyP_n; 75 mM MgCl₂, and the following enzymes: 0.06 µg/µL UDK; 0.08 µg/µL UMPK/PPK3; 0.76 µg/µL GLK; 0.14 µg/µL MANB/C; 0.12 µg/µL GALU, and 0.04 µg/µL PPA in a total volume of 200 µL.

3.3.1.2 Synthesis of GDP-sugars

3.3.1.2.1 Synthesis of GDP-Man

The reaction conditions for synthesis of GDP-Man were as follows: 200 mM Tris-HCl (pH 8.5); 75 mM MgCl₂; 10 mM Man; 12.8 mM Guo (in DMSO); 5.8 mM ATP; 13.5 mM PolyP_n; 0.11 µg/µL GSK; 0.49 µg/µL GMPK; 0.02 µg/µL PPK3; 0.33 µg/µL GLK; 0.17 µg/µL MANB/C, and PPA 0.03 µg/µL with a final volume of 200 µL. The final DMSO content of the reaction matrix was 1% v/v. Results of this cascade are presented in section 4.1.2.1.

3.3.1.2.2 Synthesis of GDP-Fuc from Fuc and Guo

The reaction mixture for GDP-Fuc synthesis contained 200 mM Tris-HCl (pH 7.5); 10 mM Fuc; 10 mM Guo (in DMSO); 2.5 mM ATP; 7.5 mM PolyP_n; 45 mM MgCl₂, and the following enzymes: GSK 0.22 µg/µL; GMPK 0.78 µg/µL; PPK3 0.05 µg/µL; FKP 0.31 µg/µL, and PPA 0.03 µg/µL in a final volume of

200 μL . The final DMSO content of the reaction matrix was 1% v/v. Results of this cascade are presented in section 4.1.2.2.1.

3.3.1.2.3 Synthesis of GDP-Fuc from GDP-Man

The reaction mixtures contained 150 mM Tris-HCl (various pH values); 10 mM MgCl_2 ; 3–4 mM GDP-Man; 4 mM nicotinamide adenine dinucleotide phosphate (NADPH); WCAG 0.45 $\mu\text{g}/\mu\text{L}$, and GMD 1.03 $\mu\text{g}/\mu\text{L}$ in a final volume of 33 μL . To evaluate the role of the pH value on the conversion of GDP-Man to GDP-Fuc, the following pH values were tested: 7.0, 7.5, 8.0, 8.5, 9.0.

3.3.1.2.4 Synthesis of GDP-Fuc from Man and Guo

The cascade reactions contained 200 mM Tris-HCl (pH 8.5); 75 mM MgCl_2 ; 10.5 mM Man; 10.5 mM Guo; 50 mM L-glutamic acid (L-Glu); 1 mM NADPH; 5.5 mM ATP; 13.5 mM PolyP_n; GSK 0.11 $\mu\text{g}/\mu\text{L}$; GMPK 0.49 $\mu\text{g}/\mu\text{L}$; PPK3 0.02 $\mu\text{g}/\mu\text{L}$; GLK 0.33 $\mu\text{g}/\mu\text{L}$; MANB/C 0.17 $\mu\text{g}/\mu\text{L}$; WCAG 0.07 $\mu\text{g}/\mu\text{L}$; GMD 0.17 $\mu\text{g}/\mu\text{L}$; PPA 0.03 $\mu\text{g}/\mu\text{L}$, and 10 units of GLDH (2.99 $\mu\text{g}/\mu\text{L}$) in a final volume of 200 μL . The final DMSO content of the reaction matrix was 1% v/v. Results of this cascade are presented in section 4.1.2.2.2.

3.3.1.3 Synthesis of CMP-Neu5Ac

3.3.1.3.1 Synthesis of CMP-Neu5Ac from Neu5Ac and Cyt

The reaction mixture for synthesis of CMP-Neu5Ac consisted of 150 mM Tris-HCl (pH 8.5); 10 mM Cyt; 10 mM Neu5Ac; 3 mM ATP; 4 mM PolyP_n; 50 mM MgCl_2 and the following enzymes: UDK 0.06 $\mu\text{g}/\mu\text{L}$; UMPK/PPK3 0.11 $\mu\text{g}/\mu\text{L}$; CSS 1.27 $\mu\text{g}/\mu\text{L}$, and PPA 0.04 $\mu\text{g}/\mu\text{L}$ in a final volume of 200 μL . Results of this cascade is presented in section 4.1.3.1.

3.3.1.3.2 Synthesis of CMP-Neu5Ac from GlcNAc, Pyr, and Cyt

The first experiment to synthesize CMP-Neu5Ac starting from GlcNAc and Pyr contained 140 mM Tris-HCl (pH 8.5); 35 mM Cyt; 39 mM GlcNAc; 39 mM Pyr; 3.5 mM ATP; 14.1 mM PolyP_n; 53 mM MgCl_2 and the following enzymes: UDK 0.09 $\mu\text{g}/\mu\text{L}$; UMPK/PPK3 0.15 $\mu\text{g}/\mu\text{L}$; CSS 1.22 $\mu\text{g}/\mu\text{L}$; AGE 0.03 $\mu\text{g}/\mu\text{L}$; NANA 0.08 $\mu\text{g}/\mu\text{L}$, and PPA 0.05 $\mu\text{g}/\mu\text{L}$ in a final volume of 282 μL .

After initial efforts for establishment of the cascade, it was hypothesized that CTP might have an inhibitory role possibly on AGE. To confirm the hypothesis of AGE inhibition by cytidine triphosphate (CTP), four rounds of experiments were carried out. Experiments performed with 150 mM Tris-HCl (pH 8.5); 20 mM MgCl_2 ; 20 mM CTP; 30 mM Pyr; 0.05 $\mu\text{g}/\mu\text{L}$ AGE; 1.5 $\mu\text{g}/\mu\text{L}$ NANA; 1 $\mu\text{g}/\mu\text{L}$ CSS and 0.04 $\mu\text{g}/\mu\text{L}$ PPA in a total volume of 150 μL . The 1st experiment contained 30 mM GlcNAc (AGE_1); the 2nd experiment contained 30 mM *N*-acetylmannosamine (ManNAc) (AGE_2); the 3rd experiment contained 30 mM GlcNAc, and 0.3 mM ATP (AGE_3); and the 4th experiment contained 30 mM ManNAc, and 0.3 mM ATP (AGE_4).

For optimization of CMP-Neu5Ac synthesis, at first, the ratio of GlcNAc/Cyt, and Pyr/Cyt was increased from 1 to 7.4 and 7.9, respectively. The reaction consisted of 145 mM Tris-HCl (pH 8.5); 10 mM Cyt; 74 mM GlcNAc; 79 mM Pyr; 3 mM ATP; 4 mM PolyP_n; 74 mM MgCl_2 and the following enzymes: UDK 0.06

$\mu\text{g}/\mu\text{L}$; UMPK/PPK3 0.08 $\mu\text{g}/\mu\text{L}$; CSS 1.67 $\mu\text{g}/\mu\text{L}$; AGE 0.04 $\mu\text{g}/\mu\text{L}$; NANA 1.15 $\mu\text{g}/\mu\text{L}$, and PPA 0.05 $\mu\text{g}/\mu\text{L}$ in a final volume of 203 μL .

In the next step, different concentrations of PolyP_n were evaluated. The tested PolyP_n concentrations of experiments were 4, 5, 6, 7, and 8 mM. The rest of the experimental conditions were as follows: 150 mM Tris-HCl (pH 8.5); 10 mM Cyt; 75 mM GlcNAc; 70 mM Pyr; 3 mM ATP; 75 mM MgCl₂ and the following enzymes: UDK 0.06 $\mu\text{g}/\mu\text{L}$; UMPK/PPK3 0.08 $\mu\text{g}/\mu\text{L}$; CSS 1.27 $\mu\text{g}/\mu\text{L}$; AGE 0.04 $\mu\text{g}/\mu\text{L}$, and NANA 1.16 $\mu\text{g}/\mu\text{L}$ in a final volume of 200 μL .

Based on the series of optimization reactions, the following were the best performing conditions: 190 mM Tris-HCl (pH 8.5); 34 mM Cyt; 72 mM GlcNAc; 79 mM Pyr; 2 mM ATP; 23 mM PolyP_n; 72 mM MgCl₂ and the following enzymes: UDK 0.05 $\mu\text{g}/\mu\text{L}$; UMPK/PPK3 0.07 $\mu\text{g}/\mu\text{L}$; CSS 1.05 $\mu\text{g}/\mu\text{L}$; AGE 0.03 $\mu\text{g}/\mu\text{L}$; NANA 0.96 $\mu\text{g}/\mu\text{L}$, and PPA 0.03 $\mu\text{g}/\mu\text{L}$ with a final volume of 242 μL . Results of these cascades are presented in section 4.1.3.2.

3.3.2 Synthesis of HMOs

3.3.2.1 *The coupling approach*

3.3.2.1.1 Synthesis of 3-FL

Synthesis of 3-FL from Man: The reactions consisted of: 160 mM Tris-HCl (pH 8.5); 60 mM MgCl₂; 24 mM Lac; 24 mM Man; 4 mM Guo; 87 mM L-Glu; 0.8 mM NADPH; 4.4 mM ATP; 10.8 mM PolyP_n; GSK 0.09 $\mu\text{g}/\mu\text{L}$; GMPK 0.39 $\mu\text{g}/\mu\text{L}$; PPK3 0.01 $\mu\text{g}/\mu\text{L}$; GLK 0.4 $\mu\text{g}/\mu\text{L}$; MANB/C 0.15 $\mu\text{g}/\mu\text{L}$; WCAG 0.05 $\mu\text{g}/\mu\text{L}$; GMD 0.14 $\mu\text{g}/\mu\text{L}$; PPA 0.02 $\mu\text{g}/\mu\text{L}$; 3/4-FT 0.11 $\mu\text{g}/\mu\text{L}$, and 10 units of GLDH (2.39 $\mu\text{g}/\mu\text{L}$) in a final volume of 251 μL . The final DMSO content of the reaction matrix was 0.4% v/v.

Synthesis of 3-FL from Fuc: The reaction mixture consisted of 200 mM Tris-HCl (pH 7.5); 29 mM Fuc; 38 mM Lac; 3.8 mM Guo (in DMSO); 2.8 mM ATP; 11.5 mM PolyP_n; 57 mM MgCl₂ and the following enzymes: GSK 0.09 $\mu\text{g}/\mu\text{L}$; GMPK 0.51 $\mu\text{g}/\mu\text{L}$; PPK3 0.02 $\mu\text{g}/\mu\text{L}$; FKP 0.32 $\mu\text{g}/\mu\text{L}$; PPA 0.02 $\mu\text{g}/\mu\text{L}$, and 3/4-FT 0.09 $\mu\text{g}/\mu\text{L}$ in a final volume of 261 μL . The final DMSO content of the reaction matrix was 0.4% v/v.

Results of these cascades are presented in section 4.2.1.1.

3.3.2.1.2 Synthesis of 6'-SL

The experimental conditions were as follows: 150 mM Tris-HCl (pH 8.5); 30 mM Lac; 8 mM Cyt; 60 mM GlcNAc; 64 mM Pyr; 1.6 mM ATP; 19.2 mM PolyP_n; 60 mM MgCl₂ and the following enzymes: UDK 0.05 $\mu\text{g}/\mu\text{L}$; UMPK/PPK3 0.05 $\mu\text{g}/\mu\text{L}$; CSS 0.87 $\mu\text{g}/\mu\text{L}$; AGE 0.02 $\mu\text{g}/\mu\text{L}$; NANA 0.8 $\mu\text{g}/\mu\text{L}$; PPA 0.02 $\mu\text{g}/\mu\text{L}$, and 2,6-ST 0.11 $\mu\text{g}/\mu\text{L}$ in a final volume of 251 μL . Results of this cascade are presented in section 4.2.1.2.

3.3.2.2 *The modular approach*

In the modular approach, all the sugar nucleotides and HMOs, except Lac, were produced based on the developed multi-enzyme cascades and used without any purification. UDP-GlcNAc was produced as described in section 4.1.1.1, UDP-Gal was produced as described in section 4.1.1.2, GDP-Fuc was

synthesized as described in section 4.1.2.2.2, and CMP-Neu5Ac was produced as described in section 4.1.3.2.

3.3.2.2.1 Synthesis of LacNAc

The reaction mixture for LacNAc synthesis contained 94 mM MES buffer (pH 6.0); 31 mM GlcNAc; 30 mM UDP-Gal; β 1,4GalT 0.01 μ g/ μ L, and 10 units of AP in a final volume of 160 μ L. Results of this experiment are presented in section 4.2.2.1.

3.3.2.2.2 Synthesis of LNT II

For the synthesis of LNT II, reaction conditions were as follows: 210 μ L of a reaction mixture containing 20 mM UDP-GlcNAc; β 1,3GlcNAcT 0.08 μ g/ μ L; 10 units of AP; 28.5 mM Lac; 150 mM Tris-HCl (pH 8.5), and 20 mM manganese (II) chloride (MnCl₂) (Merck, Germany) in a total volume of 210 μ L. Results of this experiment are presented in section 4.2.2.2.

3.3.2.2.3 Synthesis of LNnT

The reaction mixture for LNnT synthesis contained 156 mM MES buffer (pH 5.5); 3.7 mM LNT II; 11 mM UDP-Gal; β 1,4GalT 0.01 μ g/ μ L, and 20 units of AP in a total volume of 320 μ L. After 48 h of incubation at 37°C, LNnT was produced to a final concentration of ~2.9 mM (~2 g/L). Results of this experiment are presented in section 4.2.2.3.

3.3.2.2.4 Synthesis of *para*-LNnH

At first, *para*-Lacto-*N*-neopentaose was produced by combination of 75 μ L of UDP-GlcNAc cascade product (~10 mM UDP-GlcNAc); 75 μ L of LNnT reaction products; 30 units of AP, and 0.06 μ g/ μ L of β 1,3GlcNAcT in 150 mM Tris-HCl (pH 8.5) in a total volume of 270 μ L. After 24 h of incubation (at 30°C), 50 μ L reaction containing *para*-Lacto-*N*-neopentaose was mixed with 50 μ L of UDP-Gal cascade reaction product in addition to 20 units of AP, and 0.02 μ g/ μ L of β 1,4GalT in 240 MES buffer (pH 6.5) in a total volume of 210 μ L. Results of this experiment are presented in section 4.2.2.4.

3.3.2.2.5 Synthesis of 6'-SL

The reaction solution contained: 18 mM CMP-Neu5Ac; 20 mM Lac; 133 mM Tris-HCl (pH 8.5), and 0.13 μ g/ μ L 2,6-ST in a final volume of 150 μ L. Results of this experiment are presented in section 4.2.2.5.

3.3.2.2.6 Synthesis of LST_c and DSLNnT

The reaction mixture for LST_c and DS-LNnT synthesis contained: 5 mM CMP-Neu5Ac; 0.7 mM LNnT; 0.14 μ g/ μ L 2,6-ST, and 240 mM Tris-HCl (pH 9) with a total volume of 210 μ L. Results of this experiment are presented in section 4.2.2.6.

3.3.2.2.7 Synthesis of 3-FL

The following condition was used for 3-FL synthesis: 4 mM GDP-Fuc; 10 mM Lac; 0.17 μ g/ μ L 3/4-FT, and 130 mM Tris-HCl (pH 8.5) in a total volume of 118 μ L. Results of this experiment are presented in section 4.2.2.7.

3.3.2.2.8 Synthesis of LNFP III and DF-LNnT

Similar to 3-FL, synthesis of LNFP III and DF-LNnT by using *H. pylori* 3/4-FT has been reported before [209]. For synthesis of LNFP III and DF-LNnT, reaction conditions were as follows: 3 mM GDP-Fuc; 0.9

mM LNnT; 0.15 $\mu\text{g}/\mu\text{L}$ 3/4-FT; 146 mM Tris-HCl (pH 8.5), and 20 units of AP in a total volume of 205 μL . Results of this experiment are presented in section 4.2.2.8.

3.3.2.2.9 Synthesis of LNFP V

The steps for LNFP V synthesis is illustrated in Figure 3.1 [125]. The reaction mixture for synthesis of fucosylated tetrasaccharide consisted of LNT II; 210 mM Tris-HCl (pH 8.5); 0.07 $\mu\text{g}/\mu\text{L}$ 3/4-FT, and 2 mM GDP-Fuc in a total volume of 190 μL . After 24 h of incubation at 37°C, 100 μL of the reaction mixture transferred to a new vial containing: 5 mM UDP-Gal; 0.01 $\mu\text{g}/\mu\text{L}$ β 1,4GalT, and 167 mM MES buffer (pH 6.0). Results of this experiment are presented in section 4.2.2.9.



Figure 3.1. The steps for LNFP V synthesis. The symbols are glucose, blue circle; N-acetylglucosamine, blue square; fucose, red triangle, and galactose, yellow circle.

3.3.2.2.10 Synthesis of 6'-SLN

The reaction mixture for synthesis of 6'-SLN consisted of 115 mM Tris-HCl (pH 8.5); 6.1 mM LacNAc; 8.5 mM CMP-Neu5Ac; 0.10 $\mu\text{g}/\mu\text{L}$ 2,6-ST, and 5 units of AP in a total volume of 175 μL . Results of this experiment are presented in section 4.2.2.10.

3.3.3 *In vitro* glycoengineering

The nomenclature and structure of the glycans described in this work is shown in Table 3.2.

Table 3.2. The glycan nomenclature and structure described in this work. The monosaccharide compositions are N-acetylglucosamine, blue square; mannose, green circle; fucose, red triangle, and galactose, yellow circle.

Name	Structure	Name	Structure	Name	Structure
Man9		Man5-G0		G0F	
Man5		Man3-G0		G1F	
Man3		G0		G2F	

3.3.3.1 Addition of terminal Gal

For addition of terminal Gal to Rituximab (Rituxan) (Evidentic GmbH, Germany), Trastuzumab (Herceptin) (Evidentic GmbH, Germany), Ramucirumab (Cyramza) (Evidentic GmbH, Germany), and Obinutuzumab (Gazyva) (Evidentic GmbH, Germany), 100 µg of each protein incubated in 50 mM MES buffer (pH 6.5); 50 milli units of bovine β1,4GalT (Merck, Germany); 5 mM UDP-Gal (Carbosynth Ltd, United Kingdom), and 5 mM MnCl₂ in a total volume of 100 µL.

Reaction for glycoengineering of cell culture derived IgG (produced as described in 3.6) by using *E. coli*-derived β4GALT1 was as follows: 130 µg pure IgG (cell culture derived); 190 mM MES buffer pH 6.5; 14 mM MnCl₂; 1.4 mM UDP-Gal (Carbosynth Ltd, United Kingdom), and 0.3 µg/µL β4GALT1 in a total volume of 211 µL. The glycosylation profile was analysed after 24 h of incubation at 37°C and 550 rpm. Results are described in section 4.3.1.

3.3.3.2 Synthesis of Man3-G0 from Man3

Both MGAT1 and MGAT2 were produced in their soluble and active form in *E. coli*. The purified form of enzymes used throughout the experiments. Commercial unlabeled Man3 (Agilent, USA) was APTS-labeled (as described in section 3.7.5) and used as a substrate. The reaction for conversion of Man3 to

Man3-G0 consisted of 50 μL APTS-labeled Man3; 1.8 mM UDP-GlcNAc; 93 mM HEPES buffer (pH 7.4); 9.3 mM MnCl_2 , and 0.3 $\mu\text{g}/\mu\text{L}$ MGAT1 in a total volume of 107 μL . For synthesis of Man3-G0 from Man3, a one-pot experiment containing both MGAT1 and MGAT 2 was carried out. The experiment was as follows: 100 mM HEPES buffer (pH 7.4); 10 mM MnCl_2 ; 2.5 mM UDP-GlcNAc; 50 μL Man3; 0.1 $\mu\text{g}/\mu\text{L}$ MGAT1, and 0.3 $\mu\text{g}/\mu\text{L}$ MGAT2 in a volume of 200 μL . Results are described in section 4.3.2.

3.3.3.3 Synthesis of Man5-G0 on intact IgG

At first, Man9 was trimmed to Man5 by using an *E. coli*-derived mannosidase. The experimental condition for conversion of Man9 to Man5 antibodies was as follows: 2.4 mg Man 9-containing IgG (purified – kifunensine derived); 2.6 $\mu\text{g}/\mu\text{L}$ Man I; 10 mM MgCl_2 , and 200 mM MES buffer (pH 6.5) in a total volume of 100 μL .

For synthesis of Man5-G0 the reaction contained: 1.8 mg Man9-containing IgG; 1.9 $\mu\text{g}/\mu\text{L}$ Man I; 0.4 $\mu\text{g}/\mu\text{L}$ MGAT1; 1.5 mM UDP-GlcNAc; 10 mM MgCl_2 ; 10 mM MnCl_2 , and 200 mM MES buffer (pH 6.5) in a total volume of 133 μL . Results are described in section 4.3.2.

3.4 Process development

3.4.1 Scale-up of UDP-Gal synthesis cascade

For preparation of cell lysate for synthesis of UDP-Gal the following biomass was mixed: UDK 3.46 g; UMPK/PPK3 5.20 g; GALK 5.54 g; GALU 5.70 g, and PPA 1.7 g in 120 mL of 50 mM HEPES buffer (pH 8.1); 400 mM NaCl, and 5% glycerol. The mixture passed three times through a high-pressure homogenizer. Cell-free extract was centrifuged at 11,000 $\times g$ for 45 min. Afterwards, different sets of small scale (200 μL) experiments were carried out to find a suitable biocatalyst load, based on the condition described in section 4.1.1.2. It was found out 10% of $V_{\text{lysate}}/V_{\text{reaction}}$ is sufficient to perform the synthesis. The findings based on the 200 μL reaction were directly used for 1 L scale synthesis which correlates to 5,000 \times scaling factor.

To carry out the 1 L scale experiment, a spinner flask (DASGIP, Germany) was chosen to mimic the condition of a stirred tank reactor. The synthesis condition was as follows: 150 mM Tris-HCl (pH 8.5); 55 mM Uri; 55 mM Gal; 6.2 mM ATP; 20 mM PolyP_n, and 75 mM MgCl_2 . The reaction carried out at 37°C room and 60 rpm (magnetic stirrer). To understand the role of scale-up on the performance of the cascade, a parallel 200 μL experiment was carried out. Results of this experiment is described in section 4.4.1.1.

3.4.2 Scale-up of UDP-GlcNAc synthesis cascade

For preparation of cell lysate for large-scale synthesis of UDP-GlcNAc, the following biomass was mixed: UDK 6.65 g; UMPK/PPK3 9.26 g; NAHK 11.23 g; GLMU 6.9 g, and PPA 4.94 g in 200 mL of 50 mM HEPES buffer (pH 8.1); 400 mM NaCl, and 5% glycerol. The mixture passed three times through a high-pressure homogenizer. Cell-free extract was centrifuged at 11,000 $\times g$ for 45 min to separate cell lysate (soluble fraction) from the insoluble fraction (cell pellet). Afterwards, multiple sets of small scale (200 μL) experiments were performed to find a suitable biocatalyst load for the synthesis of UDP-GlcNAc based on the cascade shown in Figure 4.2, and conditions described in the section 4.1.1.1.

The findings based on the 200 μ L synthesis directly used for 4 L scale synthesis which correlates to a 20,000 \times scale-up factor.

To carry out a 4 L scale experiment, a seven-liter single wall glass autoclavable bioreactor (Applikon Biotechnology B.V., Netherlands), equipped with two elephant ear impellers was used. The synthesis condition was as follows: 200 mM Tris-HCl (pH 8.5); 62 mM Uri; 62 GlcNAc; 1.6 mM ATP; 18 mM PolyP_n; 75 mM MgCl₂, and a total protein load of 0.5 g/L in the form of cell lysate. The reaction carried out at 37°C and 120 rpm. To understand the effect of scale-up on the performance of the cascade, a parallel 200 μ L experiment was performed. Results of this section are described in section 4.4.1.2.

3.4.3 Co-expression of enzymes

3.4.3.1 Enzyme co-expression for synthesis of UDP-GlcNAc and UDP-Gal

Three different Duet™ vectors (each containing two multiple cloning sites) with distinct ribosome binding sites and selection markers were chosen for cloning of the genes. The pRSFDuet™_NAHK_GALK and pCDFDuet™_PPA_GALU plasmids for co-expression of NAHK/GALK and GALU/PPA, respectively, were designed and prepared by Dr. Simon Boecker from the Analysis and Redesign of Biological Networks group at Max Planck Institute for Dynamics of Complex Technical Systems. The pACYCDuet™ plasmid containing UMK3 and SPO1727 genes was purchased from BioCat GmbH (Heidelberg, Germany).

Table 3.3. Enzymes and plasmids used in this study for the co-expression of the cascade. The sugar kinases and the nucleotide kinases, respectively, were grouped together on one vector. Moreover, the uridylyltransferase and phosphatase were grouped together.

Gene	Enzyme	Source	Uniprot acc. No.	Plasmid	Restriction site
Sugar kinase module					
galK	GALK	<i>B. longum</i>	B3DTF0	pRSFDuet™-1	NcoI, NotI
nahk	NAHK	<i>B. longum</i>	E8MF12	pRSFDuet™-1	NdeI, KpnI
Nucleotide kinase module					
UMK3	UMPK	<i>A. thaliana</i>	O04905	pACYCDuet™	NcoI, NotI
SPO1727	PPK3	<i>R. pomeroyi</i>	Q5LSN8	pACYCDuet™	NdeI, KpnI
Uridylyltransferase module					
galu	GALU	<i>E. coli</i>	P0AEP3	pCDFDuet™	NcoI, NotI
ppa	PPA	<i>P. multocida</i>	P57918	pCDFDuet™	NdeI, KpnI

The cultivation was performed as described in 3.2.3, except 1 mM IPTG was used for induction of expression and the following antibiotics concentration: kanamycin 30 μ g/mL, chloramphenicol 32 μ g/mL, and spectinomycin 50 μ g/mL. The His-tag purification was performed, and production of all enzymes was confirmed by SDS-PAGE (Appendix D: SDS-PAGE of purified enzymes).

3.4.3.1.1 Synthesis of UDP-GlcNAc

To perform the synthesis of UDP-GlcNAc, 3.9 g of biomass (~130 mL cultivation) was resuspended in 40 mL of 25 mM Tris-HCl (pH 7.1); 400 mM NaCl, and 5% glycerol and lysed by three passages through a high-pressure homogenizer. After removal of cell debris through centrifugation, screening experiments were carried out at 200 μ L to find an optimal biocatalyst load. The cell lysate was directly used for synthesis without any further purification. The findings were transferred for synthesis at 150 mL scale.

For synthesis of UDP-GlcNAc at 150 mL, the reaction carried out in a spinner flask at 37°C temperature-controlled room and 50 rpm. The reaction mixture consisted of 200 mM Tris-HCl (pH 8.5); 75 mM MgCl₂; 47 mM UMP; 50 mM GlcNAc; 4.7 mM ATP; 15 mM PolyP_n, and a total protein concentration of 0.5 g/L. To evaluate the scale-up effect, a parallel 200 μ L scale was carried out.

3.4.3.1.2 Synthesis of UDP-Gal

For 3 L scale synthesis of UDP-Gal, 57 g of biomass (~1.9 L of culture, produced with multiple 200 mL cultivations) was disrupted by a high-pressure homogenizer in 400 mL of lysis buffer containing 50 mM HEPES (pH 8.1); 400 mM NaCl, and 5% glycerol. Cell debris was separated by centrifugation at 11,000 \times g for 45 min. The cell lysate was directly used for synthesis without any further purification. A suitable load of biocatalyst was found through screening experiments at 200 μ L. Afterwards, the findings were directly transferred to 3 L scale experiment which translates to 15,000 \times scale-up factor.

The same set-up as section 4.4.1.2, used for synthesis of UDP-Gal at 3 L scale. The reaction mixture consisted of 200 mM Tris-HCl (pH 8.5); 75 mM MgCl₂; 55 mM UMP; 55 mM Gal; 2.7 mM ATP; 14 mM PolyP_n, and a total protein (biocatalyst) concentration of 1 g/L. The experiment was performed at 37°C and 100 rpm. A parallel experiment ran at 200 μ L scale, to compare the performance of the cascade the different scales.

Results of these experiments are presented in section 4.4.2.1.

3.4.3.2 Co-expression of 3 enzymes for synthesis CMP-Neu5Ac

The concept of co-expression of enzymes was applied to synthesize CMP-Neu5Ac based on the cascade shown in Figure 4.19, however, CMP was used instead of Cyt. The recombinant enzyme preparation was carried out as described above. In brief, plasmids carrying genes for production of CSS and UMPK/PPK3 enzymes were transformed into a single strain which was used for co-expression of mentioned enzymes. For CMP-Neu5Ac synthesis at 100 mL scale, biomass from 200 mL culture was lysed by a high-pressure homogenizer in 40 mL lysis buffer contained 25 mM Tris-HCl (pH 7.1); 400 mM NaCl, and 5% glycerol.

The 100 mL scale reaction carried out in a spinner flask. The reaction matrix contained 150 mM Tris-HCl (pH 8.5); 75 mM MgCl₂; 50 mM CMP; 51 mM Neu5Ac; 5 mM ATP, and 16 mM PolyP_n. Results of this experiment is presented in section 4.4.2.2.

3.5 Immobilization

Enzyme immobilization was carried out in 2 mL Eppendorf tubes. On average, 200 mg of beads were transferred to a new Eppendorf tube and followed by addition of 0.6 mL cell lysate of UDP-GlcNAc cascade enzymes. The same cell lysate described in section 3.4.2 was used for co-immobilization. Different epoxy functionalized Relizyme™ (Resindion S.r.l, Italy), and ECR (Purolite, USA) beads were used as immobilization support. Afterwards, cell lysate (containing a cocktail of required enzymes) was added up to 5% $W_{\text{total_protein}}/W_{\text{beads}}$. Subsequently, the beads and lysate solution were incubated at room temperature (~20°C) for 24 h with interval rotational mixing. Afterwards, the cell lysate solution was removed, and the beads were washed three times with a washing buffer containing 200 mM Tris-HCl and 600 mM NaCl at pH 8.5 to remove weakly bound proteins. To block the unreacted epoxy sites, the beads were incubated for 24 h in the storage buffer containing 200 mM Tris-HCl and 300 mM NaCl at pH 8.5.

The feed solution for testing the activity of the immobilized enzymes consisted of 200 mM Tris-HCl (pH 8.5); 75 mM MgCl₂; 25 mM Uri; 25 mM GlcNAc; 5 mM ATP, and 10 mM PolyP_n. 250 µL of feed solution was added to beads and incubated at 37°C and 600 rpm for 24 h.

For reactions in multiple cycles, reaction solution was removed, and the beads were washed twice with water (each time with 1 mL) to avoid any carry-over from previous cycles.

3.6 Cell culture methods for antibody production

CHO-DP12 cells capable of production of recombinant human anti-interleukin 8 antibody (a kind gift of Prof. Dr. Thomas Noll from Bielefeld University) were used for cell culture experiments. The cultures were seeded with 5.0×10^5 cells/mL and cultivated in 250 mL shake flasks (Corning®, USA) with 100 mL of working volume in TCX6D media (Xell AG, Germany) supplemented with 8 mM glutamine (Merck, Germany) at 37°C, 5% CO₂ atmosphere, and 130 rpm in a Multitron Pro incubator (Infors HT, Switzerland). For production of mannosylated IgGs, 25 µg/mL of kifunensine (Carbosynth Ltd, United Kingdom) was added to the cell culture upon seeding. The supernatant was harvested after 187 h (~8 days) at cell viability of 76.8%, and 71.3% for untreated and kifunensine treated cultures, respectively, through centrifugation at 1500 rpm. Both cultures were grown to a total cell density of 2.2×10^7 cells/mL with an antibody titer of approximately 480 mg/L. A Vi-CELL XR cell counter (Beckman Coulter, USA) was used to determine the cell count and viability. For quantification of IgG in cell culture supernatant, a MAbPac™ Protein A column, connected to an ICS-5000+ ion chromatography system (Thermo Fisher Scientific, USA) was used. The measurement was performed according to the manufacturer's protocol by using IgG from human serum (Merck, Germany) as standard. IgG purification from cell culture was performed with an ÄKTA start instrument (Cytiva, Sweden) equipped with a HiScreen MabSelect SuRe LX (Cytiva, Sweden). The purification was carried out according to the manufacturer's protocol.

3.7 Analytics

3.7.1 Protein quantification

Protein quantification was performed with a Pierce™ BCA Protein Assay Kit (Thermo Fisher Scientific, USA) using bovine serum albumin as standard. The assay was performed based on the manufacturer's protocol.

3.7.2 SDS-PAGE

Sodium dodecyl sulphate–polyacrylamide gel electrophoresis (SDS-PAGE) was performed with precast NuPAGE™ 10% or 12% Bis-Tris protein gels (Thermo Fisher Scientific, USA). Samples were diluted 3:1 with NuPAGE™ LDS Sample Buffer (4x) (Thermo Fisher Scientific, USA) and heated at 95°C for 5 min. PageRuler™ Prestained Protein Ladder, 10 to 180 kDa (Thermo Fisher Scientific, USA) was used as the molecular weight marker, unless stated otherwise.

3.7.3 HPAEC-UV/PAD

High-performance anion exchange chromatography equipped with an ultraviolet (UV) and a pulsed amperometry detector (PAD) was used as the main analytical instrument in this work. All the measurements were performed by an ICS-5000+ ion chromatography system (Thermo Fisher Scientific, USA). The conditions used for separation and quantification of several compounds are described below.

3.7.3.1 Nucleosides, nucleotides, and sugar nucleotides

A gradient with sodium hydroxide (NaOH) (Fluka, Germany) and sodium acetate (NaOAc) (Thermo Fisher Scientific, USA) as eluents was developed using serially connected PA200 (Thermo Fisher Scientific, USA) guard (3x50 mm) and analytical columns (3x250 mm). A sample volume of 25 µL was injected for each measurement. The separation was performed at a column temperature of 30°C and a flow rate of 0.5 mL/min. The UV detector (wavelength 260 nm) was used for detection of nucleosides, nucleotide, and sugar nucleotides. Four different eluents were prepared as described in Ref. [214], as follows: E1: Milli-Q® ultra-pure water; E2: 1 M NaOAc, 1 mM NaOH; E3: 100 mM NaOH; E4: 200 mM NaOAc, 100 mM NaOH. The presented chromatography gradients are an optimized version of a previously developed gradient which was developed during a master thesis project related to this dissertation. All the chromatography gradients were statistically validated as described by Ritter *et al.* [215] and the results are presented in the Appendix C: Validation of HPAEC-UV-PAD measurements.

3.7.3.1.1 Resolving compounds from UDP-GlcNAc cascade

For separation of UV-active compounds from the UDP-GlcNAc cascade the following gradient was developed: $t_{0 \text{ min}}$, 50.6% E2, 0.6% E3; $t_{10 \text{ min}}$, 75.3% E2, 0.3% E3; $t_{10.1 \text{ min}}$, 100% E2; $t_{12 \text{ min}}$, 100% E2; $t_{12.1 \text{ min}}$, 50.6% E2, 0.6% E3; $t_{16 \text{ min}}$, 50.6% E2, 0.6% E3. The UV chromatogram of the UDP-GlcNAc cascade component is shown in Figure 3.2.

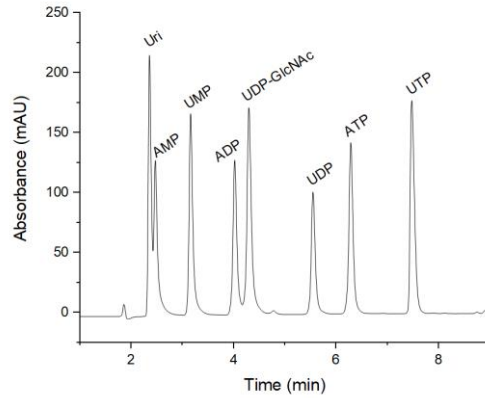


Figure 3.2. UV chromatogram of UDP-GlcNAc cascade components. Abbreviations: Uri, uridine; AMP, adenosine monophosphate; UMP, uridine monophosphate; ADP, adenosine diphosphate; UDP-GlcNAc, uridine diphosphate N-acetylglucosamine; UDP, uridine diphosphate; ATP, adenosine triphosphate; UTP, uridine triphosphate; mAU, milli absorbance unit.

3.7.3.1.2 Resolving compounds from UDP-Gal and UDP-Glc cascades

In order to separate the UV-active compounds from the UDP-Gal and UDP-Glc cascades the following gradient was developed: t_0 min, 40.6% E2, 0.6% E3; t_8 min, 80% E2, 0.6% E3; $t_{8.1}$ min, 100% E2; t_{10} min, 100% E2; $t_{10.1}$ min, 40.6% E2, 0.6% E3; t_{12} min, 40.6% E2, 0.6% E3. The UV chromatogram of UDP-Gal cascade components is shown in Figure 3.3.

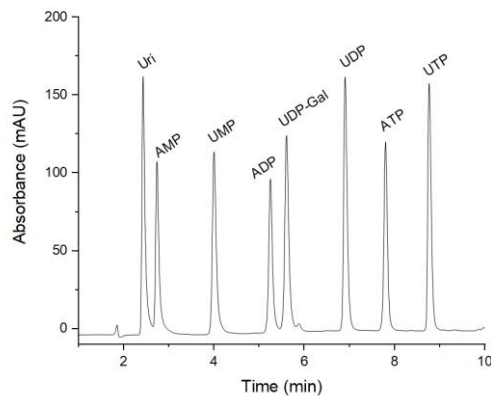


Figure 3.3. UV chromatogram of UDP-Gal cascade components. Abbreviations: Uri, uridine; AMP, adenosine monophosphate; UMP, uridine monophosphate; ADP, adenosine diphosphate; UDP-Gal, uridine diphosphate galactose; UDP, uridine diphosphate; ATP, adenosine triphosphate; UTP, uridine triphosphate; mAU, milli absorbance unit.

The chromatogram of UV-active compounds of UDP-Glc cascade is shown in Figure 3.4.

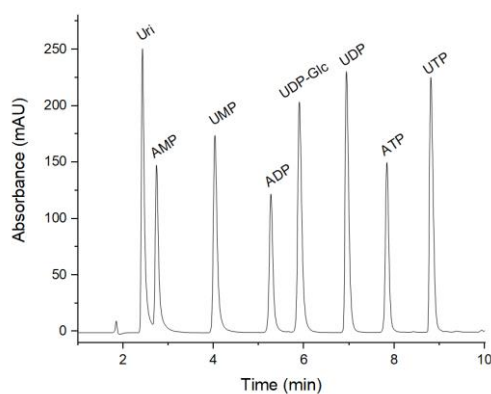


Figure 3.4. UV chromatogram of UDP-Glc cascade components. Abbreviations: Uri, uridine; AMP, adenosine monophosphate; UMP, uridine monophosphate; ADP, adenosine diphosphate; UDP-Glc, uridine diphosphate glucose; UDP, uridine diphosphate; ATP, adenosine triphosphate; UTP, uridine triphosphate; mAU, milli absorbance unit.

3.7.3.1.3 Resolving compounds from GDP-Man and GDP-Fuc cascade

For separation of UV-active compounds from the GDP-Man and GDP-Fuc cascades the following gradient was developed: t_0 min, 50.6% E2, 0.6% E3; t_{10} min, 75.3% E2, 0.3% E3; $t_{10.1}$ min, 100% E2; t_{12} min, 100% E2; $t_{12.1}$ min, 50.6% E2, 0.6% E3; t_{14} min, 50.6% E2, 0.6% E3. The UV chromatogram of GDP-Man and GDP-Fuc cascade components is shown in Figure 3.5.

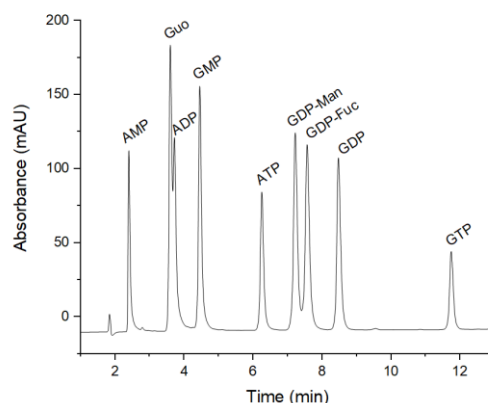


Figure 3.5. UV chromatogram GDP-Man and GDP-Fuc cascade components. Abbreviations: AMP, adenosine monophosphate; Guo, guanosine; ADP, adenosine diphosphate; GMP, guanosine monophosphate; ATP, adenosine triphosphate; GDP-Man, guanosine diphosphate mannose; GDP-Fuc, guanosine diphosphate fucose; GDP, guanosine diphosphate; GTP, guanosine triphosphate; mAU, milli absorbance unit.

3.7.3.1.4 Resolving compounds from CMP-Neu5Ac cascades

For analysis of UV-active compounds from the CMP-Neu5Ac cascade, the following gradient was developed: t_0 min, 20% E2, 1% E3; t_{20} min, 72% E2, 1% E3; $t_{20.1}$ min, 100% E2; t_{22} min, 100% E2; $t_{22.1}$ min, 20% E2, 1% E3; t_{25} min, 20% E2, 1% E3. The UV chromatogram of CMP-Neu5Ac cascade component is shown in Figure 3.6.

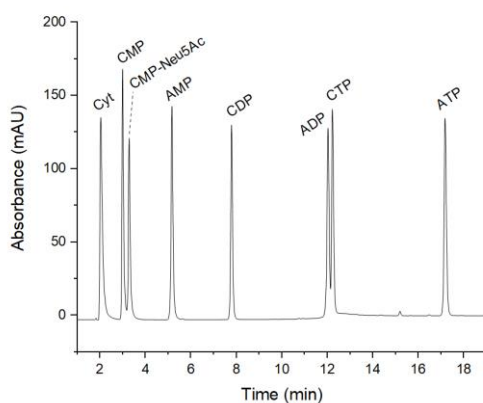


Figure 3.6. UV chromatogram of CMP-Nue5Ac cascade components. Abbreviations: Cyt, cytidine; CMP, cytidine monophosphate; CMP-Neu5Ac, cytidine monophosphate N-acetylneuraminic acid; AMP, adenosine monophosphate; CDP, cytidine diphosphate; ADP, adenosine diphosphate; CTP, cytidine triphosphate; ATP, adenosine triphosphate; mAU, milli absorbance unit.

3.7.3.1.5 Resolving compounds from UDP-GalNAc cascade

For quantification of UDP-GalNAc cascade intermediate compounds, separation was performed on an ICS-5000 chromatography system using IonPac AS11 (2x250 mm; Thermo Fisher Scientific, USA) as an analytical column. Potassium hydroxide (KOH) was used as the main eluent (flow rate: 0.35 mL/min) and was automatically generated from Milli-Q® ultra-pure water using an in-line eluent generator. The separation was carried out based on the following concentration of KOH: $t_{0 \text{ min}}$, 20 mM; $t_{1 \text{ min}}$, 20 mM; $t_{9 \text{ min}}$, 75 mM; $t_{9.1 \text{ min}}$, 100 mM; $t_{14 \text{ min}}$, 100 mM; $t_{14.1 \text{ min}}$, 10 mM; $t_{18 \text{ min}}$, 10 mM.

3.7.3.2 HMOs analysis with HPAEC-PAD

The gradients used in this study for separation and quantification of HMOs are the same as reported in Thurl *et al.* [216]. Moreover, both single and mixture of standard HMOs (commercial) were injected to identify each peak. For separation of neutral HMOs, the following gradient was used: $t_{0 \text{ min}}$, 30% E3; $t_{20 \text{ min}}$, 30% E3; $t_{34 \text{ min}}$, 100% E3; $t_{48 \text{ min}}$, 86% E3, 14% E4; $t_{55 \text{ min}}$, 100% E4; $t_{60 \text{ min}}$, 100% E4; $t_{60.1 \text{ min}}$, 30% E3; $t_{65 \text{ min}}$, 30% E3.

For separation of acidic HMOs, the gradient was as follows: $t_{0 \text{ min}}$, 90% E3, 10% E4; $t_{20 \text{ min}}$, 90% E3, 10% E4; $t_{30 \text{ min}}$, 60% E3, 40% E4; $t_{55 \text{ min}}$, 100% E4; $t_{60 \text{ min}}$, 100% E4; $t_{60.1 \text{ min}}$, 90% E3, 10% E4; $t_{65 \text{ min}}$, 90% E3, 10% E4.

3.7.4 MALDI-TOF-MS

Sample desalting: Desalting of samples containing oligosaccharides (prior to mass spectrometry analysis) was carried out through cotton hydrophilic interaction chromatography (cotton-HILIC) as described in Ref. [217,218]. In short, 15 μL of reaction products were mixed with 85 μL of 100% acetonitrile (ACN). Approximately one fifth of a 200 μL pipette tip was filled with cotton. Prior to equilibration with 85% ACN, the cotton was washed with water to remove any contamination. Samples were loaded by pipetting up and down (~20 times). After loading, the cotton was washed five times with 85% ACN containing 1% trifluoroacetic acid (TFA) and five times with 85% ACN. Afterwards, oligosaccharides were eluted in three steps, each one including 50 μL of water.

Mass spectrometry: The UltraFlex extreme matrix-assisted laser desorption/ionization time of flight mass spectrometry (MALDI-TOF-MS) (Bruker Daltonics, Germany) was used for sample analysis. For sugar nucleotides analysis, 9-aminoacridine (9-AA) (10 mg/mL in acetone) was used as the matrix. For glycan and HMOs analysis, 2, 5-dihydroxybenzoic acid and 2-hydroxy-5-methoxybenzoic acid (S-DHB) (10 mg/mL in TA30 solvent including 2 mM NaCl) were used the matrix. TA30 solvent is composed of 70% ACN and 0.1% TFA. Briefly, 1 μ L of matrix was spotted on a MTP AnchorChip 384 BC MALDI target plate (Bruker Daltonics, Germany) and left to air dry. Afterwards, 1 μ L of sample was added to the spots (containing dried matrix). After drying, 0.2 μ L of ethanol was added to the spots to allow rapid and homogenous recrystallization [217,218]. The oligosaccharides and sugar nucleotides were measured in positive- and negative-ion reflector mode, respectively.

3.7.5 xCGE-LIF

Multiplexed capillary gel electrophoresis with laser-induced fluorescence detection (xCGE-LIF) was used for glycan analysis. The measurements were carried out as described in Ref. [219]. The glycosylation profile analysis was performed with the kind help of Valerian Grote from the Bioprocess Engineering group at the Max Planck Institute for Dynamics of Complex Technical Systems. The method is briefly described below.

Glycan release: 1 to 5 μ g of protein (~1–5 μ L) were incubated with 2 μ L of 2% SDS (in phosphate-buffered saline) for 10 min at 60°C. Samples were brought to room temperature, followed by addition of 2 μ L of 8% octylphenoxy poly(ethyleneoxy)ethanol (IGEPAL[®] CA-630) in phosphate-buffered saline. Afterwards, 1 unit of peptide-N-glycosidase F (Merck, Germany) — the enzyme used for deglycosylation of proteins — was added to the samples, followed by incubation for 30 min at 37°C. Finally, the samples were vacuumed-dried.

APTS glycan labeling: For 8-aminopyrene-1,3,6-trisulfonic acid trisodium salt (APTS) (Merck, Germany) labeling, 2 μ L APTS (40 mM, in 3.6 M citric acid), 2 μ L 2-picoline borane complex solution (0.2 M in DMSO), and 2 μ L water were added to dried samples, followed by at least 3 h incubation (in dark) at 37°C. To stop the labeling reaction, 100 μ L of 80:20% ACN-water solution was added to the samples.

HILIC-SPE: Hydrophilic interaction chromatography-solid phase extraction (HILIC-SPE) — using polyacrylamide-based stationary phase Bio-Gel P-10 (Bio-Rad, USA) — was performed to separate APTS-labeled glycans from other impurities such as excess ATPS. HILIC-SPE was carried out with the aid of a vacuum manifold and a 96-well AcroPrep[™] Filter Plate (PALL, USA). The steps were as follows: 1) washing the beads with water, 2) equilibration of beads with 80:20% ACN-water, 3) sample loading (5 min incubation), 4) washing with 80:20% ACN-water containing 100 mM triethylamine (1 min incubation), 5) washing with 80:20% ACN-water (1 min incubation), and 6) elution of APTS-labeled glycan with water (5 min incubation). Samples were dried and stored at -20°C until measurements.

CGE-LIF analysis: Dried samples were resuspended in 10–20 μ L Milli-Q[®] water. Afterwards, 2 μ L of sample were mixed with 1 μ L LIZ base pair standard (GeneScan[™] 500 LIZ[™], Thermo Fischer Scientific, USA), 1 μ L 2nd NormMiX (glyXera GmbH, Germany), and 7 μ L of Hi-Di Formamide (Thermo Fischer Scientific, USA). 10 μ L of sample were transferred to a 384 well plate and analyzed by a 3130xl

Genetic Analyzer (Thermo Fischer Scientific, USA) equipped with a 50 cm capillary array. The POP-7™ polymer (Thermo Fischer Scientific, USA) was used as the separation matrix. The software package of glyXtool^{CE} 6.1.0 (glyXera GmbH, Germany) was used for electropherogram analysis such as normalization of migration time units (MTU ") and calculation of the normalized intensity (based on the total peak height).

3.7.6 ADCC assay

To evaluate the antibody-dependent cellular cytotoxicity (ADCC) activity of antibodies, an affinity-based chromatography was used. ADCC assay was performed by Dr.-Ing. Pavel Marichal-Gallardo from the Bioprocess Engineering Group at the Max Planck Institute for Dynamics of Complex Technical Systems. An ÄKTA Pure 25 liquid chromatography system, controlled by UNICORN v6.3 software (Cytiva, Sweden) was used at room temperature to perform the assay. A TSKgel FcR-III A-NPR column (Tosoh, Japan) was used according to the manufacturer's instruction.

4 Results and Discussion

The following chapter consists of four parts. In section 4.1, the establishment of novel cascades to produce sugar nucleotides is described. In section 4.2, two different strategies are presented for the synthesis of wide variety of HMOs — by using established sugar nucleotide synthesis cascades. Section 4.3 focuses on the development of an artificial Golgi for glycoengineering of therapeutic proteins. In section 4.4, process engineering strategies for large-scale production of sugar nucleotides are presented.

4.1 Multi-enzyme cascades for synthesis of sugar nucleotides

This part is subdivided into three different groups of activated sugars: UDP-sugars, GDP-sugars, and a CMP-sugar. The general aspects of each group are presented at the beginning of their section.

4.1.1 Synthesis of UDP-sugars

The general pathway for UDP-sugar synthesis is illustrated in Figure 4.1. Uri was used as the precursor for nucleotide-base of UDP-activated sugars. The conversion of Uri to UTP is catalyzed by two ATP-dependent kinases, UDK and UMPK, and one PolyP_n-dependent kinase, PPK3. UDK catalyzes the reaction of Uri to UMP and UMPK catalyzes the reaction of UMP to UDP, both by using ATP as the phosphate source. PPK3 catalyzes the conversion of UDP to UTP by using PolyP_n as the phosphate source. In each cascade, an additional kinase was used for phosphorylation of monosaccharides. Therefore, for the synthesis of each UDP-sugar molecule, three molecules of ATP are required. To avoid stoichiometric usage of costly ATP, a regeneration cycle (from ADP) was established by exploiting the affinity of PPK3 for diphosphate nucleotides. Consequently, only catalytic amounts of ATP were required to enable high yield synthesis of UDP-sugars. PPA was added to all the cascades to favor the thermodynamic equilibrium of uridylyltransferase reaction toward the product side.

The optimized reaction condition such as pH, co-factor concentration, PolyP_n, and ATP levels were found through the systematic screening of different conditions. The details of the optimization strategy are described in Ref. [220].

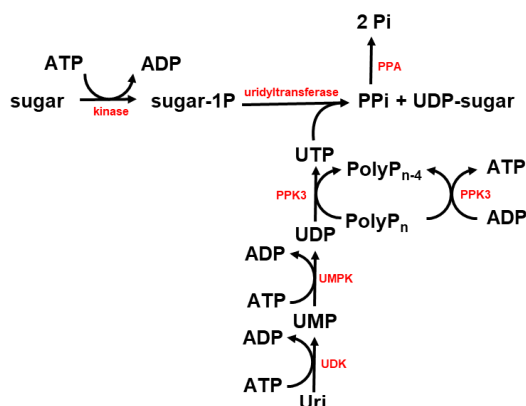


Figure 4.1. General cascade scheme for synthesis of UDP-sugars. Abbreviations: Uri, uridine; UMP, uridine monophosphate; UDP, uridine diphosphate; UTP, uridine triphosphate; PPi, diphosphate; Pi, phosphate; ADP, adenosine diphosphate; ATP, adenosine triphosphate; UDK, uridine/cytidine kinase; UMPK, UMP/CMP kinase; PPK3, PolyP_n kinase; PPA, inorganic diphosphatase.

4.1.1.1 Synthesis of UDP-GlcNAc and UDP-GalNAc

The cascade for synthesis of UDP-GlcNAc (and UDP-GalNAc) is shown in Figure 4.2. The cascade presented here is an extended version of a cascade previously developed in our research group and

published by the author [221]. Because of the bulk availability of GlcNAc [222], it was directly used as the sugar base for synthesis of UDP-GlcNAc.

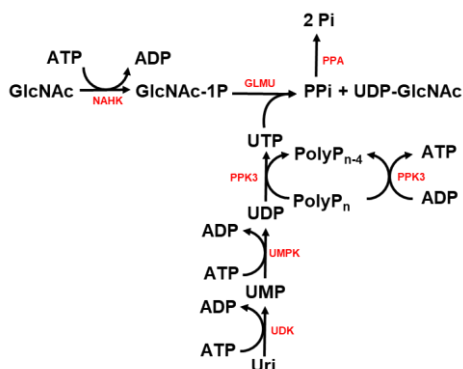


Figure 4.2. Multi-enzyme cascade of six enzymes and seven reactions for synthesis of uridine diphosphate N-acetylglucosamine (UDP-GlcNAc) from uridine (Uri), N-acetylglucosamine (GlcNAc), polyphosphate (PolyP_n), and catalytic amounts of adenosine triphosphate (ATP). Thanks to the affinity of N-acetylhexosamine 1-kinase (NAHK) and GlcNAc 1-phosphate uridylyltransferase (GLMU) for N-acetylgalactosamine (GalNAc) and N-acetylgalactosamine 1-phosphate (GalNAc-1P), respectively, UDP-GalNAc can also be synthesized with the same cascade. Abbreviations: UMP, uridine monophosphate; UDP, uridine diphosphate; UTP, uridine triphosphate; GlcNAc-1P, N-acetylglucosamine 1-phosphate; PPi, diphosphate; Pi, phosphate; ADP, adenosine diphosphate; UDK, uridine/cytidine kinase; UMPK, UMP/CMP kinase; PPK3, PolyP_n kinase; PPA, inorganic diphosphatase.

GlcNAc is converted to N-acetylglucosamine 1-phosphate (GlcNAc-1P) through the reaction catalyzed by NAHK and using ATP as a phosphate source. Simultaneously, conversion of Uri to UTP is carried out through the series of reactions described above. Afterwards, UDP-GlcNAc is produced through the reaction catalyzed by GLMU from UTP and GlcNAc-1P. It should be noted that GALU can also be used for synthesis of UDP-GlcNAc [221]. For the establishment of the cascade, purified enzymes were used.

The optimized reaction conditions — i.e., enzyme concentration, pH, co-factor, PolyP_n, and substrate concentrations — were found through screening experiments. The time course of reaction compounds is shown in Figure 4.3.

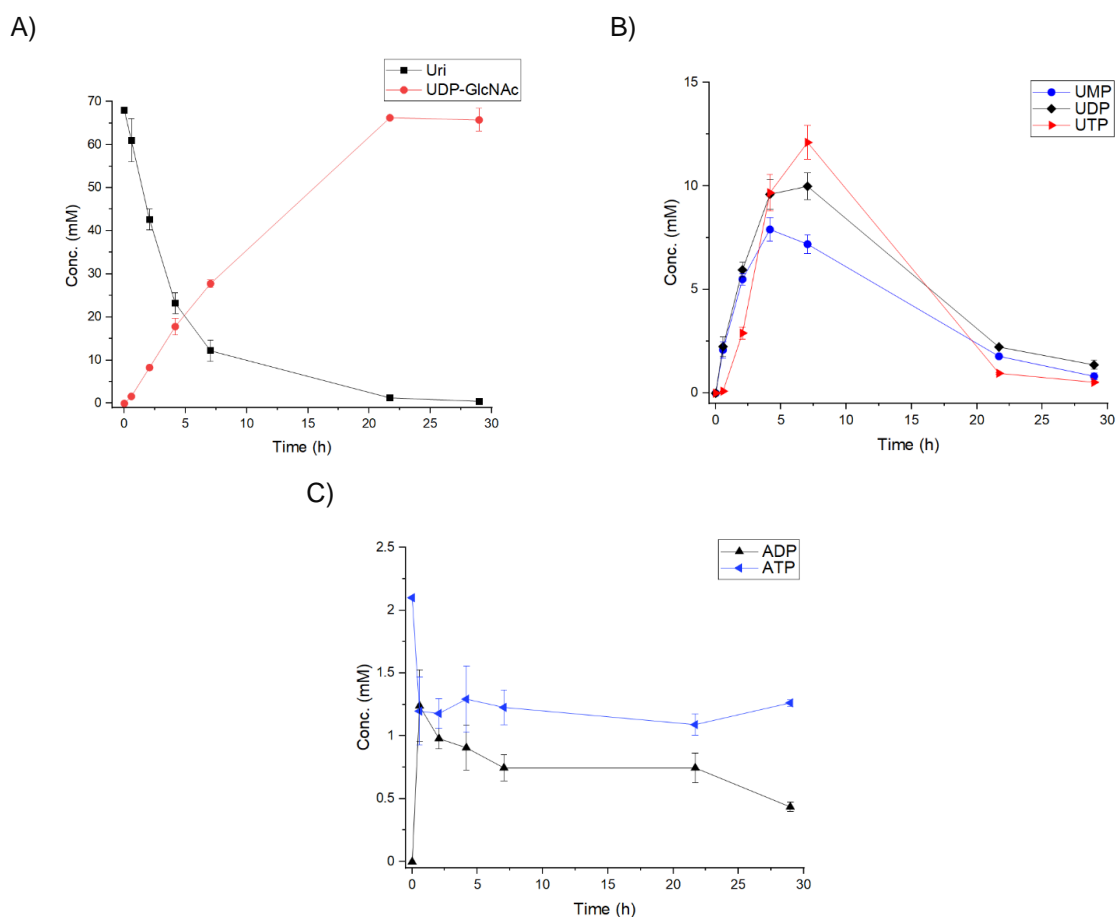


Figure 4.3. Reaction time course of substrates, intermediates, and products in the cascade. The reaction conditions were as follows: Tris-HCl (pH, 8.5) 150 mM; MgCl₂ 75 mM; Uri 68 mM; GlcNAc 68 mM; ATP 2.1 mM; PolyP_n 21 mM; UDK 0.07 µg/µL; UMPK/PPK3 0.11 µg/µL; NAHK 0.18 µg/µL; GLMU 0.2 µg/µL, and PPA 0.05 µg/µL. (A) Shows the consumption of Uri and sequential production of UDP-GlcNAc. (B) Represents the stepwise production follows by consumption of UMP, UDP, and UTP. (C) Shows the time course of ATP and ADP during the batch. The experiments were carried out in triplicates. Error bars represent the standard deviation.

Complete consumption of Uri followed by production of UDP-GlcNAc demonstrates successful establishment of the cascade. Considering the starting concentration of Uri and GlcNAc i.e., 68 mM, a total of 208 mM ATP would be required to achieve the a very high synthesis yield. However, thanks to the ATP regeneration cycle, ATP was applied only up to 2.1 mM, which is ~100-fold less than the stoichiometric amount. The cascade was successfully established to a final UDP-GlcNAc concentration of 66.2 mM (40.2 g/L) and a synthesis yield of 97.4% with respect to Uri and GlcNAc in a reaction time of 22 h. The biocatalyst load and productivity of the cascade were 0.01 g_{enzyme}/g_{product}, and 1.8 g/L/h, respectively. The reaction chromatogram of the cascade products is shown in Figure 4.4.

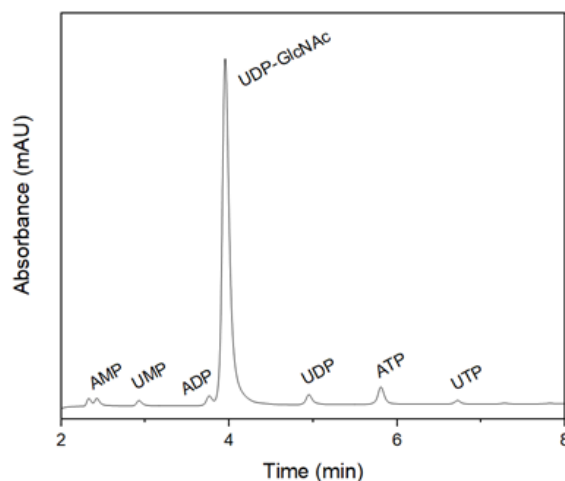


Figure 4.4. The chromatogram of the UDP-GlcNAc cascade after 22 h. The high synthesis yield and catalytic usage of ATP resulted in UDP-GlcNAc as the major product of the cascade.

The cascade shown in Figure 4.2 has the potential for synthesis of UDP-GalNAc, thanks to the affinity of NAHK and GLMU for GalNAc, and GalNAc-1P, respectively. As can be seen in Figure 4.5, UDP-GalNAc was produced with a similar yield.

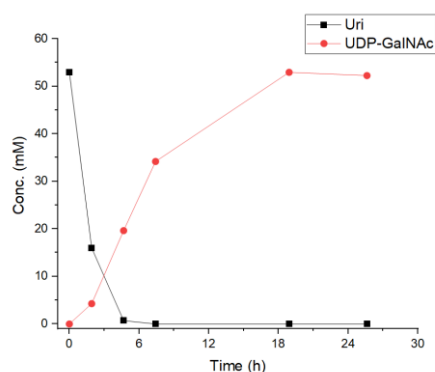


Figure 4.5. Time course of Uri consumption and UDP-GalNAc production with the proposed cascade. The reaction conditions were as follows: Tris-HCl (pH, 8.5) 150 mM; $MgCl_2$ 75 mM; Uri 53 mM; GalNAc 53 mM; ATP 2.6 mM; PolyP_n 20 mM; UDK 0.07 $\mu\text{g}/\mu\text{L}$; UMPK/PPK3 0.11 $\mu\text{g}/\mu\text{L}$; NAHK 0.15 $\mu\text{g}/\mu\text{L}$; GLMU 0.27 $\mu\text{g}/\mu\text{L}$, and PPA 0.08 $\mu\text{g}/\mu\text{L}$ in a total volume of 200 μL .

4.1.1.2 Synthesis of UDP-Gal

The cascade for synthesis of UDP-Gal is shown in Figure 4.6. The results in this chapter were filed as a patent application under PCT/EP2020/077396 [223], and published in Ref. [220]. Gal was used as the sugar source, thanks to its bulk availability and low cost. Gal-1P is produced from the reaction of Gal and ATP catalysed by GALK. Afterwards, through the steps as described above, Uri is converted to UTP. By exploiting the promiscuity of GalU, UTP, and Gal-1P are converted to UDP-Gal [200]. The optimization of the UDP-Gal synthesis cascade was carried out in context of the bachelor thesis of Pia Grimpe, whose work was performed and supervised in association with this dissertation [224].

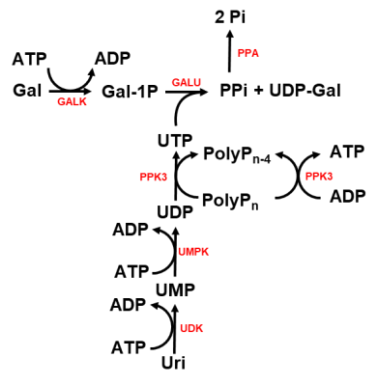


Figure 4.6. Multi-enzyme cascade of six enzymes and seven reactions for synthesis of uridine diphosphate galactose (UDP-Gal) from uridine (Uri), galactose (Gal), polyphosphate (PolyP_n), and catalytic amounts of adenosine triphosphate (ATP). Abbreviations: UMP, uridine monophosphate; UDP, uridine diphosphate; UTP, uridine triphosphate; Gal-1P, galactose 1-phosphate; PPI, diphosphate; Pi, phosphate; ADP, adenosine diphosphate; UDK, uridine/cytidine kinase; UMPK, UMP/CMP kinase; PPK3, PolyP_n kinase; GALU, glucose 1-phosphate uridylyltransferase; GALK, galactokinase; PPA, inorganic diphosphatase.

The time course of reaction compounds is shown in Figure 4.7. The Figure 4.7A is reproduced from Ref. [224].

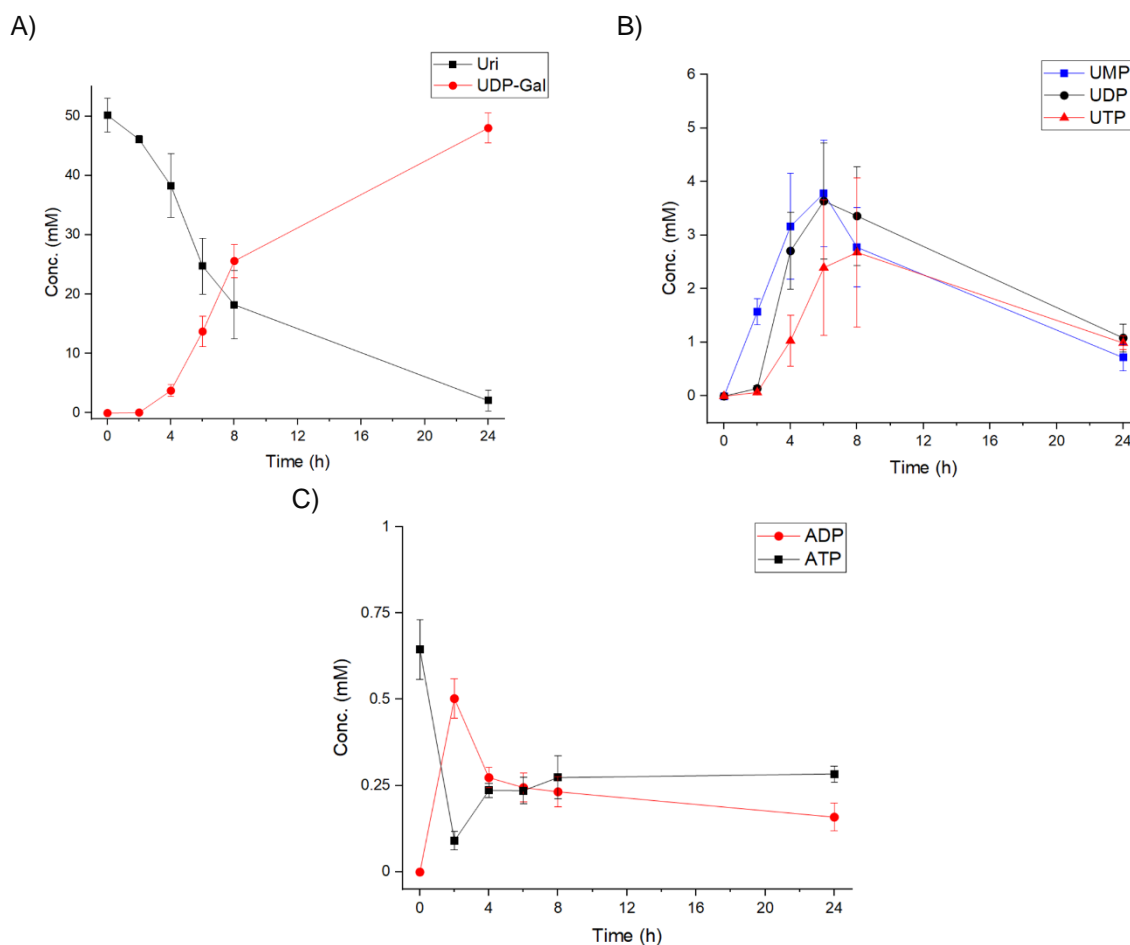


Figure 4.7. Time course of substrates, intermediates, and products for synthesis of UDP-Gal under optimized condition: Tris-HCl (pH, 8.5) 150 mM; MgCl₂ 75 mM; Uri 50 mM; Gal 52 mM; ATP 0.6 mM; PolyP_n 20 mM; UDK 0.07 µg/µL; UMPK/PPK3 0.11 µg/µL; GALK 0.16 µg/µL; GALU 0.12 µg/µL, and PPA 0.06 µg/µL. A) Concentration of Uri and UDP-Gal. B) Concentration of UMP, UDP, and UTP. C) Concentration of ADP and ATP. Reactions were carried out in triplicate and error bars represent the standard deviation.

The stoichiometric amount of ATP required in the cascade were 150 mM, however, it was applied to a catalytic amount of 0.6 mM. This means that ATP was used ~250-fold less than the stoichiometric amount as it was constantly regenerated by PolyP_n. UDP-Gal was successfully produced to a final concentration of 48 mM (27.2 g/L) and a synthesis yield of 96% with respect to Uri in a reaction time of 24 h. The biocatalyst load of the cascade was 0.02 g_{enzyme}/g_{product}.

4.1.1.3 Synthesis of UDP-Glc and UDP-Man

The cascade developed for production of UDP-Glc is shown in Figure 4.8. GLK together with ATP catalyzes the phosphorylation of Glc on the sixth carbon to yield glucose 6-phosphate (Glc-6P). Afterwards, by taking advantage of the promiscuity of MANB, Glc-6P is converted to glucose 1-phosphate (Glc-1P). In the next step, UTP (started from Uri) and Glc-1P are converted to UDP-Glc through the reaction catalyzed by GALU. Like other above-mentioned cascades, diphosphatase is also

part of the cascade. The optimized conditions found in the UDP-Gal synthesis cascade were directly used for synthesis of UDP-Glc. The time course of reaction intermediates is shown in Figure 4.9.

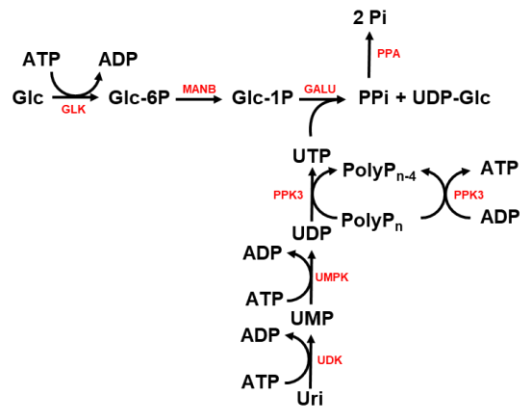


Figure 4.8. Multi-enzyme cascade of seven enzymes and eight reactions for synthesis of uridine diphosphate glucose (UDP-Glc) from uridine (Uri), glucose (Glc), polyphosphate (PolyP_n), and catalytic amounts of adenosine triphosphate (ATP). Abbreviations: UMP, uridine monophosphate; UDP, uridine diphosphate; UTP, uridine triphosphate; Glc-6P, glucose 6-phosphate; Glc-1P, glucose 1-phosphate; PPi, diphosphate; Pi, phosphate; ADP, adenosine diphosphate; UDK, uridine/cytidine kinase; UMPK, UMP/CMP kinase; PPK3, PolyP_n kinase; GALU, glucose 1-phosphate uridylyltransferase; GLK, glucokinase; MANB, phosphomannomutase; PPA, inorganic diphosphatase.

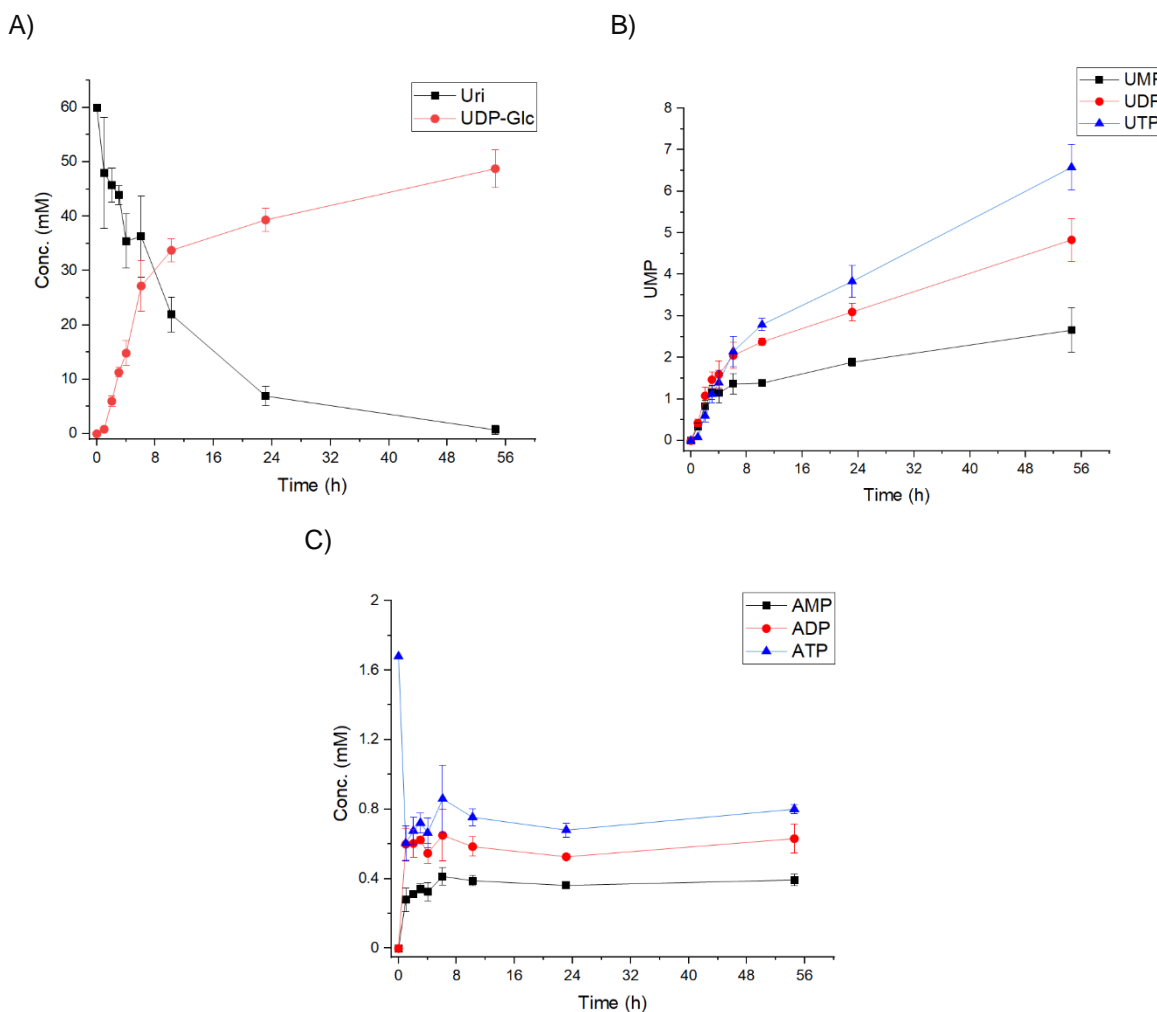


Figure 4.9. Time course of reaction substrates, intermediates, and products of the UDP-Glc cascade. The reaction conditions were as follows: 150 mM Tris-HCl (pH 8.5); 75 mM MgCl₂; 62.5 mM Glc; 60 mM Uri; 1.7 mM ATP; 19 mM PolyP_n; 0.86 μg/μL GLK; 0.06 μg/μL UDK; 0.1 μg/μL UMPK/PPK3; 0.14 μg/μL MANB/C; 0.15 μg/μL GALU, and 0.04 μg/μL PPA. A) Concentration of Uri and UDP-Glc. B) Concentration of UMP, UDP, and UTP. C) Concentration of AMP, ADP, and ATP. Reactions were carried out in triplicate and error bars represent the standard deviation.

Production of UDP-Glc upon starting the reaction demonstrates successful establishment of the cascade. The stoichiometric amount of ATP needed (assuming full conversion) in the cascade was 180 mM, however, it was added to a catalytic amount of 1.7 mM. It means that ATP was used approximately 106x less than the stoichiometric amount and it was constantly regenerated from ADP by PolyP_n. With this cascade, UDP-Glc was produced after 55 h to a final concentration of 48.8 mM (27.6 g/L) and a reaction yield of 81.3% from Uri. The biocatalyst load was 0.04 g_{enzyme}/g_{product}.

The cascade for synthesis of UDP-Glc can also be used for synthesis of the recently discovered UDP-Man [225], thanks to the promiscuity of GLK and GALU, both of which have an affinity for Man, and mannose 1-phosphate (Man-1P), respectively. The affinity of GALU for Man-1P was investigated in the context of the master thesis of Cláudia Bento, whose work was performed and supervised in association with this dissertation [226]. The UV chromatogram of the UDP-Man synthesis reaction after 24 h of incubation at 37°C is shown in Figure 4.10. The formation of UDP-Man was confirmed by mass spectrometry (see Appendix E: MS of sugar nucleotides).

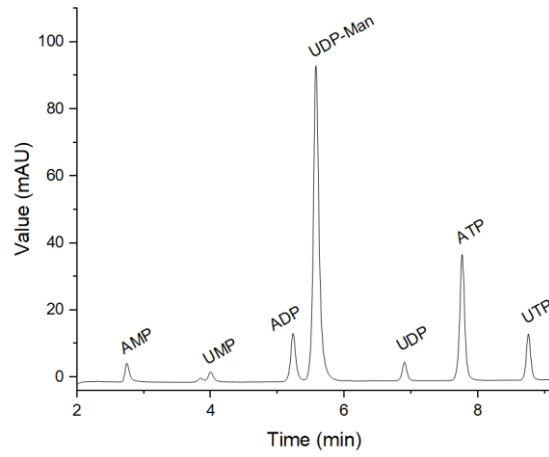


Figure 4.10. UV chromatogram of UDP-Man synthesis cascade reaction. The reaction contained 200 mM Tris-HCl (pH 8.5); 26 mM Man; 25 mM Uri; 7.3 mM ATP; 9.7 mM PolyP_n; 75 mM MgCl₂, and the following enzymes: 0.06 µg/µL UDK; 0.08 µg/µL UMPK/PPK3; 0.76 µg/µL GLK; 0.14 µg/µL MANB/C; 0.12 µg/µL GALU, and 0.04 µg/µL PPA in a final volume of 200 µL.

4.1.2 Synthesis of GDP-sugars

Results from this section have been filed as a patent application under PCT/EP2020/059182 [227], and published in Ref. [228].

For synthesis of GDP-sugars, Guo was used as the GDP-base of this family of sugar nucleotides. Due to the low water solubility of Guo (~1.82 mM), a co-solvent was required to enable Guo utilization for biocatalysis. It was found that DMSO was able to dissolve Guo up to 0.5 M at 25°C and 1 M at 75°C. Therefore, pure DMSO was used to generate Guo stock solutions that were used as a substrate in all GDP-sugar cascades. The conversion pathway of Guo to guanosine triphosphate (GTP) is similar for all the GDP-sugar cascades. GSK catalyses the conversion of Guo to guanosine monophosphate (GMP) using ATP as the phosphate source. The conversion of GMP to GDP is catalyzed by GMPK in an ATP-dependent reaction. Afterwards, PPK3 — a polyphosphate-dependent kinase — catalyses the conversion of GDP to GTP. In both GDP-sugar cascades (i.e., GDP-Man and GDP-Fuc), a sugar kinase was used to enable the synthesis of phosphorylated sugars. Therefore, three molecules of ATP were required for quantitative synthesis yield of one GDP-sugar molecule. Similar to UDP-sugar cascades, the promiscuity of PPK3 allowed the catalytic application of expensive ATP.

4.1.2.1 Synthesis of GDP-Man

The cascade for production of GDP-Man consisted of seven enzymes and eight reactions (see Figure 4.11). Man was used as the sugar base for production of GDP-Man, because of its bulk availability and low cost. The affinity of GLK for Man allows the synthesis of mannose 6-phosphate (Man-6P) from Man and ATP [131]. The enzyme MANB converts Man-6P to Man-1P through an isomerization reaction. Afterwards, in the presence of GTP and Man-1P, MANC catalyses GDP-Man synthesis. In order to shift the equilibrium towards GDP-Man, PPA was added to hydrolyse PPi to Pi.

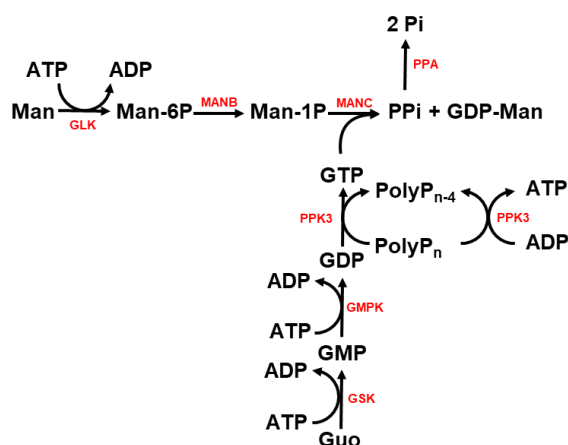


Figure 4.11. Cascade of seven enzymes and eight reactions for synthesis of guanosine diphosphate mannose (GDP-Man) from mannose (Man), guanosine (Guo), polyphosphate (PolyP_n), and catalytic amounts of adenosine triphosphate (ATP). Abbreviations: GMP, guanosine monophosphate; GDP, guanosine diphosphate; GTP, guanosine triphosphate; Man-6P, mannose 6-phosphate; Man-1P, mannose 1-phosphate; PPi, diphosphate; Pi, phosphate; ADP, adenosine diphosphate; GSK, guanosine kinase; GMPK, GMP kinase; PPK3, PolyP_n kinase; MANC, mannose 1-phosphate guanylyltransferase; GLK, glucokinase; MANB, phosphomannomutase; PPA, inorganic diphosphatase.

The time course of GDP-Man cascade components is shown in Figure 4.12. GDP-Man was produced to a final concentration of 6.7 mM equivalent to a yield of 52%, and 67% after 45 h from Guo and Man, respectively. The biocatalyst load was 0.35 g_{enzyme}/g_{product}

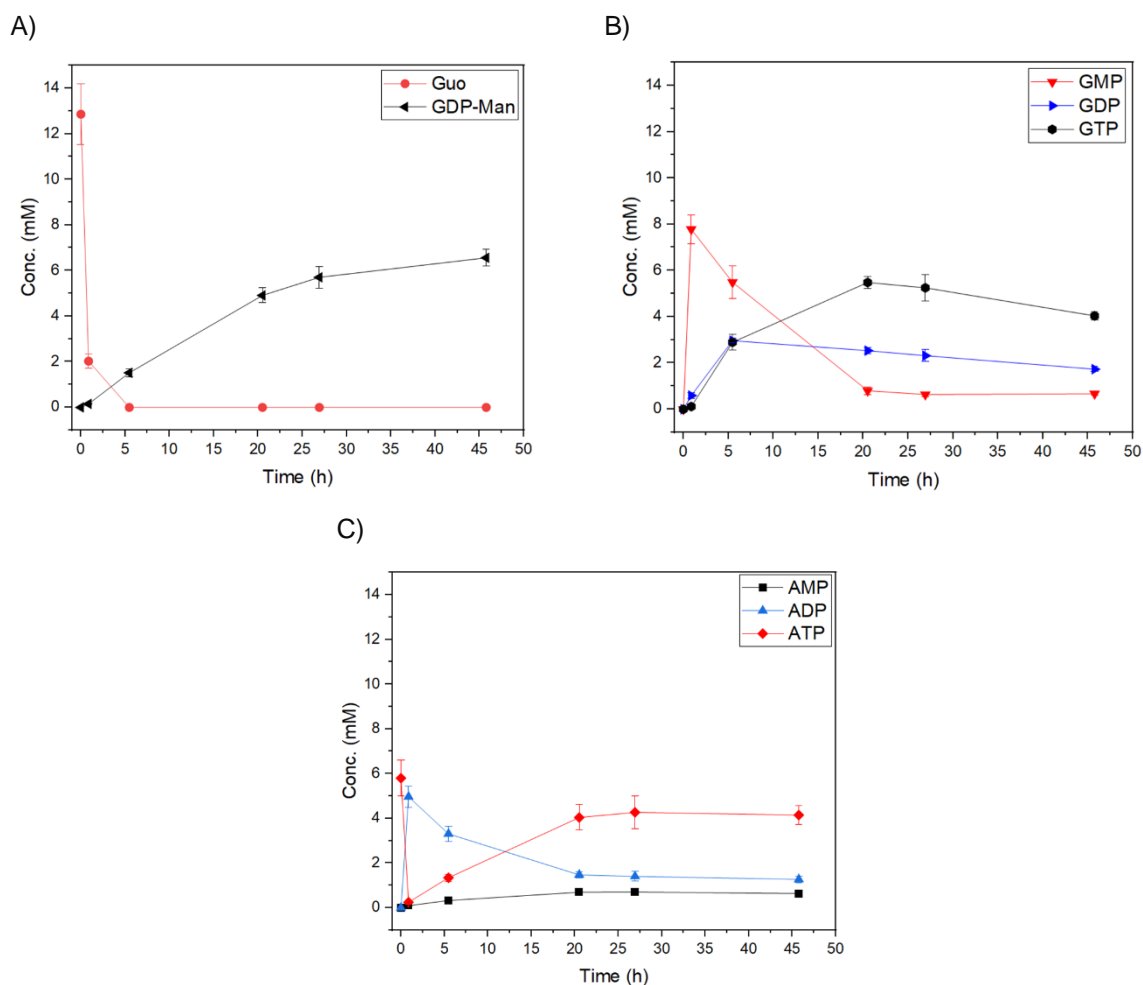


Figure 4.12. Time course of GDP-Man cascade substrates, intermediates, and products. The reaction conditions were as follows: 200 mM Tris-HCl (pH 8.5); 75 mM MgCl₂; 10 mM Man; 12.8 mM Guo; 5.8 mM ATP; 13.5 mM PolyP_n; 0.11 μg/μL GSK; 0.49 μg/μL GMPK; 0.02 μg/μL PPK3; 0.33 μg/μL GLK; 0.17 μg/μL MANB/C, and PPA 0.03 μg/μL with a final volume of 200 μL. The final DMSO content of the reaction matrix was 1% v/v. (A) Shows the consumption of Guo and production of GDP-Man. (B) Shows the reaction time courses of GMP, GDP, and GTP. (C) Shows the reaction time courses of ATP, ADP, and AMP. The production of AMP might be due to chemical conversion of ADP to AMP during the reaction. Experiments were performed in triplicates and error bars represent the standard deviation.

4.1.2.2 Synthesis of GDP-Fuc

The development of two cascades for the synthesis of GDP-Fuc from inexpensive precursors is reported in this section. The first cascade consisted of five enzymes and seven reactions for the synthesis of GDP-Fuc from Fuc as the sugar source. However, due to the relatively high costs of Fuc compared to the other substrates, a second pathway was constructed using Man as the sugar source. A cascade consisting of ten enzymes and eleven reactions was designed and established to synthesize GDP-Fuc from Man, Guo, PolyP_n, L-Glu, and catalytic amounts of NADPH and ATP.

4.1.2.2.1 Synthesis of GDP-Fuc from Guo and Fuc

The cascade for synthesis of GDP-Fuc starting from Fuc consisted of five enzymes and seven reactions (Figure 4.13). The conversion of Fuc to Fuc-1P and GDP-Fuc takes place by using bifunctional FKP [199]. This enzyme catalyses the conversion of Fuc to Fuc-1P with ATP as the phosphate source, as well as conversion of Fuc-1P and GTP to GDP-Fuc.

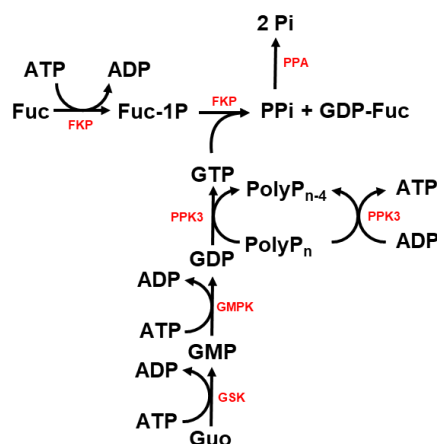


Figure 4.13. Multi-enzyme cascade for synthesis of guanosine diphosphate fucose (GDP-Fuc) starting from fucose (Fuc), guanosine (Guo), polyphosphate (PolyP_n), and catalytic amounts of adenosine triphosphate (ATP). Abbreviations: GMP, guanosine monophosphate; GDP, guanosine diphosphate; GTP, guanosine triphosphate; Fuc-1P, fucose 1-phosphate; PPi, diphosphate; Pi, phosphate; ADP, adenosine diphosphate; GSK, guanosine kinase; GMPK, GMP kinase; PPK3, PolyP_n kinase; FKP, fucokinase/ fucose 1-phosphate guanylyltransferase; PPA, inorganic diphosphatase.

The time course of reaction intermediates is shown in Figure 4.14. A steep decline of Guo and a production of GMP, GDP, GTP, and GDP-Fuc was observed. GDP-Fuc was produced to a final concentration of 7 mM (4.1 g/L) equivalent to a yield of 68% from Guo and Fuc, respectively, after 48 h. The biocatalyst load was 0.34 g_{enzyme}/g_{product}. ATP was used ~12x less than the stoichiometric amount which illustrates the successful ATP regeneration.

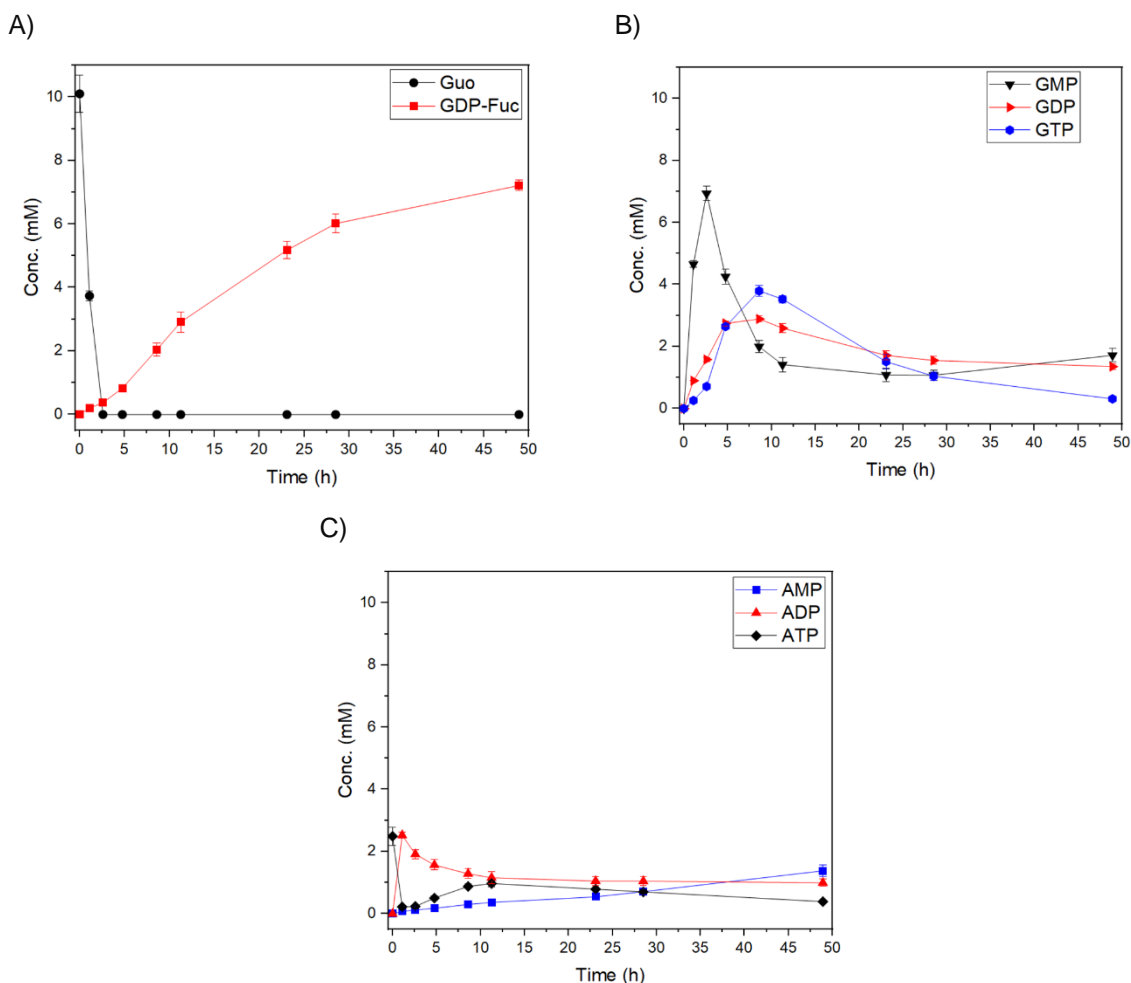


Figure 4.14. Time course of reaction substrates, intermediates, and products for synthesis of GDP-Fuc from Guo, and Fuc. (A) Shows the consumption of Guo and production of GDP-Fuc. (B) Shows the reaction time courses of GMP, GDP, and GTP. (C) Shows the reaction time courses of ATP, ADP, and AMP. The production of AMP might be due to chemical conversion of ADP to ATP during the reaction. The reaction mixture contained 200 mM Tris-HCl (pH 7.5); 10 mM Fuc; 10 mM Guo (in DMSO); 2.5 mM ATP; 7.5 mM PolyP_n; 45 mM MgCl₂, and the following enzymes: GSK 0.22 μg/μL; GMPK 0.78 μg/μL; PPK3 0.05 μg/μL; FKP 0.31 μg/μL, and PPA 0.03 μg/μL in a final volume of 200 μL. Experiments were performed in triplicates and error bars represent the standard deviation.

Despite the successful establishment of the GDP-Fuc synthesis cascade from Guo and Fuc, true large-scale application of such a cascade is severely limited by the lack of availability and high costs of Fuc. In order to overcome this issue, another cascade was developed in which GDP-Fuc is produced from GDP-Man, and thus, Man as the sugar source.

4.1.2.2.2 Synthesis of GDP-Fuc from Guo and Man

At first, a two-enzyme cascade containing GMD and WCAG was established to study the conversion of GDP-Man to GDP-Fuc (Figure 4.15). A low conversion yield of GDP-Fuc synthesis from GDP-Man due to the inhibitory role of GDP-Fuc on GMD has been reported in various studies [229–231]. The role of pH was investigated here with the aim of improving the conversion yield.

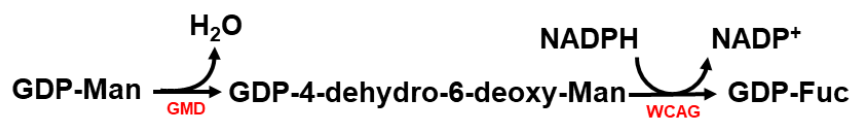


Figure 4.15. A two-enzyme cascade for synthesis of guanosine diphosphate fucose (GDP-Fuc) from guanosine diphosphate mannose (GDP-Man). Abbreviations: GDP-4-dehydro-6-deoxy-Man, guanosine diphosphate-4-keto-6-deoxy -mannose; NADPH, reduced nicotinamide adenine dinucleotide phosphate; NADP⁺, nicotinamide adenine dinucleotide phosphate; H₂O, water; GMD, guanosine diphosphate mannose 4,6-dehydratase; WCAG, guanosine diphosphate L-fucose synthase.

The influence of pH (pH 7.0, 7.5, 8.0, 8.5, and 9.0) on the synthesis yield of GDP-Fuc from GDP-Man is shown in Figure 4.16. A very high conversion was obtained at alkaline pHs. On the other hand, at pH 7.0 and 7.5, only ~20% synthesis yield was obtained, and longer incubation time did not result in higher conversion yields.

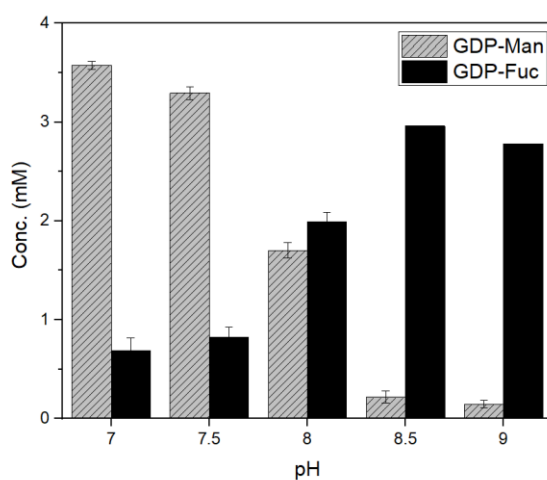


Figure 4.16. Conversion of GDP-Man to GDP-Fuc after 5 h incubation with a two-enzyme cascade. The conditions were as follows: 150 mM Tris-HCl; 10 mM MgCl₂; 3–4 mM GDP-Man; 4 mM NADPH; WCAG 0.45 μg/μL, and GMD 1.03 μg/μL with a final volume of 33 μL. Experiments were carried out in triplicate and error bars represent the standard deviation.

To avoid direct usage of expensive GDP-Man, a novel cascade was constructed (see Figure 4.17) starting from Man, Guo, PolyP_n, L-Glu, and catalytic amounts of NADPH and ATP. L-Glu and PolyP_n were used as the substrate for regeneration of expensive NADPH and ATP, respectively, since they were used in catalytic amounts.

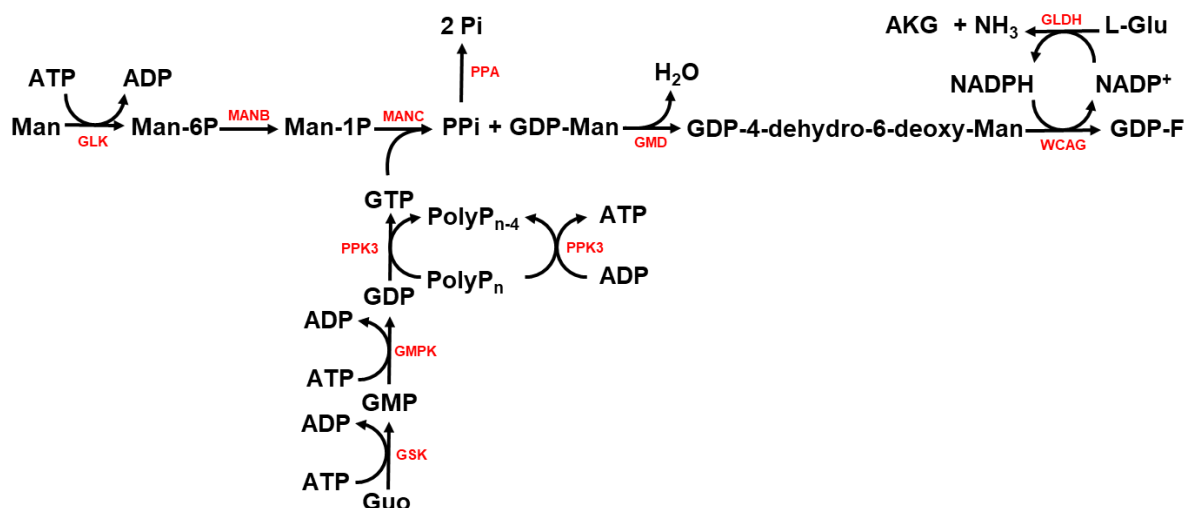


Figure 4.17. Extended cascade for the synthesis of guanosine diphosphate fucose (GDP-Fuc) from mannose (Man), guanosine (Guo), polyphosphate (PolyP_n), L-glutamate (L-Glu), and catalytic amounts of adenosine triphosphate (ATP) and reduced nicotinamide adenine dinucleotide phosphate (NADPH). Abbreviations: GMP, guanosine monophosphate; GDP, guanosine diphosphate; GTP, guanosine triphosphate; ADP, adenosine diphosphate; Man-6P, mannose 6-phosphate; Man-1P, mannose 1-phosphate; GDP-Man, guanosine diphosphate mannose; GDP-4-dehydro-6-deoxy-Man, guanosine diphosphate-4-keto-6-deoxy-mannose; NADP⁺, nicotinamide adenine dinucleotide phosphate; NH₃, ammonia; AKG, α-ketoglutaric acid; H₂O, water; PPI, diphosphate; Pi, phosphate; GSK, guanosine kinase; GMPK, GMP kinase; PPK3, PolyP_n kinase; GLK, glucokinase; MANB, phosphomannomutase; MANC, mannose 1-phosphate guanylyltransferase; PPA, inorganic diphosphatase; GMD, guanosine diphosphate mannose 4,6-dehydratase; WCAG, guanosine diphosphate L-fucose synthase; GLDH, glutamate dehydrogenase.

As high conversion yields were only obtained at alkaline pH for synthesis of GDP-Fuc from GDP-Man, pH 8.5 was selected as the operating pH. The time course of reaction components is shown in Figure 4.18. The reaction starts with immediate conversion of Guo to GMP, and further into GDP and GTP. The higher concentration of GDP-Fuc with regard to GDP-Man during the reaction demonstrates the high catalytic activity of GMD and WCAG enzymes. Moreover, the stepwise production of GDP-Fuc up to 7.6 mM shows the successful function of NADPH and ATP regeneration cycles.

GDP-Fuc was produced to a concentration of 7.6 mM (4.5 g/L) and a reaction yield of 72% after 48 h with a biocatalyst load of 0.97 g_{enzyme}/g_{product}. ATP and NADPH were used 5.7-fold and 10.5-fold less than the stoichiometric amounts, respectively.

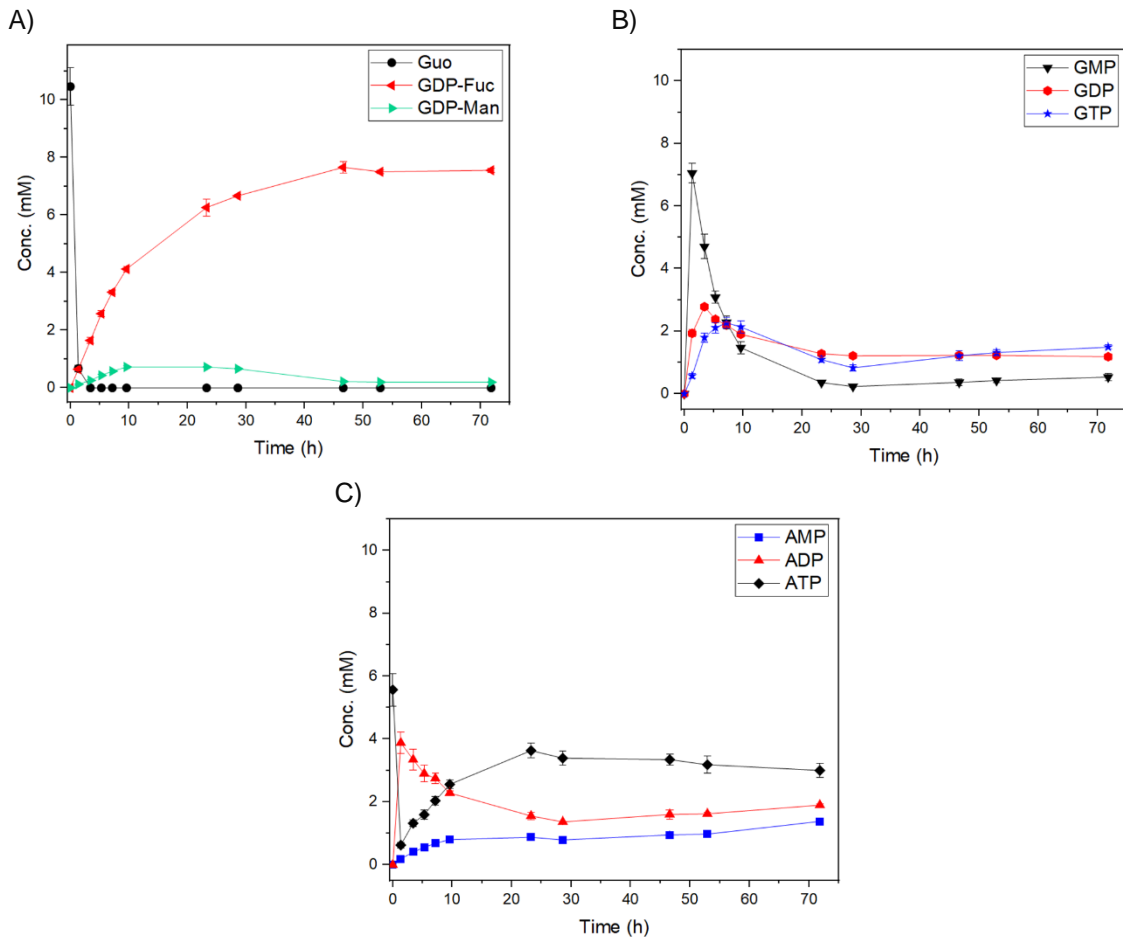


Figure 4.18. Time course of cascade substrates, intermediates, and products for synthesis of GDP-Fuc from Man and Guo. (A) Shows the consumption of Guo, the production of GDP-Man, and its consumption for synthesis of GDP-Fuc; (B) shows the production of GMP followed by its consumption for production of GDP and GTP. (C) Shows the concentration of ATP, ADP as well as AMP. The production of AMP might be due to chemical conversion of ADP to AMP. The cascade reactions contained 200 mM Tris-HCl (pH 8.5); 75 mM MgCl₂; 10.5 mM Man; 10.5 mM Guo; 50 mM L-Glu; 1 mM NADPH; 5.5 mM ATP; 13.5 mM PolyP_n; GSK 0.11 μg/μL; GMPK 0.49 μg/μL; PPK3 0.02 μg/μL; GLK 0.33 μg/μL; MANB/C 0.17 μg/μL; WCAG 0.07 μg/μL; GMD 0.17 μg/μL; PPA 0.03 μg/μL, and 10 units of GLDH 2.99 μg/μL in a final volume of 200 μL. Experiments were carried out in triplicates and error bars represent the standard deviation.

4.1.3 Synthesis of CMP-Neu5Ac

Results in this section are filed as a patent application under PCT/EP2021/059101 [232]. For synthesis of CMP-Neu5Ac, Cyt was used as the CMP-base of this sugar nucleotide. Similar to other nucleosides, Cyt is widely produced through established fermentation-based processes [233,234]. Cyt availability and low costs were the main reasons for choosing it as the synthesis precursor.

At first, a multi-enzyme cascade was developed to synthesize CMP-Neu5Ac from Neu5Ac as the sugar source. However, due to the high costs of Neu5Ac, an extended version of the cascade was developed that enabled usage of GlcNAc and Pyr instead of Neu5Ac. In both cascades, conversion of Cyt to CTP takes place through a similar enzymatic pathway. UDK catalyses the conversion of Cyt to CMP, and UMPK catalyses the conversion of CMP to cytidine diphosphate (CDP), both by using ATP as the phosphate source. Afterwards, CTP is produced from CDP by using PPK3 and PolyP_n as enzyme and phosphate donor, respectively. Similar to UDP- and GDP-sugar cascades, ATP was used in catalytic amounts for CMP-Neu5Ac synthesis.

4.1.3.1 Synthesis of CMP-Neu5Ac from Cyt and Neu5Ac

In this cascade (Figure 4.19), CMP-Ne5Ac is produced through the reaction catalyzed by CSS. PPA is added to the cascade to favor the cascade towards the product side.

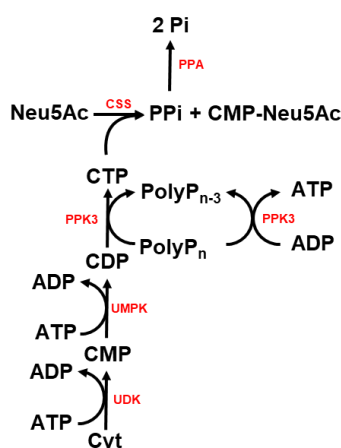


Figure 4.19. Multi-enzyme cascade of five enzymes and six reactions for synthesis of cytidine monophosphate N-acetylneuraminic acid (CMP-Neu5Ac) from cytidine (Cyt), N-acetylneuraminic acid (Neu5Ac), polyphosphate (PolyP_n), and catalytic amounts of adenosine triphosphate (ATP). Abbreviations: CMP, cytidine monophosphate; CDP, cytidine diphosphate; CTP, cytidine triphosphate; PPI, diphosphate; Pi, phosphate; ADP, adenosine diphosphate; UDK, uridine/cytidine kinase; UMPK, UMP/CMP kinase; PPK3, PolyP_n kinase; CSS, N-acetylneuraminyltransferase; PPA, inorganic diphosphatase.

The reaction chromatogram after 12 h of incubation at 37°C and 550 rpm demonstrates the high-yield synthesis of CMP-Neu5Ac (Figure 4.20).

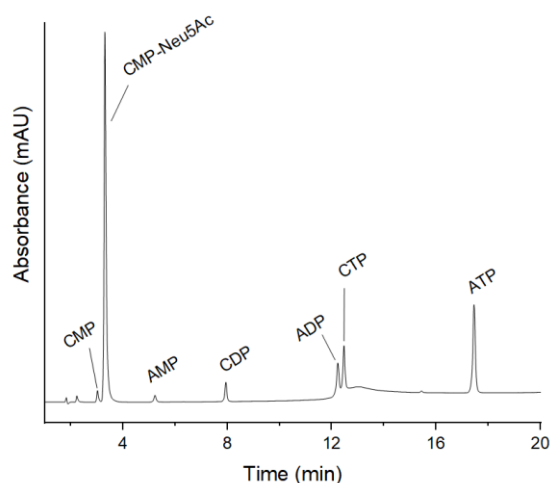


Figure 4.20. The UV chromatogram of CMP-Neu5Ac cascade reaction product after 12 h. The reaction mixture consisted of 150 mM Tris-HCl (pH 8.5); 10 mM Cyt; 10 mM Neu5Ac; 3 mM ATP; 4 mM PolyP_n; 50 mM MgCl₂, and the following enzymes: UDK 0.06 μg/μL; UMPK/PPK3 0.11 μg/μL; CSS 1.27 μg/μL, and PPA 0.04 μg/μL in a final volume of 200 μL.

However, the main disadvantage of this cascade (Figure 4.19) is using expensive and low-abundant Neu5Ac directly as a precursor. Consequently, an extended cascade was established to use inexpensive and industrially abundant compounds (i.e., GlcNAc and Pyr) to produce CMP-Neu5Ac.

4.1.3.2 Synthesis of CMP-Neu5Ac from GlcNAc, Pyr, and Cyt

The extended version of CMP-Neu5Ac synthesis cascade is shown in Figure 4.21. AGE catalyses the conversion of GlcNAc to ManNAc. Afterwards, through the reaction catalyzed by NANA, Neu5Ac is synthesized from Pyr and ManNAc.

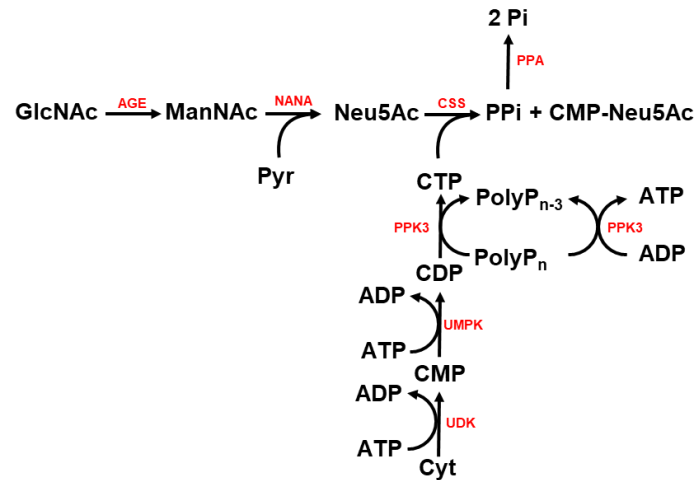


Figure 4.21. Multi-enzyme cascade of seven enzymes and eight reactions for synthesis of N-acetylneuraminic acid (CMP-Neu5Ac) from N-acetylglucosamine (GlcNAc), pyruvate (Pyr), cytidine (Cyt), polyphosphate (PolyP_n), and catalytic amounts of adenosine triphosphate (ATP). Abbreviations: CMP, cytidine monophosphate; CDP, cytidine diphosphate; CTP, cytidine triphosphate; PPI, diphosphate; Pi, phosphate; ADP, adenosine diphosphate; ManNAc, N-acetylmannosamine; UDK, uridine/cytidine kinase; UMPK, UMP/CMP kinase; PPK3, PolyP_n kinase; AGE, N-acylglucosamine 2-epimerase; NANA, N-acetylneuraminic lyase; CSS, N-acylneuraminic cytidyltransferase; PPA, inorganic diphosphatase.

The chromatogram of the reaction product is shown in Figure 4.22. After overnight incubation at 37°C, the synthesis yield was found to be low and a longer incubation of up to 48 h did not result in higher yields. Interestingly, despite high amounts of CTP, no increase in the synthesis of CMP-Neu5Ac was observed. This observation suggests an inhibition in the cascade, perhaps caused by CTP.

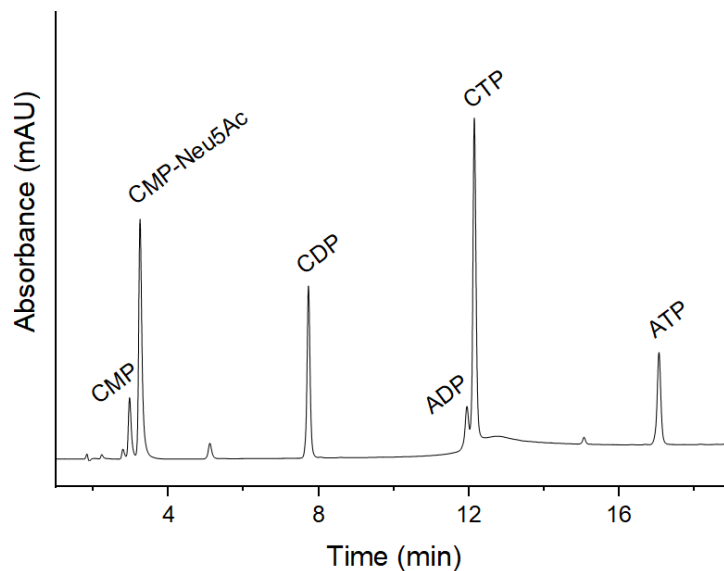


Figure 4.22. UV chromatogram of the cascade product for synthesis of CMP-Neu5Ac using GlcNAc as the sugar source. The following conditions were used: 140 mM Tris-HCl (pH 8.5); 35 mM Cyt; 39 mM GlcNAc; 39 mM Pyr; 3.5 mM ATP; 14.1 mM PolyP_n; 53 mM MgCl₂, and the following enzymes: UDK 0.09 µg/µL; UMPK/PPK3 0.15 µg/µL; CSS 1.22 µg/µL; AGE 0.03 µg/µL; NANA 0.08 µg/µL, and PPA 0.05 µg/µL in a final volume of 282 µL.

Due to low CMP-Neu5Ac synthesis yield and accumulation of CTP, it was hypothesized that CTP might inhibit AGE, as reported by Klermund *et al.* [235]. To confirm the hypothesis of AGE inhibition by CTP, a shortened version of the cascade consisting of AGE, NANA, and CSS was established to evaluate CMP-Neu5Ac synthesis from GlcNAc, ManNAc, Pyr, and CTP. As ATP is known to be an allosteric activator of AGE [203,236], its role was also evaluated. The results are shown in Figure 4.23.

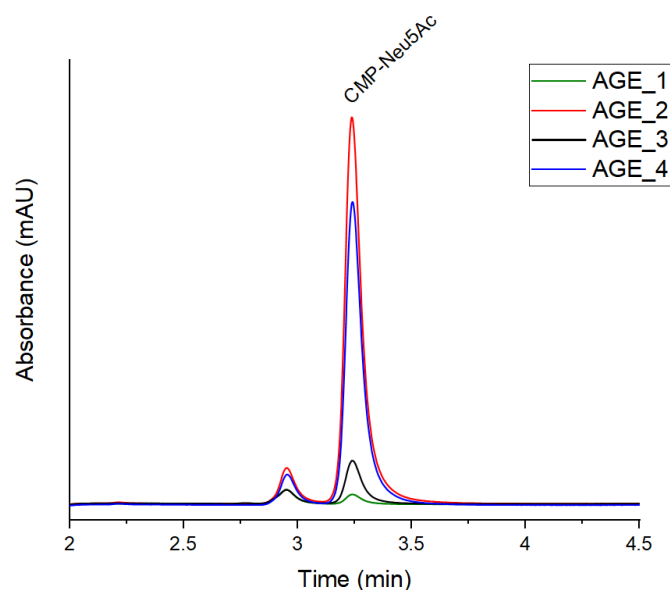


Figure 4.23. AGE inhibition by CTP. Reactions starting from ManNAc had the highest production of CMP-Neu5Ac (AGE_2, and AGE_4) while reactions starting from GlcNAc did not result in significant production of CMP-Neu5Ac (AGE_1, and AGE_3). Experiments performed with 150 mM Tris-HCl (pH 8.5); 20 mM MgCl₂; 20 mM CTP; 30 mM Pyr; 0.05 µg/µL AGE; 1.5 µg/µL NANA; 1 µg/µL CSS, and 0.04 µg/µL PPA in a total volume of 150 µL. The 1st experiment contained 30 mM GlcNAc (AGE_1), the 2nd experiment contained 30 mM ManNAc (AGE_2), the 3rd experiment contained 30 mM GlcNAc and 0.3 mM ATP (AGE_3), and the 4th experiment contained 30 mM ManNAc and 0.3 mM ATP (AGE_4). The experiments were running for 5 h.

Experiments starting from ManNAc resulted in CMP-Neu5Ac production, however, reactions starting from GlcNAc resulted in a very low amount of CMP-Neu5Ac. Moreover, addition of ATP — a known activator of AGE [236] — did not improve the synthesis yield. This observation — no synthesis starting from GlcNAc — suggests inhibition of AGE by CTP, as described in literature [235].

To overcome the inhibition of AGE by CTP, two strategies were considered. First, increasing the molar ratio of GlcNAc/Cyt, along with Pyr/Cyt, and second, controlling the concentration of CTP by modulation of PolyP_n level. Originally, the molar ratio of GlcNAc/Cyt and Pyr/Cyt was 1:1 simply due to cost. By increasing the concentration of GlcNAc and Pyr, the chemical potential of these molecules increases and theoretically, reactions catalyzed by AGE and NANA would shift more toward the product. It means that more Neu5Ac will be produced and, subsequently, CTP will be consumed faster than before (i.e., for the GlcNAc/Pyr/Cyt ratio of 1/1/1). At best, inhibition of the cascade would be avoided, or at least be minimized. Both strategies were carried out independently and simultaneously.

At first, the ratio of GlcNAc/Cyt, and Pyr/Cyt was increased from 1 to 7.4 and 7.9, respectively. After 24 h of incubation at 37°C, high conversion of CMP-Neu5Ac and very low accumulation of CTP was observed (Figure 4.24). However, a large amount of CMP remained in the reaction. Moreover, the higher peak height of ADP compared to ATP suggests inefficient ATP regeneration. It can be concluded from this that the amount of PolyP_n was insufficient.

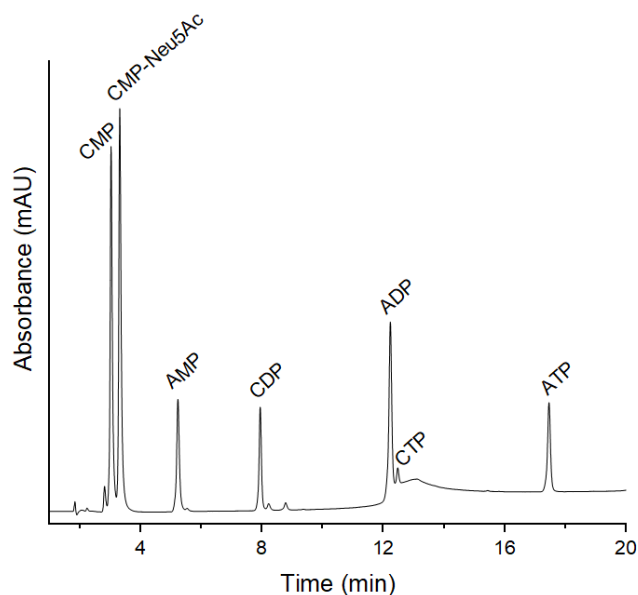


Figure 4.24. Reaction chromatogram after 24 h incubation at 37°C using increased ratio of GlcNAc/Cyt and Pyr/Cyt. The reaction consisted of 145 mM Tris-HCl (pH 8.5); 10 mM Cyt; 74 mM GlcNAc; 79 mM Pyr; 3 mM ATP; 4 mM PolyP_n; 74 mM MgCl₂; UDK 0.06 µg/µL; UMPK/PPK3 0.08 µg/µL; CSS 1.67 µg/µL; AGE 0.04 µg/µL; NANA 1.15 µg/µL, and PPA 0.05 µg/µL in a final volume of 203 µL.

Accordingly, additional experiments were done to scout for sufficient PolyP_n as the phosphate source to supply the cascade while avoiding AGE inhibition by CTP. The tested PolyP_n concentrations of scouting experiments were 4, 5, 6, 7, and 8 mM. The overlay of the scouting experiments is presented in Figure 4.25. The data shows that 7 mM PolyP_n gives the highest concentration of CMP-Neu5Ac.

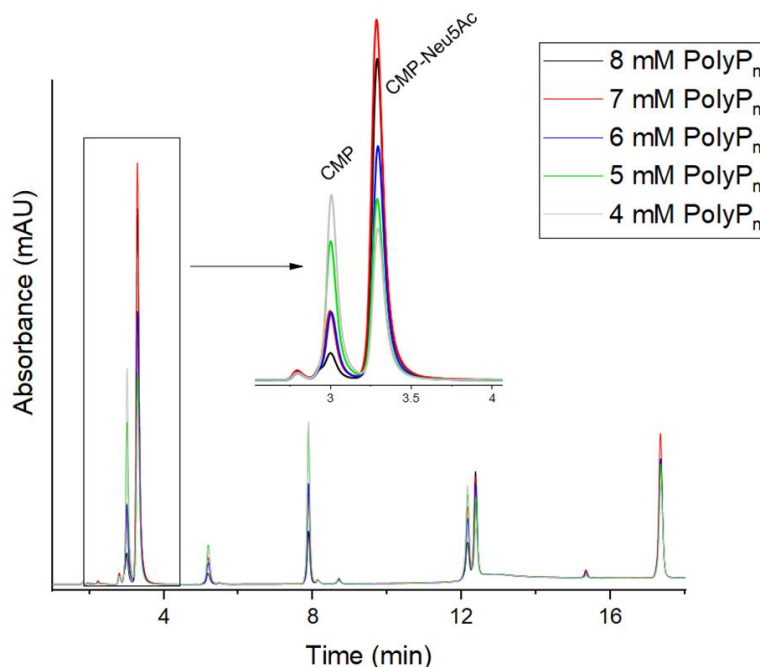


Figure 4.25. Overlay of reaction chromatograms from incremental amounts of PolyP_n after 24 h of incubation at 37°C. The experimental conditions were as follows: 150 mM Tris-HCl (pH 8.5); 10 mM Cyt; 75 mM GlcNAc; 70 mM Pyr; 3 mM ATP; and 75 mM MgCl₂; UDK 0.06 µg/µL; UMPK/PPK3 0.08 µg/µL; CSS 1.27 µg/µL; AGE 0.04 µg/µL, and NANA 1.16 µg/µL in a final volume of 200 µL.

It should be noted that the optimized concentration of PolyP_n heavily depends on the starting amounts of Cyt and ATP. High conversion of Cyt to CMP-Neu5Ac demonstrates the successful implementation of the proposed strategies.

To further improve the performance of the cascade in terms of product titer, the concentration of Cyt was increased. The purpose of these experiments was to reduce the cost by decreasing the ratios of GlcNAc/Cyt and Pyr/Cyt. The time course of reaction substrates, intermediates, and products is shown in Figure 4.26. In the developed cascade, CMP-Neu5Ac was produced to a final concentration of 24.6 mM (15.1 g/L) in a reaction time of 48.5 h and a synthesis yield of 77%, 34%, and 31% regarding Cyt, GlcNAc, and Pyr, respectively.

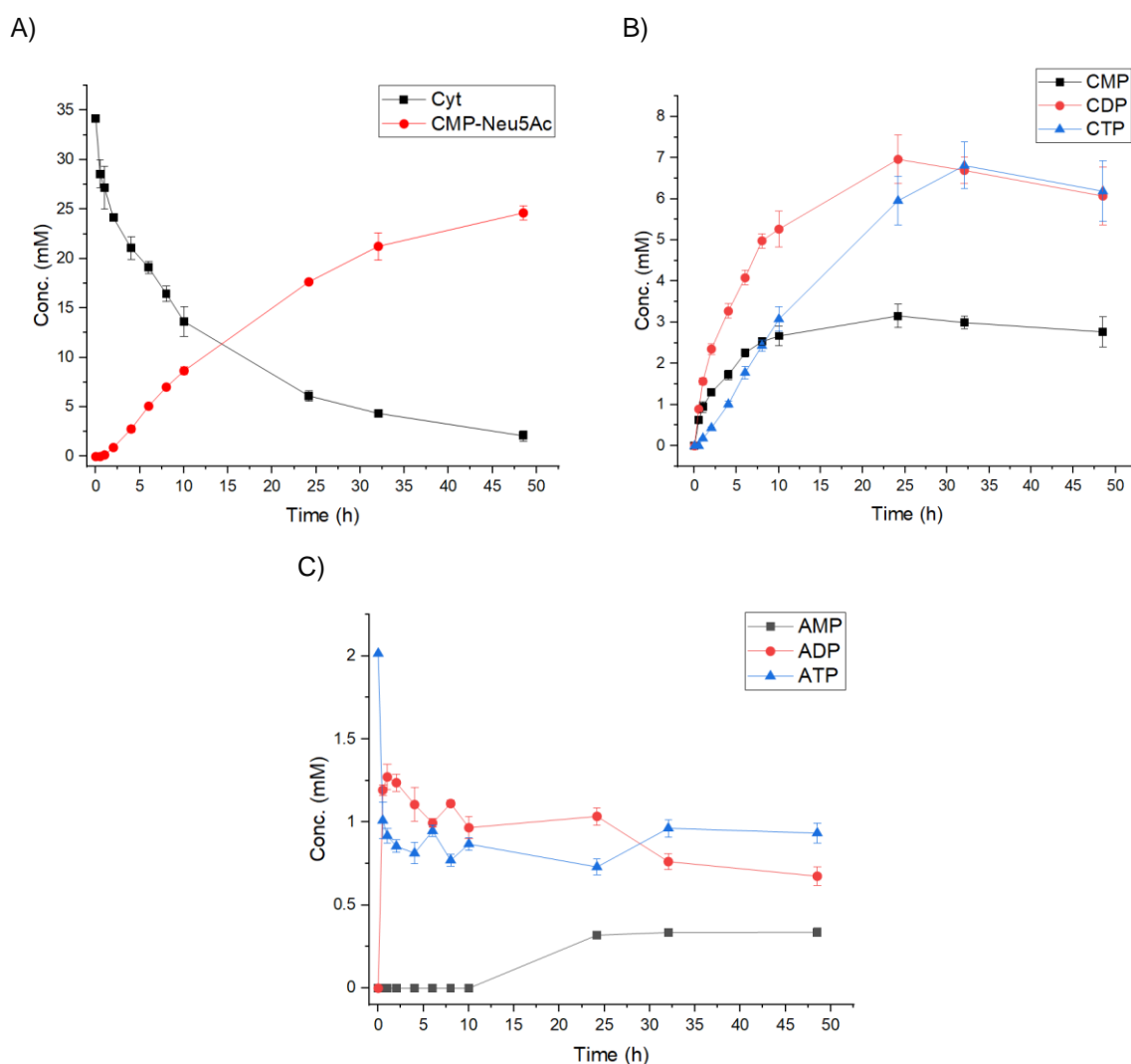


Figure 4.26. Time course of cascade substrates, products, and intermediates of CMP-Neu5Ac cascade from GlcNAc, Pyr, Cyt, PolyP_n, and catalytic amounts of ATP. (A) Consumption of Cyt and sequential production of CMP-Neu5Ac. (B) Production and consumption of CMP, CDP, and CTP. (C) Concentration of ATP, ADP, and AMP during the reaction. The reaction contained 190 mM Tris-HCl (pH 8.5); 34 mM Cyt; 72 mM GlcNAc; 79 mM Pyr; 2 mM ATP; 23 mM PolyP_n; 72 mM MgCl₂; UDK 0.05 μg/μL; UMPK/PPK3 0.07 μg/μL; CSS 1.05 μg/μL; AGE 0.03 μg/μL; NANA 0.96 μg/μL, and PPA 0.03 μg/μL with a final volume of 242 μL. The experiments were performed in triplicate and the error bars represent the standard deviation.

4.1.4 Discussion on synthesis of sugar nucleotides

In the previous sections, novel multi-enzyme cascades were presented for synthesis of UDP-, GDP-, and CMP-sugars. The main idea for development of each cascade was its potential for large-scale applications. Therefore, industrial availability of the precursors was the most important factor for development of cascades in this work. For each three groups of sugar nucleotides (UDP-, GDP-, and CMP-sugars), nucleosides — i.e., Uri, Guo, and Cyt — were used. All the nucleosides are mainly produced based on established fermentation-based processes by world-known chemical manufacturers such as Ajinomoto Co., Inc. and Takeda Chemical Industries, Ltd. [233,237,238].

Avoiding stoichiometric usage of ATP in the cascades was another strategy to optimize multi-enzymatic based sugar nucleotide production in terms of reducing the cost of precursors. Despite availability of ATP in kg scale, its stoichiometric utilization in large scale is costly and should be minimized. There are different strategies reported for regeneration of ATP from ADP by using different sources of phosphate such as acetylphosphate [239,240], PEP [189,241], and PolyP_n [146,242]. Among these compounds, PolyP_n is by far the cheapest phosphate source and it is available in ton scales because of its application in different industries, e.g., agriculture and food [243]. Therefore, it was the first choice for regeneration of ATP in this work. Moreover, thanks to the promiscuity of PPK3, all the diphosphate nucleotides — i.e., UDP, GDP, and CDP — were converted to their triphosphate form by using PolyP_n as the phosphate source — without addition of any extra enzyme to the cascades.

However, application of PolyP_n in multi-enzyme systems, specifically in the presence of enzymes that are dependent on divalent cations (e.g., Mg²⁺) for their activity, can be challenging. PolyP_n is known to form complexes with divalent cations with different dissociation constants [244,245]. Furthermore, interaction of PolyP_n with proteins is also expected in biological solutions because of its highly anionic nature [246]. Due to the existence of too many factors such as pH, salt concentration, protein amount, and nucleotides–Mg²⁺ interactions, explicit elucidation of the PolyP_n behaviour in the cascades is not feasible. Therefore, screening experiments were essential for finding the optimal conditions [220,224]. The relatively high concentration (50–80 mM) of MgCl₂ was needed for optimal performance of all the cascades, specifically for UDP-sugars. Meanwhile, most of reported cascades for sugar nucleotide synthesis used relatively lower concentrations (~5–20 mM) of MgCl₂ (see Table 4.1, Table 4.2, and Table 4.5). The high concentration of MgCl₂ could be explained by interaction of PolyP_n and Mg²⁺. In a mechanistic study of polyphosphate kinase 2 [247], it was reported that binding of Mg²⁺ and PolyP_n is essential for the enzyme activity. Despite the study being performed on a different family of polyphosphate kinase, I hypothesized that higher concentrations of Mg²⁺ would increase the activity of PPK3 by providing more Mg²⁺–PolyP_n complex. High concentrations of Mg²⁺ (50 mM) were reported in Ref. [129,248] in which PPK3 was used as a nucleotide diphosphate regenerator. Another reason for the high concentration of Mg²⁺ could be related to the phosphate ions that are released from diphosphatase reaction. Similar to a Mg²⁺–PolyP_n complex, Mg²⁺ can create a complex with phosphate ions and might avoid Mg²⁺ participation in enzymatic reactions. Moreover, it might result in precipitation of Mg²⁺ ions through the sequestration process [249]. The addition of Mg²⁺ during the batch time (for multi-enzyme synthesis of UDP-GlcNAc) to maintain the high productivity was reported in Ref. [250]. For example, interval supply of divalent cations (i.e., Mg²⁺ and Mn²⁺ in an enzymatic mixture) was the

subject of an invention in the patent regarding synthesis of oligosaccharides as a problem-solving approach for overcoming diphosphate or phosphate complexes with Mg^{2+} and Mn^{2+} [251]. In the following, the results obtained for synthesis of sugar nucleotides are discussed in detail.

4.1.4.1 Discussion on multi-enzyme synthesis of UDP-sugars

For synthesis of UDP-sugars, Uri was used as the nucleotide pair of UDP-activated sugars. Uri is the raw material for production of UMP which is highly used in infant formula [252] and in pharmaceutical products such as Sofosbuvir and Xuriden (uridine triacetate) [253–257]. Interestingly, Uri has recently been used as one of the key precursors for synthesis of Molnupiravir — an investigational antiviral drug for the treatment of coronavirus disease 2019 (COVID-19) [258]. In one of the benchmark papers, Uri was produced through fermentation (using a mutant of the *Bacillus subtilis* strain) in a 6000 L bioreactor with a titer of 65 g/L [259]. Recent advances in *E. coli*-based fermentation show a very similar performance (titer of 70.3 g/L) [260]. The robust industrial process shown in Ref. [259], demonstrates inexpensive and industrial scale production of Uri. In all the UDP-sugars, the set of enzymes were used for synthesis of UTP from Uri were the same. For conversion of Uri to UTP, two ATP-dependent kinases — i.e., UDK and UMPK — and one PolyP_n-dependent — i.e., PPK3 — were used.

All the monosaccharides used in synthesis of UDP-sugars are available in bulk except GalNAc. For UDP-GalNAc, there is still no clear bulk scale demand, therefore GalNAc was directly used as the sugar base. However, there are efforts on development of microbial O-glycosylation platform through expression of human *N*-acetylgalactosaminyl transferase in microbial hosts such as *E. coli* [261,262]. Therefore, another strategy for synthesis of UDP-GalNAc from inexpensive precursors is proposed in section 5.

In this work, I presented three novel cascades for synthesis of five different UDP-sugars. By exploiting the promiscuity of enzymes in the cascades, UDP-GlcNAc and UDP-GalNAc are produced from the same set of enzymes. For the synthesis of UDP-Glc and UDP-Man, the same set of enzymes were also used to carry out the synthesis. A novel cascade for synthesis of UDP-Gal was also presented.

Except UDP-GalNAc, GALU could be used as a sugar-1 phosphate uridylyltransferase in all the other UDP-sugar cascades. Taking advantage of the promiscuity of enzymes in multi-enzyme synthesis can be greatly beneficial, specifically when it comes to cascade optimization for synthesis of different products. Furthermore, in upstream processing for producing the required enzymes, it will be very convenient to minimize the number of different enzymes and maximize the number of different products. In this way, the efforts for process validation or process optimization can be reduced significantly.

In the following, literature focusing on the synthesis of UDP-GlcNAc is discussed. Regarding the potentially scalable synthesis of UDP-GlcNAc, two papers were separately published in 2000 by two major chemical producers in Japan. In the work that was carried out by researchers at Kyowa Hakko Kogyo Co., Ltd. [263], orotic acid and glucosamine were used as the raw materials. Both precursors are available in bulk and easily affordable, however, the proposed production strategy suffers from an extremely high biocatalyst load in the form of seven different permeabilized microbial cells (300 g/L) and low synthesis yield (17.5% regarding orotic acid and 2.8% regarding glucosamine) [263]. Moreover,

using seven different permeabilized *E. coli* cells might cause mass transfer problems, specifically at large scales. In another work by researchers in the biochemical division of the Yamasa corporation [148], a titer of 47 g/L of UDP-GlcNAc was achieved by using UMP and GlcNAc as precursors in combination of three enzymes and yeast cells as biocatalysts (see Table 4.1).

Large scale fermentation-based production of UMP was established in the 90s by Kyowa Hakko Kogyo Co., Ltd., with a titer as high as 28.6 g/L [264] which makes UMP an industrially available precursor. However, productivity of the cascade at large scales would be highly dominated by yeast cells (50 g/L) as they supply UTP for the synthesis. Considering the heterogeneities in the metabolism of living cells at large scales [265], practical implementation of such processes (e.g., the combination of enzymes and yeast cells for final product synthesis) might need a very complex process design. Moreover, due to the differing nature of enzymes and whole microorganisms in handling shear stress, providing appropriate mixing while controlling the shear stress for both enzymes and yeast cells at the same time will be challenging. In this work, to establish the cascade for synthesis of UDP-GlcNAc from Uri, GlcNAc, PolyP_n, and catalytic amounts of ATP, purified enzymes were used. All of the required six enzymes were His-tagged and recombinantly produced in *E. coli* and further purified with established immobilized metal affinity chromatography methods. UDP-GlcNAc was synthesized up to a titer of 66.2 mM (40.2 g/L) and a synthesis yield of 97.4%. No accumulation of intermediates (Figure 4.3) as well as the high yield of the cascade suggest the activity and stability of all the enzymes during the batch time. Moreover, the designed cascade was able to produce UDP-GalNAc with a titer of 53 g/L and a quantitative yield. Despite the biocatalyst load being in the range of industrially relevant processes [176], implementation of purified enzymes can significantly increase the process cost (~6× higher enzyme production cost) [176,178]. Therefore, in section 4.4.1.2, crude form enzymes were used for the scale-up of the cascade to 4 L since they are the second simplest form of biocatalyst formulation, second to whole-cell catalysis, with similar cost advantages.

Table 4.1. Summary of previous works on multi-enzyme synthesis of UDP-GlcNAc.

Precursors			Titer (g/L)	Reaction time (h)	Yield (%)	Biocatalyst	operation	Reaction condition	Scale (mL)	Ref.
Stoichiometric	Catalytic	Pi source								
100 mM GlcNAc; 100 mM UMP; 200 mM Glc	n.a.	n.a.	47.4	48	78	3 enzymes, 0.19 g/L; yeast cells, 5% w/v	Interval addition of Glc	200 mM KH ₂ PO ₄ , pH 8, 20 mM MgCl ₂ , 23 °C	5	[148]
65 mM orotic acid; 400 mM glucosamine; 50 g/L fructose	n.a.	n.a.	7.4	8	17.5	Combination of 7 different engineered <i>E. coli</i> , 300 g/L	Batch	25 g/L KH ₂ PO ₄ , pH 7.2, 5 g/L MgSO ₄ ·7H ₂ O, 32 °C	30	[263]
20 mM GlcNAc; 20 mM UTP; 0.4 mM glucose 1,6-bisphosphate	1 mM ATP	20 mM PEP	10.9	20	90	10 mL of 5 immobilized enzymes on agarose beads	7 batch	50 mM Tris-HCl, pH 7, 10 mM MgCl ₂ , 30 °C	100	[189]
50 mM GlcNAc; 50 mM UMP; 200 mM Glc	n.a.	n.a.	19.1	72	63	3 enzymes; yeast cells, 5% w/v	Interval addition of Glc	200 mM KH ₂ PO ₄ , pH 8, 20 mM MgCl ₂ , 20 °C	10	[266]
39.5 mM GlcNAc; 47.4 mM ATP; 47.4 mM UTP	n.a.	n.a.	19.4	36	81	NAHK, 0.2 g/L; GLMU, 0.31 g/L; PPA, 0.19 g/L	Batch	100 mM Tris-HCl, pH 8, 10 mM MgCl ₂ , 37 °C	20	[201]
25 mM GlcNAc; 30 mM ATP; 30 mM UTP	n.a.	n.a.	13.4	20	88	NAHK-GLMU (fused), 0.96 g/L; 50 U PPA	Batch	50 mM Tris-HCl, pH 8, 10 mM MgCl ₂ , 40 °C	5	[267]
20 mM GlcNAc; 20 mM ATP; 20 mM UTP	n.a.	n.a.	59.5	14.75	92	NAHK, 0.2 g/L; GLMU, 0.2 g/L; PPA, 500	Fed-batch, interval addition of 10 mM GlcNAc, 10 mM ATP, 10 mM UTP; 47 mg MgCl ₂ added after 5.25 h	200 mM Tris-HCl, pH 8.5, 5 mM MgCl ₂ , 37 °C	100	[250]
1 mM GlcNAc; 0.8 mM UMP; 2.5 mM ATP; 2 mM PolyP _n	n.a.	n.a.	0.6	2	100	NAHK, 0.1 g/L; GALU, 0.1 g/L; URA6, 0.1 g/L; PPK3, 0.1 g/L; PPA, 0.03 g/L	Batch	50 mM Tris-HCl, pH 7.5, 45 mM MgCl ₂ , 40 °C	1	[221]
10 mM GlcNAc; 10 mM ATP; 10 mM UTP	n.a.	n.a.	6.6	0.5 – per batch	81.33	NAHK, 40 U; GLMU, 40 U; PPA, 40 U; overall, 1.14 g/L	Repetitive batch – 120 batch	50 mM Tris-HCl, pH 8, 20 mM MgCl ₂ , 37 °C	20	[151]

68 mM GlcNAc; 68 mM Uri	2.1 mM ATP	21 mM mM PolyP _n	40.2	22	97.4	UDK, 0.07 g/L; UMPK/PPK3, 0.11 g/L; NAHK, 0.18 g/L; GLMU, 0.2 g/L; PPA, 0.05 g/L	Batch	150 mM Tris-HCl, pH 8.5, 75 mM MgCl ₂ , 37 °C	0.2	This work
50 mM GlcNAc; 47 mM UMP	4.7 mM ATP	15 mM PolyP _n	25.9	18	90	NAHK, GALK, UMPK, PPK3, GALU, PPA; cell lysate 0.5 g/L	Batch	200 mM Tris-HCl, pH 8.5, 75 mM MgCl ₂ , 37 °C	150	This work
62 mM GlcNAc; 62 mM Uri	1.6 mM ATP	18 mM PolyP _n	32.2	25.2	85.6	UDK; UMPK/PPK3; NAHK; GLMU; PPA; cell lysate, overall, 0.5 g/L	Batch	200 mM Tris-HCl, pH 8.5, 75 mM MgCl ₂ , 37 °C	4000	This work

Abbreviations: URA6, uridine-monophosphate kinase; n.a.: not available.

Table 4.2. Summary of UDP-Gal synthesis described in literature based on whole cell and multi-enzyme catalysis.

Stoichiometric	Precursors		Titer (g/L)	Reaction time (h)	Yield (%)	Biocatalyst	Operation	Reaction condition	Scale (mL)	Ref.
	Catalytic	Pi source								
20 mM Gal; 20 mM UMP	2 mM ATP; 2 mM Glc-1P	2% w/v PolyP _n	3.9	24	35	7 enzymes immobilized on agarose beads	Circulation via packed bed column	50 mM Tris-HCl, pH 7.4; 10 mM, KCl; 10, mM MgCl ₂ ; 37 °C	200	[146]
12 mM Gal; 10 mM UMP	1 mM ATP; 2 mM Glc-1P	40 mM acetyl phosphate	5.4	7	95	<i>E. coli</i> extract of 6 different enzymes	Batch	50 mM Tris-HCl, pH 7.5; 5 mM MgCl ₂ ; 37 °C	0.1	[239]
110 mM orotic acid; 250 mM Gal; 666 mM Glc	n.a.	n.a.	44	21	65	Combination of 2 engineered <i>E. coli</i> cells, 200 g/L	Batch	15 g/L KH ₂ PO ₄ , pH 7.2; 5 g/L MgSO ₄ ·7H ₂ O; 32 °C	2500	[147]
2.1 mM UDP-Glc; 2.8 mM Gal-1P; 2.5 mM NADP; 500 mM sucrose	n.a.	n.a.	1.2	2.3 – per batch	75	3 purified enzymes	Repetitive batch – 16 batch	50 mM Tris-acetate, pH 7.7; 2 mM MgSO ₄ , 37 °C	100	[268]
10 mM Gal; 10 mM ATP; 10 mM UTP	n.a.	n.a.	7.1	0.5 – per batch	94.48	3 purified enzymes overall, 1.30 g/L	Repetitive batch – 120 batch with same enzyme mixture	50 mM Tris-HCl, pH 7.5; 20 mM MgCl ₂ ; 37 °C	20	[151]
50 mM Uri; 52 mM Gal	0.6 mM ATP	20 mM PolyP _n	27.1	24	96	6 purified enzymes, overall, 0.5 g/L	Batch	150 mM Tris-HCl, pH 8.5; 75 mM MgCl ₂ ; 37 °C	20	This work
58 mM Uri; 55 mM Gal	2.5 mM ATP	20 mM PolyP _n	23.4	23	71	6 enzymes, cell lysate, overall, 0.5 g/L	Batch	150 mM Tris-HCl, pH 8.5; 75 mM MgCl ₂ ; 37 °C	1000	This work
55 mM Gal; 55 mM UMP	2.7 mM ATP	14 mM PolyP _n	26.9	35.5	86	GALK, NAHK, UMPK, PPK3, GALU, PPA; cell lysate, overall, 1.1 g/L	n.a.	200 mM Tris-HCl, pH 8.5; 75 mM MgCl ₂ ; 37 °C	3000	This work

Table 4.3. Summary of developed UDP-Glc synthesis cascade described in literature.

Stoichiometric	Precursors		Titer (g/L)	Reaction time (h)	Yield (%)	Biocatalyst	Operation	Reaction condition	Scale (mL)	Ref.
	Catalytic	Pi source								
80 mM Glc-1P; 20 mM UMP	1 mM ATP	100 mM acetylphosphate	4.5	4	40	3 enzymes, purified	Batch	50 mM Tris-HCl, pH 7.5, 20 mM MgCl ₂ , 37 °C	n.a.	[269]
50 mM sucrose; 10 mM UMP; 100 mM Glc;	2 mM ATP; 2 mM NAD ⁺	n.a.	3.4	20.5	60	Permeabilized engineered <i>E. coli</i>	Batch	100 mM NH ₄ HCO ₃ , pH 7; 20 mM MnSO ₄ ; 33 °C	1	[270]
1500 mM sucrose; 300 mM UDP	n.a.	n.a.	144	6	85	1 enzyme, purified, 0.1 g/L; 10 mg BSA*	Batch	pH 5, 10 mM MgCl ₂ , 45 °C	100	[271]
1500 mM sucrose; 210.25 mM UDP	n.a.	n.a.	100	22	86	<i>E. coli</i> cell, 1 g/L	Batch	pH 5, 10 mM MgCl ₂ , 37 °C	400	[272]
60 mM Uri; 60 mM Glc	1.7 mM ATP	19 mM PolyP _n	27.6	54.5	81	7 enzymes, purified, overall, 1.3 g/L	Batch	150 mM Tris-HCl, pH 8.5, 75 mM MgCl ₂ , 37 °C	0.2	This work

Abbreviations: KCl, potassium chloride; BSA, bovine serum albumin; n.a.: not available.

Several studies on the enzymatic synthesis of UDP-Gal have been previously published (see Table 4.2). Koizumi *et al.* developed a process using permeabilized engineered microbial cells for large scale production of UDP-Gal, which a titer of 44 g/L with yields of 65% and 29% from orotic acid and Gal, respectively, were obtained [147]. While the precursors used in Koizumi *et al.* are inexpensive and the titer is the highest reported in the literature, the high cell concentration (200 g/L or biocatalyst load of 4.5 g_{biocatalyst}/g_{product}) used makes scale-up difficult. In another multi-enzymatic approach, UDP-Gal was synthesized in a repetitive batch mode in gram scale from UDP-Glc, Gal-1P, and nicotinamide adenine dinucleotide (NADP) with a yield of 75% with respect to UDP-Glc [268]. However, UDP-Glc and NADP are expensive substances and their use in large-scale processes is economically unfeasible. The approach was improved by Fischöder *et al.* by using Gal, ATP, and UTP as substrates [151]. In a batch time of 0.5 h and a reaction volume of 20 mL, a titer of 7.1 g/L was achieved, and the enzyme showed high recyclability for 120 cycles [151].

Liu *et al.* established a system of seven enzymes to produce UDP-Gal from UMP, Gal, PolyP_n, and catalytic amounts of ATP, Glc-1P, and UDP-Glc [146]. PolyP_n was used as the phosphate source for the regeneration of ATP from ADP. Under optimized conditions — enzymes immobilized on agarose beads — a final titer of 3.9 g/L and a yield of 35% with respect to UMP and Gal was obtained. The same synthesis route was used by Lee *et al.*, except using acetylphosphate instead of PolyP_n for the regeneration of ATP [239]. In a batch process (100 µL), an improved yield of 95% and a final titer of 5.4 g/L was obtained by using crude extracts of six enzymes [239].

In this dissertation one of the main objectives was to develop a scalable biocatalytic process for the synthesis of UDP-Gal in multi-gram amounts that is economically viable. This encompasses the utilization of inexpensive substrates available in bulk amounts as well as significantly enhanced titers compared to previous studies (>20 g/L). The performance of UDP-Gal cascade was evaluated in the pH range of 7.0–9.0 based on the screening experiments described in Ref. [220]. It was found out pH≥8.5 result in higher conversion compared to lower pHs [220]. Therefore, it was selected as the operating pH for UDP-Gal cascade, and other UDP-sugar cascades. Through optimization, the amounts of ATP supplementation could be reduced to 0.6 mM, which is around 240 less than what is required for complete turnover of Uri and Gal without ATP regeneration. In section 4.4.1.1, scale-up of the cascade to 1 L for synthesis of UDP-Gal by using crude cell extract of enzymes is described.

UDP-Glc is an another important member of the UDP-sugars family whose application is extensively reported in Ref. [273,274]. It also serves as a substrate for production of other sugar nucleotides such as uridine diphosphate glucuronic acid and uridine diphosphate rhamnose. In this work, a novel cascade was designed (Figure 4.8) and established to synthesize UDP-Glc from Uri, Glc, PolyP_n, and catalytic amounts of ATP. The performance of the developed cascade is listed alongside other reported cascades in literature in Table 4.3.

Despite the high titers achieved in the work of Gutmann *et al.* and Schmölder *et al.*, utilizing UDP as the starting material for large-scale synthesis of UDP-Glc would not be a realistic option due to the high cost of UDP (~16 €/g) [271,272]. On the other hand, Uri (~0.2 €/g) is significantly cheaper and available

compared to UDP. Using inexpensive precursors is crucial when it comes to synthesis of UDP-Glc since it has applications in commodity products such as sweeteners [274].

The time course of UMP, UDP, and UTP in the UDP-Glc cascade show a different behavior compared to other UDP-sugars. In other cascades, the production of intermediates is followed by their consumption. However, in the UDP-Glc cascade, the intermediates accumulate slowly during the reaction. This suggests fast production and consumption of intermediates. Interestingly, UDP-Glc synthesis starting from 76 mM Uri and Glc resulted in 53.3 mM UDP-Glc (data not shown). Therefore, it might be that UDP-Glc has an inhibitory effect at concentrations of ~50 mM which hampers further product synthesis. This also supports the accumulation of intermediates at the end of the reaction.

The designed cascade for synthesis of UDP-Glc (Figure 4.8) can produce UDP-Man because of the affinity of GLK and GALU for Man and Man-1P, respectively. Since UDP-Man was biologically discovered at the beginning of 2018 [225], a scalable and straightforward production of UDP-Man can help to unravel its biological potential.

So far, novel sets of scalable multi-enzyme cascades were presented for synthesis of UDP-sugars. For establishment and optimization, purified enzymes were used, which can significantly hamper the industrial implementation of the cascades due to the high costs of enzyme purification. In sections 4.4.1.1 and 4.4.1.2, the scale-up of UDP-GlcNAc and UDP-Gal cascades by using crude enzymes is presented. Furthermore, to minimize the number of independent fermentations for recombinant production of enzymes, co-expression of said enzymes is demonstrated in section 4.4.2.1.

4.1.4.2 Discussion on multi-enzyme synthesis of GDP-sugars

In this work, one of the major achievements in the development of GDP-sugars was using Guo as the precursor. Guo is heavily used in food industry as a precursor for synthesis of GMP for its umami taste [275]. Due to high hydrogen bonding within Guo molecules, its presence in the aqueous phase results in strong hydrogel formation [276]. In this work, DMSO was found to be able to solubilize Guo up to 0.5 M at 25°C and 1 M at 75°C. DMSO and Guo interaction overcomes the hydrogen bonding within Guo molecules and results in its solubility [277] as well as avoiding any hydrogel formation. The mass balance of Guo-containing compounds was closed at each of the reaction measurement time points (Figure 4.14 and Figure 4.18), which ensures Guo availability for the enzymatic reactions in the cascade.

To synthesize GDP-Fuc, a cascade was initially established by using Fuc, Guo, PolyP_n, and catalytic amounts of ATP as precursors. Due to the high cost and low availability of Fuc, a second cascade was developed to produce GDP-Fuc from Man. In the later, NADPH was used to reduce GDP-4-dehydro-6-deoxy-Man to GDP-Fuc. In order to avoid stoichiometric usage of expensive NADPH, L-Glu was used in combination with GLDH to regenerate NADPH from NADP⁺. L-Glu is heavily consumed in food industry as a flavor enhancer and thus readily available at low costs [275].

It has been suggested that GDP-Fuc is a competitive inhibitor of GMD by binding to the active site [229–231,278]. Both enzymes, GMD and WCAG, belong to the short-chain dehydrogenases/reductases family and during the conversion of GDP-Man to GDP-Fuc, both the release and consumption of

hydrogen ions are part of the reaction mechanism [229,279]. To improve the synthesis yield, a pH screening was carried out to evaluate its effect on the synthesis of GDP-Fuc from GDP-Man, since pH could have an effect on dissociation constants [279]. Interestingly, it was found that at alkaline conditions, a high conversion of GDP-Man to GDP-Fuc can be obtained. The pH screening was also performed on the cascade (GDP-Fuc synthesis from Man) and as expected, high conversion was only obtained in alkaline conditions (data not shown). This might be because of low binding of GDP-Fuc to GMD at alkaline pH values.

The results obtained for synthesis of GDP-Fuc based on the developed cascades are compared to previously reported methods in Table 4.4. Pfeiffer *et al.* achieved a high concentration of 50 g/L GDP-Man by using GTP as a precursor [280], which can be very costly at large-scales (~21 €/g). On the other hand, using Guo (~0.1 €/g) or even GMP (~0.1 €/g) as precursors, as illustrated in this work, significantly reduces the synthesis cost. Koizumi *et al.* reported the highest GDP-Fuc concentration (18.4 g/L) described in literature by using whole-cell catalysis at a 15 L scale and utilizing Man and GMP as precursors [202]. However, low synthesis yields of 17% and 52% regarding Man and GMP, respectively and very high biocatalyst amount (215 g/L) in the form of four different permeabilized microbial cells make large-scale applications challenging. Moreover, since the one-pot experiment resulted in high accumulation of GDP-Man (15.6 mM vs. 5.9 mM GDP-Fuc), the conversion was carried out in two separate steps [202].

Table 4.4. Comparison of reported processes for the *in vitro* biocatalytic production of GDP-Man and GDP-Fuc.

Precursors										
Stoichiometric	Catalytic	Pi source	Titer (g/L)	Reaction time (h)	Yield (%)	Biocatalyst load (g _{enzyme} /g _{product})	Mode of operation	Reaction condition	Scale (mL)	Ref.
GDP-Man										
1.2 mM Man-1P; 2.4 mM GTP	n.a.	n.a.	0.4	0.34	60	n.a.	Continuous	Tris-HCl, pH 8, 1.8 mM MgCl ₂ , 2 mM DTT; 25 °C	3	[281]
15 mM Man; 35 mM GTP	n.a.	n.a.	14.1	24	94	0.04	Batch	100 mM Tris-HCl, pH 8; 10 mM MgCl ₂ , 37 °C	12	[282]
119 mM sucrose; 119 mM Pi; 400 mM Man; 70 mM GTP	n.a.	n.a.	50	20	100	0.01	Batch	100 mM MES, pH 7; 10 mM MgCl ₂ ; 37 °C	4	[280]
0.8 mM GDP; 6 mM Man; 0.8 mM ADP	n.a.	4 mM PolyP _n	0.3	4	71	3.1	Batch	50 mM Tris-HCl, pH 7.5; 10 mM MgCl ₂ , 30 °C	1	[131]
12.8 mM Guo, 10 mM Man	5.8 mM ATP	13.5 mM PolyP _n	4	45	52	0.35	Batch	200 mM Tris-HCl, pH 8.5; 75 mM MgCl ₂ , 37 °C	0.2	This work
GDP-Fuc										
27.5 mM GDP-Man; 33 mM NADPH	n.a.	n.a.	12.9	2	80	0.22	2-step batch	50 mM Tris-HCl, pH 7.5; 10 mM MgCl ₂ , 37 °C	6	[283]
333 mM fructose; 166 mM Man; 56 mM GMP	n.a.	n.a.	18.4	22	51	11.6	2-step batch	25 g/L KH ₂ PO ₄ , pH 7.2; 5 g/L MgSO ₄ ·7H ₂ O; 32 °C	30	[202]
91 mM Fuc; 54 mM ATP; 53 mM GTP	n.a.	n.a.	n.a.	48	n.a.	n.a.	Batch	50 mM Tris-HCl, pH 7.5; 50 mM MgCl ₂ , 25 °C	10	[150]
10.5 mM Man, 10.5 mM Guo, 50 mM L-Glu	5.5 mM ATP, 1 mM NADPH	13.5 mM PolyP _n	4.5	48	72	0.97	Batch	200 mM Tris-HCl, pH 8.5; 75 mM MgCl ₂ , 37 °C	0.2	This work
10 mM Fuc, 10 mM Guo	2.5 mM ATP	4.5 mM PolyP _n	4.1	48	70	0.34	Batch	200 mM Tris-HCl, pH 7.5; 45 mM MgCl ₂ , 37 °C	0.2	This work

Abbreviations: DTT, dithiothreitol; n.a., not available.

4.1.4.3 Discussion on multi-enzyme synthesis of CMP-Neu5Ac

Cyt was used as the precursor for synthesis of CMP-Neu5Ac. Cyt is used as the main precursor for synthesis of CMP [192] and therapeutic compounds such as cytidine diphosphate-choline [264]. Therefore, industrial processes have been developed for the large-scale production of Cyt [284,285].

The conversion of Cyt to CTP takes place through the same pathway as UDP-sugars since UDK, UMPK, and PPK3 are active on Cyt, CMP, and CDP, respectively.

However, the main challenge in the synthesis of CMP-Neu5Ac is the availability of Neu5Ac. Neu5Ac is isolated from natural sources such as milk, eggs, and edible birds' nest which contain very low amounts of it [107]. Despite the significant application of Neu5Ac in infant formula and in the pharmaceutical industry (e.g., main precursor of anti-flu drugs), Neu5Ac is still expensive and is not available in industrial amounts [286,287].

The existence of multiple challenges in enzymatic synthesis of Neu5Ac makes this valuable product an expensive and industrially unavailable compound. Neu5Ac is biologically produced from ManNAc and Pyr which is catalyzed by NANA. However, ManNAc is expensive (~4 €/g) and not commercially available in bulk amounts. ManNAc is produced from GlcNAc either by chemical epimerization at high pHs or enzymatic epimerization catalyzed by AGE. However, the equilibrium in enzymatic epimerization is in favor of GlcNAc [288]. Therefore, in a coupled approach (combination of AGE and NANA), Pyr is used in excess to push the reaction toward the Neu5Ac side which causes significant downstream challenges due to the difficulties in the separation of Pyr and Neu5Ac [286].

In a pioneering study, Mahmoudian *et al.* developed a chemo-enzymatic process to synthesize Neu5Ac from GlcNAc and Pyr. At first, GlcNAc was chemically epimerized to ManNAc. The concentration of ManNAc was further increased through selective precipitation of GlcNAc with isopropanol. Afterwards, only 1.5-fold excess of Pyr was necessary to achieve high Neu5Ac titer catalyzed by immobilized NANA [286]. However, the produced Neu5Ac was intended to be used for pharmaceutical purposes, and thus, cost-efficiency of the process had completely different metrics compared to food industry.

Synthesis of CMP-Neu5Ac from Neu5Ac and CMP has been achieved previously and it can be considered as a relatively straightforward multi-enzyme approach (Table 4.5). However, one-pot synthesis of CMP-Neu5Ac starting from GlcNAc has not been described previously. Therefore, multi-enzyme cascades were developed to use ManNAc as the sugar precursors (Table 4.5).

Strategies such as compartmentalization of enzymes to avoid direct interaction of CTP and AGE have been developed for synthesis of CMP-Neu5Ac [235]. Klermund *et al.* reported a 2.2-fold improvement of CMP-Neu5Ac titer (600 mg/L) upon capturing AGE in polymersomes while NANA and CSS were being immobilized on the surface [235]. It should be noted that the focus of the study was to demonstrate the role of compartmentalization in multi-enzyme synthesis rather than efficient synthesis of CMP-Neu5Ac. Hamamoto *et al.* synthesized CMP-Neu5Ac at 1 L scale starting from CMP, GlcNAc, and Glc by using *E. coli*, baker's yeast, and CSS to a titer of 30 mM [289]. Despite the demonstration at the 1 L scale, large-scale synthesis of such systems (i.e., mixture of microbial cells and enzymes) would be challenging due to their different physical properties. Heterogeneity of microbial cells in large scales

might also cause unpredictable issues and challenges in the synergistic behavior of *E. coli*, baker's yeast, and the enzyme.

In this work, as expected, the first effort for one-pot synthesis of CMP-Neu5Ac from GlcNAc and Cyt resulted in high accumulation of CTP and low synthesis yield of CMP-Neu5Ac (Figure 4.22). The hypothesis of an inhibitory effect of CTP on AGE was confirmed through a series of experiments (Figure 4.23). To overcome the inhibitory role of CTP on AGE in one-pot, the concentration of GlcNAc and Pyr was increased compared to Cyt, with the goal of a faster synthesis rate of Neu5Ac and subsequently faster consumption of CTP. Furthermore, the concentration of PolyP_n was screened to control the synthesis of CTP from Cyt, since PolyP_n acted as the main phosphate supply of the cascade. Therefore, by increasing the rate of Neu5Ac synthesis and controlled synthesis of CTP, the aim was for high yield (regarding Cyt) synthesis of CMP-Neu5Ac.

Based on the proposed strategy, CMP-Neu5Ac could be synthesized to a titer 24.6 mM (15.1 g/L) with the synthesis yields of 77%, 34%, and 31% regarding Cyt, GlcNAc, and Pyr, respectively. The results obtained in this work for synthesis of CMP-Neu5Ac is compared to previously reported values in Table 4.5. The precursors used in this study are among the most inexpensive starting materials ever used for multi-enzyme synthesis of CMP-Neu5Ac.

Table 4.5. Comparison of reported processes for the *in vitro* biocatalytic production of CMP-Neu5Ac.

Stoichiometric	Precursors		Titer (g/L)	Reaction time (h)	Yield (%)	Biocatalyst	Mode of operation	Reaction condition	Scale (mL)	Ref.
	Catalytic	Pi source								
60 mM ManNAc; 120 mM Pyr; 20 mM CMP	0.2 mM ATP	80 mM PEP	12	48	98	5 enzymes	Batch	200 mM HEPES, pH 7.5; room temperature	100	[241]
56 mM orotic acid; 100 mM Neu5Ac; 333 mM fructose	n.a.	n.a.	17	27	48	150 g/L of 3 different microbial cells	Batch	15 g/L KH ₂ PO ₄ , pH 7.2; 5 g/L MgSO ₄ ·7H ₂ O; 32 °C	30	[290]
15 mM CMP; 15 mM Neu5Ac	n.a.	150 mM PolyP _n (in terms of Pi)	6.1	22	67	1 U/mL PPA; 0.08 U/mL PPK; 10 U/mL CMK; 0.2 U/mL CSS	Batch	100 mM Tris-HCl, pH 8; 50 mM (NH ₄) ₂ SO ₄ ; 50 mM MgCl ₂ ; 37 °C	n.a.	[248]
20 mM CMP; 40 mM ManNAc; 60 mM Pyr	1 mM ATP	60 mM acetylphosphate	11	2	90	25 g/L of permeabilized <i>E. coli</i> cells (one strain)	Batch	200 mM Tris-HCl, pH 8; 20 mM MgCl ₂ ; 37 °C	0.1	[291]
40 mM CMP; 30 mM ManNAc; 75 mM Pyr	2.5 mM ATP	10 g/L PolyP _n	12	24–48	50–100	permeabilized <i>E. coli</i> or entrapped whole cell	Repetitive batch, two-pot*	50 mM Tris-HCl, pH 7.8; 50 mM MgCl ₂ ; 23 °C, 30 °C	100, 0.5	[242]
100 mM GlcNAc; 50 mM CMP; Glc	n.a.	n.a.	18.4	32	60	permeabilized <i>E. coli</i> ; yeast cells; CSS	Batch, interval addition of Glc	200 mM KH ₂ PO ₄ , pH 8; 30 mM MgCl ₂ ; 28 °C	1000	[289]
150 mM Pyr; 75 mM ManNAc; 75 mM CMP	5 mM CTP	150 mM PolyP _n (in terms of Pi)	34	12	73	0.48 g/L CMK; 0.92 PPK3; 5 g/L permeabilized <i>E. coli</i> cells; aggregated enzymes	Batch	50 mM Tris-HCl, pH 7.8; 50 mM MgCl ₂ ; 30 °C	10	[129]
50 mM CMP; 51 mM Neu5Ac	5 mM ATP	16 mM PolyP _n	27.8	6.6	90	UMPk; PPK3; CSS; cell lysate	Batch	150 mM Tris-HCl, pH 8.5, 75 mM MgCl ₂ ; 37 °C	100	This work
10 mM Cyt; 10 mM Neu5Ac	3 mM ATP	4 mM PolyP _n	~5.8	12	~95	0.06 g/L UDK; 0.11 g/L UMPk/PPK3; 1.27 g/L CSS; 0.04 g/L PPA	Batch	150 mM Tris-HCl, pH 8.5, 50 mM MgCl ₂ ; 37 °C	0.2	This work
34 mM Cyt; 72 mM GlcNAc; 79 mM Pyr	2 mM ATP	23 mM PolyP _n	15.1	48.5	77	0.05 g/L UDK; 0.07 g/L UMPk/PPK3; 1.05 g/L CSS; 0.03 g/L AGE; 1 g/L NANA, 0.03 g/L PPA	Batch	190 mM Tris-HCl, pH 8.5, 72 mM MgCl ₂ ; 37 °C	0.2	This work

* Repetitive batch, CMP to CTP in one pot in large scale, CMP-Neu5Ac in another pot in small scale. Abbreviations: CMK, cytidylate kinase; (NH₄)₂SO₄, ammonium sulfate.

4.2 Synthesis of HMOs

The two main approaches used for synthesis of HMOs are described. In the first approach (coupling strategy), two simple HMOs (i.e., 3-FL, and 6'-SL) were synthesized by coupling sugar nucleotide synthesis cascades and the relevant glycosyltransferases. In the second approach (modular strategy), a modular platform is proposed to potentially synthesize any type of HMOs. Here, products of sugar nucleotide synthesis cascades and glycosyltransferases are combined for HMOs synthesis.

4.2.1 Coupling strategy for synthesis of HMOs

Through the coupling approach, both synthesis of sugar nucleotide and HMO (or any other oligosaccharide) takes place in one pot. During synthesis, the released mono- or diphosphate nucleotide is regenerated, with the added advantage of using the nucleotides in catalytic amounts.

4.2.1.1 Synthesis of 3-FL

Synthesis of 3-FL based on the OPME approach, starting from Fuc, ATP, and GTP by using *H. pylori* 3/4-FT, has been reported before [209]. Here, the cascade is extended to use Man and Guo as the main precursors (see Figure 4.27). A cascade of 11 enzymes and 12 reactions was established, through the coupling of a GDP-Fuc synthesis cascade and 3/4-FT in one-pot. ATP and NADPH are used in catalytic amounts and are constantly regenerated from PolyP_n and L-Glu, respectively. As depicted in Figure 4.27, Guo can be used in catalytic amounts since released GDP from the 3/4-FT reaction is converted to GTP by PPK3.

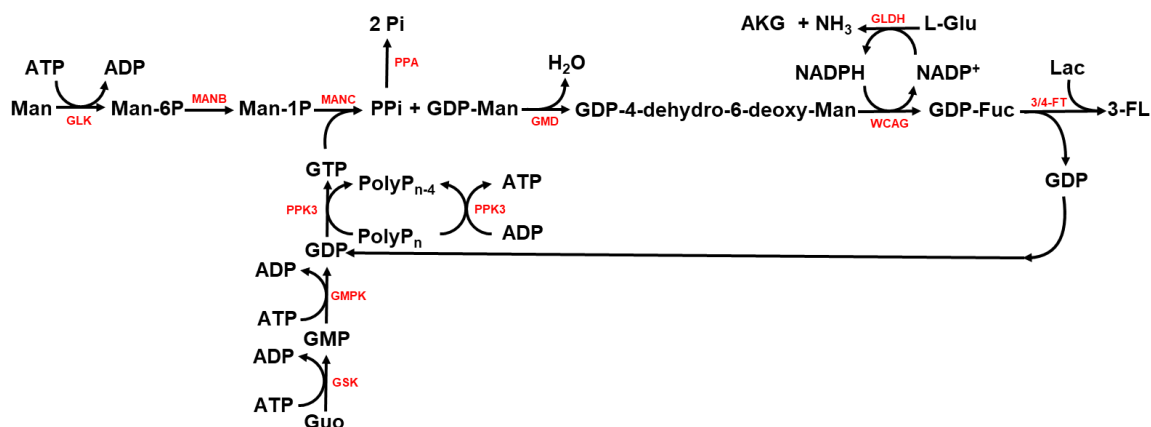


Figure 4.27. Coupling strategy for synthesis of 3-fucosyllactose (3-FL) through a cascade of 11 enzymes and 12 reactions from mannose (Man), lactose (Lac), polyphosphate (PolyP_n), L-glutamate (L-Glu), catalytic amounts of adenosine triphosphate (ATP), reduced nicotinamide adenine dinucleotide phosphate (NADPH), and guanosine (Guo). Abbreviations: GMP, guanosine monophosphate; GDP, guanosine diphosphate; GTP, guanosine triphosphate; ADP, adenosine diphosphate; Man-6P, mannose 6-phosphate; Man-1P, mannose 1-phosphate; GDP-Man, guanosine diphosphate mannose; GDP-Fuc, guanosine diphosphate fucose; GDP-4-dehydro-6-deoxy-Man, guanosine diphosphate-4-keto-6-deoxy-mannose; NADP⁺, nicotinamide adenine dinucleotide phosphate; NH₃, ammonia; AKG, α-ketoglutaric acid; H₂O, water; PPI, diphosphate; Pi, phosphate; GSK, guanosine kinase; GMPK, GMP kinase; PPK3, PolyP_n kinase; GLK, glucokinase; MANB, phosphomannomutase; MANC, mannose 1-phosphate guanylyltransferase; PPA, inorganic diphosphatase; GMD, guanosine diphosphate mannose 4,6-dehydratase; WCAG, guanosine diphosphate L-fucose synthase; GLDH, glutamate dehydrogenase; 3/4-FT, α1-3/4-fucosyltransferase.

The successful production of 3-FL from Lac, Man, Guo, L-Glu, and PolyP_n as the main precursors is shown in Figure 4.28. 3-FL was produced to a final concentration of 7.9 mM (3.8 g/L) after 72 h of reaction time at 37°C and 550 rpm. Guo, ATP, and NADPH were used 2, 5.2, and 9.8 times, respectively, lower than the stoichiometric amounts.

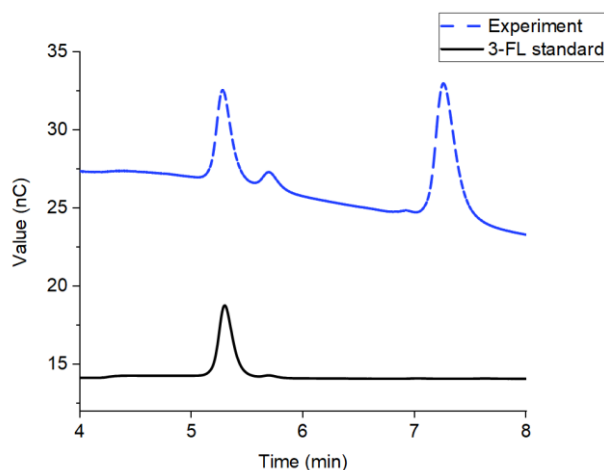


Figure 4.28. The HPAEC-PAD chromatogram of 3-FL synthesis based on the coupling approach. The second peak on the right (~7 min) is the remaining Lac. The reactions consisted of: 160 mM Tris-HCl (pH 8.5); 60 mM MgCl₂; 24 mM Lac; 24 mM Man; 4 mM Guo; 87 mM L-Glu; 0.8 mM NADPH; 4.4 mM ATP; 10.8 mM PolyP_n; GSK 0.09 μg/μL; GMPK 0.39 μg/μL; PPK3 0.01 μg/μL; GLK 0.4 μg/μL; MANB/C 0.15 μg/μL; WCAG 0.05 μg/μL; GMD 0.14 μg/μL; PPA 0.02 μg/μL; 3/4-FT 0.11 μg/μL, and 10 units of GLDH (2.39 μg/μL) in a final volume of 251 μL. Abbreviations: nC, nano-coulombs (dimension of PAD signal).

The concept of 3-FL synthesis based on the coupling approach was also evaluated by directly using Fuc as a precursor (Figure 4.29). Based on this cascade, 3-FL was successfully produced to a concentration of 27.3 mM (13.3 g/L) in a reaction time of 72 h and synthesis yield of 94% and 71% in respect to Fuc and Lac, respectively.

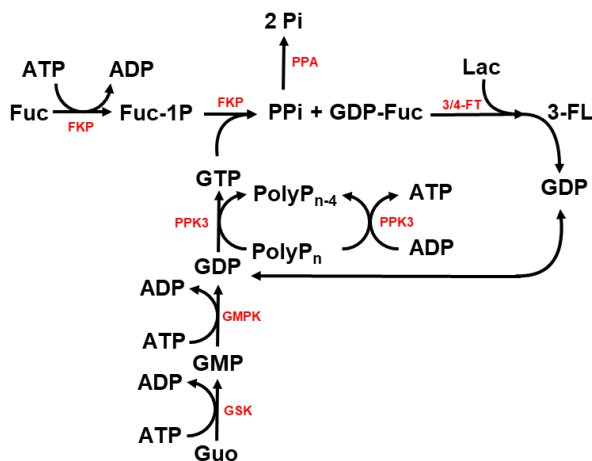


Figure 4.29. Synthesis of 3-fucosyllactose (3-FL) in the coupling approach through a cascade of six enzymes and eight reactions using fucose (Fuc), lactose (Lac), polyphosphate (PolyP_n), and catalytic amounts of guanosine (Guo), and adenosine triphosphate (ATP). Abbreviations: GMP, guanosine monophosphate; GDP, guanosine diphosphate; GTP, guanosine triphosphate; ADP, adenosine diphosphate; Fuc-1P, fucose 1-phosphate; GDP-Fuc, guanosine diphosphate fucose; PPi, diphosphate; Pi, phosphate; GSK, guanosine kinase; GMPK, GMP kinase; PPK3, PolyP_n kinase; FKP, fucokinase/ fucose 1-phosphate guanylyltransferase; PPA, inorganic diphosphatase; 3/4-FT, α1-3/4-fucosyltransferase.

4.2.1.2 Synthesis of 6'-SL

The sialyltransferase used here has been previously characterized and used for addition of α -2,6-linked sialic acid to free galactosylated glycans [208]. The cascade for synthesis of 6'-SL is illustrated in Figure 4.30. Through this enzymatic cascade, CMP-Neu5Ac is produced from GlcNAc, Pyr, and Cyt, afterwards, 6'-SL is produced through the reaction catalyzed by 2,6-ST. By coupling CMP-Neu5Ac synthesis enzymes and 2,6-ST in one-pot, a cascade of eight enzymes and nine reactions was established. As depicted in Figure 4.30, Cyt can be used in catalytic amounts since released CMP is regenerated to CTP through UMPK and PPK3. After 72 h of reaction time, 6'-SL was produced to a concentration of 9.4 mM (5.9 g/L) and synthesis yields of 31% and 15% in respect to Lac and GlcNAc, respectively.

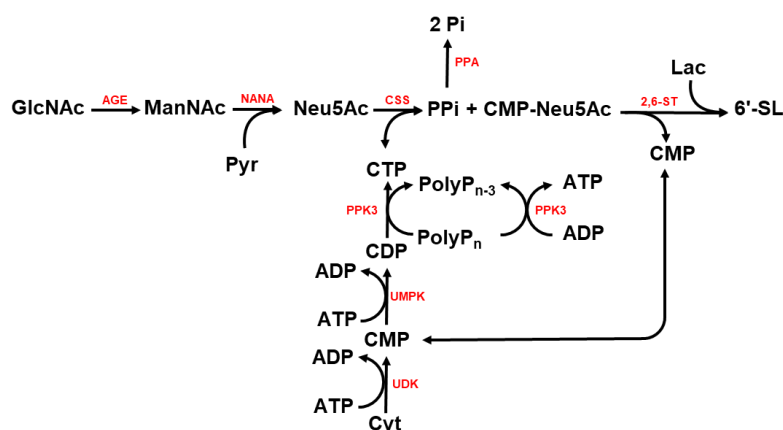


Figure 4.30. Synthesis of 6'-sialyllactose 6'-SL based on the coupling approach with a cascade of eight enzymes and nine reactions from *N*-acetylglucosamine (GlcNAc), pyruvate (Pyr), polyphosphate (PolyP_n), and catalytic amounts of adenosine triphosphate (ATP), and cytidine (Cyt). Abbreviations: CMP, cytidine monophosphate; CDP, cytidine diphosphate; CTP, cytidine triphosphate; PPI, diphosphate; Pi, phosphate; ADP, adenosine diphosphate; ManNAc, *N*-acetylmannosamine; UDK, uridine/cytidine kinase; UMPK, UMP/CMP kinase; PPK3, PolyP_n kinase; AGE, *N*-acetylglucosamine 2-epimerase; NANA, *N*-acetylneuraminic lyase; CSS, *N*-acetylneuraminic cytidyltransferase; PPA, inorganic diphosphatase.

4.2.2 Modular strategy for synthesis of HMOs

The concept of modular synthesis of HMOs is illustrated in Figure 4.31. In this approach, all the sugar nucleotides and HMOs, except Lac, were produced based on the developed multi-enzyme cascades and used without any purification. Therefore, the solution containing sugar nucleotide (the whole reaction mixture) was mixed with an acceptor (e.g., Lac, LNT II, and LNnT), a glycosyltransferase, and optionally an AP. The reason for addition of AP was to shift the equilibrium toward the product side by removing the released nucleotides.

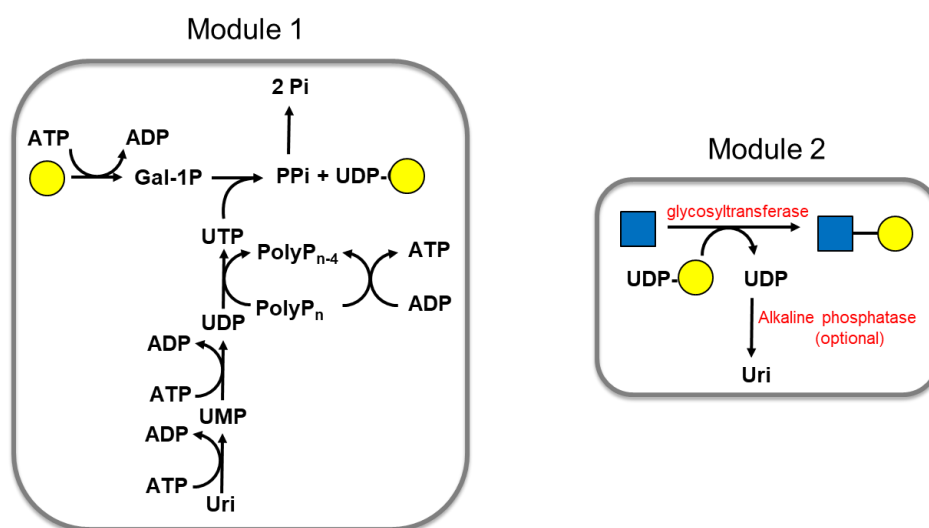


Figure 4.31. Modular approach for synthesis of HMOs. In this approach, sugar nucleotide is first produced in a separate pot. Afterwards, sugar nucleotide is mixed with an acceptor, a glycosyltransferase, and an optional AP. Abbreviations: Uri, uridine; ATP, adenosine triphosphate; ADP, adenosine diphosphate; UMP, uridine monophosphate; UDP, uridine diphosphate; UTP, uridine triphosphate; Gal-1P, galactose 1-phosphate; PPI, diphosphate; Pi, phosphate; PolyP_n; polyphosphate. Symbols: yellow circle, galactose; blue square, N-acetylglucosamine.

4.2.2.1 Synthesis of LacNAc

The galactosyltransferase for synthesis of LacNAc (as well as LNnT) has been characterized before and its affinity for GlcNAc has also been demonstrated [207]. After 20 h of incubation at 37°C, LacNAc was produced up to 14.4 mM (5.5 g/L). The reaction chromatogram is shown in Figure 4.32. The parallel reaction with the same condition but without any AP resulted in 10.2 mM (3.9 g/L) LacNAc.

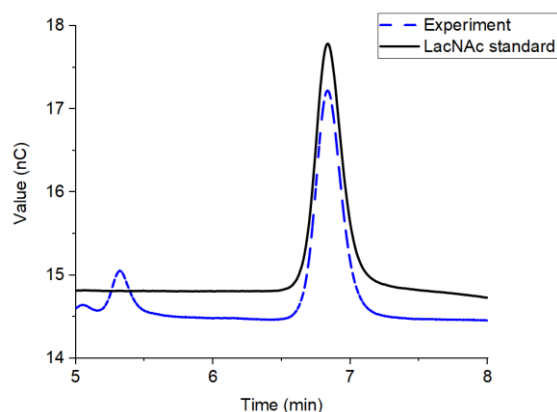


Figure 4.32. The HPAEC-PAD chromatogram of LacNAc synthesis reaction based on the modular approach. The reaction mixture for LacNAc synthesis contained 94 mM MES buffer (pH 6.0); 31 mM GlcNAc; 30 mM UDP-Gal; β 1,4GalT 0.01 μ g/ μ L, and 10 units of AP in a final volume of 160 μ L.

4.2.2.2 Synthesis of LNT II

LNT II was synthesized by incubating UDP-GlcNAc, Lac, and β 1,3GlcNAcT. After 48 h of incubation at 30°C, LNT II was produced to a final concentration of \sim 8.7 mM (\sim 4.7 g/L). The reaction chromatogram and MS/MS spectra of the peak at 568.0 Da is shown in Figure 4.33.

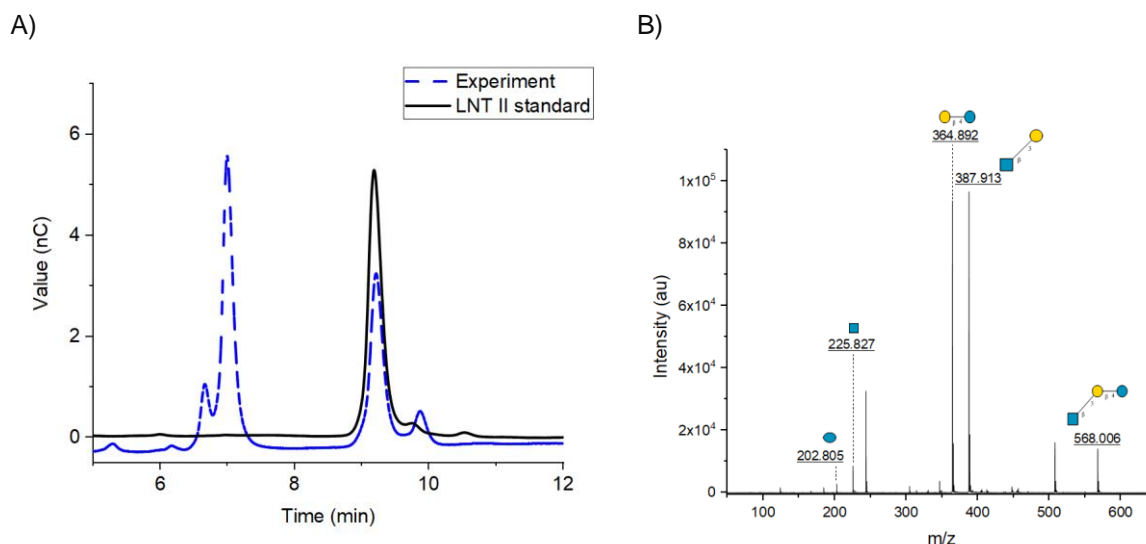


Figure 4.33. The HPAEC-PAD chromatogram of modular LNT II synthesis. (A) Reaction product and LNT II standard. The peak at \sim 7 min is the remaining Lac. (B) MS/MS spectra of the peak at 568.0 Da. Theoretical mass of LNT II is $[M+Na]^+$: 568.2 Da. The reaction conditions were as follows: 210 μ L of a reaction mixture containing 150 mM Tris-HCl (pH 8.5); 20 mM $MnCl_2$; 28.5 mM Lac; 20 mM UDP-GlcNAc; β 1,3GlcNAcT 0.08 μ g/ μ L, and 10 units of AP in a total volume of 210 μ L. Abbreviations: Da, Dalton; m/z, mass/charge ratio; au, arbitrary units.

4.2.2.3 Synthesis of LNnT

LNnT was synthesized by mixing UDP-Gal, LNT II, and β 1,4GalT. After 48 h of incubation at 37°C, LNnT was produced to a final concentration of \sim 2.9 mM (\sim 2 g/L). The reaction chromatogram and MS/MS spectra of the peak at 729.9 Da is shown in Figure 4.34.

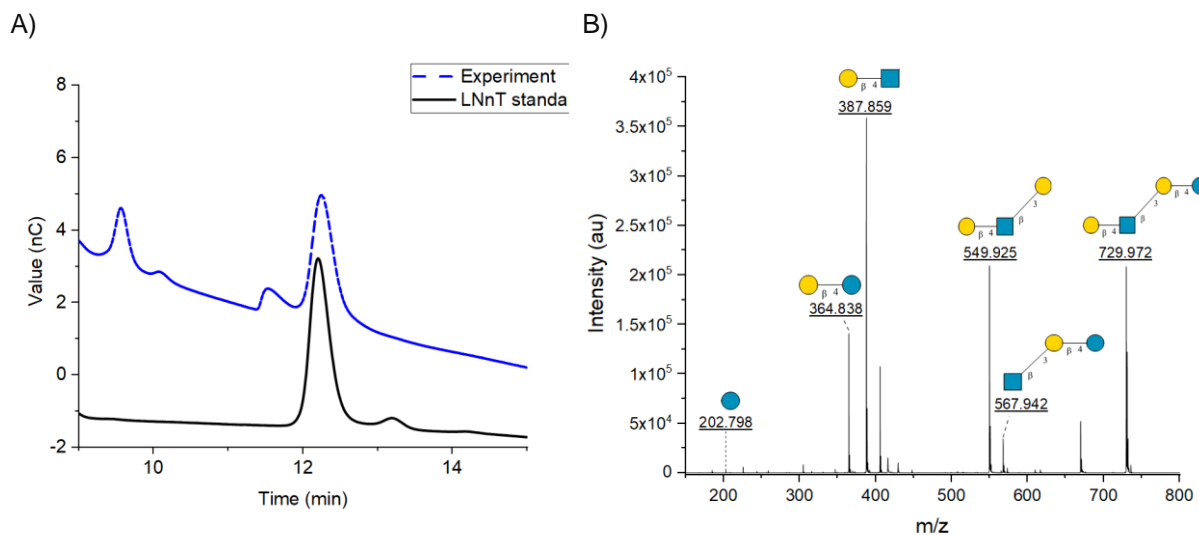


Figure 4.34. Synthesis of LNnT based on the modular approach. (A) HPAEC-PAD chromatogram of reaction product and LNnT standard. The peak at \sim 9 min is remaining LNT II. (B) MS/MS of peak at m/z 729.9. Theoretical mass of LNnT is $[M+Na]^+$: 730.2 Da. The reaction mixture contained 156 mM MES buffer (pH 5.5); 3.7 mM LNT II; 11 mM UDP-Gal; β 1,4GalT 0.01 μ g/ μ L, and 20 units of AP in a total volume of 320 μ L.

4.2.2.4 Synthesis of *para*-LNnH

The synthesis of *para*-LNnH is essentially as the same as the previously described steps. The successful production is shown in Figure 4.35.

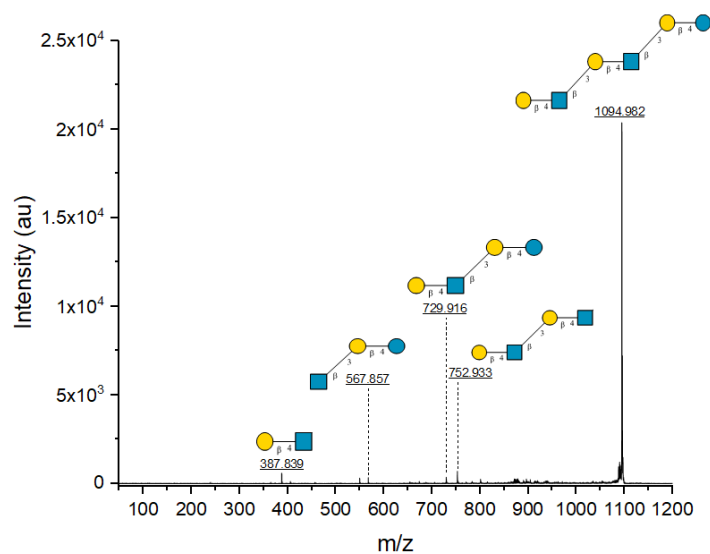


Figure 4.35. Synthesis of *para*-LNnH based on the modular approach. MS/MS of peak at *m/z* 1094.9. Theoretical mass of *para*-LNnH is $[M+Na]^+$: 1095.3 Da. At first, *para*-Lacto-*N*-neopentaose was produced through the combination of 75 μ L of UDP-GlcNAc cascade product (~10 mM UDP-GlcNAc); 75 μ L of LNnT reaction products; 30 units of AP; 0.06 μ g/ μ L of β 1,3GlcNAcT, and 150 mM Tris-HCl (pH 8.5) in a total volume of 270 μ L. After 24 h of incubation (at 30°C), 50 μ L reaction containing *para*-Lacto-*N*-neopentaose was mixed with 50 μ L of UDP-Gal cascade reaction product in addition to 20 units of AP; 0.02 μ g/ μ L β 1,4GalT, and 240 MES buffer (pH 6.5) in a total volume of 210 μ L.

4.2.2.5 Synthesis of 6'-SL

6'-SL was synthesized by mixing CMP-Neu5Ac, Lac and 2,6-ST. Through this reaction, 6'-SL was produced to a concentration of 16.8 mM (10.6 g/L) after 48 h with synthesis yields of 93% and 84% regarding CMP-Neu5Ac and Lac, respectively. The reaction chromatogram and MS/MS spectra of the product are shown in Figure 4.36.

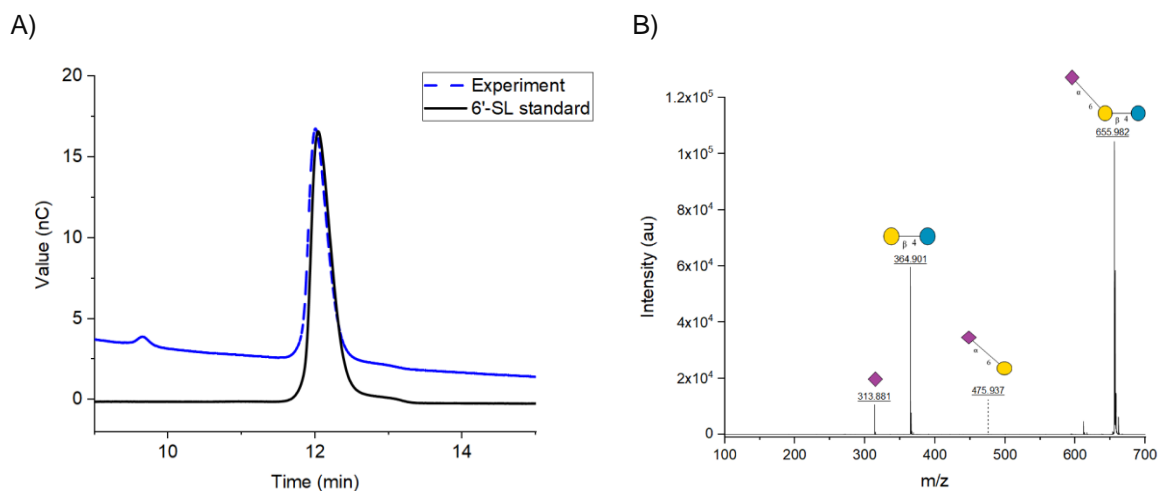


Figure 4.36. Modular synthesis of 6'-SL. (A) HPAEC-PAD chromatogram of reaction products for synthesis of 6'-SL. (B) MS/MS spectra of peak at m/z of 655.9. Theoretical mass of 6'-SL is $[M+Na]^+$: 656.2 Da. For synthesis of 6'-SL. The reaction solution contained: 18 mM CMP-Neu5Ac; 20 mM Lac; 133 mM Tris-HCl (pH 8.5), and 0.13 $\mu\text{g}/\mu\text{L}$ 2,6-ST in a final volume of 150 μL .

4.2.2.6 Synthesis of LST_c and $DSLNNt$

Synthesis of LST_c and $DSLNNt$ by using bacterial α -2,6-sialyltransferase has been demonstrated before [292,293]. Basically, $DSLNNt$ is a side product of LST_c synthesis due to high affinity of bacterial α -2,6-sialyltransferase to Gal. Here, both LST_c and $DSLNNt$ could be successfully synthesized by using reaction products of CMP-Neu5Ac cascade and $LNNt$ synthesis module. The mass spectra of reaction product after 24 h is shown in Figure 4.37.

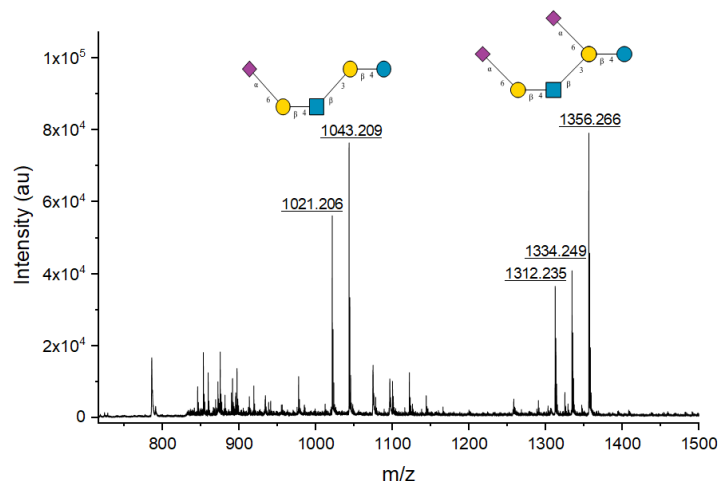


Figure 4.37. MS spectra of LST_c and $DSLNNt$ synthesis based on modular concept. Theoretical masses are as follows: LST_c , $[M+Na]^+$: 1021.3 Da; LST_c , $[M+2Na]^+$: 1044.2 Da; $DSLNNt$, $[M Na]^+$: 1312.4 Da; $DSLNNt$ $[M+2Na]^+$: 1335.3 Da; $DSLNNt$, $[M + 3Na]^+$: 1358.2 Da. The reaction contained: 5 mM CMP-Neu5Ac; 0.7 mM $LNNt$; 0.14 μ g/ μ L 2,6-ST, and 240 mM Tris-HCl (pH 9), in a total volume of 210 μ L.

4.2.2.7 Synthesis of 3-FL

Synthesis of 3-FL by using *H. pylori* 3/4-FT has been reported previously [209]. The synthesized GDP-Fuc was used without any purification for synthesis of 3-FL. By incubating GDP-Fuc, Lac, and 3/4-FT for 24 h, 3-FL was produced to a final concentration of 3.6 mM (1.7 g/L).

4.2.2.8 Synthesis of LNFP III and DF-LNnT

Similar to 3-FL, synthesis of LNFP III and DF-LNnT by using *H. pylori* 3/4-FT has been reported before [209]. Based on the modular approach, both LNFP III and DF-LNnT was produced (Figure 4.38).

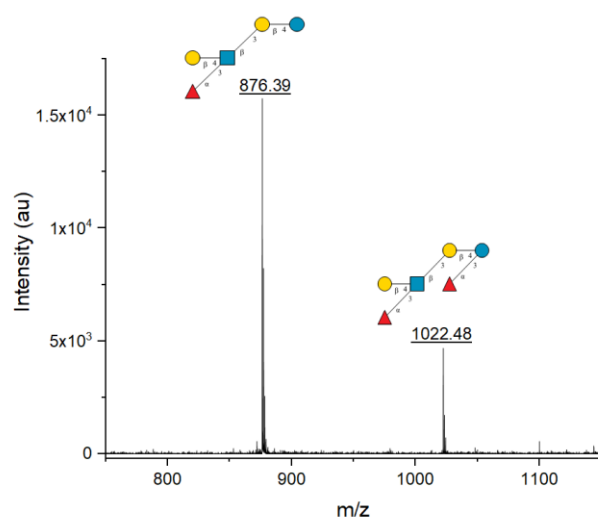


Figure 4.38. MS spectra of reaction product for synthesis of LNFP III and DF-LNnT based on modular concept. Theoretical mass of LNFP III is $[M+Na]^+$: 876.3 Da. Theoretical mass of DF-LNnT is $[M+Na]^+$: 1022.3 Da. The reaction contained 3 mM GDP-Fuc; 0.9 mM LNnT; 0.15 $\mu\text{g}/\mu\text{L}$ 3/4-FT; 146 mM Tris-HCl (pH 8.5), and 20 units of AP in a total volume of 205 μL .

4.2.2.9 Synthesis of LNFP V

For synthesizing LNFP V without having any undesired fucosylated by-products, at first, LNT II needs to be fucosylated. The steps for LNFP V synthesis are illustrated in Figure 4.39 [125]. Based on the modular approach, LNFP V was produced as shown in Figure 4.40.

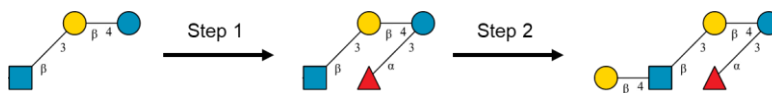


Figure 4.39. The steps for LNFP V synthesis.

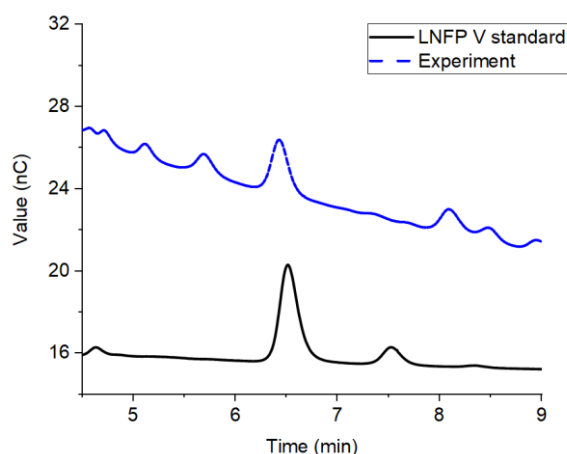


Figure 4.40. HPAEC-PAD chromatogram of LNFP V synthesis. The impurities (i.e., peaks before and after LNFP V) were not identified. At first, LNT II was produced as described in section 4.2.2.2. The reaction mixture for synthesis of fucosylated LNT II consisted of 210 mM Tris-HCl (pH 8.5); LNT II (~2.6 mM); 0.07 $\mu\text{g}/\mu\text{L}$ 3/4-FT, and 2 mM GDP-Fuc in a total volume of 190 μL . After 24 h of incubation at 37°C, 100 μL of the reaction mixture was transferred to a new vial containing: 5 mM UDP-Gal; 0.01 $\mu\text{g}/\mu\text{L}$ β 1,4GalT, and 167 mM MES buffer (pH 6.0).

4.2.2.10 Synthesis of 6'-SLN

At first LacNAc was produced as described in section 4.2.2.1. Based on the modular approach, the synthesized LacNAc was mixed with CMP-Neu5Ac and 2,6-ST. After 20 h of incubation at 37°C, 6'-SLN was produced to a final concentration of ~5.2 mM (~3.5 g/L). The chromatogram and MS spectra of reaction product are shown in Figure 4.41.

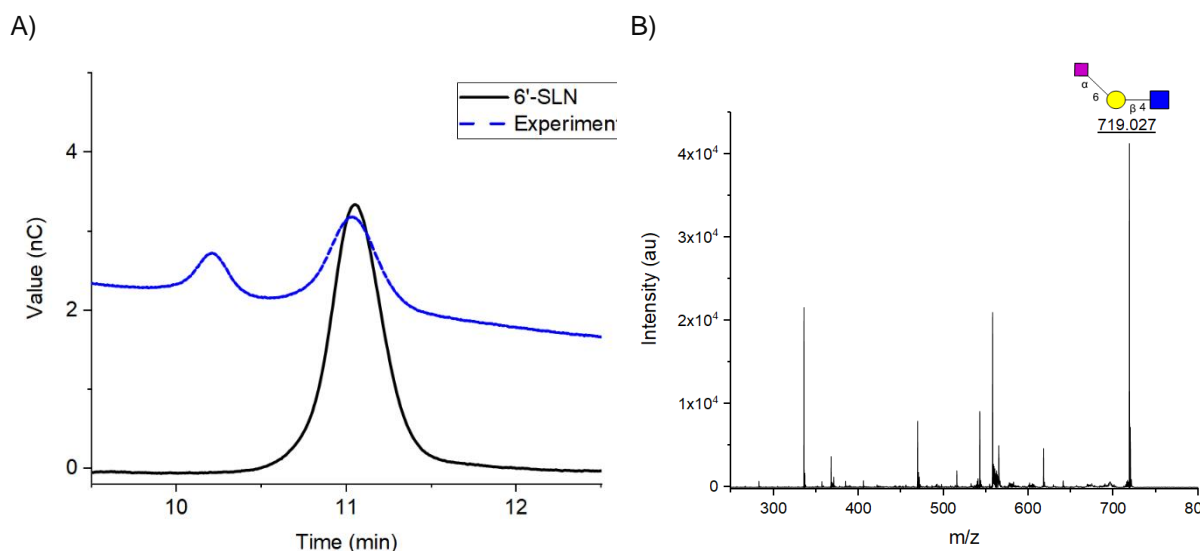


Figure 4.41. Synthesis of 6'-SLN based on the modular concept. (A) Overlay of HPAEC-PAD chromatogram of reaction product and pure 6'-SLN. (B) MS spectra of reaction product. Theoretical mass of 6'-SLN is $[M+2Na]^+$: 720.0 Da. The reaction consisted of 115 mM Tris-HCl (pH 8.5); 6.1 mM LacNAc; 8.5 mM CMP-Neu5Ac; 0.10 $\mu\text{g}/\mu\text{L}$ 2,6-ST, and 5 units of AP in a total volume of 175 μL .

4.2.3 Discussion on synthesis of HMOs

Two different strategies — coupling and modular — have been proposed and developed for HMOs synthesis. Different aspects of each strategy, with the goal of large-scale application, are discussed below.

4.2.3.1 Coupling strategy

Synthesis of oligosaccharides, including HMOs through coupling of sugar nucleotide synthesis and glycosyltransferases together with nucleotide regeneration (or co-factor regeneration), has been investigated in various studies [128,130].

Wong *et al.* synthesized 12.5 g of LacNAc in a cascade of five enzymes and five reactions starting from Glc-6P, GlcNAc, PEP, and catalytic amounts of UDP [294]. Ichikawa *et al.* synthesized 6'-SLN in a cascade of four enzymes and six reactions starting from LacNAc, Neu5Ac, PEP, and catalytic amounts of CMP and ATP [133]. In a comprehensive study by Tsai *et al.*, multigram scale synthesis of oligosaccharides was demonstrated through regeneration of sugar nucleotides including UDP-Gal, UDP-GalNAc, GDP-Fuc, and CMP-Neu5Ac [128]. All nucleotides were used in catalytic amounts and PEP was used as the phosphate source for regeneration of sugar nucleotides. Despite successful gram scale synthesis of functional oligosaccharides through the sugar nucleotide regeneration approach, the use of purified enzymes, diphosphate nucleotides, and expensive phosphate sources such as PEP (~20 €/g) make such approaches unattractive for large-scale synthesis of HMOs.

To bypass the costly step of enzyme purification, the coupling of engineered bacteria was investigated for synthesis of functional oligosaccharides [147,149,202,295]. In this strategy, permeabilized microbial cells act as the enzyme source. Titers reported based on this approach for sugar nucleotide and oligosaccharides synthesis are among the highest reported values in literature which demonstrate its potential for industrial applications [296]. However, a high concentration of microbial cells (e.g., >200 g/L) might cause scale-up of such processes to be challenging, both in terms of process economics (e.g., numbers and volume of required fermentation units) and technical points such as mixing and mass transfer.

OPME is another strategy which focuses on synthesis of HMOs and other oligosaccharides from simpler precursors such as monosaccharides and triphosphate nucleotides, however without any nucleotide regeneration [124]. There are a significant number of reports on gram scale synthesis of HMOs based on the OPME approach [124–126,297]. Despite being an attractive strategy for lab-scale synthesis of HMOs (or in general, oligosaccharides), stoichiometric utilization of expensive ATP and nucleotide triphosphates (i.e., UTP, CTP, and GTP) as well as purified enzymes would significantly hinder OPME applicability for manufacturing purposes. To overcome the mentioned shortages, the OPME approach was extended in this study to the coupling approach for increasing the scalability potential. This means that because of the catalytic usage of nucleosides and ATP, industrial implementation would be more economically viable. In a proof-of-concept study, two different HMOs were synthesized to demonstrate the concept of the coupling approach.

3-FL has been reported to be in the range of 50–231 mg/L in human milk [298]. Two different cascades were developed for 3-FL synthesis. In the first step, a cascade of 11 enzymes and 12 reactions, starting from 24 mM Lac, 24 mM Man, 4 mM Guo, 87 mM L-Glu, 0.8 mM NADPH, 4.4 mM ATP, and 10.8 mM PolyP_n was developed. In a batch time of 72 h, 3-FL was produced to a titer of 7.9 mM (3.8 g/L). Therefore, Guo, ATP, and NADPH were used 2, 5.2, and 9.8-fold, respectively, lower than the stoichiometric amounts.

In the second cascade, 3-FL was produced by directly using Fuc as the source of sugar. Starting from 29 mM Fuc, 38 mM Lac, 3.8 mM Guo, 2.8 mM ATP, and 11.5 mM PolyP_n, 3-FL was produced to a concentration of 27.3 mM (13.3 g/L) in a reaction time of 72 h. Therefore, Guo and ATP were used 7.1 and 30-fold less than the stoichiometric amounts, respectively. Despite 3-FL being synthesized to a concentration of 13.3 g/L and a high yield of 95% (regarding Fuc), direct usage of expensive Fuc as the sugar source challenges the process applicability of the cascade.

Yu *et al.* synthesized 3-FL with a yield of 90% (after purification — in the reaction it correlates to 18 mM 3-FL) starting from 26 mM Fuc, 26 mM ATP, and 26 mM GTP [209]. Choi *et al.* synthesized 3-FL to a titer of 4.8 mM starting from 15 mM Lac and 5 mM GDP-Fuc [299]. Synthesis of 3-FL based on fermentation has been reported to be ~11.5 g/L (~23.6 mM) by using only glycerol and Lac as the carbon source and substrate, respectively [300]. Recently, titers of ~60 g/L for fermentation-based synthesis of a similar HMO — i.e., 2'-FL by using sucrose as both carbon source and substrate — has been reported [120].

Despite reported titers for 3-FL in this work being among the highest reported in literature based on enzymatic synthesis, the final large-scale application will be limited by the cost of Fuc as well as usage of purified enzymes. As commercial production of 2'-FL is carried out through fermentation methods [24], it can be assumed that the same strategy would apply for industrial scale production of 3-FL.

The concentration of 6'-SL is reported to be in the range of 126–564 mg/L in human milk [298]. For synthesis of 6'-SL, a cascade of eight enzymes and nine reactions was developed. Starting from 30 mM Lac, 8 mM Cyt, 60 mM GlcNAc, 64 mM Pyr, 1.6 mM ATP, and 19.2 mM PolyP_n, 6'-SL was produced to a concentration of 9.4 mM (5.9 g/L). To the best of author's knowledge, one-pot synthesis of 6'-SL starting from Cyt and GlcNAc has been demonstrated for the first time in this study.

In a recent study, Schelch *et al.* synthesized 17 mM (10.4 g/L) 3'-SL starting from 20 mM ManNAc, 20 mM PEP, 25 mM CTP, and 20 mM Lac through a three-enzyme cascade [301]. However, no CMP regeneration was implemented in the cascade. Gilbert *et al.* synthesized 100 g of 3'-SL starting from 75 mM Lac, Neu5Ac, PEP, 4 mM CMP, and 0.4 mM ATP at 2.2 L scale [302]. Nahálka *et al.* presented the concept of CMP regeneration by using PolyP_n for synthesis of 3'-SL from ManNAc, however, it was not experimentally demonstrated [129]. Woo *et al.* synthesized 3'-SL to a titer of 40 g/L (63 mM) from 80 mM of GlcNAc, Pyr, Lac, 10 mM CMP, 1 mM CTP, and 200 mM acetylphosphate [240]. The study was performed by an industrial company (GeneChem Inc., South Korea) and the produced 3'-SL and 6'-SL are claimed to be available at industrial scales under the Siallac3® and Siallac6® brands, respectively.

The results obtained in this work for synthesis of 6'-SL are 6.6 and 3.7-fold less than reported titers by Woo *et al.* [240], based on the coupling and modular approaches, respectively. However, PolyP_n is significantly cheaper than acetylphosphate and is easily available at industrial scales. Therefore, with further optimization, the industrial applicability of the developed strategies would be very promising.

In all three cascades based on the coupling approach, PolyP_n was used as the phosphate source, which offers significant cost advantages compared to PEP and acetylphosphate. The developed cascades for synthesis of HMOs with sugar nucleotide regeneration were presented as the proof-of-concept study in this work. Clearly, usage of purified enzymes and relatively low titers are among the disadvantages of the presented cascades.

The costs of enzyme production have been estimated to be in the range of ~8–35 € per kg of protein [158,171]. In the study by Tufvesson *et al.* [176], enzyme costs were estimated to be ~180 and ~1100 €/kg of crude extract and purified enzymes, respectively. For instance, the minimum and maximum enzyme cost for synthesis of 1 kg 6'-SL would fall in the range of 3–360 €. Considering the current performance of the cascade, the cost of raw material is ~680 € for a kg of 6'-SL. However, if the titer can be improved to ~40 g/L, the cost of 6'-SL would decrease to ~100 €/kg. Therefore, combination of reaction engineering and usage of crude enzymes would make such cascades as an economically viable strategy.

4.2.3.2 Modular strategy

At first, sugar nucleotides were produced through the cascades presented in the section 4.1. Afterwards, synthesis of HMOs was performed by mixing the cascade products with a glycosyltransferase and an acceptor.

The concept of modular synthesis was practically demonstrated by Prudden *et al.*, who synthesized a broad spectrum of simple and complex HMOs [26]. However, excess amounts of sugar nucleotides were used to allow the high-yield synthesis by using mammalian cell-derived glycosyltransferases.

Large-scale synthesis of HMOs based on the modular strategy has been performed in an industrial setting [28]. In a 100 L scale, 250 g of LNT II was produced from UDP-GlcNAc and Lac through a reaction catalysed by β 1,3GlcNAcT (LgtA). In the subsequent 100 L scale synthesis, more than 300 g of LNnT was produced from LNT II and UDP-Gal by using β 1,4GalT (LgtB). In the next step, 50 g of LST_D was produced from LNnT and 3'-SL at a 5 L scale [28]. The results by Johnson *et al.* clearly illustrate the scalability of HMOs synthesis based on the modular approach [28]. However, no information was provided on the source of the sugar nucleotides.

Modular approach synthesis can be evaluated as a plug-and-play process in which essentially any type of HMOs (or other oligosaccharides) can be synthesized. One of the disadvantages of the modular strategy can be accumulation of by-products such as phosphate and mono- or diphosphate nucleotides. In the work of Prudden *et al.*, AP was used in high amounts to shift the equilibrium toward the synthesis of HMOs [26]. Rech *et al.* avoided the inhibitory role of UDP during poly-*N*-acetyllactosamine synthesis by using AP [303]. It has also been suggested that the presence of released nucleotides might result in low yields of glycosylation as well as an increase in hydrolysis of sugar nucleotides (by

glycosyltransferases) [26,41,217,303,304]. In this work, the role of AP was investigated in the synthesis of LacNAc. The addition of AP to the reaction mixture resulted in a 13% higher synthesis yield. On the other hand, there are multiple reports on high-yield (>90%) synthesis of HMOs based on OPME systems in which high accumulation of nucleotides takes place [125,126]. It can be concluded that the presence of AP is beneficial rather than mandatory in glycosylation reactions and that each case needs to be investigated individually. A significant advantage of synthesizing sugar nucleotides starting from nucleosides can be highlighted once AP is used in oligosaccharide synthesis. Through the development of efficient separation methods, released nucleosides can be separated and re-used for synthesis of sugar nucleotides. This concept can offer significant cost advantages for large-scale production of HMOs.

In a sequential modular synthesis, dilution of the compounds due to addition of donor or acceptor solutions can be a disadvantage. For instance, complex HMOs, such as LNFP V and *para*-LNnH that are synthesized through modular synthesis in this work had very low titers due to dilution from previous steps. Therefore, for large-scale applications, intermediary purification steps might be beneficial to achieve relatively high titers.

A simple cost calculation for modular synthesis of 6'-SL (based on current process metrics) results in ~400 €/kg. Therefore, in comparison to coupling approach, it is ~40% cheaper to synthesize 6'-SL through modular synthesis. However, this comparison was for demonstration purposes, and a detailed techno-economic analysis needs to be performed to have a systematic comparison.

One of the advantages of the modular approach compared to the coupling approach is the low number of enzymes in the system. Since only a glycosyltransferase (and AP) is required, reaction optimization will be relatively simple compared to multi-enzyme systems. The main purpose of this study was to demonstrate the synthesis of HMOs by using sugar nucleotides cascade products (without any purification) and Leloir-glycosyltransferases. As human milk consists of multiple oligosaccharides, a potential technology for their synthesis would therefore ideally need to allow the synthesis of the maximum number of HMOs. This idea was the main driving force for developing the modular synthesis approach as a platform technology for HMOs synthesis. Evidently, for practical scale synthesis of HMOs based on the modular approach, optimization, specifically in terms of product titer, should be performed.

4.3 Development of an artificial Golgi for protein glycoengineering

Here, the developed strategies for glycoengineering of therapeutic glycoproteins are described. In the first step, *in vitro* addition of terminal Gal to a few therapeutic antibodies were investigated. In the next step, the efforts for establishment of an *E. coli*-based artificial Golgi platform are described.

4.3.1 *In vitro* glycoengineering of therapeutic antibodies

In this section, commercial β 1,4GalT and UDP-Gal were used to investigate the galactosylation of mAbs — a known engineering strategy for enhancement of ADCC activity [41]. The glycosylation profiles were analyzed by xCGE-LIF and the electropherogram of glycans before and after *in vitro* addition of Gal are shown in Figure 4.42.

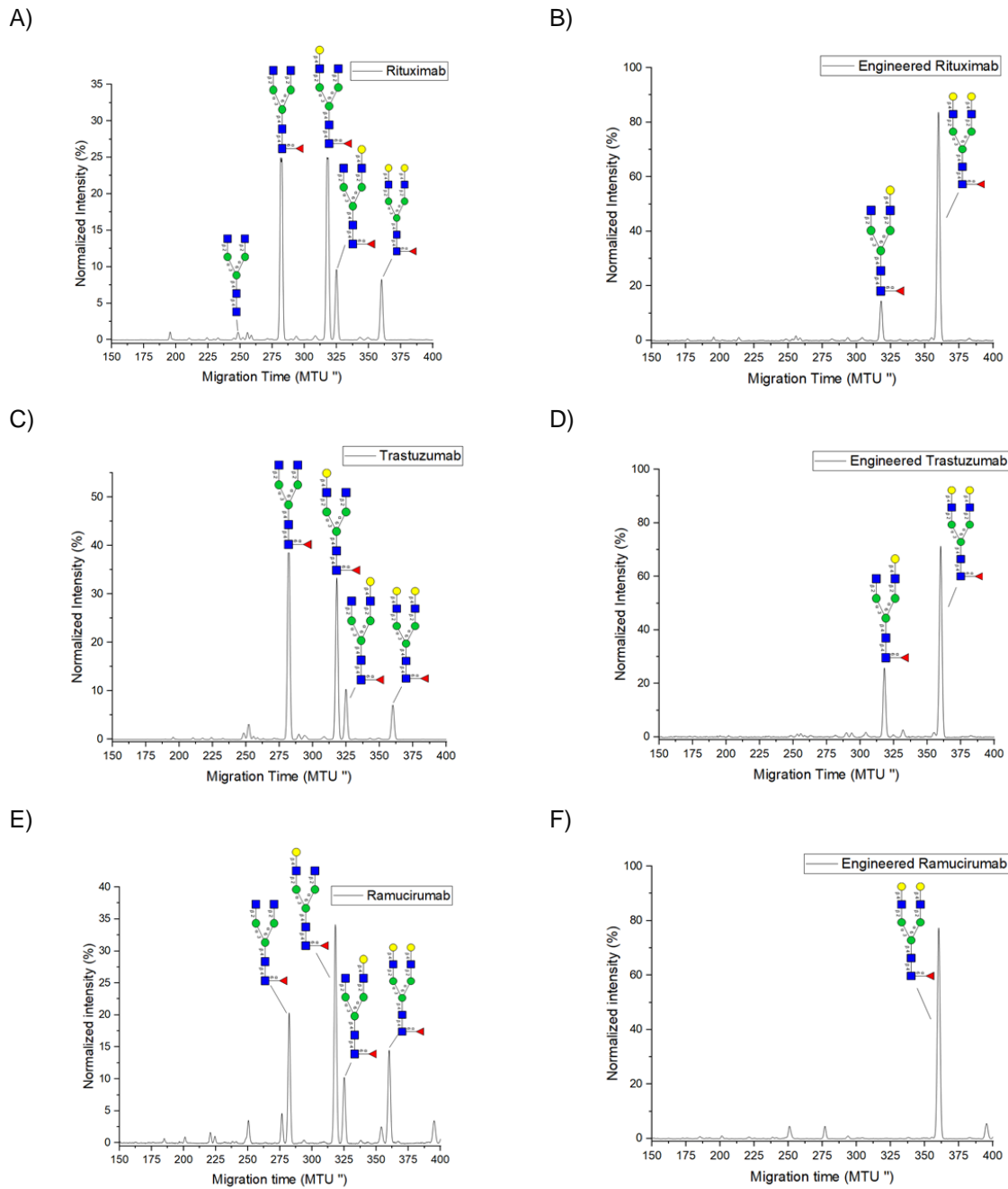


Figure 4.42. Glycosylation profile of therapeutic antibodies before and after in vitro glycoengineering. (A) Glycosylation profile of Rituximab. (B) Glycosylation profile of in vitro glycoengineered Rituximab. (C) Glycosylation profile of Trastuzumab. (D) Glycosylation profile of in vitro glycoengineered Trastuzumab. (E) Glycosylation profile of Ramucirumab. (F) Glycosylation profile of in vitro glycoengineered Ramucirumab. Experiments were performed as follows: 100 μg of each protein was incubated in 50 mM MES buffer (pH 6.5), 50 milli units of $\beta 1,4\text{GalT}$ (from bovine milk, Merck, Germany); 5 mM UDP-Gal, and 5 mM MnCl_2 in a total volume of 100 μL for ~ 20 h at 37°C and 550 rpm. Abbreviation: MTU'', migration time unit. The "''" means that the MTU was normalized for two times.

To evaluate the ADCC activity of mAbs before and after glycoengineering, low affinity immunoglobulin gamma Fc region receptor III-A (Fc γ RIIIa¹) affinity chromatography was performed as described in the

¹ Fc γ RIIIa is a receptor expressed on the surface of natural killer cells that facilitates ADCC by binding to Fc region of antibodies [366].

section 3.7.6. Samples were injected onto the column and eluted by a linear pH gradient from 6.5 to 4.5. The results are illustrated in Figure 4.43.

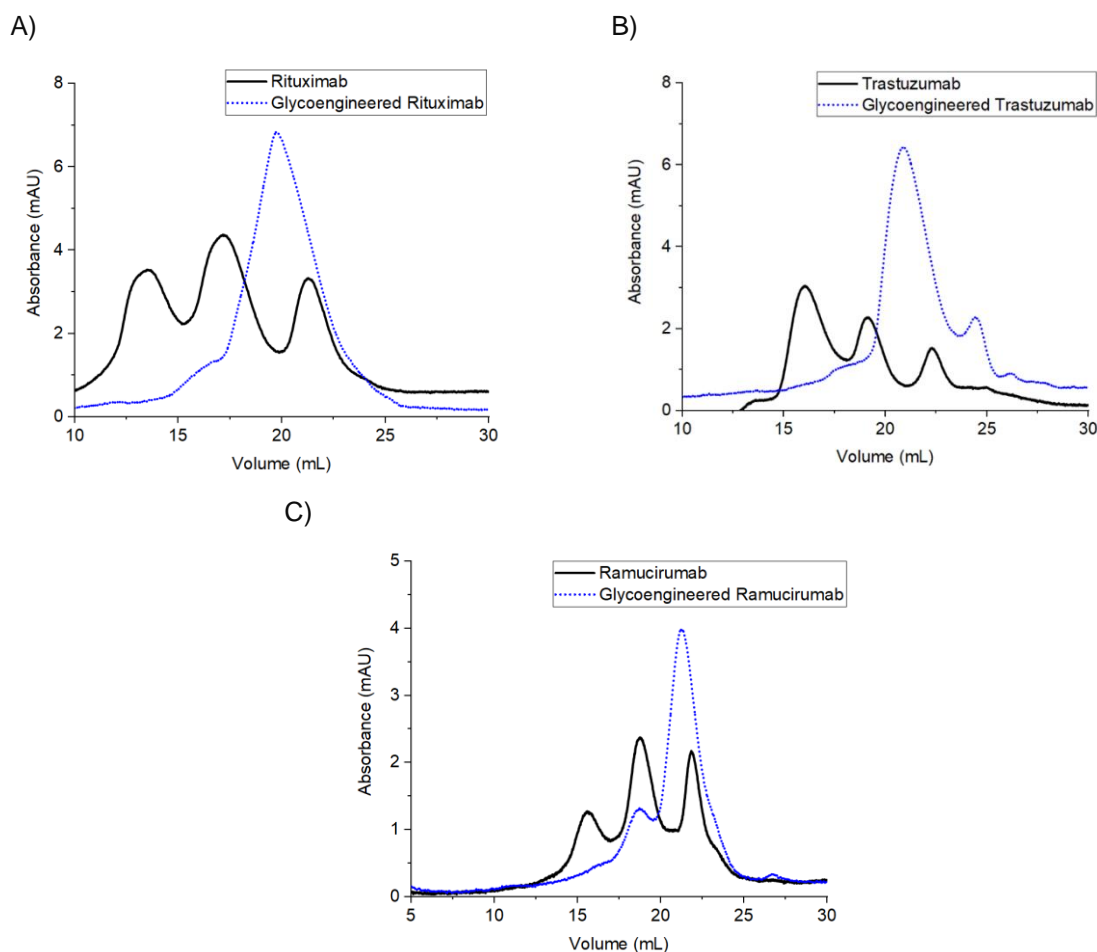


Figure 4.43. UV chromatogram of Fc γ R-IIIa affinity chromatography of original and engineered mAbs. (A) Rituximab and glycoengineered Rituximab. (B) Trastuzumab and glycoengineered Trastuzumab. (C) Ramucirumab and glycoengineered Ramucirumab. The elution after higher amount of desorption buffer (more acidic condition) represents stronger binding of glycoengineered antibodies to the Fc γ R-IIIa receptors and accordingly, higher ADCC activity.

The original mAbs showed three major peaks in the ADCC assay, which correlate to the three main glycans of G0F, G1F, and G2F structures. Based on the literature describing the ADCC chromatography of the original material (black curve, from left to right in each graph) the first peak refers to G0F structure, the second peak refers to G1F structure, and the last peak refers to G2F structure [305,306]. Therefore, among these three major glycoforms, G2F has the strongest binding to Fc γ RIIIa receptors since it elutes in the more acidic condition. After *in vitro* glycoengineering through addition of terminal Gal, these three major structures (i.e., G0F, G1F, and G2F) were mainly converted to G2F structure (see Figure 4.42). Therefore, it is expected that in the ADCC assay the majority of glycoengineered mAbs will elute as one dominant peak in the more acidic conditions than G0F and G1F. As it is shown in Figure 4.43, glycoengineered mAbs are eluting in the more acidic condition compared to their original form. Therefore, enzymatic addition of terminal Gal to mAbs resulted in the enhancement of their ADCC activity.

The first approved glycoengineered antibody — i.e., Obinutuzumab, produced by Roche GlycoMAB® technology — used a different engineering approach. The glycoengineering was performed by overexpression of Golgi α -mannosidase II (Man II) and β -1,4-mannosyl-glycoprotein 4- β -*N*-acetylglucosaminyltransferase (MGAT3) — the latter of which is responsible for addition of bisecting GlcNAc [307,308]. The reason behind this strategy is that bisecting GlcNAc inhibits addition of core Fuc [9,309]. Therefore, the increase of ADCC activity is achieved by lack of core Fuc [310].

I hypothesized that the addition of terminal Gal can even further contribute to ADCC activity of Obinutuzumab. Upon addition of terminal Gal, Fc γ RIIIa affinity chromatography was performed (Figure 4.44). Interestingly, addition of terminal Gal resulted in stronger binding to human Fc γ RIIIa receptors, which essentially emphasizes enhanced ADCC activity compared to the reference materials.

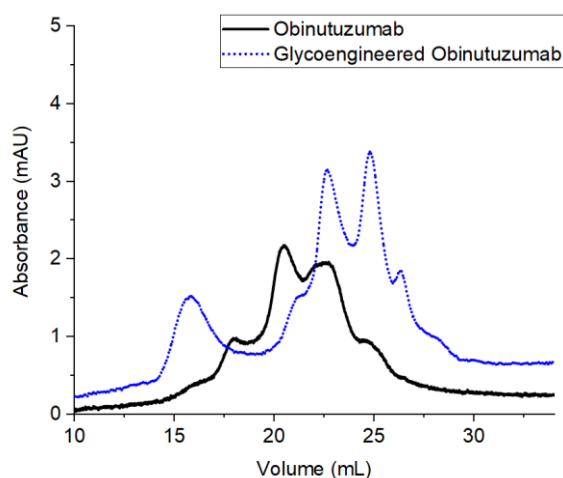


Figure 4.44. Overlay of FcR-IIIa affinity chromatography of Obinutuzumab and *in vitro* glycoengineered Obinutuzumab. Clearly, galactosylated version of Obinutuzumab is even further increase its ADCC activity.

Despite clear evidence from *in vitro* assays on ADCC enhancement of mAbs upon galactosylation, industrial implementation of *in vitro* glycoengineering at large scales can be very costly. This could be mainly due to the high cost of recombinant production of β 1,4GalT in mammalian cells and of UDP-Gal. In previous sections, a cost-efficient platform for synthesis of UDP-Gal was demonstrated. Therefore, I hypothesized that recombinant production of human β 1,4GALT1 (Gene: β 4GalT1) in low-cost expression hosts (e.g., *E. coli*) could bring *in vitro* glycoengineering closer to large scale applications.

The truncated version of β 1,4GALT1 (the luminal side of the enzyme) was recombinantly produced as a soluble protein in *E. coli* and was purified in its active form. In Figure 4.45, addition of terminal Gal to IgG (produced by CHO-DP12 cells) by means of *E. coli*-derived β 1,4GALT1 is illustrated.

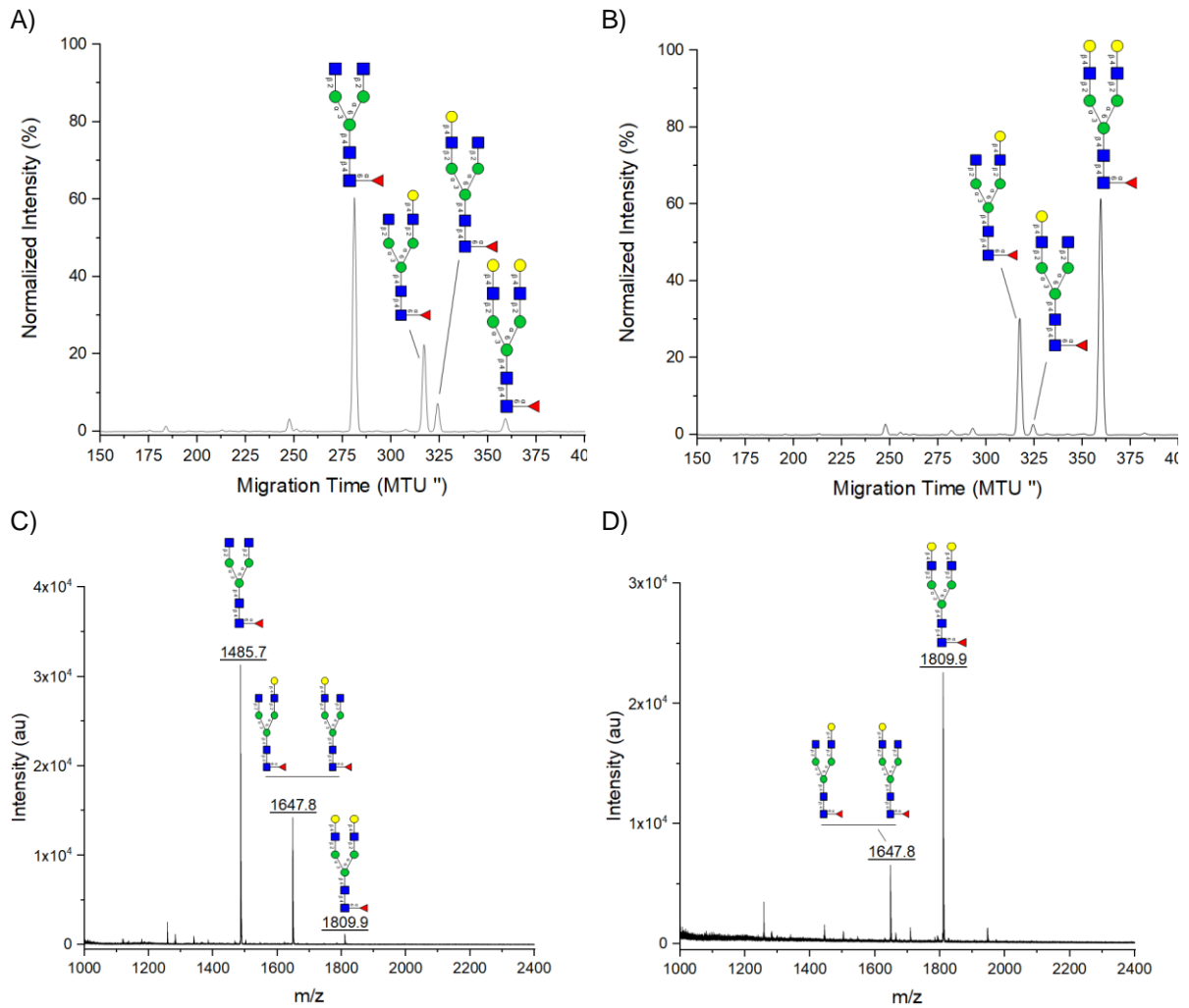


Figure 4.45. Results of *in vitro* addition of terminal Gal to CHO-DP12 derived IgG. A) Electropherogram of APTS-labeled glycan from IgG. B) Electropherogram of APTS-labeled glycan from glycoengineered IgG. C) Mass spectra of released glycan from IgG, G0F theoretical mass $[M+Na]^+$:1485.5 Da, G1F theoretical mass $[M+Na]^+$:1647.6 Da, G2F theoretical mass $[M+Na]^+$:1809.6 Da. The reaction contained 0.13 mg pure IgG (cell culture derived); 190 mM MES buffer pH 6.5; 14 mM $MnCl_2$; 1.4 mM UDP-Gal (pure, commercial), and 0.3 $\mu\text{g}/\mu\text{L}$ $\beta 1,4\text{GALT1}$ in a total volume of 211 μL . The samples were analysed after 24 h of incubation at 37°C and 550 rpm.

This observation demonstrates the active expression of human $\beta 4\text{GalT1}$ gene in *E. coli* which increase the potential of *in vitro* glycoengineering for large-scale applications.

4.3.2 Design and development of an artificial Golgi platform

As clearly stated in literature, lack of core Fuc can substantially contribute to an increase in ADCC activity [9]. Furthermore, terminal Gal can also positively contribute to enhancement of ADCC [9]. Therefore, the construction of a platform for the production of antibodies with no Fuc but containing terminal Gal, can be a very promising technology for development of glycoengineered antibodies. The concept can also be used for development of glycoproteins with any desired glycoforms as long as the glycans are accessible by enzymes. Here, a microbial-based platform is proposed to act as an artificial Golgi for tailoring the glycosylation profile of antibodies. The concept of an artificial Golgi is illustrated in Figure 4.46 — which is essentially similar to the *in vivo* process [31]. This platform is a combination of the *in vivo* and *in vitro* glycoengineering approaches in which high mannose (Man9) antibodies would be converted to fully galactosylated antibodies — without any core Fuc.

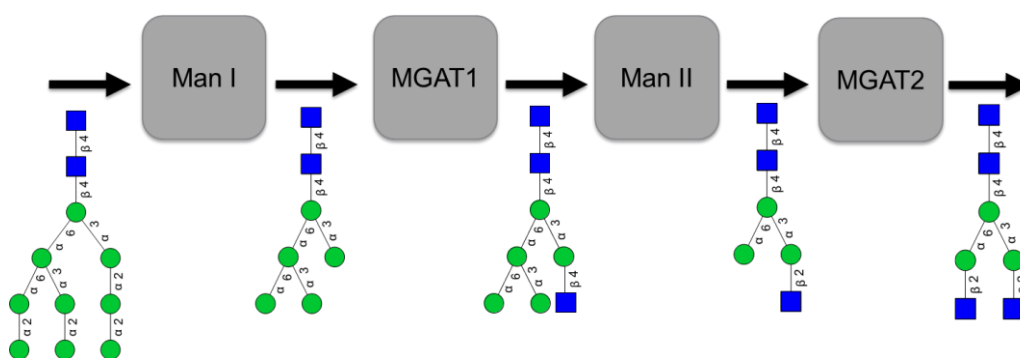


Figure 4.46. Illustration of the concept of artificial Golgi. Man9 glycoproteins are produced by treatment of the host cells with a mannosidase I inhibitor e.g., kifunensine. Afterwards, Man9 structure can be trimmed and tailored into any desired structure. It should be noted that the concept is only practical once the glycans are available to glycosidase and glycosyltransferases. Abbreviation: Man I, α -1,2-mannosidase; MGAT1, α -1,3-mannosyl-glycoprotein 2-beta-N-acetylglucosaminyltransferase; Man II, Golgi α -mannosidase II; MGAT2, α -1,6-mannosyl-glycoprotein 2-beta-N-acetylglucosaminyltransferase.

APTS-labeled glycan was used for demonstration of the concept of the artificial Golgi. Both MGAT1 and MGAT2 were used in their purified form. At first, Man3-G0 structure was synthesized from Man3 (Figure 4.47A) through the reaction catalysed by MGAT1 (Figure 4.47B). Synthesis of G0 structure was performed in a one-pot approach starting from Man3 in the presence of MGAT1 and MGAT2 (Figure 4.47C). Both MGAT1 and MGAT2 were produced in their soluble and active form in *E. coli*. To the best of author's knowledge, the active expression of MGAT2 in *E. coli* is reported for the first time in this work.

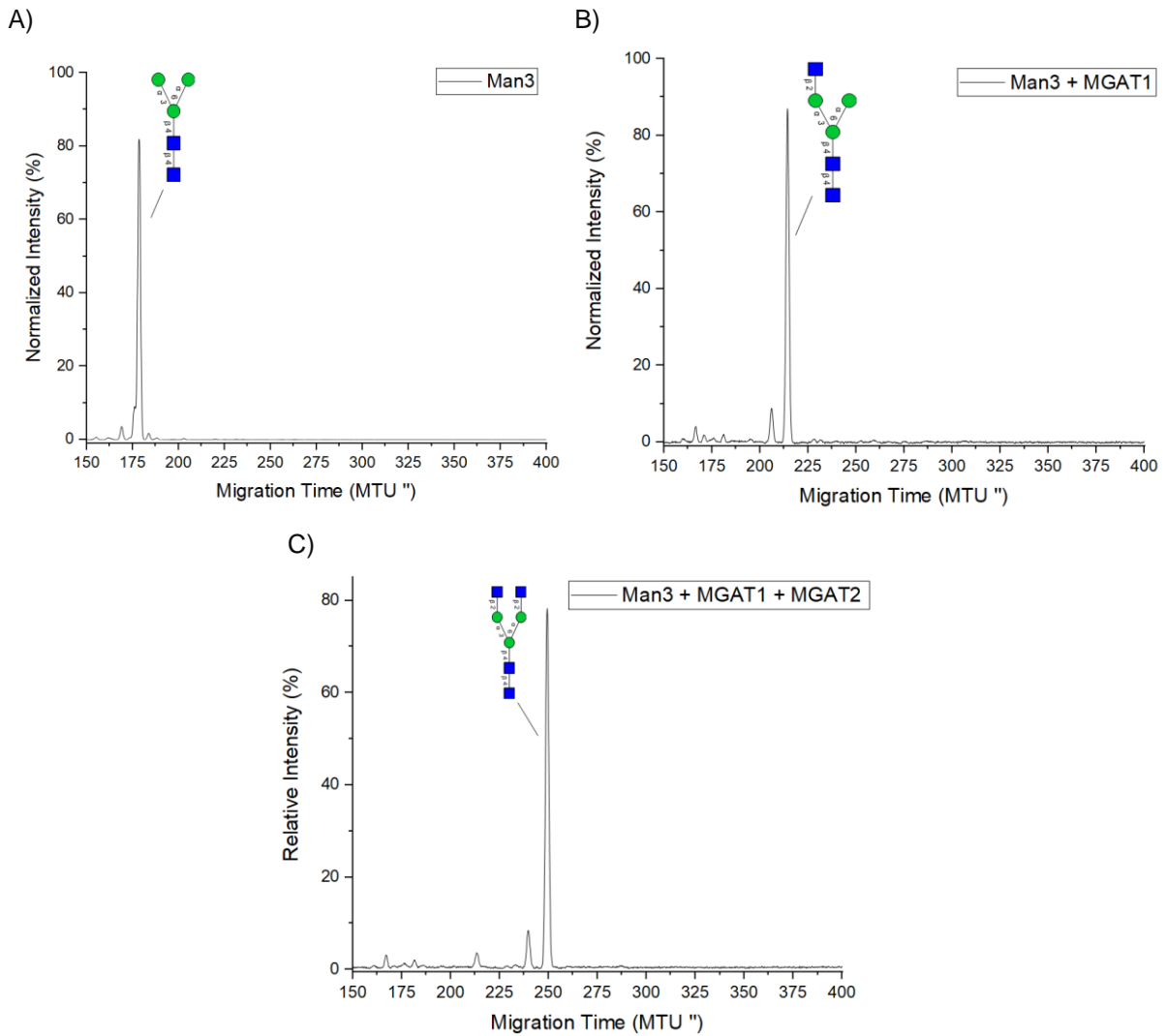


Figure 4.47. Results of different steps for synthesis of Man3-G0 from Man3. A) Analysis of APTS-labeled Man3 which was used as the substrate. B) Activity of MGAT1 on APTS-labeled Man3. C) One-pot conversion of Man3 to G0 by using MGAT1 and MGAT2. The reaction for conversion of Man3 to Man3-G0 consisted of 50 μ L APTS-labeled Man3; 1.8 mM UDP-GlcNAc; 93 mM HEPES buffer (pH 7.4); 9.3 mM $MnCl_2$, and 0.3 μ g/ μ L MGAT1 in a total volume of 107 μ L. The experiment for synthesis of Man3-G0 from Man3 was as follows: 100 mM HEPES buffer (pH 7.4); 10 mM $MnCl_2$; 2.5 mM UDP-GlcNAc; 50 μ L Man3; 0.1 μ g/ μ L MGAT1, and 0.3 μ g/ μ L MGAT2 in a volume of 200 μ L. The samples were analyzed after 6 h incubation at 37°C and 550 rpm.

Addition of terminal Gal can be carried out as described in the section 4.3.1. However, the main challenge in developing an artificial Golgi platform is the synthesis of G0 structure on intact proteins. Therefore, I decided to use intact proteins to realize the concept of artificial Golgi in practical conditions.

For production of Man9 mAbs, kifunensine — a known inhibitor of Man I — was added to the cell culture as described in section 3.6. Therefore, by inhibiting the removal of Man from Man9 structure, further glycan processing will not take place. The glycosylation profile of antibodies from kifunensine treated cell culture is shown in Figure 4.48.

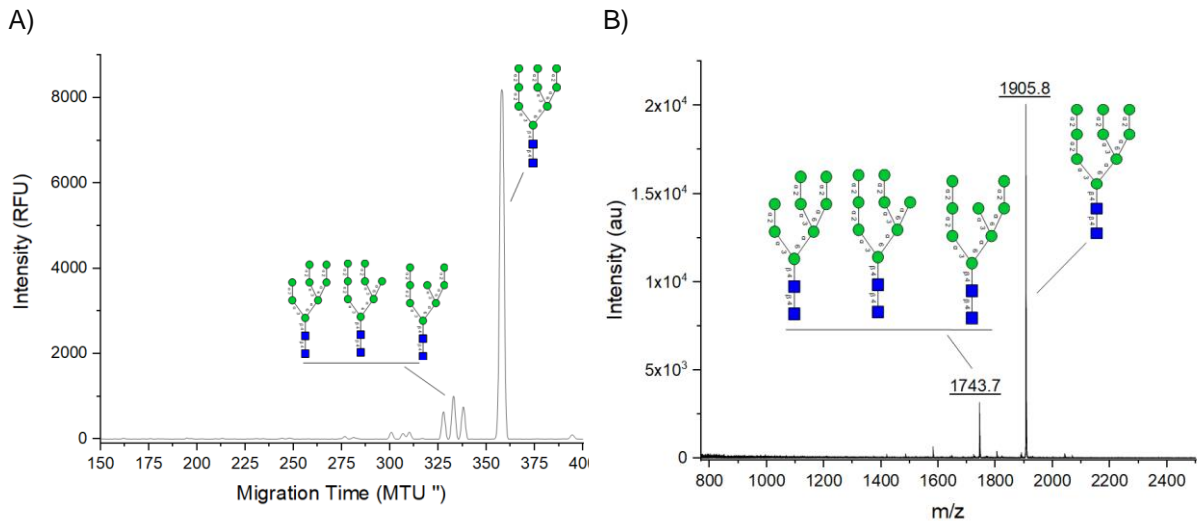


Figure 4.48. Production of anti-interleukin 8 antibody with Man9 glycosylation profile. A) CGE-LIF electropherogram of glycans from kifunensin-derived IgG. B) Mass spectra of released glycan from kifunensin-derived IgG, theoretical Man9 mass $[M+Na]^+$:1905.6 Da, theoretical Man8 mass $[M+Na]^+$:1743.6 Da. Abbreviation: RFU, relative fluorescence unit.

In the next step, intact Man9 containing antibodies (kifunensine derived IgG), was treated with bacterial α -1,2-mannosidase to produce antibodies with Man5 structure. Bacterial α -1,2-mannosidase was produced as described in Ref. [210]. After ~20 h of incubation, full conversion of Man9 to Man5 antibodies was achieved (Figure 4.49).

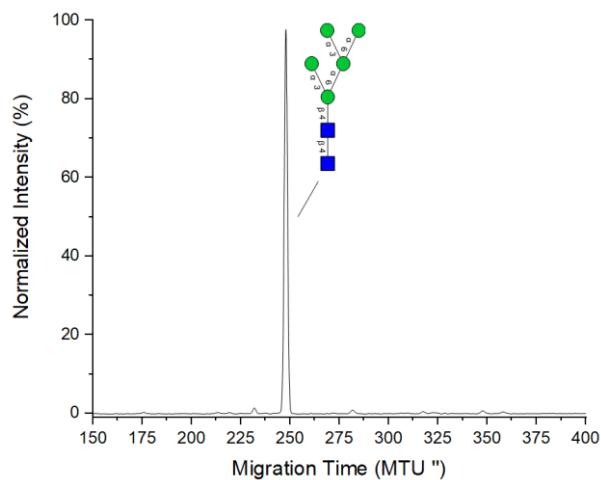


Figure 4.49. Synthesis of antibodies with Man5 structure from Man9-containing antibodies. The conversion was achieved by using bacterial α -1,2-mannosidase. The experimental condition for conversion of Man9 to Man5 antibodies was as follows: 2.4 mg IgG (purified – kifunensine derived); 2.6 μ g/ μ L Man I; 10 mM MgCl₂, and 200 mM MES buffer (pH 6.5) in a total volume of 100 μ L.

After successful synthesis of Man5 containing antibodies, efforts were made for addition of GlcNAc on α -1,3-antenna through the reaction catalyzed by MGAT1. To avoid extra incubation of antibodies in different reaction pots, as well as developing a more practical process, the mannosidase reaction and addition of GlcNAc were carried out in one-pot. The successful one-pot synthesis of Man-G0 structure from Man9 glycans on intact antibody is shown in Figure 4.50.

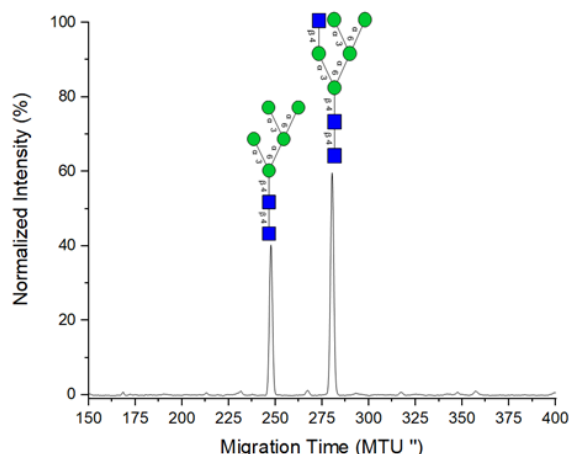


Figure 4.50. One-pot conversion of Man9-containing IgG into Man5 and Man5-G0 IgG. The reaction contained: 1.8 mg Man9 IgG; 1.9 μ g/ μ L Man I; 1.9 μ g/ μ L MGAT1; 1.5 mM UDP-GlcNAc; 10 mM $MgCl_2$; 10 mM $MnCl_2$, and 200 mM MES buffer (pH 6.5) in a total volume of 133 μ L. The experiment was running for 24 h.

As illustrated in Figure 4.46, two Man on the α -1,6-antenna should be trimmed by α -mannosidase 2 (Man II) in the next step. Unfortunately, *E. coli* expression of *Drosophila melanogaster* (fruit fly) Man II was found to be inactive. Therefore, in order to continue the concept of an artificial Golgi, an active Man II is required. There are multiple reports on active expression of Man II in insect or mammalian cell lines [311–313]. However, the purpose of this study was to develop an *E. coli*-based glycoengineering platform. Further work is required for active expression of Man II (or any other specific mannosidase) in microbial hosts which specifically cuts two Man (α -1,6 and α -1,3) on the α -1,6-antenna.

4.3.3 Discussion of *in vitro* glycoengineering of therapeutic proteins

Two different approaches were used for the modification of glycans on therapeutic antibodies. In the first approach, terminal Gal was added to mAb glycans for enhancement of ADCC activity. In the second approach, in combination with an *in vivo* method, high Man containing antibodies were produced and further tailored into Man5-G0 structure.

Gal content in the glycosylation profile of therapeutic antibodies has been the subject of various studies [27,45,314,315]. The main interest in galactosylation of antibodies comes from *in vitro* observations that galactosylated antibodies show higher affinity toward FcγRIIIa receptors, and thus, higher ADCC as well as higher CDC activity [44,45,306]. Therefore, there is growing interest in production of antibodies with high content of terminal Gal [9].

Rituximab was the first mAb approved (in 1997) for treatment of oncology patients [316]. It is still one of the first-line treatment options for mainly all B-cell non-Hodgkin lymphomas [317] and some autoimmune diseases such as rheumatoid arthritis [318]. Therefore, it has a very high clinical value, making it a major blockbuster [34]. Since ADCC is involved in the efficacy of Rituximab [319], this drug was selected as a target for glycoengineering. Due to the resistance of some patients to Rituximab, an improved version of it — Obinutuzumab — was developed to overcome the resistance with improved activity [320].

Trastuzumab is a mAb that was approved in 1998 for treatment of breast cancer that overexpresses human epidermal growth factor receptor 2 [321]. Trastuzumab has been a major success in the field of targeted cancer therapy, making this drug extremely useful and a huge commercial success [34]. As Trastuzumab induces a significant ADCC response [322], it was selected as a model drug for glycoengineering.

Ramucirumab is a mAb (approved in 2014) for treatment of advanced gastric cancer [323]. The role of ADCC has not been clearly investigated in the Ramucirumab mechanism of action, however, the demonstration of the enhancement of ADCC activity might contribute to future drug development efforts.

In the first step, galactosylation of approved antibodies (model glycoproteins) — i.e., Rituximab, Trastuzumab, Ramucirumab, and Obinutuzumab — was achieved by using a commercial galactosyltransferase and UDP-Gal. Afterwards, enhancement of ADCC activity of glycoengineered antibodies was demonstrated through column chromatography. Glycoengineered (galactosylated) mAbs eluted at more acidic conditions than the original ones, which shows the stronger binding to the FcγRIIIa receptors. Interestingly, galactosylation of Obinutuzumab, which is already glycoengineered in terms of having no Fuc, further increased its ADCC activity. This means that combination of afucosylation and galactosylation could be a complementary action for the development of mAbs with superior performance. It has also been suggested that galactosylation increases CDC activity, which results in better efficacy of antibodies [324,325].

In the next step, galactosylation of a CHO cell-derived antibody was demonstrated by using an *E. coli*-derived human β1,4GALT1. This result shows the application of low-cost enzyme production process for engineering of antibodies. Similar to HMOs synthesis, galactosylation of mAbs could be performed

either based on the coupling or modular approach. Both approaches have been used for galactosylation of mAbs (results are reported by the author in Ref. [223]).

There are multiple reports on glycoengineering — e.g., galactosylation and sialylation of different therapeutic proteins — based on Leloir glycosyltransferases [41,44,71,72]. The scalability of this strategy was demonstrated by Warnock *et al.*, where full galactosylation of an IgG was achieved at 1 kg scale (40 L) by using UDP-Gal (source was not mentioned) and a murine cell-derived galactosyltransferase [27]. There are also glycoengineering toolboxes that are commercially available by Roche CustomBiotech (Roche, Germany) for galactosylation and sialylation of glycoproteins. Therefore, it can be concluded that glycoengineering by using Leloir glycosyltransferases, specifically galactosylation, is relatively straightforward. Despite enzymatic glycoengineering having been shown to be one of the main strategies for obtaining homogenous glycoforms [6,10], there is no information on its applicability at industrial scales. One of the reasons might be the high cost of glycosyltransferase production in mammalian cell lines. This challenge was solved in this work through production of human β 1,4GALT1 in a low-cost expression host. Moreover, the unavailability and high cost of UDP-Gal and CMP-Neu5Ac might be among the reasons that *in vitro* glycoengineering has not been realized at industrial scales. This issue was also addressed in this work by developing efficient multi-enzyme cascades for synthesis of UDP-Gal and CMP-Neu5Ac.

There are many reports on modulation of the glycosylation profile of therapeutic proteins by means of media supplementation such as feeding glycosylation precursors [61,64]. For example, Ehret *et al.* achieved 40.9% increase in galactosylation of IgG upon addition of 120 mM Gal, 24 μ M Uri, and 48 μ M Mn²⁺ [62]. However, due to the inherent heterogeneity of cell culture processes and biological limitation of cells in handling media supplements, achieving a homogenous glycosylation profile has not been demonstrated yet.

Despite significant advances in the development of stable glycoengineered cell lines, production of glycoproteins with a homogenous structure has not been achieved [47]. On the contrary, enzymatic glycoengineering has been shown to be a very promising approach for obtaining homogenous glycoforms [10,66,67].

Genetic glycoengineering of mammalian cell lines has been demonstrated in multiple studies [7,47] and commercially developed by different companies such as Glycotope GmbH (Germany), GlycoDisplay (Denmark), Glycart (Now Roche, Germany), and ProBioGen AG (Germany). In the case of mAbs, the majority (if not all) of *in vivo* glycoengineering approaches are focused on the inhibition of core Fuc linkage from glycosylation profile for improvement of ADCC [7].

Recently, patients with severe COVID-19 infection have been discovered to contain afucosylated antibodies [326,327]. This modification in Fc glycosylation of IgGs — performed by the human immune system — could enhance the binding to the Fc γ R1IIa receptors [326,327]. These reports are the first evidence of natural glycosylation modification for enhancement of therapeutic performances of IgGs. A recently approved glycoengineered (afucosylated) antibody, Margetuximab, has been shown to outperform its originator, Trastuzumab, through a head-to-head comparison [328]. Such direct

comparison provides significant insights into developments of glycoengineered drugs with high clinical values.

Despite a high number of *in vitro* studies on ADCC activity enhancement of mAbs upon galactosylation, it is noteworthy to mention that no clinical data is available to prove superior performance (compared to original drugs) of fully galactosylated mAbs in the human body.

Overall, the recent findings on the importance of Fc galactosylation in activation of complement system (part of immune system which enhances the functionality of antibodies) highlight the potential of glycoengineering — in terms of galactosylation — for development of enhanced therapeutic IgGs [329,330].

In the next stage of development, I hypothesized that a platform — an artificial Golgi — for tailoring glycosylation profile of theoretically any glycoprotein to desired structures would add significant values to the glycoengineering field. Evidently, only glycans accessible by enzymes could be modified.

Kifunensine is a known inhibitor of Man I whose usage in cell culture results in production of mannosylated IgGs [331,332] — without sacrificing product titer [331,333]. Kifunensine has been used in various studies and different cell lines for production of homogenous high Man *N*-glycosylated proteins [331,332,334]. Recently, lower-cost Man I inhibitors (e.g., tris, which is 35x more cost effective than kifunensine) have been developed for the production of high Man antibodies [333]. This demonstrates the interests in such an approach for the production of mAbs with homogenous glycoforms.

In this work, kifunensine was used to produce high Man IgGs (Figure 4.48). Full conversion of Man9 to Man5 was achieved by using a recently reported bacterial Man I [210].

It has been reported that the presence of GlcNAc on α -1,3-antenna (i.e., Man5-G0 structure) is required for activity of Man II [311]. Therefore, before experimenting the activity of Man II, addition of GlcNAc to Man5 was performed. Since activity of MGAT1 and bacterial Man I overlap in terms of pH, co-factor, and temperature, a one-pot experiment was performed to convert Man9 IgG into Man5-G0 structure (Figure 4.50).

Further expansion of the platform requires an active Man II. Unfortunately, bacterial expression of fruit fly Man II was found to be inactive. Evidently, insect cell or mammalian cell derived Man II can be used to extend the platform, however, the high cost of enzyme production in such hosts could challenge the advantage of a low-cost artificial Golgi platform. Therefore, active expression of Man II in *E. coli* or other low-cost microbial expression host will be the subject of further studies.

The developed artificial Golgi in this work can be very well-suited in combination with other glycoprotein expression hosts such as insect cell lines where Man3 structures are the main form of glycosylation [335]. This idea was demonstrated in a study by our group in Ref. [336]. The developed platform — a combination of MGAT1, MGAT2, and β 1,4GALT1 — was used in a sequential one-pot approach for glycoengineering insect cell-derived severe acute respiratory syndrome coronavirus 2 (SARS-CoV-2)

spike glycoprotein [336]. A fraction of fucosylated Man3 structures were successfully converted to G2F structure [336].

Furthermore, the concept of a low-cost microbial-based artificial Golgi platform can be a valuable complement to low-cost microbial hosts (e.g., yeast) for glycoprotein production. For instance, De Pourcq *et al.* glycoengineered *Yarrowia lipolytica* to produce glycoproteins with Man3 structure [337]. In such cases, further glycan modification could be achieved through combination of MGAT1, MGAT2, and β 1,4GALT1. This was an example of how microbial-based processes could contribute to production of complex therapeutic biologics by combining *in vivo* and *in vitro* glycoengineering. Therefore, through the advancement of concepts such as artificial Golgi, microbial-based processes could gain great potentials in usage for low-cost production of therapeutic glycoproteins.

Despite sialylation of glycoproteins not being investigated in this study, there are reports on the activity of microbial sialyltransferases for the addition of sialic acid on terminal Gal of glycoprotein [338,339]. Therefore, the multi-enzyme cascades for synthesis of CMP-Neu5Ac could be very practical for sialylation of glycoproteins and, together with 2,6ST, further expand the concept of an artificial Golgi.

The theoretical concept of an artificial Golgi has been previously demonstrated in Ref. [340]. In an experimental study, Hamilton *et al.* showed the synthesis of different lipid-linked glycoforms by means of microbial-derived glycosyltransferases [341]. However, no Man II was used, and utilization of *Canavalia ensiformis* (jack bean) α -mannosidase resulted in trimming the core structure into only one Man. The concept of glycoprotein production with linear glycoforms by using engineered *E. coli* lysate has been shown in these Ref. [342,343].

The presented methods for glycoengineering have high potential for large-scale implementation, especially for development of fully galactosylated mAbs. However, in order to confidently comment on the practicality of *in vitro* glycoengineering methods for development of superior drugs, clinical data is required. Therefore, development of processes for clinical trial of mAbs would significantly contribute to the development of next generation of therapeutic glycoproteins.

4.4 Process development and scale-up of multi-enzyme systems

Application of purified enzymes for large-scale synthesis is largely limited due to the high cost of purification process [176]. Moreover, some common purification methods, e.g., nickel-nitrilotriacetic acid (Ni-NTA) chromatography, can cause problems such as leaching of metal ions into enzyme solutions and in product streams up to, for example, nickel concentration of 20 mM [344].

In this section, three different strategies are described for the development of large-scale multi-enzyme production of sugar nucleotides.

At first, direct usage of cell lysate was evaluated as the final form of biocatalyst to synthesize sugar nucleotides. In the next step, co-expression of six enzymes was performed to minimize the number of fermentations for production of biocatalysts. In the last step, co-immobilization of enzymes on solid supports are demonstrated to allow the multiple usage of biocatalysts.

4.4.1 Scale-up of multi-enzyme cascades

In this part, direct application of centrifugally clarified cell lysate was used instead of purified enzymes for scale-up of multi-enzyme systems.

4.4.1.1 Large-scale synthesis of UDP-Gal

The biocatalyst for synthesis of UDP-Gal at 1 L scale was prepared as described in section 3.4.1. To understand the role of scale-up on the performance of the cascade, a parallel 200 μ L experiment was carried out. The time course of Uri consumption and UDP-Gal production at both scales are shown in Figure 4.51. In a batch time of 23 h, UDP-Gal was successfully produced to a concentration of 41.3 mM (23.4 g/L) and synthesis yield of 75% respect to Uri and Gal. The ATP was used 26 \times less than the stoichiometric amounts and the biocatalyst load was 0.05 $\text{g}_{\text{total_protein}}/\text{g}_{\text{product}}$.

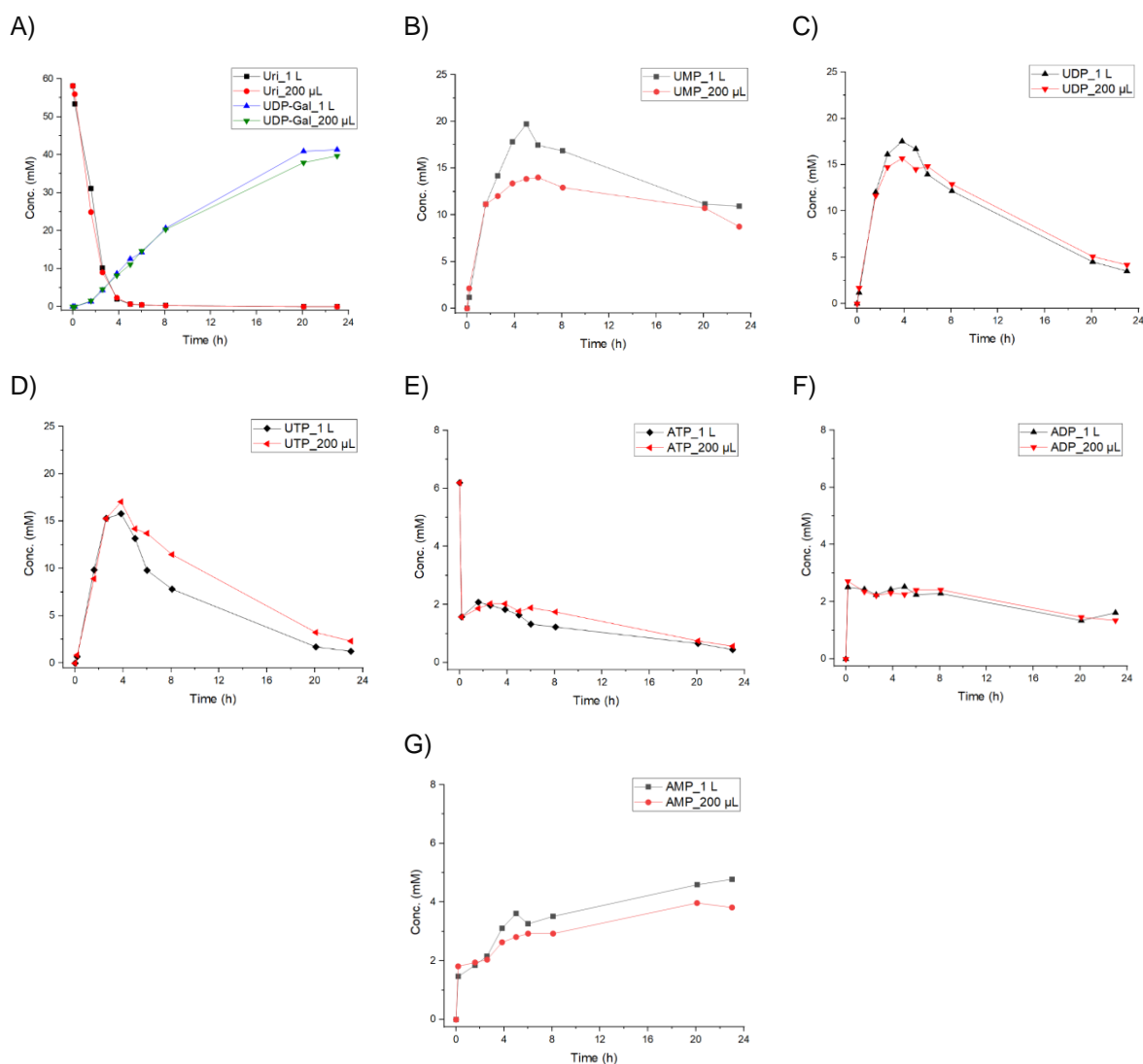


Figure 4.51. 1 L scale and 200 μL synthesis of UDP-Gal using the supernatant from a cell lysate at 37°C and 60 rpm (magnetic stirrer): A) Uri and UDP-Gal; B) UMP; C) UDP; D) UTP; E) ATP; F) ADP; G) AMP. The synthesis condition was as follows: 150 mM Tris-HCl (pH 8.5); 55 mM Uri; 55 mM Gal; 6.2 mM ATP; 20 mM PolyP_n, and 75 mM MgCl₂.

4.4.1.2 Large-scale synthesis of UDP-GlcNAc

The results presented here are also described in a patent application under PCT/EP2020/077383 [345]. The biocatalyst was prepared as described in section 3.4.2. To understand the effect of scale-up on the performance of the cascade, a parallel 200 μL experiment was performed. The time course of the cascade components is shown in Figure 4.52. During the batch time of 25.2 h, UDP-GlcNAc was produced to a final concentration of 53 mM (32.2 g/L) and a synthesis yield of 85.6% (regarding Uri). The ATP was used $\sim 100\times$ less than the stoichiometric amount and the biocatalyst load was 0.01 $\text{g}_{\text{total_protein}}/\text{g}_{\text{product}}$.

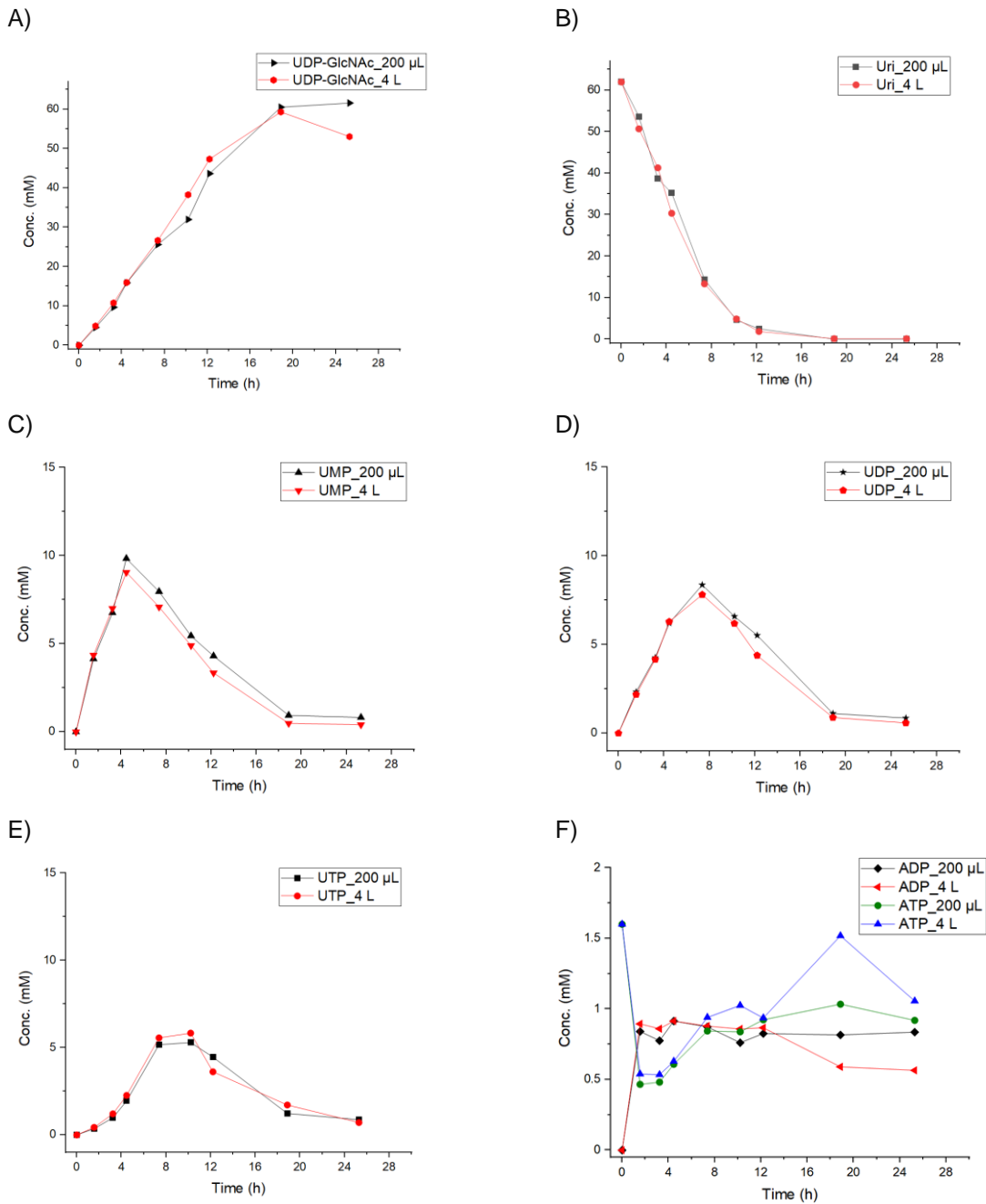


Figure 4.52. Time course of reaction substrates, intermediate, and products for large-scale synthesis of UDP-GlcNAc. (A) UDP-GlcNAc, (B) Uri, (C) UMP, (D) UDP, (E) UTP, (F) ADP and ATP. The synthesis condition was as follows: 200 mM Tris-HCl (pH 8.5); 62 mM Uri; 62 GlcNAc; 1.6 mM ATP; 18 mM PolyP_n; 75 mM MgCl₂, and a total protein load of 0.5 g/L in the form of cell lysate. The reaction carried out at 37°C and 120 rpm.

4.4.2 Co-expression of enzymes

One of the strategies to bring the concept of multi-enzyme synthesis closer to large-scale implementation is co-expression of needed enzymes in a single strain. Therefore, in this part of the thesis, a strategy is proposed for recombinant production of all necessary enzymes for synthesis of a sugar nucleotide(s) in one strain.

At first, a strategy is proposed for co-expression of six enzymes to enable the synthesis of UDP-GlcNAc and UDP-Gal. In another example, three enzymes were co-expressed for synthesis of CMP-Neu5Ac.

4.4.2.1 Co-expression of six enzymes for synthesis of UDP-GlcNAc and UDP-Gal

The concept of a six-enzyme cascade for synthesis of UDP-GlcNAc and UDP-Gal is shown in Figure 4.53. The cascade for synthesis of UDP-GlcNAc was previously published by the author [221]. The enzyme promiscuity of GALU facilitates the synthesis of UDP-GlcNAc and UDP-Gal, respectively, from UTP and the respective sugar-1 phosphate.

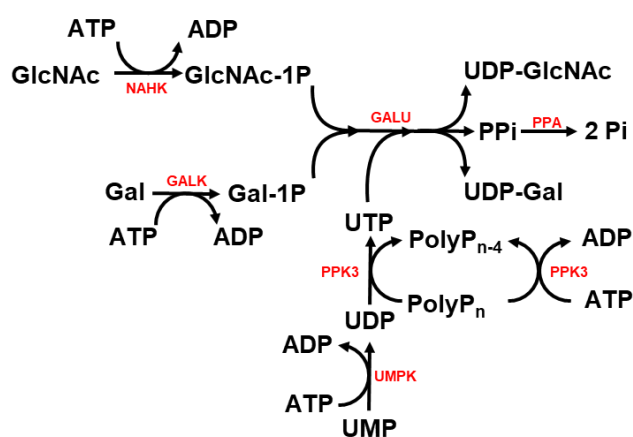


Figure 4.53. Combination of six enzymes for production of uridine diphosphate N-acetylglucosamine (UDP-GlcNAc) and uridine diphosphate galactose (UDP-Gal) from uridine monophosphate (UMP), N-acetylglucosamine (GlcNAc), galactose (Gal), polyphosphate (PolyP_n), and catalytic amounts of adenosine triphosphate (ATP). Abbreviations: UDP, uridine diphosphate; UTP, uridine triphosphate; GlcNAc-1P, N-acetylglucosamine 1-phosphate; Gal-1P, galactose 1-phosphate; PPi, diphosphate; Pi, phosphate; ADP, adenosine diphosphate; UMPK, UMP/CMP kinase; PPK3, PolyP_n kinase; GALU, glucose 1-phosphate uridylyltransferase; NAHK, N-acetylhexosamine 1-kinase; GALK, galactokinase; PPA, inorganic diphosphatase.

To limit the number of enzyme expression runs, all gene were cloned into compatible Duet™ vectors (see section 3.4.33.4.3.1) [173]. Subsequently, an *E. coli* strain was generated harboring all three plasmids and all six enzymes were successfully produced in their soluble form in one fermentation run. Since each enzyme was His-tagged, one single immobilized metal affinity chromatography run was performed to purify all enzymes. The activity of the purified cascade was confirmed by the successful production of UDP-GlcNAc, and UDP-Gal in individual reaction runs (data not shown). However, as mentioned earlier, using crude form enzymes has significant cost advantages over using purified enzymes.

The biocatalyst for synthesis of UDP-GlcNAc by using co-expressed enzymes was prepared as describe in section 3.4.3.1.1. In order to find the optimal substrate and biocatalyst load, several

screening runs were performed in volumes of 200 μL at 37°C. After screening various conditions, it was found out substrate loads of 50 mM UMP, GlcNAc and a biocatalyst amount of 0.5 g/L resulted in the highest yield. Therefore, these concentrations were used subsequently in the synthesis scale-up. To evaluate the scale-up effect, a parallel 200 μL scale was carried out. The time course of reaction components is shown in Figure 4.54. After a batch time of 18 h, UDP-GlcNAc was produced to a titer of 42.7 mM (25.9 g/L) and synthesis yield of 90% (regarding UMP). The ATP was used 20x less than the stoichiometric amount and the biocatalyst load was 0.02 $\text{g}_{\text{total_protein}}/\text{g}_{\text{product}}$. The similar behavior of cascade intermediates at 200 μL and 150 mL scale emphasizes the linearity of scale-up.

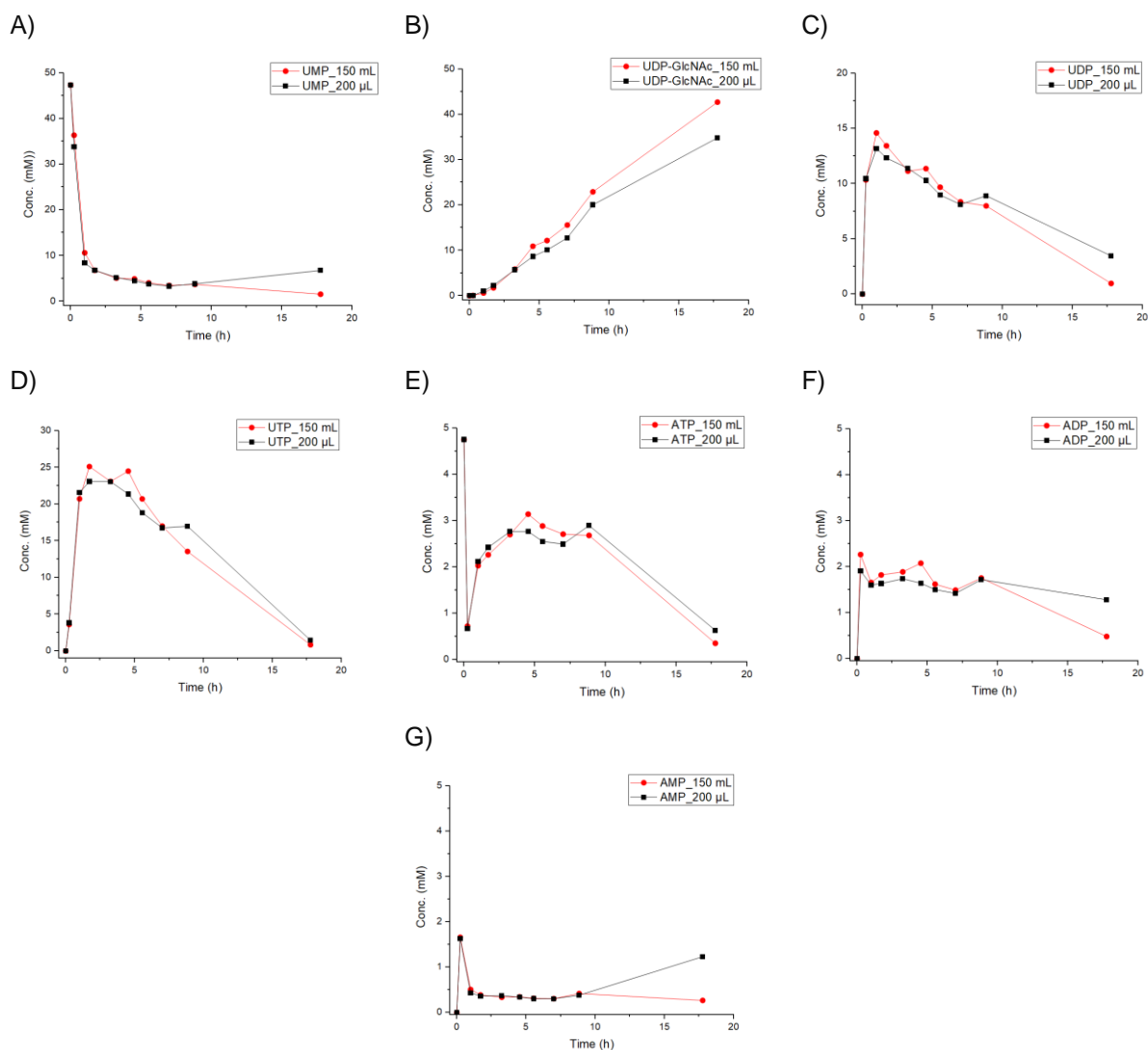


Figure 4.54. Time course of substrates, intermediates, and products of UDP-GlcNAc synthesis cascade based on co-expressed enzymes at 150 mL scale. In each graph, time course of each compound is compared at both scales. (A) UMP; (B) UDP-GlcNAc; (C) UDP; (D) UTP; (E) ATP; (F) ADP; (G) AMP. The reaction mixture consisted of 200 mM Tris-HCl (pH 8.5); 75 mM MgCl_2 ; 47 mM UMP; 50 mM GlcNAc; 4.7 mM ATP; 15 mM PolyP_n, and a total protein concentration of 0.5 g/L.

The same set-up as section 4.4.1.2 was used for synthesis of UDP-Gal at 3 L scale. The biocatalyst was prepared as described in section 3.4.3.1.2. Before scale-up, series of screening experiments were performed to find an optimal condition.

A parallel experiment ran at 200 μL scale to compare the performance of the cascade at the different scales. The time course of reaction components is shown in

Figure 4.55. During the batch time of 35.5 h, UDP-Gal was produced to a final concentration of 47.6 mM (26.9 g/L) and synthesis yield of 86% (regarding UMP). The ATP was used 35x less than the stoichiometric amount and the biocatalyst load was 0.04 $\text{g}_{\text{total_protein}}/\text{g}_{\text{product}}$.

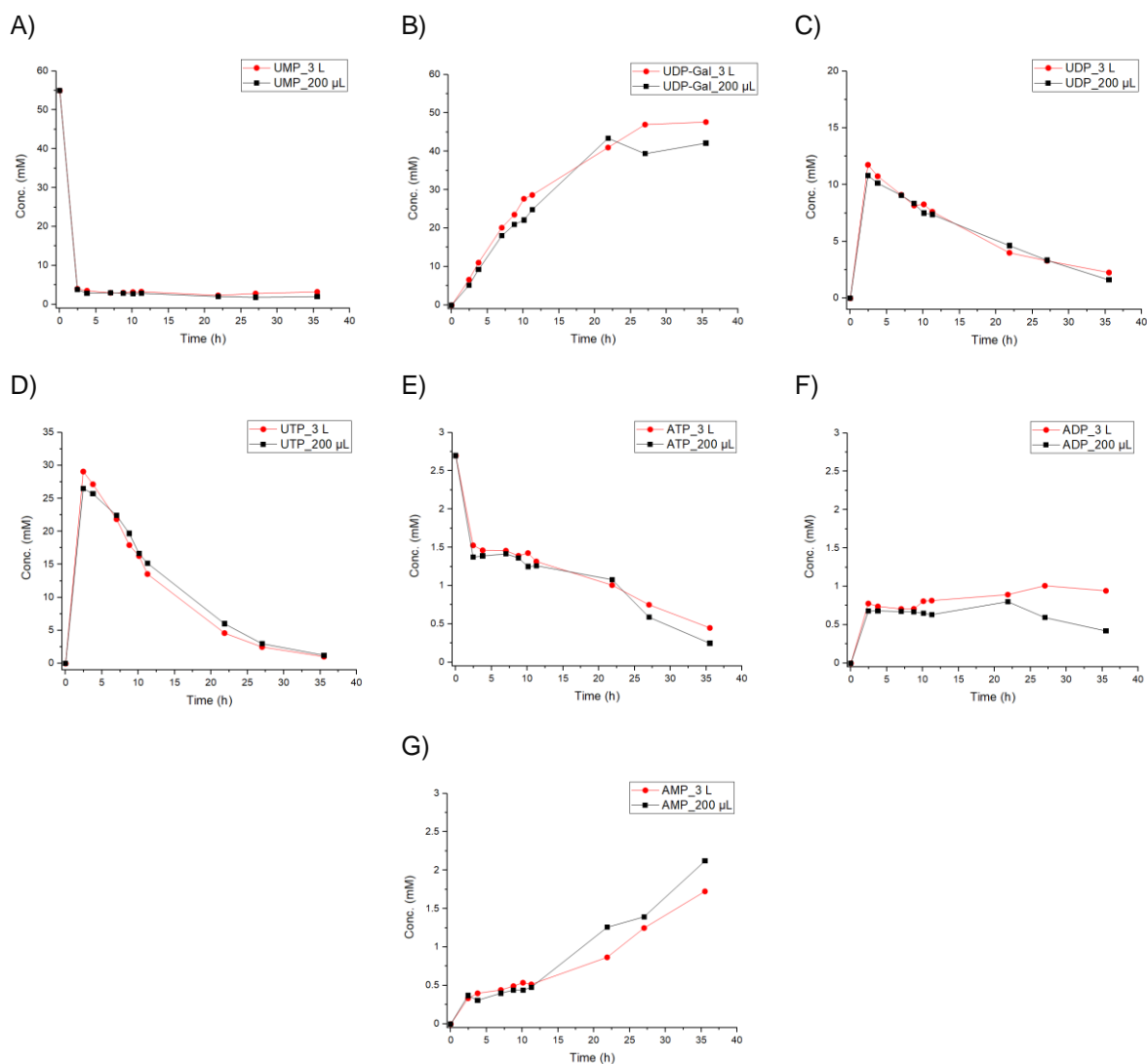


Figure 4.55. Time course of substrates, intermediates, and products of UDP-Gal synthesis cascade based on co-expressed enzymes at 3 L. (A) UMP; (B) UDP-Gal; (C) UDP; (D) UTP; (E) ATP; (F) ADP; (G) AMP. The reaction mixture consisted of 200 mM Tris-HCl (pH 8.5); 75 mM MgCl_2 ; 55 mM UMP; 55 mM Gal; 2.7 mM ATP; 14 mM PolyP_n, and a total protein (biocatalyst) concentration of 1 g/L.

4.4.2.2 Co-expression of three enzymes for synthesis of CMP-Neu5Ac

The concept of co-expression of enzymes was applied to synthesize CMP-Neu5Ac based on the cascade shown in Figure 4.19, however, CMP was used instead of Cyt. The recombinant enzyme preparation was carried out as described in section 3.4.3.2.

Starting from 50 CMP and 51 mM Neu5Ac, CMP-Neu5Ac was produced to a final concentration of 45.3 mM (27.8 g/L) and synthesis yield of 90% in a batch time of 6.6 h. The chromatogram of reaction mixture at the end of the reaction is shown in Figure 4.56.

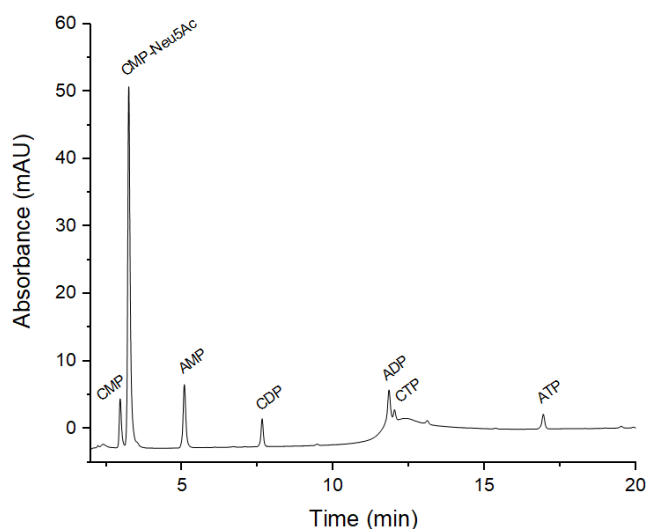


Figure 4.56. HPAEC-UV chromatogram of large-scale synthesis of CMP-Neu5Ac from CMP, Neu5Ac, PolyP_n, and catalytic amounts of ATP. The reaction matrix contained 150 mM Tris-HCl (pH 8.5); 75 mM MgCl₂; 50 mM CMP; 51 mM Neu5Ac; 5 mM ATP, and 16 mM PolyP_n in a total volume of 100 mL.

So far, all the strategies for synthesis of sugar nucleotides and HMOs were based on homogenous catalysis. This means that enzymes were used in their soluble form. In the following, the co-immobilization of a multi-enzyme system which allows the synthesis of sugar nucleotides based on heterogenous catalysis is described.

4.4.3 Co-immobilization of a multi-enzyme cascade

The results obtained in this part were filed as a patent application under PCT/EP2020/077383 [345]. As explained above, using crude enzymes has significant cost benefits. Therefore, these were used for co-immobilization.

For co-immobilization of enzymes for synthesis of UDP-GlcNAc (see Figure 4.2), the same cell lysate solution as described in the section 3.4.2 was used. The tested beads for co-immobilization of enzymes are listed in Table 4.6. It should be noted that the price of the immobilization resin has significant cost contribution to process economics, therefore, selected beads should be available in bulk amounts with reasonable pricing.

Table 4.6. List of resins used in this study as a support for co-immobilization of enzymes.

Bead	Matrix	Pore size (nm)	Size (µm)	Oxiran content (µmol/g _{wet})
Relizyme EP 112/S	epoxy/polymethacrylate	40–60	100–300	115
Relizyme EP 112/M	epoxy/polymethacrylate	40–60	200–500	112
Relizyme EP 113/S	epoxy/polymethacrylate	40–60	100–300	87
Relizyme EP 113/M	epoxy/polymethacrylate	40–60	200–500	94
Relizyme HFA 403/S	epoxy/polymethacrylate	40–60	100–300	43
Relizyme HFA 403/M	epoxy/polymethacrylate	40–60	200–500	47
Relizyme EP 403/S	epoxy/polymethacrylate	40–60	100–300	60
Relizyme EP 403/M	epoxy/polymethacrylate	40–60	200–500	56
ECR8204F	epoxy/methacrylate	30–60	150–300	n.a.
ECR8204M	epoxy/methacrylate	30–60	300–710	n.a.
ECR8215F	epoxy/methacrylate	120–180	150–300	n.a.
ECR8215M	epoxy/methacrylate	120–180	300–710	n.a.
ECR8285	epoxy/butyl methacrylate	40–60	250–1000	n.a.
ECR8209F	epoxy/methacrylate	60–120	150–300	n.a.
ECR8209M	epoxy/methacrylate	60–120	300–710	n.a.

Abbreviation: n.a., not available.

As mentioned in section 3.3.1, on average 200 mg of beads (Table 4.6) were transferred into 2 mL Eppendorf tubes, followed by the addition of 0.6 mL cell lysate solution (see section 3.4.2) containing a cocktail of enzymes required for synthesis of UDP-GlcNAc (Figure 4.2). The ratio of beads over total protein was approximately 20 (i.e., 20 mg_{beads}/mg_{protein}). After 24 h of incubation at room temperature with interval rotational mixing, the solution containing enzymes was removed. Afterwards, the beads were washed three times with a washing buffer containing a high salt concentration (200 mM Tris-HCl and 600 mM NaCl at pH 8.5) to remove weakly bound proteins. Upon washing, the beads were incubated for 24 h in a storage buffer containing 200 mM Tris-HCl and 300 mM NaCl at pH 8.5 to block the uncoupled binding sites. The percentage of bound protein is described in Figure 4.57.

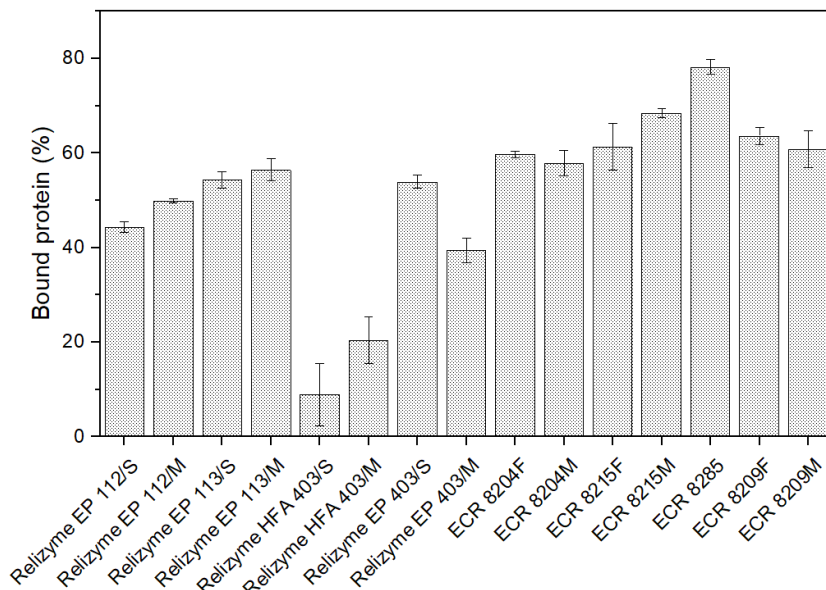
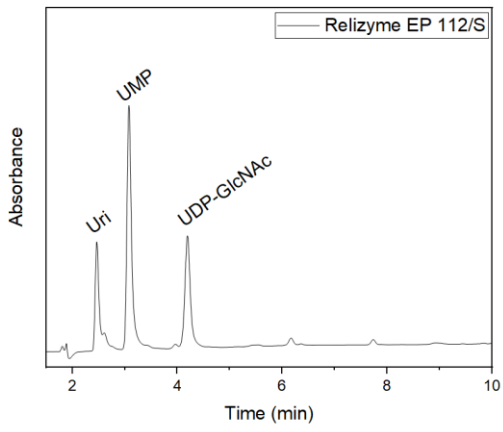


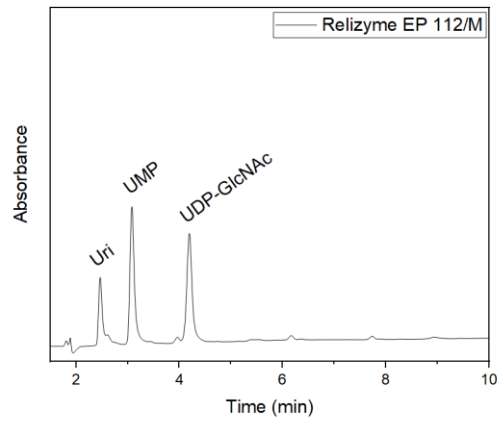
Figure 4.57. Percentage of bound protein to each bead. On average total protein mass in each immobilization vial was 10 mg. Considering the mass of resin in each vial e.g., 200 mg, the ratio of protein to resin was 20. The experiments were performed in triplicate and errors bars represent the standard deviation.

Afterwards, the storage solution was removed and the activity of each bead for synthesis of UDP-GlcNAc was evaluated. The chromatogram of the reaction product in the first cycle for each set of beads is shown in Figure 4.58. By analyzing the reaction chromatogram, one can understand the distribution of intermediates, which directly provides information on the performance of individual enzymes.

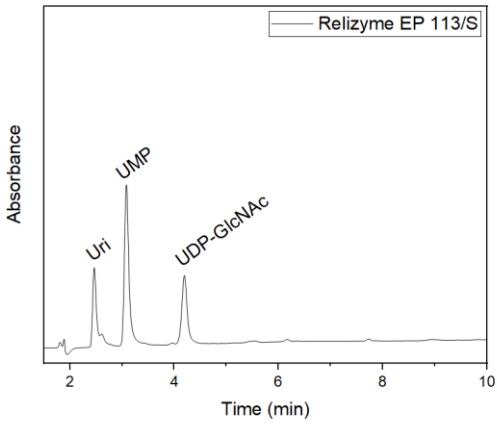
A)



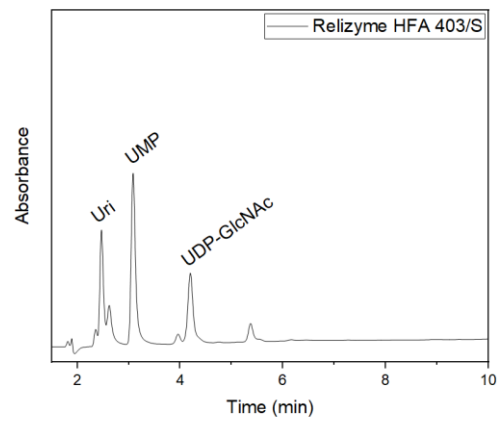
B)



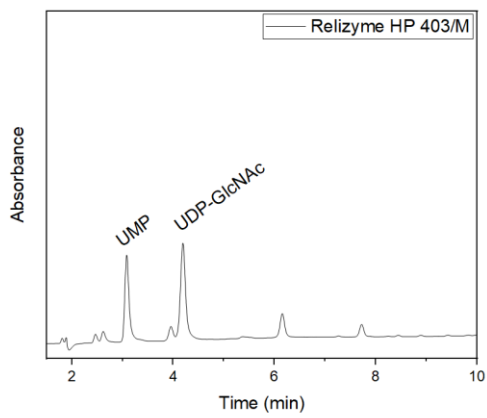
C)



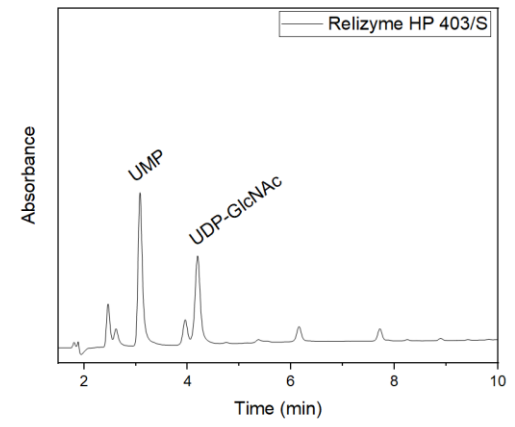
D)



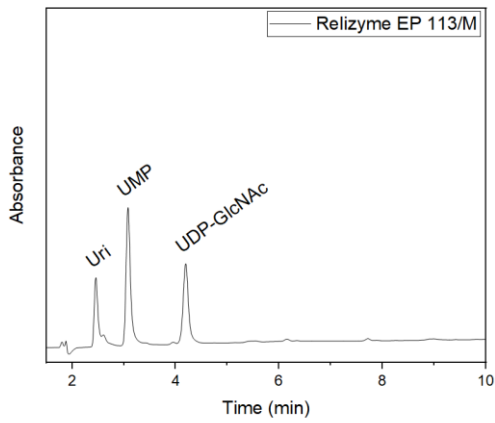
E)



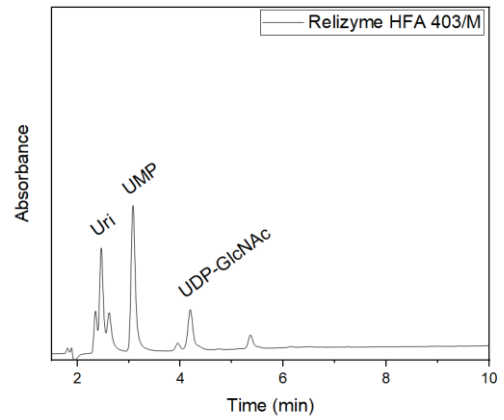
F)



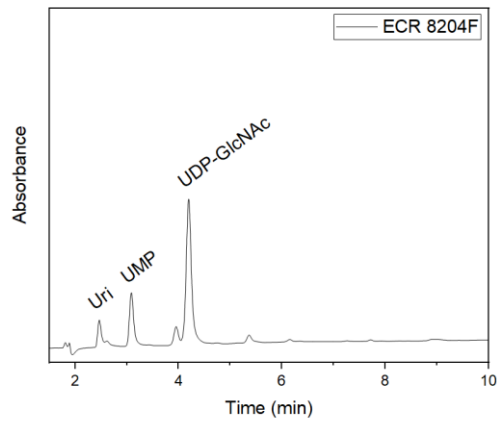
G)



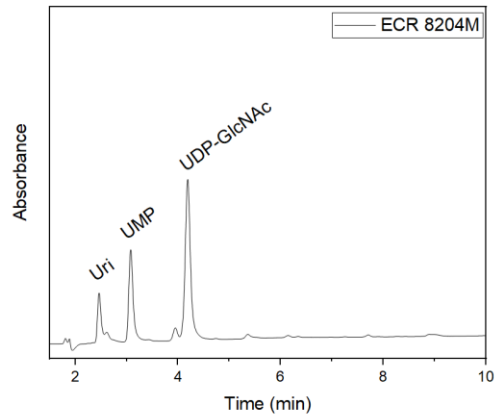
H)



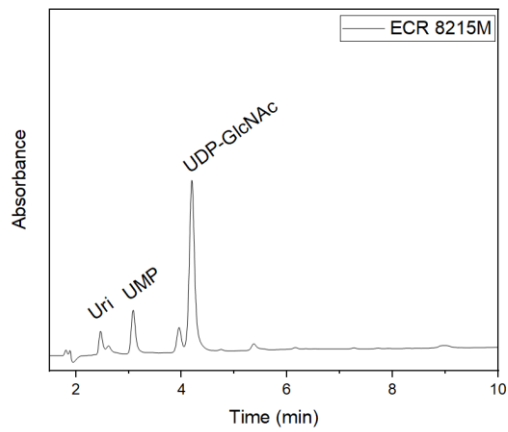
I)



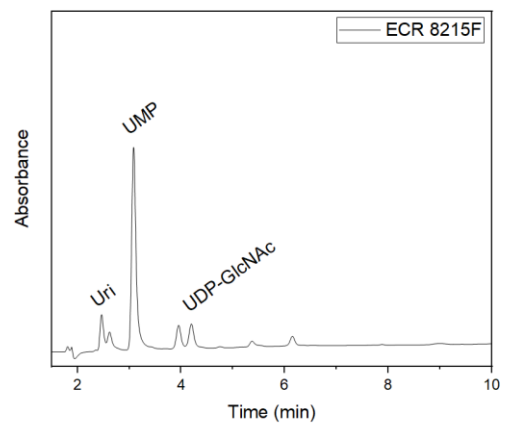
J)



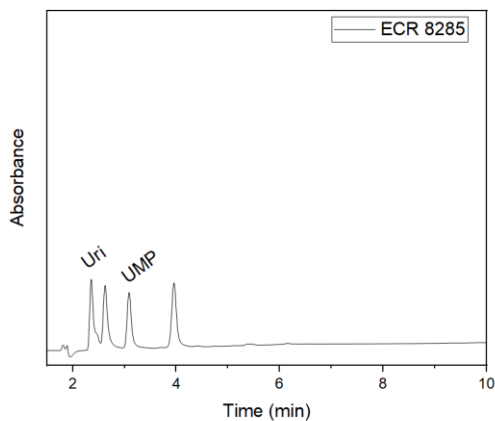
K)



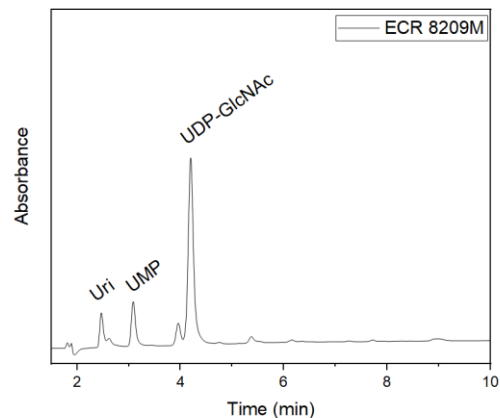
L)



M)



N)



O)

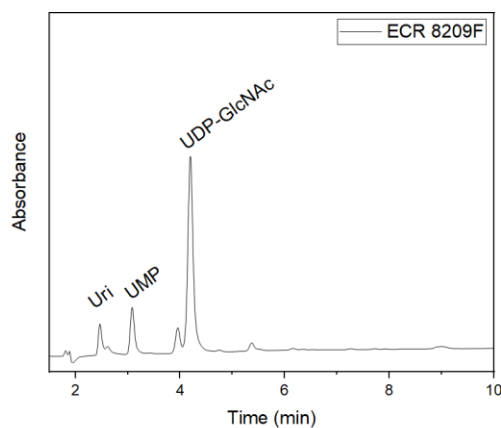


Figure 4.58. HPAEC-UV chromatogram of reaction products of each bead after 24 h of reaction time (end point). The beads with UDP-GlcNAc as the major peak were selected for further activity tests. The feed solution consisted of 200 mM Tris-HCl (pH 8.5); 75 mM $MgCl_2$; 25 mM Uri; 25 mM GlcNAc; 5 mM ATP, and 10 mM PolyP_n. 250 μ L of feed solution was added to beads and incubated at 37°C and 600 rpm for 24 h.

The performance of the beads for synthesis of UDP-GlcNAc (area under the UV chromatogram peak) is compared in Figure 4.59. Through this comparison, certain beads were selected for further experiments to evaluate the potential of co-immobilized enzymes for reusability.

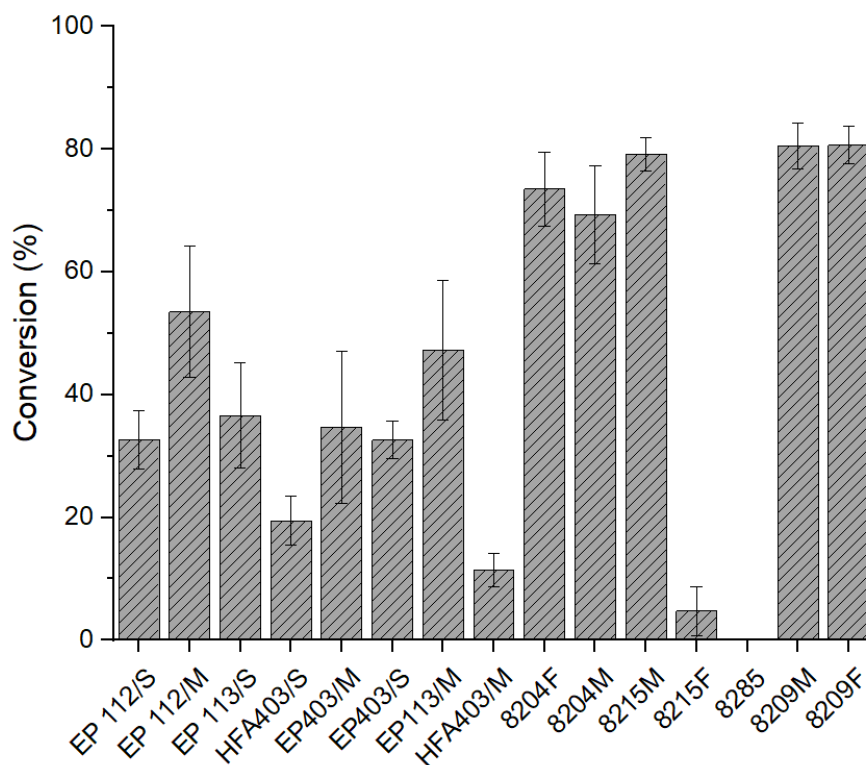


Figure 4.59. The area under the curve of UDP-GlcNAc peak was normalized to the area of all uridine-containing compounds and reported as conversion percentage. The experiments were carried out in triplicate, except for Relizyme HFA 403/S and Relizyme HFA 403/M, for which the average of three consecutive cycles are shown. Error bars represent the standard deviation.

Based on the performance of the beads, the following were selected to evaluate their performance in synthesis of UDP-GlcNAc over multiple cycles: Relizyme EP 113/M, ECR 8204F, ECR 8204M, ECR 8215M, ECR 8209F, and ECR 8209M. In each cycle, 250 μ L of feed solution (200 mM Tris-HCl; 75 mM MgCl₂; 25 mM Uri; 25 mM GlcNAc; 5 mM ATP, and 10 mM PolyP_n at pH 8.5) were added to each vial (containing beads) and incubated at 600 rpm and 37°C for 24 h. Afterwards, the reaction solution was removed, and the beads were washed twice with Milli-Q® ultra-pure water (each time with 1 mL) to avoid any carry-over from previous cycles. The activity of beads was tested for 20 cycles and results are shown in Figure 4.60.

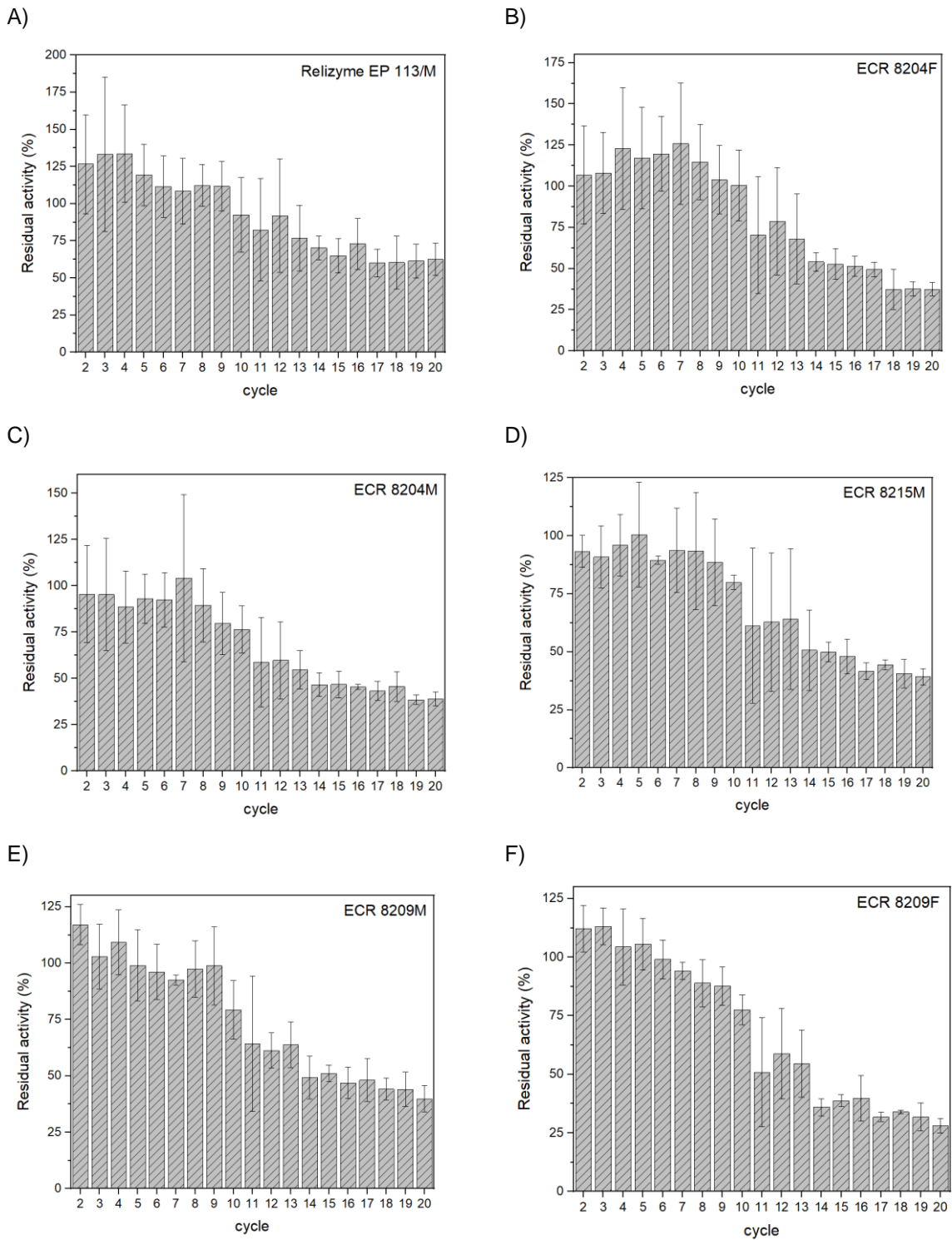


Figure 4.60. Activity of each bead in 20 different cycles. In each cycle, the area under the UDP-GlcNAc peak was normalized to the area under the peak in the first batch. (A) Relizyme EP113/M; (B) ECR 8204F; (C) ECR 8204M; (D) ECR8215M; (E) ECR8209M; (F) ECR 8209F. Error bars represent the standard deviation.

4.4.4 Discussion on process engineering strategies

Three different strategies are proposed and developed for potential large-scale synthesis of sugar nucleotides. At first, direct usage of cell lysate from individually produced enzymes was evaluated for large-scale synthesis of sugar nucleotides. In the second approach, a co-expression strategy was proposed to simultaneously produce the required enzymes for synthesis of UDP-GlcNAc and UDP-Gal as well as CMP-Neu5Ac. In the third strategy, application of immobilized enzymes was investigated by co-immobilization of six enzymes on commercially available beads. Results obtained in each approach are discussed in the following.

4.4.4.1 Scale-up of multi-enzyme cascades using cell lysate

Utilization of purified enzymes at large-scales is associated with several challenges. It has been shown that using purified enzymes results in high process costs [176] and severely challenges the implementation of multi-enzyme processes [161]. Additionally, the leakage of metal ions from common resins used in immobilized metal affinity chromatography (e.g., nickel, copper, cobalt) [344,346] is another challenge due to toxicity of metals [347–349].

In this work, crude form enzymes were used at 150 mL, 1 L, 3 L, and 4 L scale synthesis to bypass the costly step of enzyme purification as well as to make the process closer to industrial application. Enzymes in their crude form are the second simplest form of biocatalyst formulation, second only to whole-cell catalysis (with similar cost advantages) [176].

For 3 L and 4 L scale synthesis, a 7 L, single-wall, baffled bioreactor equipped with three Elephant ear impellers (similar to pitched blade) was used in order to mimic industrial scale bioreactors. As shear stress could have significant effects on the performance of enzymes (e.g., affecting activity and stability) and could even result in complete enzyme deactivation [350,351]. The Elephant ear impeller — which has been shown to cause less shear compared to other common impellers (e.g., Rushton impellers [352]) — was selected as the impeller of choice.

At 1 L scale synthesis, UDP-Gal was successfully produced to a concentration of 41.3 mM (23.4 g/L) with a biocatalyst load of 0.05 $\text{g}_{\text{total_protein}}/\text{g}_{\text{product}}$ in a batch time of 23 h (Table 4.2).

The 4 L scale synthesis, starting from 62 mM GlcNAc, 62 mM Uri, 18 mM PolyP_n, and 1.6 mM ATP, resulted in 53 mM (32.2 g/L) UDP-GlcNAc in a batch time of 25.2 h and a synthesis yield of 85.6% (regarding Uri). Based on the stoichiometry of the cascade and considering the large-scale reaction condition, 159 mM ATP was required. However, despite the direct usage of cell lysates, ATP was used ~100x less than the stoichiometric amount and was sufficient for high yield synthesis of UDP-GlcNAc. The 4 L scale synthesis of UDP-GlcNAc is among the highest scales reported for synthesis of this molecule (Table 4.1).

Interestingly, no significant formation of AMP was observed during the large-scale experiments. One of the common concerns of using cell lysate in enzymatic synthesis is the side reactions which could result in production of undesired products and thus decrease the synthesis yield (through consumption of substrates, intermediates, or products). However, the closed mass balance for Uri- and adenosine-containing compounds during the time course of the reaction, demonstrates that no significant side

reactions took place. For instance, for the case of UDP-Gal synthesis at 1 L scale, the mass balance for Uri-, and adenosine-containing compounds were $102\pm 5\%$, and $108\pm 10\%$, respectively, during the batch time. Moreover, no foaming was observed throughout the scale-up reactions.

Due to inherent differences in the structure of enzymes, they have different biophysical properties, and thus, different shear tolerance [351,353]. Therefore, it is important to understand the behavior of each individual enzyme throughout the scale-up process, especially for multi-enzyme synthesis in which a low-performing or outperforming enzyme would change the performance of the whole cascade. Consequently, parallel to the scale-up experiments, a 200 μL experiment — the scale at which preliminary experiments were performed — was carried out in order to have a direct comparison of performances at different scales. The dynamics of intermediates — which essentially represent the activity of individual enzymes — were compared at both μL and L scales. The similar dynamics of the cascade components at both scales suggests the linearity of the scale-up, indicating that sufficient mixing provided at L scales did not cause deactivating shear stress to the enzymes. Moreover, it shows that the 200 μL scale reaction is a good representative scale-down model for optimization purposes.

4.4.4.2 Discussion on co-expression of enzymes

Recombinant production of enzymes for a multi-enzyme process, for example in the case of a six-enzyme cascade requires six different fermentations, which significantly increases the overall cost. On the other hand, one fermentation unit instead of six fermentation units would significantly lower the process development costs and time, especially since fermentation is considered the most expensive and challenging step in scale-up of bioprocesses [166]. To implement the idea of reducing the number of fermentation units for production of enzymes required for multi-enzyme processes, concepts such as gene fusion or co-expression can be used.

The gene fusion strategy has been used for gene co-expression in a single host [172]. For example, for a cascade of two enzymes and two reactions, the corresponding two genes will be fused together and in the case of successful translation, a bifunctional enzyme will be produced which is able to perform the two reactions [172]. However, this strategy can be very complicated for cascades requiring more than two enzymes due to the complexity of protein structures.

Multiple Duet™ vectors capable of co-expression of two genes per vector and with compatible antibiotic selection markers and origins of replication were developed to enable co-expression of multiple genes in one strain [173]. These vectors are highly used in metabolic engineering and biocatalysis studies for co-expression of multiple genes [173–175].

Interestingly, it was demonstrated that co-expression leads to higher conversion values in the following enzymatic reactions compared to separate expression of genes for enzyme production [172,354,355]. Physical proximity of co-expressed enzymes was suggested to be the reason for improved performance [172]. Wu *et al.* developed a modular platform using *E. coli* cells to co-express four to eight genes for amino- and oxy-functionalization of alkenes [175]. In another study, Chen *et al.* co-expressed four genes for multi-enzyme synthesis of ribulose 5-phosphate from maltodextrin [356]. Zhang *et al.* designed a

plasmid for co-expression of five genes in a single strain of *E. coli* to synthesize globotriose from Gal, Glc, Lac, and catalytic amounts of ATP, PEP, UDP-Glc, and Glc-1P by using permeabilized cells [357].

As a first step in this work, a cascade of six enzymes and seven reactions was designed to enable the synthesis of both UDP-GlcNAc and UDP-Gal — with essentially the same enzymes — from industrially available chemicals: UMP, Gal, GlcNAc, PolyP_n, and catalytic amounts of ATP (Figure 4.53). UMP has many applications in the industry such as infant formula [252] or precursor of pharmaceutical products [358], and thus, processes have been developed for its large-scale manufacturing [264,275]. Therefore, similar to Uri, UMP is also inexpensively available in bulk amounts.

To implement the co-expression of the six enzymes shown in Figure 4.53, three different Duet™ vectors were used. The plasmids were categorized into three modules: First, a sugar kinase module containing the genes for NAHK and GALK (cloned into the pRSFDuet™-1 vector) that catalyzes the phosphorylation of GlcNAc and Gal, respectively. Second, a nucleotide kinase module composed of a pACYCDuet™ vector carrying the genes for UMPK and PPK3 that catalyzes the generation of nucleotide triphosphate from their di- and monophosphate counterparts. Therefore, genes for UMPK and PPK3 were cloned together into the pACYCDuet™ vector. The third module, a pCDFDuet™ vector harboring the genes for GALU and PPA into the pCDFDuet™ vector, catalyses the product formation with high yields. The latter is achieved through the presence of PPA that hydrolyzes inhibitory PPI. As part of a platform technology, the modules can be mixed and matched with other modules or used individually. For instance, the nucleotide kinase module developed can also be used for the conversion of CMP to CTP. For instance, the nucleotide kinase module developed in this work has the potential for conversion of CMP to its triphosphate form based on the promiscuity of UMPK and PPK3 [129,194], as shown in section 4.4.2.2.

All six genes required for synthesis of UDP-GlcNAc and UDP-Gal were successfully co-expressed in an *E. coli* strain and all enzymes were produced in their active form. The centrifugally clarified cell lysate was used as the final form of biocatalyst to avoid enzyme purification and the challenges associated with it (discussed in section 4.4.4.1). UDP-GlcNAc (150 mL) and UDP-Gal (3 L) were successfully produced to titers of 25.9 g/L and 26.9 g/L, respectively.

The time course of compounds in the cascades showed small difference between the small-scale experiments (200 μ L) and the large-scale experiments (150 mL and 3 L) for both UDP-GlcNAc and UDP-Gal, confirming both the scalability of the processes and the utility of a 200 μ L volume reaction as a reliable scale-down model. The performance of the developed cascade is compared to previous works regarding synthesis of UDP-GlcNAc and UDP-Gal (Table 4.1 and Table 4.2). Okuyama *et al.* synthesized UDP-GlcNAc through co-expression of three enzymes in one *E. coli* strain and further mixing with yeast cells to a high titer of 47 g/L from industrially available UMP and GlcNAc [148]. However, providing enough mixing for a mixture of enzymes and yeast cells in large scales seems to be challenging due to the different physical properties of enzymes and yeast cells. Zhai *et al.* fused NAHK and GLMU and in combination with separately expressed PPA, they synthesized UDP-GlcNAc from GlcNAc, UTP, and ATP [267].

In another example, the concept of co-expression was used to synthesize CMP-Neu5Ac. The nucleotide kinase module was used in combination with CSS to enable the synthesis from CMP, Neu5Ac, PolyP_n, and catalytic amounts of ATP. The cascade was performed at 100 mL scale by using cell lysate as the biocatalyst. The biotransformation delivered 27.8 g/L of CMP-Neu5Ac in less than 7 h (Table 4.5). However, the high-cost and unavailability of Neu5Ac challenge the large-scale implementation of this cascade.

4.4.4.3 Discussion on co-immobilization of multi-enzyme systems

Immobilized enzymes have been highly used in industrial processes [180,185,359]. Advantages such as significant improvement in process stability (i.e., usage in multiple cycles) and thermal stability, as well as freedom in bioreactor design are among the main reasons for immobilization of enzymes for industrial purposes [180,184,185,359]. Moreover, synthesis based on immobilized enzymes offers significant advantages for downstream processing by avoiding the costly separation of enzymes (proteins) from the product stream.

Different mechanisms of enzyme immobilization have been thoroughly described in Ref. [360,361]. Covalent binding of enzymes on solid supports has been reported to be the strongest type of immobilization, which results in minimum leakage of enzymes [179]. The role of physical properties of solid supports such as particle size, pore size, porosity, and the nature and length of the spacer has been thoroughly discussed in Ref. [179,184]. However, due to the extremely complex interactions involved in enzyme immobilization, the performance of immobilized enzymes cannot be predicted and needs to be investigated experimentally [362].

Recently, co-immobilization of multi-enzyme systems has been gaining significant attention as a strategy for process establishment and development [186–188]. Co-immobilization vs. immobilization (separate immobilization of each enzyme) of multi-enzymes system offers certain advantages (e.g., enhanced mass-transfer and more favorable thermodynamic equilibrium) which result in enhanced process performance [188].

In this work, it was assumed that co-immobilization of enzymes could bring multi-enzyme synthesis of sugar nucleotides closer to practical large-scale implementation — as an alternative strategy to soluble enzymes. Because of the advantages offered by covalent immobilization (i.e., strongest linkage), it was considered as the main mechanism for co-immobilization in this work. Moreover, in the context of this dissertation, almost 40 different commercially available resins with various mechanisms for co-immobilization of UDP-GlcNAc enzyme were evaluated and the results are presented in Ref. [345].

The advantage of using immobilized enzymes for multiple cycles significantly reduces the cost of enzyme production. However, it comes with the additional costs of resins. Therefore, the cost and industrial availability of immobilization resins should be considered for process development. The resins used in this work are listed in Table 4.6. All the tested resins are available in industrial amounts from world-known resin suppliers. The purpose of co-immobilization in this work was to demonstrate the feasibility of sugar nucleotide synthesis as a proof-of-concept study. The preliminary steps for immobilization of enzymes for synthesis of UDP-GlcNAc was carried out in master thesis of Suzana

Cvijetinovic, whose work was performed and supervised in association with this dissertation [363]. After successful immobilization, the concept of co-immobilization was realized by providing a cocktail of all required enzymes for synthesis of UDP-GlcNAc. The multi-enzyme solution prepared in section 3.4.2 was directly used for co-immobilization. Evidently, in order to have functional co-immobilized enzymes, six enzymes must bind to resins in their active form.

The amounts of total adsorbed protein were significantly different for each bead (Figure 4.57). Because of changes in protein structure upon immobilization, no direct correlation between bound enzymes and their activity can be drawn. For instance, in the case of ERC8285, ~80% of total protein was bound, however, no activity in terms of UDP-GlcNAc production was observed. Interestingly, ERC8285 resin has a highly hydrophobic nature (because of butyl methacrylate matrix) compared to other enzyme carriers which might be an explanation for inactive co-immobilization of enzymes in the UDP-GlcNAc cascade. However, the presence of UMP and ADP (Figure 4.58M) suggests active immobilization of UDK.

To evaluate re-usability of the co-immobilized enzymes, the following beads were selected based on high yield synthesis in the first cycle: Relizyme EP113/M, ECR 8204F, ECR 8204M, ECR 8215M, ECR 8209M, and ECR 8209F. On average, the selected beads were able to synthesize UDP-GlcNAc up to a titer of ~11 g/L with an average conversion of 72%. The activity of beads was tested for 20 cycles (Figure 4.60). The majority of the beads did not significantly lose any activity up to 10th cycle; however, loss of activity was gradually observed in the later reaction cycles.

Previous efforts for synthesis of UDP-GlcNAc based on covalent immobilization were not successful — specifically NAHK was found to be inactive upon epoxy-based immobilization [364]. However, in this work I was able to successfully demonstrate the synthesis of UDP-GlcNAc through the co-immobilization of enzymes on industrially relevant beads. To the best of author's knowledge, this is the first time that successful co-immobilization of six enzymes on epoxy functionalized beads has been described. As it can be concluded from Figure 4.58, the key factor for successful co-immobilization was the screening of different beads. As mentioned above, due to high level of complexity of interactions in co-immobilization of multiple enzymes, it is not possible to theoretically predict the results of immobilization. Therefore, screening resins is a crucial practice in finding an optimal immobilization support.

Shao *et al.* synthesized UDP-GlcNAc from GlcNAc, UTP, PEP, and catalytic amounts of ATP through (separate) immobilization of five enzymes on Ni-NTA agarose beads [189]. The beads retained 50% of their initial activity after seven cycles [189]. Liu *et al.* individually immobilized seven enzymes on Ni-NTA agarose beads for synthesis of UDP-Gal from UMP, Gal, PolyP_n, catalytic amounts of ATP, UDP-Glc, and Glc-1P [146]. However, some enzymes (e.g., polyphosphate kinase) needed to be recharged after each batch [146]. Despite successful synthesis of UDP-GlcNAc and UDP-Gal using immobilized enzymes, the high cost of Ni-NTA agarose beads poses a significant challenge for large-scale applications. Moreover, most Ni-NTA agarose beads have gel-like structure and do not have high mechanical stability which limits their application in process conditions (e.g., when high mixing is

required). The performance of Ni-NTA agarose beads for co-immobilization of UDP-GlcNAc cascade enzymes was evaluated by the author and results are presented in Ref. [345]. It was found out that co-immobilized enzymes on Ni-NTA beads completely lost activity after the 10th cycle, however, epoxy-based resins were active up to the 20th cycle [345].

Direct comparison of UDP-GlcNAc synthesis based on co-immobilized enzymes and soluble enzymes suggests superior performance of soluble enzymes. However, no optimization work was performed on improvement of co-immobilized enzymes. Moreover, co-immobilized enzymes offer advantages such as continuous production by using suitable reactors such as packed bed reactors. Accordingly, selection of a production strategy highly depends on many factors (e.g., downstream units, available infrastructure) and thus, each case needs to be evaluated individually.

5 Conclusions and Outlook

The main aim of this dissertation was to exploit the engineering opportunities in the field of glycosylation. The two major considered opportunities were: first, synthesis of functional oligosaccharides such as HMOs and second, glycoengineering of therapeutic glycoproteins. Both opportunities were mainly based on reactions catalysed by Leloir glycosyltransferases using sugar nucleotides as substrates. However, sugar nucleotides are too expensive to be used for any engineering purposes. For instance, in 1988, Simon *et al.* clearly stated that the high cost of CMP-Neu5Ac ($\sim 10^6$ \$/mol in 1988) was the main reason for the development of a multi-enzyme cascade for its synthesis for further development of sialylated molecules [145]. Interestingly, despite the advances in various techniques associated with enzymatic technologies and after three decades, in 2021 the price of CMP-Neu5Ac is still in the same order. The same story applies to other sugar nucleotides as they are very expensive and are not available in bulk amounts. Therefore, large-scale synthesis of sugar nucleotides was the major milestone in this work. I hypothesized that upon bulk availability of sugar nucleotides, significant advances in the glycoengineering field could be made and relevant ideas could be applied in large scales.

At first, I decided to develop multi-enzymatic platforms for large-scale synthesis of sugar nucleotides to achieve the major milestones. The most important factor was designing a multi-enzyme cascade to enable the synthesis by using industrially available precursors.

For synthesis of UDP-sugars i.e., UDP-GlcNAc, UDP-GalNAc, UDP-Gal, and UDP-Glc, Uri was used as the Uri-based on these family of sugar nucleotides. Industrial availability of Uri ensures sustainable process development for industrial production of UDP-sugars. The monosaccharide form of sugar nucleotides was directly used as the source of sugar. Since sugar nucleotides are thermodynamically active molecules, a relatively high amount of energy is required for their enzymatic synthesis. Based on the designed cascades, three molecules of ATP were required per molecule of a UDP-sugar. To avoid usage of expensive ATP at stoichiometric amounts, PolyP_n was used as the main energy source to constantly regenerate ATP from ADP. This allows the catalytic utilization of ATP in the cascade. PolyP_n is industrially available at a low cost. In all the developed cascades ATP was used as low as 250× less than the stoichiometric amount. Therefore, an efficient ATP regeneration module was established. The cascades for synthesis of UDP-sugars have a synthesis yield of more than 95% (except UDP-Glc, which was 81%) and product titer in the range of 27–40 g/L. The biocatalyst load was also in the range of 0.01–0.04 g_{enzyme}/g_{product}. Through systematic comparison to previously reported enzymatic methods for synthesis of UDP-sugars, the cascades developed in this work are among the most efficient in terms of used precursors, scale, and titer.

To bring UDP-sugars closer to the form of a final product — i.e., solid powders — industrially applicable downstream methods should be developed. High yield synthesis of UDP-sugars from Uri and the corresponding sugars as well as catalytic utilization of ATP could be a significant advantage in development of chromatography-free downstream methods. Strategies such as the addition of cations

for precipitation of PolyP_n followed by treatment with cation exchange resins or using nanofiltration systems are suggested to be evaluated for purification of UDP-sugars.

The established UDP-Glc cascade can be further coupled to other enzymes for production of other valuable UDP-sugars such as uridine diphosphate glucuronic acid and uridine diphosphate rhamnose. Therefore, by only using inexpensive precursors (i.e., Uri and Glc), other valuable UDP-sugars can be synthesized.

The cascade for synthesis of UDP-GlcNAc can also be used for synthesis of UDP-GalNAc by extending the cascade through addition of an epimerase. By using this strategy, there is no need to use expensive GalNAc for synthesis of its UDP-activated form.

For synthesis of GDP-sugars, Guo was used as one of the main precursors. The key element for using Guo was using DMSO as the solvent for preparation of Guo stock solution, and thus, as the co-solvent in the reactions. Since Guo and GMP have unique self-assembly properties which result in hydrogel formation, using DMSO was crucial to solubilize Guo at high concentrations and avoid hydrogel formation in enzymatic reactions. In synthesis of GDP-Fuc, besides synthesis starting from Fuc, a cascade containing ten enzymes and eleven reactions was developed to allow synthesis of GDP-Fuc from Man as the sugar source. Since the stoichiometric amount of NADPH was required for the cascade, a regeneration cycle was established by employing GLDH and L-Glu as the substrate. Additionally, in these cascades three moles of ATP were required per mole of the products — i.e., GDP-Man and GDP-Fuc. As described above, an ATP regeneration system was established using PolyP_n. It was also found that an alkaline pH of 8.5 is necessary for high yield synthesis of GDP-Fuc starting from Man. By using the latter cascade, GDP-Fuc was produced to a concentration of 7.6 mM (4.5 g/L) and a reaction yield of 72% with a biocatalyst load of 0.97 g_{enzyme}/g_{product}. ATP and NADPH were used 5.7-fold and 10.5-fold less than the stoichiometric amounts, respectively. The precursors used for synthesis of GDP-sugars are the most inexpensive compounds reported in literature, which represents a promising future large-scale application.

Despite the obtained data for synthesis of GDP-sugars being among the most efficient systems reported in literature — especially regarding used precursors and biocatalyst load — the current reaction metrics are not suitable for large-scale applications. Systematic optimization to further improve the titer as well as strategies such as co-expression of required enzymes are suggested to be evaluated to improve the performance of the cascade in terms of process-scale applicability. Evidently, by decreasing the cost of enzyme production, its load could be further increased to enhance the titer level. Direct usage of cell lysate is also suggested to be evaluated to decrease the biocatalyst preparation. Moreover, the presence of native NADPH from cell lysate could offer certain advantages by eliminating the need for exogenous addition. Due to certain inhibitions existing in the cascade, co-immobilization would offer certain advantages which might result in improvement of reaction metrics.

In synthesis of CMP-Neu5Ac, Cyt was used as the source of nucleoside. At first, a cascade starting from Neu5Ac was designed and established. However, Neu5Ac is an expensive compound with limited availability. Therefore, an extended version of the cascade was established to carry out the synthesis

from GlcNAc and Pyr. The issue with the extended version of the cascade was the inhibition of AGE by CTP which led to inefficient Neu5Ac, and thus, CMP-Neu5Ac synthesis. To overcome this phenomenon, the concentration of GlcNAc and Pyr was increased (while keeping the concentration of Cyt constant) to push the reaction toward the product side — i.e., ManNAc and Neu5Ac. At the same time, the concentration of PolyP_n was tested to control the synthesis rate of CTP. Through multiple screening reactions, a condition was found where inhibition could be minimized. CMP-Neu5Ac was synthesized to a titer of 24.6 mM CMP-NeuAc (15.1 g/L) with the synthesis yields of 77%, 34%, and 31% regarding Cyt, GlcNAc and Pyr, respectively.

It is suggested that kinetic dynamic modeling be performed to quantitatively understand inhibition of AGE by CTP as well as the conversion of GlcNAc to Neu5Ac. In the case of successful establishment of a kinetic model, the cascade performance could be improved by controlling the intermediate levels.

Another strategy which fits all the enzyme production processes described in this work is evaluating endotoxin-free organisms, e.g., engineered *E. coli*. This approach can significantly reduce the additional cost of endotoxin removal in downstream processing and increase the potential of the purified sugar nucleotides for food and pharmaceutical applications.

The major milestone of the work was accomplished after successful development of multi-enzyme cascades for potentially scalable synthesis of sugar nucleotides. In the next step, application of developed sugar nucleotide synthesis cascades was evaluated for synthesis of wide variety of HMOs. In total, two strategies were proposed for synthesis of HMOs. The first approach was based on the coupling strategy in which a sugar nucleotide cascade is coupled to a glycosyltransferase where released mono- or diphosphate nucleotide enters the cascade after releasing from the transferring reaction. Therefore, nucleosides are used in catalytic amounts. In a proof-of-concept study, two HMOs — i.e., 3-FL, and 6'-SL — were synthesized to a final titer in the range of 3–13 g/L. However, due to the high number of enzymes involved in such cascades, the titer and biocatalyst load should be further optimized to make such approaches more attractive for large-scale applications.

For practical implementation of the coupling approach, developing *in situ* product removal strategies to enhance the productivity and overall performance of the process can be very advantageous.

The second approach for synthesis of HMOs was based on modular synthesis in which produced sugar nucleotide (module 1) is separately mixed with an acceptor(s) and a glycosyltransferase(s) (module 2), without any purification steps. AP could be used in module 2 to shift the transferase reaction more toward the product side. Based on the modular synthesis concept more than ten different HMOs — i.e., LacNAc, LNT II, LNnT, *para*-LNnH, 6'-SL, LST_c, DSLNnT, 3-FL, LNFP III, DF-LNnT, LNFP V, and 6'-SLN — were sequentially synthesized in a proof-of-concept study — starting from the Lac and sugar nucleotides produced in this work.

Immobilization of glycosyltransferases is suggested to be performed to bring the idea of modular synthesis closer to process scale implementations. Like sugar nucleotides, a downstream process needs to be developed which is (in the best case) suitable for vast majority of HMOs. Nanofiltration in combination with ion exchange could be a viable strategy to enable purification of a high number of

different HMOs. Recycling released nucleotides (or nucleosides once AP is used), can offer significant cost advantages in large scales since they can be used again for synthesis of sugar nucleotides.

In the section of *in vitro* glycoengineering, it was shown that ADCC activity of mAbs is increased upon addition of terminal Gal. It was assumed that availability of UDP-Gal and affordable β -1,4-galactosyltransferase could bring glycoengineering (in terms of addition of terminal Gal), closer to practical implementation. Since UDP-Gal was produced through a multi-enzyme cascade with high titers, the focus in this step was to express human β 1,4GalT1 gene in *E. coli* cells (as a low-cost expression host) to have a cost-efficient platform for large-scale applications. The truncated (soluble part) version of human β 1,4GALT1 was produced in its active form in *E. coli* cells and was used for galactosylation of a cell culture derived mAb. Accordingly, an *E. coli*-based platform was established for galactosylation of mAbs. Even though there is still no clinical data which proves the benefits of fully galactosylated antibodies, results based on *in vitro* assays are very promising for development of biobetters of approved drugs, biosimilars, or development of new drugs.

Without any support from clinical data, it is challenging to claim the application of *in vitro* glycoengineering as a potential method for the production of biologics with high clinical value. However, this strategy is proven to deliver homogenous and fully galactosylated mAbs and can be further expanded to other biologics. Evidently, the corresponding downstream step needs to be developed for removal of the enzymes.

The concept of glycoengineering was further expanded to construct a toolbox to materialize the idea of an artificial Golgi to generate, theoretically, any type of glycan on intact proteins. In the first step of implementing this idea, IgG with Man9 glycan was produced through addition of kifunensine to the cell culture. Afterwards, in a one-pot reaction, Man9 was trimmed to Man5 while simultaneously GlcNAc was added by using MGAT1 to synthesize Man5-G0. To further expand the cascade, active Man II was required, which was found out to be inactive upon expression in *E. coli*.

Therefore, active microbial expression of Man II was found to be the bottleneck for the development of an artificial Golgi, as MGAT1, MGAT2 and β 1,4GALT1 were already shown to be active once they are recombinantly produced in *E. coli*. Therefore, the active expression of Man II from various organisms may be extended in the future to establish a fully bacterial based artificial Golgi. Having functional artificial Golgi in a cell-free format can be coupled to cell-free glycoprotein synthesis for development of new biological entities or any other yet to come therapeutic glycoproteins.

In the last step, some strategies were proposed and demonstrated as solutions for industrial implementation of developed multi-enzyme cascades. Scalability of the cascades for synthesis of CMP-Neu5Ac, UDP-Gal, and UDP-GlcNAc was carried out at 100 mL, 3 L, and 4 L, respectively. The maximum scale-up factor in this study was 20,000 \times (from 200 μ L to 4 L). At these scales, cell lysate was used as the biocatalyst because of the significant cost advantages compared to the utilization of purified enzymes. The similar kinetic behavior of the cascades at μ L and L scale suggests that μ L scale reactions can be used as a representative scale-down model for optimization of the cascade.

To further optimize the developed processes for synthesis of sugar nucleotides, fed-batch addition of substrates and co-factors should be evaluated to increase the titer even further. Moreover, designing membrane bioreactors for recycling enzymes would further optimize the processes by decreasing the cost of biocatalysts.

Another idea for bringing the sugar nucleotide synthesis closer to manufacturing purposes was co-expression of required enzymes in a single strain. This means that in one fermentation unit, all necessary enzymes are produced and there is no need for individual production of enzymes. By using three different Duet™ vectors, six different enzymes were recombinantly produced in one strain. The enzymes were chosen in a way to allow the synthesis of both UDP-Gal and UDP-GlcNAc from UMP, Gal or GlcNAc, PolyP_n, and catalytic amounts of ATP. The practicality of this approach was demonstrated at 150 mL for synthesis of UDP-GlcNAc and 3 L scale for synthesis of UDP-Gal by using cell lysate as the biocatalyst.

Of course, the co-expression strategy could be expanded to other sugar nucleotides and HMOs synthesis cascades. Developing and applying synthetic biology methods to eliminate the need for addition of various selection markers — i.e., antibiotics — could significantly improve such systems. Moreover, evaluating controlled co-expression would lead to more optimized systems.

Co-immobilization of enzymes was demonstrated to enable the heterogenous catalysis for production of sugar nucleotides. The cascade for synthesis of UDP-GlcNAc was co-immobilized on industrially available epoxy-functionalized solid supports. To find a suitable support, 15 different commercially available resins were screened and six of them — beads which resulted in conversion yields of ~80% — were chosen to show the activity of beads over multiple cycles. The activity of co-immobilized enzymes was shown up to 20 sequential cycles, however, the activity started to decrease after 10th cycle. The key factor in successful co-immobilization of six enzymes on solid supports was the screening of multiple beads. Production of sugar nucleotides or any other products based on immobilized enzymes can offer significant advantages such as lower downstream processing costs, multiple usage of biocatalyst, and continuous synthesis. However, for making a solid decision between choosing free enzyme solution or immobilized enzymes for a given product, a detailed techno-economic analysis needs to be performed individually.

Screening of various co-immobilization condition such as pH, salt concentration, co-factor addition, biomass ratio of each enzyme, etc. should be considered as optimization parameters to improve the performance of co-immobilized enzymes. Moreover, various reaction conditions should be evaluated to find the condition in which co-immobilized enzymes operate in their optimal condition.

At the beginning of this work, I hypothesized that the availability of sugar nucleotides in bulk amounts would be considered a breakthrough innovation in the field of glycoengineering — from free oligosaccharide synthesis to modification of glycosylation on intact proteins. Therefore, I have tried to explore bioprocess engineering strategies to make the bulk scale synthesis of sugar nucleotides feasible. I have demonstrated these achievements through the design, development, optimization, and scale-up of multi-enzyme systems, not only for sugar nucleotides synthesis, but also for the production

of HMOs and, to some extent, for *in vitro* glycoengineering of therapeutic proteins. Overall, I believe that the processes developed in the framework of this dissertation can significantly contribute to future works on exploiting engineering opportunities offered in the world of glycosylation to better the quality of human life.

List of Figures

Figure 2.1. Schematic representation of major types of glycosylation in humans. Abbreviations are as follows: EGF, epidermal growth factor; TSR, thrombospondin type 1 repeats; GPI, glycosylphosphatidylinositol; GAG, glycosaminoglycans; N, Asn; S, Ser; T, Thr; 2S, sulfation at C-2 carbon; 3S, sulfation at C-3 carbon; 4S, sulfation at C-4; 6S, sulfation at C-6 carbon; NS, N-sulfation; GlcA, glucuronic acid; GlcN, glucosamine; IdoA, iduronic acid. Adapted with permission from Ref. [31]. 5

Figure 2.2. Most abundant glycans found on the Fc region of therapeutic mAbs. Values were obtained from Ref. [37]. Blue squares, N-acetylglucosamine; green circle, mannose; yellow circle, galactose; pink square, sialic acid; red triangles, fucose. 6

Figure 2.3. concepts used in in vitro or enzymatic glycoengineering. (A) Glycoengineering by using oxazoline glycans as the substrate and ENGase (EndoS2) and its engineered variants (EndoS2-D184M) as the biocatalyst [6]. (B) Glycoengineering by using sugar nucleotides and Leloir-glycosyltransferases. Abbreviations: β 1,4GALT1, β -1,4-Galactosyltransferase 1; UDP-Gal, uridine diphosphate galactose. 7

Figure 2.4. Concept of OPME for synthesis of lacto-N-tetraose (LNT) based on Ref. [125]. In this approach both syntheses of sugar nucleotide and HMO are carried out in one-pot. SpGalk, *Streptococcus pneumoniae* TIGR4 galactokinase; BLUSP, *Bifidobacterium longum* UDP-sugar pyrophosphorylase; PmPpA, *Pasteurella multocida* inorganic pyrophosphatase; Cv β 3GalT, *C. violaceum* β -1,3-galactosyltransferase; Gal, galactose, Gal-1P, galactose 1-phosphate; PPi, diphosphate; Pi, phosphate; ATP, adenosine triphosphate; ADP, adenosine diphosphate; UTP, uridine triphosphate; LNT II, lacto-N-triose II. 11

Figure 2.5. Illustration of coupling approach for synthesis of 6'-sialyl-N-acetylglucosamine (6'-SLN) from N-acetylglucosamine (LacNAc) as described in Ref. [133]. Neu5Ac, N-acetylneuraminic acid; ADP, adenosine diphosphate; ATP, adenosine triphosphate; CMP, cytidine monophosphate; CDP, cytidine diphosphate; CTP, cytidine triphosphate; CMP-NeuAc, cytidine monophosphate N-acetylneuraminic acid; PPi, inorganic pyrophosphate; Pi, inorganic phosphate; PEP, phosphoenolpyruvate; Pyr, pyruvate; PK, pyruvate kinase; NMK, nucleoside monophosphate kinase; PPase, inorganic pyrophosphorylase. 12

Figure 3.1. The steps for LNFP V synthesis. The symbols are glucose, blue circle; N-acetylglucosamine, blue square; fucose, red triangle, and galactose, yellow circle. 24

Figure 3.2. UV chromatogram of UDP-GlcNAc cascade components. Abbreviations: Uri, uridine; AMP, adenosine monophosphate; UMP, uridine monophosphate; ADP, adenosine diphosphate; UDP-GlcNAc, uridine diphosphate N-acetylglucosamine; UDP, uridine diphosphate; ATP, adenosine triphosphate; UTP, uridine triphosphate; mAU, milli absorbance unit. 31

Figure 3.3. UV chromatogram of UDP-Gal cascade components. Abbreviations: Uri, uridine; AMP, adenosine monophosphate; UMP, uridine monophosphate; ADP, adenosine diphosphate; UDP-Gal, uridine diphosphate galactose; UDP, uridine diphosphate; ATP, adenosine triphosphate; UTP, uridine triphosphate; mAU, milli absorbance unit. 31

Figure 3.4. UV chromatogram of UDP-Glc cascade components. Abbreviations: Uri, uridine; AMP, adenosine monophosphate; UMP, uridine monophosphate; ADP, adenosine diphosphate; UDP-Glc, uridine diphosphate glucose; UDP, uridine diphosphate; ATP, adenosine triphosphate; UTP, uridine triphosphate; mAU, milli absorbance unit. 32

Figure 3.5. UV chromatogram GDP-Man and GDP-Fuc cascade components. Abbreviations: AMP, adenosine monophosphate; Guo, guanosine; ADP, adenosine diphosphate; GMP, guanosine monophosphate; ATP, adenosine triphosphate; GDP-Man, guanosine diphosphate mannose; GDP-Fuc, guanosine diphosphate fucose; GDP, guanosine diphosphate; GTP, guanosine triphosphate; mAU, milli absorbance unit. 32

Figure 3.6. UV chromatogram of CMP-Nue5Ac cascade components. Abbreviations: Cyt, cytidine; CMP, cytidine monophosphate; CMP-Neu5Ac, cytidine monophosphate N-acetylneuraminic acid; AMP, adenosine monophosphate; CDP, cytidine diphosphate; ADP, adenosine diphosphate; CTP, cytidine triphosphate; ATP, adenosine triphosphate; mAU, milli absorbance unit. 33

Figure 4.1. General cascade scheme for synthesis of UDP-sugars. Abbreviations: Uri, uridine; UMP, uridine monophosphate; UDP, uridine diphosphate; UTP, uridine triphosphate; PPi, diphosphate; Pi,

phosphate; ADP, adenosine diphosphate; ATP, adenosine triphosphate; UDK, uridine/cytidine kinase; UMPK, UMP/CMP kinase; PPK3, PolyP_n kinase; PPA, inorganic diphosphatase. 37

Figure 4.2. Multi-enzyme cascade of six enzymes and seven reactions for synthesis of uridine diphosphate N-acetylglucosamine (UDP-GlcNAc) from uridine (Uri), N-acetylglucosamine (GlcNAc), polyphosphate (PolyP_n), and catalytic amounts of adenosine triphosphate (ATP). Thanks to the affinity of N-acetylhexosamine 1-kinase (NAHK) and GlcNAc 1-phosphate uridylyltransferase (GLMU) for N-acetylgalactosamine (GalNAc) and N-acetylgalactosamine 1-phosphate (GalNAc-1P), respectively, UDP-GalNAc can also be synthesized with the same cascade. Abbreviations: UMP, uridine monophosphate; UDP, uridine diphosphate; UTP, uridine triphosphate; GlcNAc-1P, N-acetylglucosamine 1-phosphate; P_i, diphosphate; P_i, phosphate; ADP, adenosine diphosphate; UDK, uridine/cytidine kinase; UMPK, UMP/CMP kinase; PPK3, PolyP_n kinase; PPA, inorganic diphosphatase. 38

Figure 4.3. Reaction time course of substrates, intermediates, and products in the cascade. The reaction conditions were as follows: Tris-HCl (pH, 8.5) 150 mM; MgCl₂ 75 mM; Uri 68 mM; GlcNAc 68 mM; ATP 2.1 mM; PolyP_n 21 mM; UDK 0.07 µg/µL; UMPK/PPK3 0.11 µg/µL; NAHK 0.18 µg/µL; GLMU 0.2 µg/µL, and PPA 0.05 µg/µL. (A) Shows the consumption of Uri and sequential production of UDP-GlcNAc. (B) Represents the stepwise production follows by consumption of UMP, UDP, and UTP. (C) Shows the time course of ATP and ADP during the batch. The experiments were carried out in triplicates. Error bars represent the standard deviation. 39

Figure 4.4. The chromatogram of the UDP-GlcNAc cascade after 22 h. The high synthesis yield and catalytic usage of ATP resulted in UDP-GlcNAc as the major product of the cascade. 40

Figure 4.5. Time course of Uri consumption and UDP-GalNAc production with the proposed cascade. The reaction conditions were as follows: Tris-HCl (pH, 8.5) 150 mM; MgCl₂ 75 mM; Uri 53 mM; GalNAc 53 mM; ATP 2.6 mM; PolyP_n 20 mM; UDK 0.07 µg/µL; UMPK/PPK3 0.11 µg/µL; NAHK 0.15 µg/µL; GLMU 0.27 µg/µL, and PPA 0.08 µg/µL in a total volume of 200 µL. 40

Figure 4.6. Multi-enzyme cascade of six enzymes and seven reactions for synthesis of uridine diphosphate galactose (UDP-Gal) from uridine (Uri), galactose (Gal), polyphosphate (PolyP_n), and catalytic amounts of adenosine triphosphate (ATP). Abbreviations: UMP, uridine monophosphate; UDP, uridine diphosphate; UTP, uridine triphosphate; Gal-1P, galactose 1-phosphate; P_i, diphosphate; P_i, phosphate; ADP, adenosine diphosphate; UDK, uridine/cytidine kinase; UMPK, UMP/CMP kinase; PPK3, PolyP_n kinase; GALU, glucose 1-phosphate uridylyltransferase; GALK, galactokinase; PPA, inorganic diphosphatase. 41

Figure 4.7. Time course of substrates, intermediates, and products for synthesis of UDP-Gal under optimized condition: Tris-HCl (pH, 8.5) 150 mM; MgCl₂ 75 mM; Uri 50 mM; Gal 52 mM; ATP 0.6 mM; PolyP_n 20 mM; UDK 0.07 µg/µL; UMPK/PPK3 0.11 µg/µL; GALK 0.16 µg/µL; GALU 0.12 µg/µL, and PPA 0.06 µg/µL. A) Concentration of Uri and UDP-Gal. B) Concentration of UMP, UDP, and UTP. C) Concentration of ADP and ATP. Reactions were carried out in triplicate and error bars represent the standard deviation. 42

Figure 4.8. Multi-enzyme cascade of seven enzymes and eight reactions for synthesis of uridine diphosphate glucose (UDP-Glc) from uridine (Uri), glucose (Glc), polyphosphate (PolyP_n), and catalytic amounts of adenosine triphosphate (ATP). Abbreviations: UMP, uridine monophosphate; UDP, uridine diphosphate; UTP, uridine triphosphate; Glc-6P, glucose 6-phosphate; Glc-1P, glucose 1-phosphate; P_i, diphosphate; P_i, phosphate; ADP, adenosine diphosphate; UDK, uridine/cytidine kinase; UMPK, UMP/CMP kinase; PPK3, PolyP_n kinase; GALU, glucose 1-phosphate uridylyltransferase; GLK, glucokinase; MANB, phosphomannomutase; PPA, inorganic diphosphatase. 43

Figure 4.9. Time course of reaction substrates, intermediates, and products of the UDP-Glc cascade. The reaction conditions were as follows: 150 mM Tris-HCl (pH 8.5); 75 mM MgCl₂; 62.5 mM Glc; 60 mM Uri; 1.7 mM ATP; 19 mM PolyP_n; 0.86 µg/µL GLK; 0.06 µg/µL UDK; 0.1 µg/µL UMPK/PPK3; 0.14 µg/µL MANB/C; 0.15 µg/µL GALU, and 0.04 µg/µL PPA. A) Concentration of Uri and UDP-Glc. B) Concentration of UMP, UDP, and UTP. C) Concentration of AMP, ADP, and ATP. Reactions were carried out in triplicate and error bars represent the standard deviation. 44

Figure 4.10. UV chromatogram of UDP-Man synthesis cascade reaction. The reaction contained 200 mM Tris-HCl (pH 8.5); 26 mM Man; 25 mM Uri; 7.3 mM ATP; 9.7 mM PolyP_n; 75 mM MgCl₂, and the following enzymes: 0.06 µg/µL UDK; 0.08 µg/µL UMPK/PPK3; 0.76 µg/µL GLK; 0.14 µg/µL MANB/C; 0.12 µg/µL GALU, and 0.04 µg/µL PPA in a final volume of 200 µL. 45

Figure 4.11. Cascade of seven enzymes and eight reactions for synthesis of guanosine diphosphate mannose (GDP-Man) from mannose (Man), guanosine (Guo), polyphosphate (PolyP_n), and catalytic amounts of adenosine triphosphate (ATP). Abbreviations: GMP, guanosine monophosphate; GDP, guanosine diphosphate; GTP, guanosine triphosphate; Man-6P, mannose 6-phosphate; Man-1P, mannose 1-phosphate; P_i, phosphate; ADP, adenosine diphosphate; GSK, guanosine kinase; GMPK, GMP kinase; PPK3, PolyP_n kinase; MANC, mannose 1-phosphate guanylyltransferase; GLK, glucokinase; MANB, phosphomannomutase; PPA, inorganic diphosphatase. 46

Figure 4.12. Time course of GDP-Man cascade substrates, intermediates, and products. The reaction conditions were as follows: 200 mM Tris-HCl (pH 8.5); 75 mM MgCl₂; 10 mM Man; 12.8 mM Guo; 5.8 mM ATP; 13.5 mM PolyP_n; 0.11 µg/µL GSK; 0.49 µg/µL GMPK; 0.02 µg/µL PPK3; 0.33 µg/µL GLK; 0.17 µg/µL MANB/C, and PPA 0.03 µg/µL with a final volume of 200 µL. The final DMSO content of the reaction matrix was 1% v/v. (A) Shows the consumption of Guo and production of GDP-Man. (B) Shows the reaction time courses of GMP, GDP, and GTP. (C) Shows the reaction time courses of ATP, ADP, and AMP. The production of AMP might be due to chemical conversion of ADP to ATP during the reaction. Experiments were performed in triplicates and error bars represent the standard deviation. 47

Figure 4.13. Multi-enzyme cascade for synthesis of guanosine diphosphate fucose (GDP-Fuc) starting from fucose (Fuc), guanosine (Guo), polyphosphate (PolyP_n), and catalytic amounts of adenosine triphosphate (ATP). Abbreviations: GMP, guanosine monophosphate; GDP, guanosine diphosphate; GTP, guanosine triphosphate; Fuc-1P, fucose 1-phosphate; P_i, phosphate; ADP, adenosine diphosphate; GSK, guanosine kinase; GMPK, GMP kinase; PPK3, PolyP_n kinase; FKP, fucokinase/ fucose 1-phosphate guanylyltransferase; PPA, inorganic diphosphatase. 48

Figure 4.14. Time course of reaction substrates, intermediates, and products for synthesis of GDP-Fuc from Guo, and Fuc. (A) Shows the consumption of Guo and production of GDP-Fuc. (B) Shows the reaction time courses of GMP, GDP, and GTP. (C) Shows the reaction time courses of ATP, ADP, and AMP. The production of AMP might be due to chemical conversion of ADP to ATP during the reaction. The reaction mixture contained 200 mM Tris-HCl (pH 7.5); 10 mM Fuc; 10 mM Guo (in DMSO); 2.5 mM ATP; 7.5 mM PolyP_n; 45 mM MgCl₂, and the following enzymes: GSK 0.22 µg/µL; GMPK 0.78 µg/µL; PPK3 0.05 µg/µL; FKP 0.31 µg/µL, and PPA 0.03 µg/µL in a final volume of 200 µL. Experiments were performed in triplicates and error bars represent the standard deviation. 49

Figure 4.15. A two-enzyme cascade for synthesis of guanosine diphosphate fucose (GDP-Fuc) from guanosine diphosphate mannose (GDP-Man). Abbreviations: GDP-4-dehydro-6-deoxy-Man, guanosine diphosphate-4-keto-6-deoxy -mannose; NADPH, reduced nicotinamide adenine dinucleotide phosphate; NADP⁺, nicotinamide adenine dinucleotide phosphate; H₂O, water; GMD, guanosine diphosphate mannose 4,6-dehydratase; WCAG, guanosine diphosphate L-fucose synthase. 50

Figure 4.16. Conversion of GDP-Man to GDP-Fuc after 5 h incubation with a two-enzyme cascade. The conditions were as follows: 150 mM Tris-HCl; 10 mM MgCl₂; 3–4 mM GDP-Man; 4 mM NADPH; WCAG 0.45 µg/µL, and GMD 1.03 µg/µL with a final volume of 33 µL. Experiments were carried out in triplicate and error bars represent the standard deviation. 50

Figure 4.17. Extended cascade for the synthesis of guanosine diphosphate fucose (GDP-Fuc) from mannose (Man), guanosine (Guo), polyphosphate (PolyP_n), L-glutamate (L-Glu), and catalytic amounts of adenosine triphosphate (ATP) and reduced nicotinamide adenine dinucleotide phosphate (NADPH). Abbreviations: GMP, guanosine monophosphate; GDP, guanosine diphosphate; GTP, guanosine triphosphate; ADP, adenosine diphosphate; Man-6P, mannose 6-phosphate; Man-1P, mannose 1-phosphate; GDP-Man, guanosine diphosphate mannose; GDP-4-dehydro-6-deoxy-Man, guanosine diphosphate-4-keto-6-deoxy-mannose; NADP⁺, nicotinamide adenine dinucleotide phosphate; NH₃, ammonia; AKG, α-ketoglutaric acid; H₂O, water; P_i, phosphate; GSK, guanosine kinase; GMPK, GMP kinase; PPK3, PolyP_n kinase; GLK, glucokinase; MANB, phosphomannomutase; MANC, mannose 1-phosphate guanylyltransferase; PPA, inorganic diphosphatase; GMD, guanosine diphosphate mannose 4,6-dehydratase; WCAG, guanosine diphosphate L-fucose synthase; GLDH, glutamate dehydrogenase. 51

Figure 4.18. Time course of cascade substrates, intermediates, and products for synthesis of GDP-Fuc from Man and Guo. (A) Shows the consumption of Guo, the production of GDP-Man, and its consumption for synthesis of GDP-Fuc; (B) shows the production of GMP followed by its consumption

for production of GDP and GTP. (C) Shows the concentration of ATP, ADP as well as AMP. The production of AMP might be due to chemical conversion of ADP to ATP. The cascade reactions contained 200 mM Tris-HCl (pH 8.5); 75 mM MgCl₂; 10.5 mM Man; 10.5 mM Guo; 50 mM L-Glu; 1 mM NADPH; 5.5 mM ATP; 13.5 mM PolyP_n; GSK 0.11 µg/µL; GMPK 0.49 µg/µL; PPK3 0.02 µg/µL; GLK 0.33 µg/µL; MANB/C 0.17 µg/µL; WCAG 0.07 µg/µL; GMD 0.17 µg/µL; PPA 0.03 µg/µL, and 10 units of GLDH 2.99 µg/µL in a final volume of 200 µL. Experiments were carried out in triplicates and error bars represent the standard deviation. 52

Figure 4.19. Multi-enzyme cascade of five enzymes and six reactions for synthesis of cytidine monophosphate N-acetylneuraminic acid (CMP-Neu5Ac) from cytidine (Cyt), N-acetylneuraminic acid (Neu5Ac), polyphosphate (PolyP_n), and catalytic amounts of adenosine triphosphate (ATP). Abbreviations: CMP, cytidine monophosphate; CDP, cytidine diphosphate; CTP, cytidine triphosphate; PPI, diphosphate; Pi, phosphate; ADP, adenosine diphosphate; UDK, uridine/cytidine kinase; UMPK, UMP/CMP kinase; PPK3, PolyP_n kinase; CSS, N-acylneuraminate cytidyltransferase; PPA, inorganic diphosphatase. 53

Figure 4.20. The UV chromatogram of CMP-Neu5Ac cascade reaction product after 12 h. The reaction mixture consisted of 150 mM Tris-HCl (pH 8.5); 10 mM Cyt; 10 mM Neu5Ac; 3 mM ATP; 4 mM PolyP_n; 50 mM MgCl₂, and the following enzymes: UDK 0.06 µg/µL; UMPK/PPK3 0.11 µg/µL; CSS 1.27 µg/µL, and PPA 0.04 µg/µL in a final volume of 200 µL. 54

Figure 4.21. Multi-enzyme cascade of seven enzymes and eight reactions for synthesis of N-acetylneuraminic acid (CMP-Neu5Ac) from N-acetylglucosamine (GlcNAc), pyruvate (Pyr), cytidine (Cyt), polyphosphate (PolyP_n), and catalytic amounts of adenosine triphosphate (ATP). Abbreviations: CMP, cytidine monophosphate; CDP, cytidine diphosphate; CTP, cytidine triphosphate; PPI, diphosphate; Pi, phosphate; ADP, adenosine diphosphate; ManNAc, N-acetylmannosamine; UDK, uridine/cytidine kinase; UMPK, UMP/CMP kinase; PPK3, PolyP_n kinase; AGE, N-acylglucosamine 2-epimerase; NANA, N-acetylneuraminate lyase; CSS, N-acylneuraminate cytidyltransferase; PPA, inorganic diphosphatase. 55

Figure 4.22. UV chromatogram of the cascade product for synthesis of CMP-Neu5Ac using GlcNAc as the sugar source. The following conditions were used: 140 mM Tris-HCl (pH 8.5); 35 mM Cyt; 39 mM GlcNAc; 39 mM Pyr; 3.5 mM ATP; 14.1 mM PolyP_n; 53 mM MgCl₂, and the following enzymes: UDK 0.09 µg/µL; UMPK/PPK3 0.15 µg/µL; CSS 1.22 µg/µL; AGE 0.03 µg/µL; NANA 0.08 µg/µL, and PPA 0.05 µg/µL in a final volume of 282 µL. 56

Figure 4.23. AGE inhibition by CTP. Reactions starting from ManNAc had the highest production of CMP-Neu5Ac (AGE_2, and AGE_4) while reactions starting from GlcNAc did not result in significant production of CMP-Neu5Ac (AGE_1, and AGE_3). Experiments performed with 150 mM Tris-HCl (pH 8.5); 20 mM MgCl₂; 20 mM CTP; 30 mM Pyr; 0.05 µg/µL AGE; 1.5 µg/µL NANA; 1 µg/µL CSS, and 0.04 µg/µL PPA in a total volume of 150 µL. The 1st experiment contained 30 mM GlcNAc (AGE_1), the 2nd experiment contained 30 mM ManNAc (AGE_2), the 3rd experiment contained 30 mM GlcNAc and 0.3 mM ATP (AGE_3), and the 4th experiment contained 30 mM ManNAc and 0.3 mM ATP (AGE_4). The experiments were running for 5 h. 57

Figure 4.24. Reaction chromatogram after 24 h incubation at 37°C using increased ratio of GlcNAc/Cyt and Pyr/Cyt. The reaction consisted of 145 mM Tris-HCl (pH 8.5); 10 mM Cyt; 74 mM GlcNAc; 79 mM Pyr; 3 mM ATP; 4 mM PolyP_n; 74 mM MgCl₂; UDK 0.06 µg/µL; UMPK/PPK3 0.08 µg/µL; CSS 1.67 µg/µL; AGE 0.04 µg/µL; NANA 1.15 µg/µL, and PPA 0.05 µg/µL in a final volume of 203 µL. 58

Figure 4.25. Overlay of reaction chromatograms from incremental amounts of PolyP_n after 24 h of incubation at 37°C. The experimental conditions were as follows: 150 mM Tris-HCl (pH 8.5); 10 mM Cyt; 75 mM GlcNAc; 70 mM Pyr; 3 mM ATP; and 75 mM MgCl₂; UDK 0.06 µg/µL; UMPK/PPK3 0.08 µg/µL; CSS 1.27 µg/µL; AGE 0.04 µg/µL, and NANA 1.16 µg/µL in a final volume of 200 µL. 58

Figure 4.26. Time course of cascade substrates, products, and intermediates of CMP-Neu5Ac cascade from GlcNAc, Pyr, Cyt, PolyP_n, and catalytic amounts of ATP. (A) Consumption of Cyt and sequential production of CMP-Neu5Ac. (B) Production and consumption of CMP, CDP, and CTP. (C) Concentration of ATP, ADP, and AMP during the reaction. The reaction contained 190 mM Tris-HCl (pH 8.5); 34 mM Cyt; 72 mM GlcNAc; 79 mM Pyr; 2 mM ATP; 23 mM PolyP_n; 72 mM MgCl₂; UDK 0.05 µg/µL; UMPK/PPK3 0.07 µg/µL; CSS 1.05 µg/µL; AGE 0.03 µg/µL; NANA 0.96 µg/µL, and PPA 0.03 µg/µL with a final volume of 242 µL. The experiments were performed in triplicate and the error bars represent the standard deviation. 59

Figure 4.27. Coupling strategy for synthesis of 3-fucosyllactose (3-FL) through a cascade of 11 enzymes and 12 reactions from mannose (Man), lactose (Lac), polyphosphate (PolyP_n), L-glutamate (L-Glu), catalytic amounts of adenosine triphosphate (ATP), reduced nicotinamide adenine dinucleotide phosphate (NADPH), and guanosine (Guo). Abbreviations: GMP, guanosine monophosphate; GDP, guanosine diphosphate; GTP, guanosine triphosphate; ADP, adenosine diphosphate; Man-6P, mannose 6-phosphate; Man-1P, mannose 1-phosphate; GDP-Man, guanosine diphosphate mannose; GDP-Fuc, guanosine diphosphate fucose; GDP-4-dehydro-6-deoxy-Man, guanosine diphosphate-4-keto-6-deoxy-mannose; NADP⁺, nicotinamide adenine dinucleotide phosphate; NH₃, ammonia; AKG, α-ketoglutaric acid; H₂O, water; PPi, diphosphate; Pi, phosphate; GSK, guanosine kinase; GMPK, GMP kinase; PPK3, PolyP_n kinase; GLK, glucokinase; MANB, phosphomannomutase; MANC, mannose 1-phosphate guanylyltransferase; PPA, inorganic diphosphatase; GMD, guanosine diphosphate mannose 4,6-dehydratase; WCAG, guanosine diphosphate L-fucose synthase; GLDH, glutamate dehydrogenase; 3/4-FT, α1-3/4-fucosyltransferase.

..... 75

Figure 4.28. The HPAEC-PAD chromatogram of 3-FL synthesis based on the coupling approach. The second peak on the right (~7 min) is the remaining Lac. The reactions consisted of: 160 mM Tris-HCl (pH 8.5); 60 mM MgCl₂; 24 mM Lac; 24 mM Man; 4 mM Guo; 87 mM L-Glu; 0.8 mM NADPH; 4.4 mM ATP; 10.8 mM PolyP_n; GSK 0.09 μg/μL; GMPK 0.39 μg/μL; PPK3 0.01 μg/μL; GLK 0.4 μg/μL; MANB/C 0.15 μg/μL; WCAG 0.05 μg/μL; GMD 0.14 μg/μL; PPA 0.02 μg/μL; 3/4-FT 0.11 μg/μL, and 10 units of GLDH (2.39 μg/μL) in a final volume of 251 μL. Abbreviations: nC, nano-coulombs (dimension of PAD signal)..... 75

Figure 4.29. Synthesis of 3-fucosyllactose (3-FL) in the coupling approach through a cascade of six enzymes and eight reactions using fucose (Fuc), lactose (Lac), polyphosphate (PolyP_n), and catalytic amounts of guanosine (Guo), and adenosine triphosphate (ATP). Abbreviations: GMP, guanosine monophosphate; GDP, guanosine diphosphate; GTP, guanosine triphosphate; ADP, adenosine diphosphate; Fuc-1P, fucose 1-phosphate; GDP-Fuc, guanosine diphosphate fucose; PPi, diphosphate; Pi, phosphate; GSK, guanosine kinase; GMPK, GMP kinase; PPK3, PolyP_n kinase; FKP, fucokinase/ fucose 1-phosphate guanylyltransferase; PPA, inorganic diphosphatase; 3/4-FT, α1-3/4-fucosyltransferase..... 76

Figure 4.30. Synthesis of 6'-sialyllactose 6'-SL based on the coupling approach with a cascade of eight enzymes and nine reactions from N-acetylglucosamine (GlcNAc), pyruvate (Pyr), polyphosphate (PolyP_n), and catalytic amounts of adenosine triphosphate (ATP), and cytidine (Cyt). Abbreviations: CMP, cytidine monophosphate; CDP, cytidine diphosphate; CTP, cytidine triphosphate; PPi, diphosphate; Pi, phosphate; ADP, adenosine diphosphate; ManNAc, N-acetylmannosamine; UDK, uridine/cytidine kinase; UMPK, UMP/CMP kinase; PPK3, PolyP_n kinase; AGE, N-acetylglucosamine 2-epimerase; NANA, N-acetylneuraminase lyase; CSS, N-acetylneuraminase cytidyltransferase; PPA, inorganic diphosphatase..... 77

Figure 4.31. Modular approach for synthesis of HMOs. In this approach, sugar nucleotide is first produced in a separate pot. Afterwards, sugar nucleotide is mixed with an acceptor, a glycosyltransferase, and an optional AP. Abbreviations: Uri, uridine; ATP, adenosine triphosphate; ADP, adenosine diphosphate; UMP, uridine monophosphate; UDP, uridine diphosphate; UTP, uridine triphosphate; Gal-1P, galactose 1-phosphate; PPi, diphosphate; Pi, phosphate; PolyP_n; polyphosphate. Symbols: yellow circle, galactose; blue square; N-acetylglucosamine..... 78

Figure 4.32. The HPAEC-PAD chromatogram of LacNAc synthesis reaction based on the modular approach. The reaction mixture for LacNAc synthesis contained 94 mM MES buffer (pH 6.0); 31 mM GlcNAc; 30 mM UDP-Gal; β1,4GalT 0.01 μg/μL, and 10 units of AP in a final volume of 160 μL. 79

Figure 4.33. The HPAEC-PAD chromatogram of modular LNT II synthesis. (A) Reaction product and LNT II standard. The peak at ~7 min is the remaining Lac. (B) MS/MS spectra of the peak at 568.0 Da. Theoretical mass of LNT II is [M+Na]⁺: 568.2 Da. The reaction conditions were as follows: 210 μL of a reaction mixture containing 150 mM Tris-HCl (pH 8.5); 20 mM MnCl₂; 28.5 mM Lac; 20 mM UDP-GlcNAc; β1,3GlcNAcT 0.08 μg/μL, and 10 units of AP in a total volume of 210 μL. Abbreviations: Da, Dalton; m/z, mass/charge ratio; au, arbitrary units. 79

Figure 4.34. Synthesis of LNnT based on the modular approach. (A) HPAEC-PAD chromatogram of reaction product and LNnT standard. The peak at ~9 min is remaining LNT II. (B) MS/MS of peak at m/z 729.9. Theoretical mass of LNnT is [M+Na]⁺: 730.2 Da. The reaction mixture contained 156 mM

MES buffer (pH 5.5); 3.7 mM LNT II; 11 mM UDP-Gal; β 1,4GalT 0.01 μ g/ μ L, and 20 units of AP in a total volume of 320 μ L..... 80

Figure 4.35. Synthesis of para-LNnH based on the modular approach. MS/MS of peak at m/z 1094.9. Theoretical mass of para-LNnH is $[M+Na]^+$: 1095.3 Da. At first, para-Lacto-N-neopentose was produced through the combination of 75 μ L of UDP-GlcNAc cascade product (~10 mM UDP-GlcNAc); 75 μ L of LNnT reaction products; 30 units of AP; 0.06 μ g/ μ L of β 1,3GlcNAcT, and 150 mM Tris-HCl (pH 8.5) in a total volume of 270 μ L. After 24 h of incubation (at 30°C), 50 μ L reaction containing para-Lacto-N-neopentose was mixed with 50 μ L of UDP-Gal cascade reaction product in addition to 20 units of AP; 0.02 μ g/ μ L β 1,4GalT, and 240 MES buffer (pH 6.5) in a total volume of 210 μ L..... 81

Figure 4.36. Modular synthesis of 6'-SL. (A) HPAEC-PAD chromatogram of reaction products for synthesis of 6'-SL. (B) MS/MS spectra of peak at m/z of 655.9. Theoretical mass of 6'-SL is $[M+Na]^+$: 656.2 Da. For synthesis of 6'-SL. The reaction solution contained: 18 mM CMP-Neu5Ac; 20 mM Lac; 133 mM Tris-HCl (pH 8.5), and 0.13 μ g/ μ L 2,6-ST in a final volume of 150 μ L. 82

Figure 4.37. MS spectra of LST_c and DSLNnT synthesis based on modular concept. Theoretical masses are as follows: LST_c, $[M+Na]^+$: 1021.3 Da; LST_c, $[M+2Na]^+$: 1044.2 Da; DSLNnT, $[M Na]^+$: 1312.4 Da; DSLNnT $[M+2Na]^+$: 1335.3 Da; DSLNnT, $[M + 3Na]^+$: 1358.2 Da. The reaction contained: 5 mM CMP-Neu5Ac; 0.7 mM LNnT; 0.14 μ g/ μ L 2,6-ST, and 240 mM Tris-HCl (pH 9), in a total volume of 210 μ L. 83

Figure 4.38. MS spectra of reaction product for synthesis of LNFP III and DF-LNnT based on modular concept. Theoretical mass of LNFP III is $[M+Na]^+$: 876.3 Da. Theoretical mass of DF-LNnT is $[M+Na]^+$: 1022.3 Da. The reaction contained 3 mM GDP-Fuc; 0.9 mM LNnT; 0.15 μ g/ μ L 3/4-FT; 146 mM Tris-HCl (pH 8.5), and 20 units of AP in a total volume of 205 μ L. 84

Figure 4.39. The steps for LNFP V synthesis. 85

Figure 4.40. HPAEC-PAD chromatogram of LNFP V synthesis. The impurities (i.e., peaks before and after LNFP V) were not identified. At first, LNT II was produced as described in section 4.2.2.2. The reaction mixture for synthesis of fucosylated LNT II consisted of 210 mM Tris-HCl (pH 8.5); LNT II (~2.6 mM); 0.07 μ g/ μ L 3/4-FT, and 2 mM GDP-Fuc in a total volume of 190 μ L. After 24 h of incubation at 37°C, 100 μ L of the reaction mixture was transferred to a new vial containing: 5 mM UDP-Gal; 0.01 μ g/ μ L β 1,4GalT, and 167 mM MES buffer (pH 6.0). 85

Figure 4.41. Synthesis of 6'-SLN based on the modular concept. (A) Overlay of HPAEC-PAD chromatogram of reaction product and pure 6'-SLN. (B) MS spectra of reaction product. Theoretical mass of 6'-SLN is $[M+2Na]^+$: 720.0 Da. The reaction consisted of 115 mM Tris-HCl (pH 8.5); 6.1 mM LacNAc; 8.5 mM CMP-Neu5Ac; 0.10 μ g/ μ L 2,6-ST, and 5 units of AP in a total volume of 175 μ L. ... 86

Figure 4.42. Glycosylation profile of therapeutic antibodies before and after in vitro glycoengineering. (A) Glycosylation profile of Rituximab. (B) Glycosylation profile of in vitro glycoengineered Rituximab. (C) Glycosylation profile of Trastuzumab. (D) Glycosylation profile of in vitro glycoengineered Trastuzumab. (E) Glycosylation profile of Ramucirumab. (F) Glycosylation profile of in vitro glycoengineered Ramucirumab. Experiments were performed as follows: 100 μ g of each protein was incubated in 50 mM MES buffer (pH 6.5), 50 milli units of β 1,4GalT (from bovine milk, Merck, Germany); 5 mM UDP-Gal, and 5 mM MnCl₂ in a total volume of 100 μ L for ~20 h at 37°C and 550 rpm. Abbreviation: MTU ", migration time unit. The " " means that the MTU was normalized for two times. 92

Figure 4.43. UV chromatogram of Fc γ R-IIIa affinity chromatography of original and engineered mAbs. (A) Rituximab and glycoengineered Rituximab. (B) Trastuzumab and glycoengineered Trastuzumab. (C) Ramucirumab and glycoengineered Ramucirumab. The elution after higher amount of desorption buffer (more acidic condition) represents stronger binding of glycoengineered antibodies to the Fc γ R-IIIa receptors and accordingly, higher ADCC activity. 93

Figure 4.44. Overlay of FcR-IIIa affinity chromatography of Obinutuzumab and in vitro glycoengineered Obinutuzumab. Clearly, galactosylated version of Obinutuzumab is even further increase its ADCC activity. 94

Figure 4.45. Results of in vitro addition of terminal Gal to CHO-DP12 derived IgG. A) Electropherogram of APTS-labeled glycan from IgG. B) Electropherogram of APTS-labeled glycan from glycoengineered IgG. C) Mass spectra of released glycan from IgG, G0F theoretical mass $[M+Na]^+$:1485.5 Da, G1F theoretical mass $[M+Na]^+$:1647.6 Da, G2F theoretical mass $[M+Na]^+$:1809.6 Da. The reaction contained 0.13 mg pure IgG (cell culture derived); 190 mM MES buffer pH 6.5; 14

mM MnCl₂; 1.4 mM UDP-Gal (pure, commercial), and 0.3 µg/µL β1,4GALT1 in a total volume of 211 µL. The samples were analysed after 24 h of incubation at 37°C and 550 rpm. 95

Figure 4.46. Illustration of the concept of artificial Golgi. Man9 glycoproteins are produced by treatment of the host cells with a mannosidase I inhibitor e.g., kifunensine. Afterwards, Man9 structure can be trimmed and tailored into any desired structure. It should be noted that the concept is only practical once the glycans are available to glycosidase and glycosyltransferases. Abbreviation: Man I, α-1,2-mannosidase; MGAT1, α-1,3-mannosyl-glycoprotein 2-beta-N-acetylglucosaminyltransferase; Man II, Golgi α-mannosidase II; MGAT2, α-1,6-mannosyl-glycoprotein 2-beta-N-acetylglucosaminyltransferase. 96

Figure 4.47. Results of different steps for synthesis of Man3-G0 from Man3. A) Analysis of APTS-labeled Man3 which was used as the substrate. B) Activity of MGAT1 on APTS-labeled Man3. C) One-pot conversion of Man3 to G0 by using MGAT1 and MGAT2. The reaction for conversion of Man3 to Man3-G0 consisted of 50 µL APTS-labeled Man3; 1.8 mM UDP-GlcNAc; 93 mM HEPES buffer (pH 7.4); 9.3 mM MnCl₂, and 0.3 µg/µL MGAT1 in a total volume of 107 µL. The experiment for synthesis of Man3-G0 from Man3 was as follows: 100 mM HEPES buffer (pH 7.4); 10 mM MnCl₂; 2.5 mM UDP-GlcNAc; 50 µL Man3; 0.1 µg/µL MGAT1, and 0.3 µg/µL MGAT2 in a volume of 200 µL. The samples were analyzed after 6 h incubation at 37°C and 550 rpm. 97

Figure 4.48. Production of anti-interleukin 8 antibody with Man9 glycosylation profile. A) CGE-LIF electropherogram of glycans from kifunensin-derived IgG. B) Mass spectra of released glycan from kifunensin-derived IgG, theoretical Man9 mass [M+Na]⁺:1905.6 Da, theoretical Man8 mass [M+Na]⁺:1743.6 Da. Abbreviation: RFU, relative fluorescence unit. 98

Figure 4.49. Synthesis of antibodies with Man5 structure from Man9-containing antibodies. The conversion was achieved by using bacterial α-1,2-mannosidase. The experimental condition for conversion of Man9 to Man5 antibodies was as follows: 2.4 mg IgG (purified – kifunensine derived); 2.6 µg/µL Man I; 10 mM MgCl₂, and 200 mM MES buffer (pH 6.5) in a total volume of 100 µL. 98

Figure 4.50. One-pot conversion of Man9-containing IgG into Man5 and Man5-G0 IgG. The reaction contained: 1.8 mg Man9 IgG; 1.9 µg/µL Man I; 1.9 µg/µL MGAT1; 1.5 mM UDP-GlcNAc; 10 mM MgCl₂; 10 mM MnCl₂, and 200 mM MES buffer (pH 6.5) in a total volume of 133 µL. The experiment was running for 24 h. 99

Figure 4.51. 1 L scale and 200 µL synthesis of UDP-Gal using the supernatant from a cell lysate at 37°C and 60 rpm (magnetic stirrer): A) Uri and UDP-Gal; B) UMP; C) UDP; D) UTP; E) ATP; F) ADP; G) AMP. The synthesis condition was as follows: 150 mM Tris-HCl (pH 8.5); 55 mM Uri; 55 mM Gal; 6.2 mM ATP; 20 mM PolyP_n, and 75 mM MgCl₂. 105

Figure 4.52. Time course of reaction substrates, intermediate, and products for large-scale synthesis of UDP-GlcNAc. (A) UDP-GlcNAc, (B) Uri, (C) UMP, (D) UDP, (E) UTP, (F) ADP and ATP. The synthesis condition was as follows: 200 mM Tris-HCl (pH 8.5); 62 mM Uri; 62 mM GlcNAc; 1.6 mM ATP; 18 mM PolyP_n; 75 mM MgCl₂, and a total protein load of 0.5 g/L in the form of cell lysate. The reaction carried out at 37°C and 120 rpm. 106

Figure 4.53. Combination of six enzymes for production of uridine diphosphate N-acetylglucosamine (UDP-GlcNAc) and uridine diphosphate galactose (UDP-Gal) from uridine monophosphate (UMP), N-acetylglucosamine (GlcNAc), galactose (Gal), polyphosphate (PolyP_n), and catalytic amounts of adenosine triphosphate (ATP). Abbreviations: UDP, uridine diphosphate; UTP, uridine triphosphate; GlcNAc-1P, N-acetylglucosamine 1-phosphate; Gal-1P, galactose 1-phosphate; P₂i, diphosphate; P_i, phosphate; ADP, adenosine diphosphate; UMPK, UMP/CMP kinase; PPK3, PolyP_n kinase; GALU, glucose 1-phosphate uridylyltransferase; NAHK, N-acetylhexosamine 1-kinase; GALK, galactokinase; PPA, inorganic diphosphatase. 107

Figure 4.54. Time course of substrates, intermediates, and products of UDP-GlcNAc synthesis cascade based on co-expressed enzymes at 150 mL scale. In each graph, time course of each compound is compared at both scales. (A) UMP; (B) UDP-GlcNAc; (C) UDP; (D) UTP; (E) ATP; (F) ADP; (G) AMP. The reaction mixture consisted of 200 mM Tris-HCl (pH 8.5); 75 mM MgCl₂; 47 mM UMP; 50 mM GlcNAc; 4.7 mM ATP; 15 mM PolyP_n, and a total protein concentration of 0.5 g/L. 108

Figure 4.55. Time course of substrates, intermediates, and products of UDP-Gal synthesis cascade based on co-expressed enzymes at 3 L. (A) UMP; (B) UDP-Gal; (C) UDP; (D) UTP; (E) ATP; (F) ADP; (G) AMP. The reaction mixture consisted of 200 mM Tris-HCl (pH 8.5); 75 mM MgCl₂; 55 mM UMP; 55 mM Gal; 2.7 mM ATP; 14 mM PolyP_n, and a total protein (biocatalyst) concentration of 1 g/L. 109

Figure 4.56. HPAEC-UV chromatogram of large-scale synthesis of CMP-Neu5Ac from CMP, Neu5Ac, PolyP_n, and catalytic amounts of ATP. The reaction matrix contained 150 mM Tris-HCl (pH 8.5); 75 mM MgCl₂; 50 mM CMP; 51 mM Neu5Ac; 5 mM ATP, and 16 mM PolyP_n in a total volume of 100 mL. 110

Figure 4.57. Percentage of bound protein to each bead. On average total protein mass in each immobilization vial was 10 mg. Considering the mass of resin in each vial e.g., 200 mg, the ratio of protein to resin was 20. The experiments were performed in triplicate and errors bars represent the standard deviation. 112

Figure 4.58. HPAEC-UV chromatogram of reaction products of each bead after 24 h of reaction time (end point). The beads with UDP-GlcNAc as the major peak were selected for further activity tests. The feed solution consisted of 200 mM Tris-HCl (pH 8.5); 75 mM MgCl₂; 25 mM Uri; 25 mM GlcNAc; 5 mM ATP, and 10 mM PolyP_n. 250 μL of feed solution was added to beads and incubated at 37°C and 600 rpm for 24 h. 115

Figure 4.59. The area under the curve of UDP-GlcNAc peak was normalized to the area of all uridine-containing compounds and reported as conversion percentage. The experiments were carried out in triplicate, except for Relizyme HFA 403/S and Relizyme HFA 403/M, for which the average of three consecutive cycles are shown. Error bars represent the standard deviation. 116

Figure 4.60. Activity of each bead in 20 different cycles. In each cycle, the area under the UDP-GlcNAc peak was normalized to the area under the peak in the first batch. (A) Relizyme EP113/M; (B) ECR 8204F; (C) ECR 8204M; (D) ECR8215M; (E) ECR8209M; (F) ECR 8209F. Error bars represent the standard deviation. 117

List of Tables

Table 2.1. Examples of human milk oligosaccharides (HMOs), their molecular structures, and reported concentrations in human milk. Concentrations are reported from Ref. [85].	9
Table 3.1. List of genes used in this work for recombinant enzyme production.	17
Table 3.2. The glycan nomenclature and structure described in this work. The monosaccharide compositions are <i>N</i> -acetylglucosamine, blue square; mannose, green circle; fucose, red triangle, and galactose, yellow circle.	25
Table 3.3. Enzymes and plasmids used in this study for the co-expression of the cascade. The sugar kinases and the nucleotide kinases, respectively, were grouped together on one vector. Moreover, the uridylyltransferase and phosphatase were grouped together.	27
Table 4.1. Summary of previous works on multi-enzyme synthesis of UDP-GlcNAc.	63
Table 4.2. Summary of UDP-Gal synthesis described in literature based on whole cell and multi-enzyme catalysis.	65
Table 4.3. Summary of developed UDP-Glc synthesis cascade described in literature.	66
Table 4.4. Comparison of reported processes for the in vitro biocatalytic production of GDP-Man and GDP-Fuc.	70
Table 4.5. Comparison of reported processes for the in vitro biocatalytic production of CMP-Neu5Ac.	73
Table 4.6. List of resins used in this study as a support for co-immobilization of enzymes.	111

Author statement

The majority of this dissertation has been previously filed as patent applications and published in peer reviewed journals — with the author as one of the inventors and as the first author. The results presented in chapters 4.1.1.14.1.1.1 (UDP-GlcNAc synthesis), 4.4.1.2, and 4.4.3 were filed as a patent application under PCT/EP2020/077383. The short version of the cascade presented in the chapter 4.1.1.1 was published in Mahour *et al.* [221]. The results in chapters 4.1.1.2, 4.3.1, and 4.4.1.1 were filed as a patent application under PCT/EP2020/077396 and the manuscript has been published [220]. The results in chapter 4.1.2.1, 0, 4.2.1.1, and 4.2.2.7 were filed as a patent application under PCT/EP2020/059182 and results from chapters 4.1.2.1 and 0 were published in Mahour *et al.* [228]. The results in chapters 4.1.3, 4.2.1.2, 4.2.2.5, and 4.2.2.6 were filed as a patent application under PCT/EP2021/059101. The results in chapter 4.2 was filed as an invention disclosure under MI 1402-6174-LC-WA. The results in chapter 4.3 was filed as an invention disclosure under MI 1402-6183-LC-WA.

The *manuscripts under preparation* are listed at the end of this document under List of Scientific Contributions.

The use of text passages, figures, and diagrams has been confirmed to be in accordance with the copyright guidelines of the journals — and the same will be applied for the manuscripts under preparation.

The use of the author's other published and under-preparation manuscripts are hereby fully acknowledged and text passages, figures, and diagrams from these published and under-preparation manuscripts are not further referenced in the following.

List of Scientific Contributions

Publications

Mahour R., Lee J.W., Grimpe P., Boecker S., Grote V., Seidel-Morgenstern A., Klamt S., Rexer T.F.T., Reichl U. Cell-free multi-enzyme synthesis and purification of uridine diphosphate galactose. *Accepted for publication in ChemBioChem*.

Contribution: Designed the study, designed and performed the enzyme production and scale-up biotransformation experiments, data analysis and interpretation, data visualization, writing and editing.

Ruhnau J, Grote V, Juarez-Osorio M, Bruder D, **Mahour R**, Rapp E, Rexer TFT and Reichl U. 2021. Cell-Free Glycoengineering of the Recombinant SARS-CoV-2 Spike Glycoprotein. *Front. Bioeng. Biotechnol.* 9:699025.

Contribution: Provided intellectual input to the study. Designed and developed the platform used for glycoengineering of the model protein.

Litschko, C., Budde, I., Berger, M., Bethe, A., Schulze, J., Alcala Orozco, E.A., **Mahour, R.**, Goettig, P., Führung, J.I., Rexer, T. and Gerardy-Schahn, R., 2021. Mix-and-Match System for the Enzymatic Synthesis of Enantiopure Glycerol-3-Phosphate-Containing Capsule Polymer Backbones from *Actinobacillus pleuropneumoniae*, *Neisseria meningitidis*, and *Bibersteinia trehalosi*. *Mbio*, 12(3), pp.e00897-21.

Note: The result from this work is not presented in the dissertation.

Contribution: investigation, writing—review and editing. Designed and developed a multi-enzyme cascade for synthesis of cytidine diphosphate glycerol

Mahour R., Marichal-Gallardo P., Rexer T., Reichl U. Multi-enzyme cascades for the in vitro synthesis of guanosine diphosphate L-fucose. *ChemCatChem*. 2021;13(8):1981-9.

Contribution: Designed the study and solvent selection, designed and performed the enzyme production and biotransformation optimization experiments, data analysis and interpretation, data visualization, writing and editing.

Rexer, T.F., Wenzel, L., Hoffmann, M., Tischlik, S., Bergmann, C., Grote, V., Boecker, S., Bettenbrock, K., Schildbach, A., Kottler, R., **Mahour, R.**, Rapp, E., Pietzsch, M., and Reichl, U. 2020. Synthesis of lipid-linked oligosaccharides by a compartmentalized multi-enzyme cascade for the in vitro N-glycosylation of peptides. *Journal of Biotechnology*, 322, pp.54-65.

Contribution: writing, review, and editing.

Mahour, R.*, Klapproth, J.*, Rexer, T.F., Schildbach, A., Klamt, S., Pietzsch, M., Rapp, E. and Reichl, U., 2018. Establishment of a five-enzyme cell-free cascade for the synthesis of uridine diphosphate N-acetylglucosamine. *Journal of biotechnology*, 283, pp.120-129.

Contribution: Designed and performed the biotransformation experiments, data analysis and interpretation, data visualization, writing and editing.

** Authors contributed equally.*

Rexer, T.F.T, Schildbach, A., Klapproth, J., Schierhorn, A., **Mahour, R.**, Pietzsch, M., Rapp, E. and Reichl, U., 2018. One pot synthesis of GDP-mannose by a multi-enzyme cascade for enzymatic assembly of lipid-linked oligosaccharides. *Biotechnology and bioengineering*, 115(1), pp.192-205.

Contribution: investigation, writing—review and editing.

Patents

Rexer, T.F., **Mahour, R.**, 2020. Enzymatic method for preparation of CMP- N-Acetylneuraminic acid. PCT/EP2021/059101, International Publication Date: 14th October 2021

Mahour, R., Rexer, T.F., 2019. Enzymatic method for preparation of UDP-galactose. PCT/EP2020/077396, International Publication Date: 14th May 2021

Mahour, R., Rexer, T.F., 2019. Enzymatic method for preparation of UDP-N-acetylglucosamine. PCT/EP2020/077383, International Publication Date: 14th May 2021

Mahour, R., Rexer, T.F., 2019. Enzymatic method for preparation of GDP-fucose. PCT/EP2020/059182, International Publication Date: 08th October 2020, Priority Date: 01st April 2019.

Invention disclosures

Mahour, R., Rexer, T.F., Reichl, U. Platform for the *in-vitro* glycoengineering of proteins. MI 1402-6183-LC-WA

Mahour, R., Rexer, T.F. Platform for synthesis of human milk oligosaccharides and functional oligosaccharides. MI 1402-6174-LC-WA

Talks

Mahour R., Boecker S., Babakhani M., Rexer T.F.T., Reichl U. An efficient multi-enzyme process to produce activated sugars: case of uridine diphosphate N-acetylglucosamine. MECP 2020+1, Aachen (Online due to COVID 19 restrictions), Germany

Mahour, R. *In vitro* glycoengineering: toward synthetic glycosylation. International Max Planck Research School workshop 2018, Goslar, Germany

Mahour, R. Germany Cell free metabolic engineering for production of sugar nucleotide. International Max Planck Research School workshop 2017, Tangermünde, Germany

Posters

Mahour, R., Duarte, B., Rexer, T.F. and Reichl, U. one-pot multi-enzyme synthesis of UDP-Man. poster at Biocatalysis 2018, Hamburg, Germany

Mahour, R., Klapproth, J., Rexer, T.F., Schildbach, A., Pietzsch, M., Rapp, E. and Reichl, U. In vitro multi-enzymatic network for production of UDP-GlcNAc. poster presentation at DECHEMA Biotransformation 2017, Hannover, Germany

Mahour, R., Klapproth, J., Rexer, T.F.T, Schildbach, A., Pietzsch, M., Rapp, E. and Reichl, U. In vitro multi-enzymatic network for production of UDP-GlcNAc. Glycobiotec2017, Berlin, Germany

Supervised Theses

Pia Grimpe (2020), Otto-von-Guericke-Universität Magdeburg, Germany, BSc thesis, Optimization of a multi-enzyme system for production of UDP-Gal

Suzana Cvijetinovic (2018), KTH Royal Institute of Technology, Sweden, MSc thesis, Development of cascade of immobilized enzymes for synthesis of activated sugars

Cláudia Bento (2018), Universidade NOVA de Lisboa, Portugal, MSc thesis, Advanced development of sugar nucleotides cascades (UDP-Glc and UDP-Man)

Stefanie Schmidt (2017), University of Applied Sciences Jena, Germany, MSc thesis, HPAEC-UV/PAD method development for quantification of hexosamine pathway

Supervised Internships

Hessel van der Eijk (2019), TU Delft, The Netherlands, MSc student intern, immobilization of a multienzyme cascade for production of CMP-Neu5Ac

Masoud Babakhani (2019), Otto-von-Guericke-Universität Magdeburg, Germany, MSc student guest researcher, Development of techno-economic models for multi-enzyme processes based on SuperPro Designer software

Claire Telfer (2018), Rice University, United States, BSc intern, Assistant in development of multienzyme system for synthesis of GDP-Fuc

Bibliography

1. Spiro, R.G. Glycoproteins. In *Advances in protein chemistry*; Elsevier, 1973; Vol. 27, pp. 349–467 ISBN 0065-3233.
2. Stanley, P. Golgi glycosylation. *Cold Spring Harb. Perspect. Biol.* **2011**, 3, a005199.
3. Walsh, G.; Jefferis, R. Post-translational modifications in the context of therapeutic proteins. *Nat. Biotechnol.* **2006**, 24, 1241–1252.
4. Erbayraktar, S.; Grasso, G.; Sfacteria, A.; Xie, Q.; Coleman, T.; Kreilgaard, M.; Torup, L.; Sager, T.; Erbayraktar, Z.; Gokmen, N. Asialoerythropoietin is a nonerythropoietic cytokine with broad neuroprotective activity in vivo. *Proc. Natl. Acad. Sci.* **2003**, 100, 6741–6746.
5. Geuijen, K.P.M.; Oppers-Tiemissen, C.; Egging, D.F.; Simons, P.J.; Boon, L.; Schasfoort, R.B.M.; Eppink, M.H.M. Rapid screening of IgG quality attributes—effects on Fc receptor binding. *FEBS Open Bio* **2017**, 7, 1557–1574.
6. Wada, R.; Matsui, M.; Kawasaki, N. Influence of N-glycosylation on effector functions and thermal stability of glycoengineered IgG1 monoclonal antibody with homogeneous glycoforms. *MAbs* **2019**, 11, 350–372.
7. Donini, R.; Haslam, S.M.; Kontoravdi, C. Glycoengineering Chinese hamster ovary cells: a short history. *Biochem. Soc. Trans.* **2021**.
8. Ma, B.; Guan, X.; Li, Y.; Shang, S.; Li, J.; Tan, Z. Protein Glycoengineering: An Approach for Improving Protein Properties. *Front. Chem.* **2020**, 8, 622.
9. Mastrangeli, R.; Palinsky, W.; Bierau, H. Glycoengineered antibodies: towards the next-generation of immunotherapeutics. *Glycobiology* **2019**, 29, 199–210.
10. Brühlmann, D.; Vuillemin, T.; Satwekar, A.; Galano, E.; Palmese, A.; D'Angelo, A.; Manco, Z.; Souquet, J.; Broly, H.; Sauer, M. Generation of site-distinct N-glycan variants for in vitro bioactivity testing. *Biotechnol. Bioeng.* **2019**, 116, 1017–1028.
11. Kirmiz, N.; Robinson, R.C.; Shah, I.M.; Barile, D.; Mills, D.A. Milk glycans and their interaction with the infant-gut microbiota. *Annu. Rev. Food Sci. Technol.* **2018**, 9, 429–450.
12. Comstock, S.S.; Donovan, S.M. Human Milk Oligosaccharides as Modulators of Intestinal and Systemic Immunity. In *Prebiotics and Probiotics in Human Milk: Origins and Functions of Milk-Borne Oligosaccharides and Bacteria*; Elsevier Inc., 2017; pp. 223–248 ISBN 9780128027257.
13. Bode, L. Human milk oligosaccharides: every baby needs a sugar mama. *Glycobiology* **2012**, 22, 1147–1162.
14. Ayechu-Muruzabal, V.; van Stigt, A.H.; Mank, M.; Willemsen, L.E.M.; Stahl, B.; Garssen, J.; Van't Land, B. Diversity of human milk oligosaccharides and effects on early life immune development. *Front. Pediatr.* **2018**, 6, 239.
15. Newburg, D.S.; Grave, G. Recent advances in human milk glycobiology. *Pediatr. Res.* **2014**, 75, 675–679.
16. Berger, P.K.; Plows, J.F.; Jones, R.B.; Alderete, T.L.; Yonemitsu, C.; Poulsen, M.; Ryoo, J.H.; Peterson, B.S.; Bode, L.; Goran, M.I. Human milk oligosaccharide 2'-fucosyllactose links feedings at 1 month to cognitive development at 24 months in infants of normal and overweight mothers. *PLoS One* **2020**, 15, e0228323.
17. Lagström, H.; Rautava, S.; Ollila, H.; Kaljonen, A.; Turta, O.; Mäkelä, J.; Yonemitsu, C.; Gupta, J.; Bode, L. Associations between human milk oligosaccharides and growth in infancy and early childhood. *Am. J. Clin. Nutr.* **2020**.
18. Šuligoj, T.; Vignæs, L.K.; Abbeele, P. Van den; Apostolou, A.; Karalis, K.; Savva, G.M.; McConnell, B.; Juge, N. Effects of Human Milk Oligosaccharides on the Adult Gut Microbiota and Barrier Function. *Nutrients* **2020**, 12, 2808.
19. Elison, E.; Vignæs, L.K.; Krogsgaard, L.R.; Rasmussen, J.; Sørensen, N.; McConnell, B.; Hennem, T.; Sommer, M.O.A.; Bytzer, P. Oral supplementation of healthy adults with 2'-O-fucosyllactose and lacto-N-neotetraose is well tolerated and shifts the intestinal microbiota. *Br. J. Nutr.* **2016**, 116, 1356–1368.
20. Martin, C.R.; Ling, P.-R.; Blackburn, G.L. Review of infant feeding: key features of breast milk and infant formula. *Nutrients* **2016**, 8, 279.
21. Robinson, R.C. Structures and metabolic properties of bovine milk oligosaccharides and their potential in the development of novel therapeutics. *Front. Nutr.* **2019**, 6, 50.
22. Hernell, O. Human milk vs. cow's milk and the evolution of infant formulas. *Milk milk Prod. Hum. Nutr.* **2011**, 67, 17–28.
23. Bode, L.; Contractor, N.; Barile, D.; Pohl, N.; Prudden, A.R.; Boons, G.-J.; Jin, Y.-S.; Jennewein, S. Overcoming the limited availability of human milk oligosaccharides: challenges

- and opportunities for research and application. *Nutr. Rev.* **2016**, *74*, 635–644.
24. Bych, K.; Mikš, M.H.; Johanson, T.; Hederos, M.J.; Vignsnæs, L.K.; Becker, P. Production of HMOs using microbial hosts—from cell engineering to large scale production. *Curr. Opin. Biotechnol.* **2019**, *56*, 130–137.
 25. Nidetzky, B.; Gutmann, A.; Zhong, C. Leloir glycosyltransferases as biocatalysts for chemical production. *ACS Catal.* **2018**, *8*, 6283–6300.
 26. Prudden, A.R.; Liu, L.; Capicciotti, C.J.; Wolfert, M.A.; Wang, S.; Gao, Z.; Meng, L.; Moremen, K.W.; Boons, G.-J. Synthesis of asymmetrical multiantennary human milk oligosaccharides. *Proc. Natl. Acad. Sci.* **2017**, *114*, 6954–6959.
 27. Warnock, D.; Bai, X.; Autote, K.; Gonzales, J.; Kinealy, K.; Yan, B.; Qian, J.; Stevenson, T.; Zopf, D.; Bayer, R.J. In vitro galactosylation of human IgG at 1 kg scale using recombinant galactosyltransferase. *Biotechnol. Bioeng.* **2005**, *92*, 831–842.
 28. Johnson, K.F. Synthesis of oligosaccharides by bacterial enzymes. *Glycoconj. J.* **1999**, *16*, 141–146.
 29. Varki, A.; Cummings, R.D.; Esko, J.D.; Stanley, P.; Hart, G.W.; Aebi, M.; Darvill, A.G.; Kinoshita, T.; Packer, N.H.; Prestegard, J.H. Essentials of Glycobiology [internet]. **2015**.
 30. Moremen, K.W.; Tiemeyer, M.; Nairn, A. V Vertebrate protein glycosylation: diversity, synthesis and function. *Nat. Rev. Mol. Cell Biol.* **2012**, *13*, 448–462.
 31. Reily, C.; Stewart, T.J.; Renfrow, M.B.; Novak, J. Glycosylation in health and disease. *Nat. Rev. Nephrol.* **2019**, *1*.
 32. Varki, A. Biological roles of glycans. *Glycobiology* **2017**, *27*, 3–49.
 33. Varki, A. Uniquely human evolution of sialic acid genetics and biology. *Proc. Natl. Acad. Sci.* **2010**, *107*, 8939–8946.
 34. Walsh, G. Biopharmaceutical benchmarks 2018. *Nat. Biotechnol.* **2018**, *36*, 1136–1145.
 35. O’Flaherty, R.; Bergin, A.; Flampouri, E.; Mota, L.M.; Obaidi, I.; Quigley, A.; Xie, Y.; Butler, M. Mammalian cell culture for production of recombinant proteins: A review of the critical steps in their biomanufacturing. *Biotechnol. Adv.* **2020**, 107552.
 36. Solá, R.J.; Griebenow, K. Glycosylation of therapeutic proteins. *BioDrugs* **2010**, *24*, 9–21.
 37. Reusch, D.; Tejada, M.L. Fc glycans of therapeutic antibodies as critical quality attributes. *Glycobiology* **2015**, *25*, 1325–1334.
 38. Mack, G. FDA balks at Myozyme scale-up. *Nat. Biotechnol.* **2008**, *26*, 592, doi:10.1038/NBT0608-592.
 39. Liu, L. Antibody glycosylation and its impact on the pharmacokinetics and pharmacodynamics of monoclonal antibodies and Fc-fusion proteins. *J. Pharm. Sci.* **2015**, *104*, 1866–1884.
 40. Ząbczyńska, M.; Polak, K.; Kozłowska, K.; Sokołowski, G.; Pocheć, E. The contribution of igg glycosylation to antibody-dependent cell-mediated cytotoxicity (ADCC) and complement-dependent cytotoxicity (CDC) in hashimoto’s thyroiditis: An in vitro model of thyroid autoimmunity. *Biomolecules* **2020**, *10*, 171.
 41. Thomann, M.; Schlothauer, T.; Dashivets, T.; Malik, S.; Avenal, C.; Bulau, P.; Rüger, P.; Reusch, D. In vitro glycoengineering of IgG1 and its effect on Fc receptor binding and ADCC activity. *PLoS One* **2015**, *10*.
 42. Geffner, J. Antibody-Dependent Cellular Cytotoxicity BT - Encyclopedia of Immunotoxicology. In; Vohr, H.-W., Ed.; Springer Berlin Heidelberg: Berlin, Heidelberg, 2005; pp. 1–5 ISBN 978-3-642-27786-3.
 43. Fanger, M.W.; Shen, L.; Graziano, R.F.; Guyre, P.M. Cytotoxicity mediated by human Fc receptors for IgG. *Immunol. Today* **1989**, *10*, 92–99.
 44. Raju, T.S.; Briggs, J.B.; Chamow, S.M.; Winkler, M.E.; Jones, A.J.S. Glycoengineering of therapeutic glycoproteins: in vitro galactosylation and sialylation of glycoproteins with terminal N-acetylglucosamine and galactose residues. *Biochemistry* **2001**, *40*, 8868–8876.
 45. Thomann, M.; Reckermann, K.; Reusch, D.; Prasser, J.; Tejada, M.L. Fc-galactosylation modulates antibody-dependent cellular cytotoxicity of therapeutic antibodies. *Mol. Immunol.* **2016**, *73*, 69–75.
 46. Buettner, M.J.; Shah, S.R.; Saeui, C.T.; Ariss, R.; Yarema, K.J. Improving immunotherapy through glycodeign. *Front. Immunol.* **2018**, *9*, 2485.
 47. Narimatsu, Y.; Büll, C.; Chen, Y.-H.; Wandall, H.H.; Yang, Z.; Clausen, H. Genetic glycoengineering in mammalian cells. *J. Biol. Chem.* **2021**, 100448.
 48. Schön, K.; Lepenies, B.; Goyette-Desjardins, G. Impact of Protein Glycosylation on the Design of Viral Vaccines. **2020**.
 49. Guo, J.; Tu, H.; Atouf, F. Measurement of macro-and micro-heterogeneity of glycosylation in biopharmaceuticals: a pharmacopeia perspective 2020.

50. Mariño, K.; Bones, J.; Kattla, J.J.; Rudd, P.M. A systematic approach to protein glycosylation analysis: a path through the maze. *Nat. Chem. Biol.* **2010**, *6*, 713–723.
51. Restelli, V.; Wang, M.; Huzel, N.; Ethier, M.; Perreault, H.; Butler, M. The effect of dissolved oxygen on the production and the glycosylation profile of recombinant human erythropoietin produced from CHO cells. *Biotechnol. Bioeng.* **2006**, *94*, 481–494.
52. Sou, S.N.; Sellick, C.; Lee, K.; Mason, A.; Kyriakopoulos, S.; Polizzi, K.M.; Kontoravdi, C. How does mild hypothermia affect monoclonal antibody glycosylation? *Biotechnol. Bioeng.* **2015**, *112*, 1165–1176.
53. Sajjan, E.; Matanguihan, R.; Heidemann, R.; Abu-Absi, S.; Asuncion, W.; Yamasaki, G.; Wu, X.; Chen, J.; Murphy, J.E.; Zhang, C. The effect of bioreactor pH and temperature on protein glycosylation in perfusion cultures of mammalian cells. In *Cells and culture*; Springer, 2010; pp. 785–788.
54. Costa, A.R.; Rodrigues, M.E.; Henriques, M.; Oliveira, R.; Azeredo, J. Glycosylation: impact, control and improvement during therapeutic protein production. *Crit. Rev. Biotechnol.* **2014**, *34*, 281–299.
55. Nam, J.H.; Zhang, F.; Ermonval, M.; Linhardt, R.J.; Sharfstein, S.T. The effects of culture conditions on the glycosylation of secreted human placental alkaline phosphatase produced in Chinese hamster ovary cells. *Biotechnol. Bioeng.* **2008**, *100*, 1178–1192.
56. Del Val, I.J.; Kontoravdi, C.; Nagy, J.M. Towards the implementation of quality by design to the production of therapeutic monoclonal antibodies with desired glycosylation patterns. *Biotechnol. Prog.* **2010**, *26*, 1505–1527.
57. Hossler, P. Protein glycosylation control in mammalian cell culture: past precedents and contemporary prospects. In *Genomics and Systems Biology of Mammalian Cell Culture*; Springer, 2011; pp. 187–219.
58. Ivarsson, M.; Villiger, T.K.; Morbidelli, M.; Soos, M. Evaluating the impact of cell culture process parameters on monoclonal antibody N-glycosylation. *J. Biotechnol.* **2014**, *188*, 88–96.
59. Beck, A.; Liu, H. Macro-and micro-heterogeneity of natural and recombinant IgG antibodies. *Antibodies* **2019**, *8*, 18.
60. Yamane-Ohnuki, N.; Satoh, M. Production of therapeutic antibodies with controlled fucosylation. *MAbs* **2009**, *1*, 230–236.
61. Blondeel, E.J.M.; Aucoin, M.G. Supplementing glycosylation: a review of applying nucleotide-sugar precursors to growth medium to affect therapeutic recombinant protein glycoform distributions. *Biotechnol. Adv.* **2018**, *36*, 1505–1523.
62. Ehret, J.; Zimmermann, M.; Eichhorn, T.; Zimmer, A. Impact of cell culture media additives on IgG glycosylation produced in Chinese hamster ovary cells. *Biotechnol. Bioeng.* **2019**, *116*, 816–830.
63. Kildegaard, H.F.; Fan, Y.; Sen, J.W.; Larsen, B.; Andersen, M.R. Glycoprofiling effects of media additives on IgG produced by CHO cells in fed-batch bioreactors. *Biotechnol. Bioeng.* **2016**, *113*, 359–366.
64. Brühlmann, D.; Jordan, M.; Hemberger, J.; Sauer, M.; Stettler, M.; Broly, H. Tailoring recombinant protein quality by rational media design. *Biotechnol. Prog.* **2015**, *31*, 615–629.
65. Wang, Q.; Chung, C.; Chough, S.; Betenbaugh, M.J. Antibody glycoengineering strategies in mammalian cells. *Biotechnol. Bioeng.* **2018**, *115*, 1378–1393.
66. Huang, W.; Giddens, J.; Fan, S.-Q.; Toonstra, C.; Wang, L.-X. Chemoenzymatic glycoengineering of intact IgG antibodies for gain of functions. *J. Am. Chem. Soc.* **2012**, *134*, 12308–12318.
67. Washburn, N.; Schwab, I.; Ortiz, D.; Bhatnagar, N.; Lansing, J.C.; Medeiros, A.; Tyler, S.; Mekala, D.; Cochran, E.; Sarvaiya, H. Controlled tetra-Fc sialylation of IVIg results in a drug candidate with consistent enhanced anti-inflammatory activity. *Proc. Natl. Acad. Sci.* **2015**, *112*, E1297–E1306.
68. Liu, C.-P.; Tsai, T.-I.; Cheng, T.; Shivatare, V.S.; Wu, C.-Y.; Wong, C.-H. Glycoengineering of antibody (Herceptin) through yeast expression and in vitro enzymatic glycosylation. *Proc. Natl. Acad. Sci.* **2018**, *115*, 720–725.
69. Liu, L.; Prudden, A.R.; Bosman, G.P.; Boons, G.-J. Improved isolation and characterization procedure of sialylglycopeptide from egg yolk powder. *Carbohydr. Res.* **2017**, *452*, 122–128.
70. Dekkers, G.; Plomp, R.; Koeleman, C.A.M.; Visser, R.; Von Horsten, H.H.; Sandig, V.; Rispens, T.; Wührer, M.; Vidarsson, G. Multi-level glyco-engineering techniques to generate IgG with defined Fc-glycans. *Sci. Rep.* **2016**, *6*, 36964.
71. Luley-Goedel, C.; Schmoelzer, K.; Thomann, M.; Malik, S.; Greif, M.; Ribitsch, D.; Jung, C.; Sobek, H.; Engel, A.; Mueller, R. Two N-terminally truncated variants of human β -galactoside

- α 2, 6 sialyltransferase I with distinct properties for in vitro protein glycosylation. *Glycobiology* **2016**, *26*, 1097–1106.
72. Chung, S.-W.; Joo, H.-S.; Jang, K.-S.; Lee, H.-J.; Lee, S.-G.; Kim, B.-G. Galactosylation and sialylation of terminal glycan residues of human immunoglobulin G using bacterial glycosyltransferases with in situ regeneration of sugar-nucleotides. *Enzyme Microb. Technol.* **2006**, *39*, 60–66.
 73. Tripathi, N.K.; Shrivastava, A. Recent developments in bioprocessing of recombinant proteins: expression hosts and process development. *Front. Bioeng. Biotechnol.* **2019**, *7*, 420.
 74. Puetz, J.; Wurm, F.M. Recombinant proteins for industrial versus pharmaceutical purposes: a review of process and pricing. *Processes* **2019**, *7*, 476.
 75. Docq, S.; Spoelder, M.; Wang, W.; Homberg, J.R. The Protective and Long-Lasting Effects of Human Milk Oligosaccharides on Cognition in Mammals. *Nutrients* **2020**, *12*, 3572.
 76. Lucas, A.; Morley, R.; Cole, T.J.; Lucas, P.J.; Gore, S.M.; Crowle, P.; Pearce, R.; Boon, A.J.; Powell, R. Early diet in preterm babies and developmental status at 18 months. *Lancet* **1990**, *335*, 1477–1481.
 77. Hofer, C.; Hardy, M.C. Later development of breast fed and artificially fed infants: comparison of physical and mental growth. *J. Am. Med. Assoc.* **1929**, *92*, 615–619.
 78. György, P. A hitherto unrecognized biochemical difference between human milk and cow's milk. *Pediatrics* **1953**, *11*, 98–108.
 79. Gura, T. Nature's first functional food. *Science (80-.)*. **2014**, *345*, 747–749, doi:10.1126/SCIENCE.345.6198.747.
 80. Gyorgy, P. N-Containing saccharides in human milk.' *Chem. Biol. Mucopolysaccharides* **1958**, 140–156.
 81. Kunz, C. Historical aspects of human milk oligosaccharides. *Adv. Nutr.* **2012**, *3*, 430S-439S.
 82. Kobata, A. A journey to the world of glycobiology. *Glycoconj. J.* **2000**, *17*, 443–464.
 83. Ruhaak, L.R.; Lebrilla, C.B. Advances in analysis of human milk oligosaccharides. *Adv. Nutr.* **2012**, *3*, 406S-414S.
 84. van Leeuwen, S.S. Challenges and pitfalls in human milk oligosaccharide analysis. *Nutrients* **2019**, *11*, 2684.
 85. Thurl, S.; Munzert, M.; Boehm, G.; Matthews, C.; Stahl, B. Systematic review of the concentrations of oligosaccharides in human milk. *Nutr. Rev.* **2017**, *75*, 920–933.
 86. Gibson, G.R.; Probert, H.M.; Van Loo, J.; Rastall, R.A.; Roberfroid, M.B. Dietary modulation of the human colonic microbiota: updating the concept of prebiotics. *Nutr. Res. Rev.* **2004**, *17*, 259–275.
 87. Roberfroid, M. Prebiotics: the concept revisited. *J. Nutr.* **2007**, *137*, 830S-837S.
 88. Engfer, M.B.; Stahl, B.; Finke, B.; Sawatzki, G.; Daniel, H. Human milk oligosaccharides are resistant to enzymatic hydrolysis in the upper gastrointestinal tract. *Am. J. Clin. Nutr.* **2000**, *71*, 1589–1596.
 89. Bode, L. Human milk oligosaccharides: prebiotics and beyond. *Nutr. Rev.* **2009**, *67*, S183–S191.
 90. Gao, X.; Wu, D.; Wen, Y.; Gao, L.; Liu, D.; Zhong, R.; Yang, C.; Zhao, C. Antiviral effects of human milk oligosaccharides: A review. *Int. Dairy J.* **2020**, 104784.
 91. Wiciński, M.; Sawicka, E.; Gębalski, J.; Kubiak, K.; Malinowski, B. Human milk oligosaccharides: Health benefits, potential applications in infant formulas, and pharmacology. *Nutrients* **2020**, *12*, 266.
 92. Newburg, D.S.; He, Y. Neonatal gut microbiota and human milk glycans cooperate to attenuate infection and inflammation. *Clin. Obstet. Gynecol.* **2015**, *58*, 814–826.
 93. Hester, S.N.; Chen, X.; Li, M.; Monaco, M.H.; Comstock, S.S.; Kuhlenschmidt, T.B.; Kuhlenschmidt, M.S.; Donovan, S.M. Human milk oligosaccharides inhibit rotavirus infectivity in vitro and in acutely infected piglets. *Br. J. Nutr.* **2013**, *110*, 1233–1242.
 94. Lane, J.A.; O'Callaghan, J.; Carrington, S.D.; Hickey, R.M. Transcriptional response of HT-29 intestinal epithelial cells to human and bovine milk oligosaccharides. *Br. J. Nutr.* **2013**, *110*, 2127–2137.
 95. Comstock, S.S.; Donovan, S.M. Human milk oligosaccharides as modulators of intestinal and systemic immunity. In *Prebiotics and Probiotics in Human Milk: Origins and Functions of Milk-Borne Oligosaccharides and Bacteria*; Elsevier Inc., 2016; pp. 223–248.
 96. Wickramasinghe, S.; Pacheco, A.R.; Lemay, D.G.; Mills, D.A. Bifidobacteria grown on human milk oligosaccharides downregulate the expression of inflammation-related genes in Caco-2 cells. *BMC Microbiol.* **2015**, *15*, 172.
 97. Patel, R.M.; Kandefter, S.; Walsh, M.C.; Bell, E.F.; Carlo, W.A.; Lupton, A.R.; Sánchez, P.J.;

- Shankaran, S.; Van Meurs, K.P.; Ball, M.B. Causes and timing of death in extremely premature infants from 2000 through 2011. *N. Engl. J. Med.* **2015**, *372*, 331–340.
98. Autran, C.A.; Schoterman, M.H.C.; Jantscher-Krenn, E.; Kamerling, J.P.; Bode, L. Sialylated galacto-oligosaccharides and 2'-fucosyllactose reduce necrotising enterocolitis in neonatal rats. *Br. J. Nutr.* **2016**, *116*, 294–299.
 99. Jantscher-Krenn, E.; Zherebtsov, M.; Nissan, C.; Goth, K.; Guner, Y.S.; Naidu, N.; Choudhury, B.; Grishin, A. V; Ford, H.R.; Bode, L. The human milk oligosaccharide disialyllacto-N-tetraose prevents necrotising enterocolitis in neonatal rats. *Gut* **2012**, *61*, 1417–1425.
 100. Masi, A.C.; Embleton, N.D.; Lamb, C.A.; Young, G.; Granger, C.L.; Najera, J.; Smith, D.P.; Hoffman, K.L.; Petrosino, J.F.; Bode, L.; et al. Human milk oligosaccharide DSLNT and gut microbiome in preterm infants predicts necrotising enterocolitis. *Gut* **2020**, gutjnl-2020-322771, doi:10.1136/gutjnl-2020-322771.
 101. Bode, L. Disialyllacto-N-tetraose (DSLNT) or variants, isomers, analogs and derivatives thereof to prevent or inhibit bowel disease 2017.
 102. Duska-McEwen, G.; Comstock, S.; Donovan, S.; Buck, R.; Schaller, J. Nutritional formulations using human milk oligosaccharides for modulating inflammation 2020.
 103. Chow, J.; Davis, S.R.; Buck, R.; Duska-McEwen, G.O.; Linke, H.K. Methods for decreasing the incidence of necrotizing enterocolitis in infants, toddlers, or children using human milk oligosaccharides 2017.
 104. Morrow, A.L.; Newburg, D.S.; Ruiz-Palacios, G.M. Oligosaccharide compositions and use thereof in the treatment of infection 2011.
 105. Kristmundsdottir, F. Prenatal growth and development. *Textb. Neonatol. New York Churchill Livingstone* **1992**, 162–169.
 106. Wang, B. Sialic acid is an essential nutrient for brain development and cognition. *Annu. Rev. Nutr.* **2009**, *29*, 177–222.
 107. Röhrig, C.H.; Choi, S.S.H.; Baldwin, N. The nutritional role of free sialic acid, a human milk monosaccharide, and its application as a functional food ingredient. *Crit. Rev. Food Sci. Nutr.* **2017**, *57*, 1017–1038.
 108. Springer, S.A.; Diaz, S.L.; Gagneux, P. Parallel evolution of a self-signal: humans and new world monkeys independently lost the cell surface sugar Neu5Gc. *Immunogenetics* **2014**, *66*, 671–674.
 109. Ng, P.S.K.; Böhm, R.; Hartley-Tassell, L.E.; Steen, J.A.; Wang, H.; Lukowski, S.W.; Hawthorne, P.L.; Trezise, A.E.O.; Coloe, P.J.; Grimmond, S.M. Ferrets exclusively synthesize Neu5Ac and express naturally humanized influenza A virus receptors. *Nat. Commun.* **2014**, *5*, 1–9.
 110. Paul, G.; Richard, K.; Friedrich, Z. Food compositions 1955.
 111. Paul, G.; Richard, K.; Friedrich, Z. Food products containing glucosides of nu-acetyl-d-glucosamine 1955.
 112. Paul, G.; Friedrich, Z. Enzymatic synthesis of n-acetylglucosaminido galactose and galactosido-n-acetyl glucosamine 1956.
 113. Bode, L.; Campbell, S.; Furneaux, R.; Beauprez, J.; Muscroft-Taylor, A. Making Human Milk Oligosaccharides Available for Research and Application - Approaches, Challenges, and Future Opportunities. In *Prebiotics and Probiotics in Human Milk: Origins and Functions of Milk-Borne Oligosaccharides and Bacteria*; Elsevier Inc., 2017; pp. 251–293 ISBN 9780128027257.
 114. Mestrom, L.; Przypis, M.; Kowalczykiewicz, D.; Pollender, A.; Kumpf, A.; Marsden, S.R.; Bento, I.; Jarzębski, A.B.; Szymańska, K.; Chruściel, A. Leloir glycosyltransferases in applied biocatalysis: A multidisciplinary approach. *Int. J. Mol. Sci.* **2019**, *20*, 5263.
 115. Sprenger, G.A.; Baumgärtner, F.; Albermann, C. Production of human milk oligosaccharides by enzymatic and whole-cell microbial biotransformations. *J. Biotechnol.* **2017**, *258*, 79–91.
 116. Yang, J.; Zhang, T.; Tian, C.; Zhu, Y.; Zeng, Y.; Men, Y.; Chen, P.; Sun, Y.; Ma, Y. Multi-enzyme systems and recombinant cells for synthesis of valuable saccharides: Advances and perspectives. *Biotechnol. Adv.* **2019**.
 117. Schelch, S.; Zhong, C.; Petschacher, B.; Nidetzky, B. Bacterial sialyltransferases and their use in biocatalytic cascades for sialo-oligosaccharide production. *Biotechnol. Adv.* **2020**, 107613.
 118. Walsh, C.; Lane, J.A.; van Sinderen, D.; Hickey, R.M. From lab bench to formulated ingredient: Characterization, production, and commercialization of human milk oligosaccharides. *J. Funct. Foods* **2020**, *72*, 104052.
 119. Molnar-Gabor, D.; Hederos, M.J.; Bartsch, S.; Vogel, A. Emerging Field—Synthesis of Complex Carbohydrates. Case Study on HMOs. In *Industrial Enzyme Applications*; Wiley Online Library,

- 2019; pp. 179–201.
120. Parschat, K.; Schreiber, S.; Wartenberg, D.; Engels, B.; Jennewein, S. High-Titer De Novo Biosynthesis of the Predominant Human Milk Oligosaccharide 2'-Fucosyllactose from Sucrose in *Escherichia coli*. *ACS Synth. Biol.* **2020**, *9*, 2784–2796.
 121. Lu, M.; Mosleh, I.; Abbaspourrad, A. Engineered Microbial Routes for Human Milk Oligosaccharides Synthesis. *ACS Synth. Biol.* **2021**.
 122. Zeuner, B.; Teze, D.; Muschiol, J.; Meyer, A.S. Synthesis of human milk oligosaccharides: Protein engineering strategies for improved enzymatic transglycosylation. *Molecules* **2019**, *24*, 2033.
 123. Bode, L.; Campbell, S.; Furneaux, R.; Beauprez, J.; Muscroft-Taylor, A. *Making Human Milk Oligosaccharides Available for Research and Application - Approaches, Challenges, and Future Opportunities*; 2017; ISBN 9780128027257.
 124. Yu, H.; Chen, X. One-pot multienzyme (OPME) systems for chemoenzymatic synthesis of carbohydrates. *Org. Biomol. Chem.* **2016**, *14*, 2809–2818.
 125. McArthur, J.B.; Yu, H.; Chen, X. A Bacterial β 1–3-Galactosyltransferase Enables Multigram-Scale Synthesis of Human Milk Lacto-N-tetraose (LNT) and Its Fucosides. *ACS Catal.* **2019**, *9*, 10721–10726.
 126. Li, W.; McArthur, J.B.; Chen, X. Strategies for chemoenzymatic synthesis of carbohydrates. *Carbohydr. Res.* **2019**, *472*, 86–97.
 127. Zhao, C.; Wu, Y.; Yu, H.; Shah, I.M.; Li, Y.; Zeng, J.; Liu, B.; Mills, D.A.; Chen, X. The one-pot multienzyme (OPME) synthesis of human blood group H antigens and a human milk oligosaccharide (HMOS) with highly active *Thermosynechococcus elongatus* α 1–2-fucosyltransferase. *Chem. Commun.* **2016**, *52*, 3899–3902.
 128. Tsai, T.-I.; Lee, H.-Y.; Chang, S.-H.; Wang, C.-H.; Tu, Y.-C.; Lin, Y.-C.; Hwang, D.-R.; Wu, C.-Y.; Wong, C.-H. Effective sugar nucleotide regeneration for the large-scale enzymatic synthesis of Globo H and SSEA4. *J. Am. Chem. Soc.* **2013**, *135*, 14831–14839.
 129. Nahálka, J.; Pátoprstý, V. Enzymatic synthesis of sialylation substrates powered by a novel polyphosphate kinase (PPK3). *Org. Biomol. Chem.* **2009**, *7*, 1778–1780.
 130. Ichikawa, Y.; Wang, R.; Wong, C.-H. Regeneration of sugar nucleotide for enzymatic oligosaccharide synthesis. In *Methods in Enzymology*; Elsevier, 1994; Vol. 247, pp. 107–127 ISBN 0076-6879.
 131. Rexer, T.F.T.; Schildbach, A.; Klapproth, J.; Schierhorn, A.; Mahour, R.; Pietzsch, M.; Rapp, E.; Reichl, U. One pot synthesis of GDP-mannose by a multi-enzyme cascade for enzymatic assembly of lipid-linked oligosaccharides. *Biotechnol. Bioeng.* **2018**, *115*, doi:10.1002/bit.26454.
 132. Chen, X.; Fang, J.; Zhang, J.; Liu, Z.; Shao, J.; Kowal, P.; Andreana, P.; Wang, P.G. Sugar nucleotide regeneration beads (superbeads): a versatile tool for the practical synthesis of oligosaccharides. *J. Am. Chem. Soc.* **2001**, *123*, 2081–2082.
 133. Ichikawa, Y.; Liu, J.L.C.; Shen, G.J.; Wong, C.H. A highly efficient multienzyme system for the one-step synthesis of a sialyl trisaccharide: in situ generation of sialic acid and N-acetyllactosamine coupled with regeneration of UDP-glucose, UDP-galactose and CMP-sialic acid. *J. Am. Chem. Soc.* **1991**, *113*, 6300–6302.
 134. Mikkola, S. Nucleotide Sugars in Chemistry and Biology. *Molecules* **2020**, *25*, 5755.
 135. Lilly, M.D. Extraction and separation of nucleotides from *Escherichia coli*. *Biotechnol. Bioeng.* **1965**, *7*, 335–342.
 136. Munden, J.E.; Crook, E.M.; Donald, M.B. The development of a process for recovering nucleotides from Bakers' yeast. *Biotechnol. Bioeng.* **1963**, *5*, 221–230.
 137. Rodríguez-Díaz, J.; Rubio-del-Campo, A.; Yebra, M.J. Metabolic engineering of *Lactobacillus casei* for production of UDP-N-acetylglucosamine. *Biotechnol. Bioeng.* **2012**, *109*, 1704–1712.
 138. Yang, T.; Bar-Peled, Y.; Smith, J.A.; Glushka, J.; Bar-Peled, M. In-microbe formation of nucleotide sugars in engineered *Escherichia coli*. *Anal. Biochem.* **2012**, *421*, 691–698.
 139. Broach, B.; Gu, X.; Bar-Peled, M. Biosynthesis of UDP-glucuronic acid and UDP-galacturonic acid in *Bacillus cereus* subsp. *cytotoxis* NVH 391-98. *FEBS J.* **2012**, *279*, 100–112.
 140. Wagner, G.K.; Pesnot, T.; Field, R.A. A survey of chemical methods for sugar-nucleotide synthesis. *Nat. Prod. Rep.* **2009**, *26*, 1172–1194.
 141. Ahmadipour, S.; Miller, G.J. Recent advances in the chemical synthesis of sugar-nucleotides. *Carbohydr. Res.* **2017**, *451*, 95–109.
 142. Chen, R. Enzyme and microbial technology for synthesis of bioactive oligosaccharides: an update. *Appl. Microbiol. Biotechnol.* **2018**, *102*, 3017–3026.
 143. Cai, L. Recent progress in enzymatic synthesis of sugar nucleotides. *J. Carbohydr. Chem.*

- 2012**, 31, 535–552.
144. Ahmadipour, S.; Beswick, L.; Miller, G.J. Recent advances in the enzymatic synthesis of sugar-nucleotides using nucleotidyltransferases and glycosyltransferases. *Carbohydr. Res.* **2018**, 469, 38–47.
 145. Simon, E.S.; Bednarski, M.D.; Whitesides, G.M. Synthesis of CMP-NeuAc from N-acetylglucosamine: generation of CTP from CMP using adenylate kinase. *J. Am. Chem. Soc.* **1988**, 110, 7159–7163.
 146. Liu, Z.; Zhang, J.; Chen, X.; Wang, P.G. Combined biosynthetic pathway for de novo production of UDP-galactose: catalysis with multiple enzymes immobilized on agarose beads. *ChemBioChem* **2002**, 3, 348–355.
 147. Koizumi, S.; Endo, T.; Tabata, K.; Ozaki, A. Large-scale production of UDP-galactose and globotriose by coupling metabolically engineered bacteria. *Nat. Biotechnol.* **1998**, 16, 847–850.
 148. Okuyama, K.; Hamamoto, T.; Ishige, K.; Takenouchi, K.; Noguchi, T. An efficient method for production of uridine 5'-diphospho-N-acetylglucosamine. *Biosci. Biotechnol. Biochem.* **2000**, 64, 386–392.
 149. Endo, T.; Koizumi, S.; Tabata, K.; Ozaki, A. Large-scale production of CMP-NeuAc and sialylated oligosaccharides through bacterial coupling. *Appl. Microbiol. Biotechnol.* **2000**, 53, 257–261.
 150. Zhao, G.; Guan, W.; Cai, L.; Wang, P.G. Enzymatic route to preparative-scale synthesis of UDP-GlcNAc/GalNAc, their analogues and GDP-fucose. *Nat. Protoc.* **2010**, 5, 636.
 151. Fischöder, T.; Wahl, C.; Zerhusen, C.; Elling, L. Repetitive Batch Mode Facilitates Enzymatic Synthesis of the Nucleotide Sugars UDP-Gal, UDP-GlcNAc, and UDP-GalNAc on a Multi-Gram Scale. *Biotechnol. J.* **2019**, 14.
 152. Lemmerer, M.; Schmölzer, K.; Gutmann, A.; Nidetzky, B. Downstream Processing of Nucleoside-Diphospho-Sugars from Sucrose Synthase Reaction Mixtures at Decreased Solvent Consumption. *Adv. Synth. Catal.* **2016**, 358, 3113–3122, doi:10.1002/adsc.201600540.
 153. Buchner, E. Alkoholische Gärung ohne Hefezellen. *Berichte der Dtsch. Chem. Gesellschaft* **1897**, 30, 1110–1113.
 154. Bornscheuer, U.T. The fourth wave of biocatalysis is approaching. *Philos. Trans. R. Soc. A Math. Phys. Eng. Sci.* **2018**, 376, 20170063.
 155. Huffman, M.A.; Fryszkowska, A.; Alvizo, O.; Borra-Garske, M.; Campos, K.R.; Devine, P.N.; Duan, D.; Forstater, J.H.; Grosser, S.T.; Halsey, H.M. Design of an in vitro biocatalytic cascade for the manufacture of islatravir. *Science (80-.)*. **2019**, 366, 1255–1259.
 156. Sperl, J.M.; Sieber, V. Multienzyme Cascade Reactions— Status and Recent Advances. *ACS Catal.* **2018**, 8, 2385–2396.
 157. France, S.P.; Hepworth, L.J.; Turner, N.J.; Flitsch, S.L. Constructing biocatalytic cascades: in vitro and in vivo approaches to de novo multi-enzyme pathways. *Acs Catal.* **2017**, 7, 710–724.
 158. Burgener, S.; Luo, S.; McLean, R.; Miller, T.E.; Erb, T.J. A roadmap towards integrated catalytic systems of the future. *Nat. Catal.* **2020**, 3, 186–192.
 159. Petroll, K.; Kopp, D.; Care, A.; Bergquist, P.L.; Sunna, A. Tools and strategies for constructing cell-free enzyme pathways. *Biotechnol. Adv.* **2019**, 37, 91–108.
 160. Devine, P.N.; Howard, R.M.; Kumar, R.; Thompson, M.P.; Truppo, M.D.; Turner, N.J. Extending the application of biocatalysis to meet the challenges of drug development. *Nat. Rev. Chem.* **2018**, 2, 409–421.
 161. Honda, K. Industrial applications of multistep enzyme reactions. In *Biotechnology of Microbial Enzymes*; Elsevier, 2017; pp. 433–450.
 162. Vogel, A.; May, O. *Industrial enzyme applications*; John Wiley & Sons, 2019; ISBN 3527813756.
 163. Schrittwieser, J.H.; Velikogne, S.; Hall, M.; Kroutil, W. Artificial biocatalytic linear cascades for preparation of organic molecules. *Chem. Rev.* **2018**, 118, 270–348.
 164. Li, S.; Wang, S.; Wang, Y.; Qu, J.; Liu, X.; Wang, P.G.; Fang, J. Gram-scale production of sugar nucleotides and their derivatives. *Green Chem.* **2021**, 23, 2628–2633, doi:10.1039/D1GC00711D.
 165. Kossen, N.W.F. Scale-up in biotechnology. In *Recent Advances in Biotechnology*; Springer, 1992; pp. 147–182.
 166. Crater, J.S.; Lievens, J.C. Scale-up of industrial microbial processes. *FEMS Microbiol. Lett.* **2018**, 365, fny138.
 167. Wu, S.; Snajdrova, R.; Moore, J.C.; Baldenius, K.; Bornscheuer, U.T. Biocatalysis: Enzymatic Synthesis for Industrial Applications. *Angew. Chemie Int. Ed.* **2021**, 60, 88–119,

- doi:10.1002/ANIE.202006648.
168. Hilterhaus, L.; Liese, A.; Kettling, U.; Antranikian, G. *Applied biocatalysis: from fundamental science to industrial applications*; John Wiley & Sons, 2016; ISBN 3527677135.
 169. Yang, X. Scale-up of microbial fermentation process. In *Manual of Industrial Microbiology and Biotechnology, Third Edition*; American Society of Microbiology, 2010; pp. 669–675.
 170. Guan, N.; Chen, R. Recent Technology Development for the Biosynthesis of Human Milk Oligosaccharide. *Recent Pat. Biotechnol.* **2018**, *12*, 92–100.
 171. da Gama Ferreira, R.; Azzoni, A.R.; Freitas, S. Techno-economic analysis of the industrial production of a low-cost enzyme using *E. coli*: the case of recombinant β -glucosidase. *Biotechnol. Biofuels* **2018**, *11*, 1–13.
 172. Bülow, L.; Mosbach, K. Multienzyme systems obtained by gene fusion. *Trends Biotechnol.* **1991**, *9*, 226–231.
 173. Tolia, N.H.; Joshua-Tor, L. Strategies for protein coexpression in *Escherichia coli*. *Nat. Methods* **2006**, *3*, 55–64.
 174. Krauser, S.; Hoffmann, T.; Heinzle, E. Directed multistep biocatalysis for the synthesis of the polyketide oxytetracycline in permeabilized cells of *Escherichia coli*. *ACS Catal.* **2015**, *5*, 1407–1413.
 175. Wu, S.; Zhou, Y.; Wang, T.; Too, H.-P.; Wang, D.I.C.; Li, Z. Highly regio- and enantioselective multiple oxy- and amino-functionalizations of alkenes by modular cascade biocatalysis. *Nat. Commun.* **2016**, *7*, 1–13.
 176. Tufvesson, P.; Lima-Ramos, J.; Nordblad, M.; Woodley, J.M. Guidelines and cost analysis for catalyst production in biocatalytic processes. *Org. Process Res. Dev.* **2011**, *15*, 266–274.
 177. Tufvesson, P.; Fu, W.; Jensen, J.S.; Woodley, J.M. Process considerations for the scale-up and implementation of biocatalysis. *Food Bioprod. Process.* **2010**, *88*, 3–11.
 178. Pollard, D.J.; Woodley, J.M. Biocatalysis for pharmaceutical intermediates: the future is now. *TRENDS Biotechnol.* **2007**, *25*, 66–73.
 179. Cao, L. Covalent enzyme immobilization. *Carrier-bound Immobil. Enzym.* **2006**, 169–316.
 180. Garcia-Galan, C.; Berenguer-Murcia, Á.; Fernandez-Lafuente, R.; Rodrigues, R.C. Potential of different enzyme immobilization strategies to improve enzyme performance. *Adv. Synth. Catal.* **2011**, *353*, 2885–2904.
 181. Sheldon, R.A.; van Pelt, S. Enzyme immobilisation in biocatalysis: why, what and how. *Chem. Soc. Rev.* **2013**, *42*, 6223–6235.
 182. Rodrigues, R.C.; Ortiz, C.; Berenguer-Murcia, Á.; Torres, R.; Fernández-Lafuente, R. Modifying enzyme activity and selectivity by immobilization. *Chem. Soc. Rev.* **2013**, *42*, 6290–6307.
 183. Sheldon, R.A.; Brady, D.; Bode, M.L. The Hitchhiker's guide to biocatalysis: recent advances in the use of enzymes in organic synthesis. *Chem. Sci.* **2020**, *11*, 2587–2605.
 184. Liese, A.; Hilterhaus, L. Evaluation of immobilized enzymes for industrial applications. *Chem. Soc. Rev.* **2013**, *42*, 6236–6249.
 185. Basso, A.; Serban, S. Industrial applications of immobilized enzymes—A review. *Mol. Catal.* **2019**, *479*, 110607.
 186. Arana-Peña, S.; Carballares, D.; Morellon-Sterling, R.; Berenguer-Murcia, Á.; Alcántara, A.R.; Rodrigues, R.C.; Fernandez-Lafuente, R. Enzyme co-immobilization: Always the biocatalyst designers' choice... or not? *Biotechnol. Adv.* **2020**, 107584.
 187. Orrego, A.H.; López-Gallego, F.; Fernandez-Lorente, G.; Guisan, J.M.; Rocha-Martín, J. Co-Immobilization and Co-Localization of Multi-Enzyme Systems on Porous Materials. In *Immobilization of Enzymes and Cells*; Springer, 2020; pp. 297–308.
 188. Xu, K.; Chen, X.; Zheng, R.; Zheng, Y. Immobilization of multi-enzymes on support materials for efficient biocatalysis. *Front. Bioeng. Biotechnol.* **2020**, *8*.
 189. Shao, J.; Zhang, J.; Nahálka, J.; Wang, P.G. Biocatalytic synthesis of uridine 5'-diphosphate N-acetylglucosamine by multiple enzymes co-immobilized on agarose beads. *Chem. Commun.* **2002**, 2586–2587.
 190. Schomburg, I.; Chang, A.; Schomburg, D. BRENDA, enzyme data and metabolic information. *Nucleic Acids Res.* **2002**, *30*, 47–49.
 191. Schomburg, I.; Jeske, L.; Ulbrich, M.; Placzek, S.; Chang, A.; Schomburg, D. The BRENDA enzyme information system—From a database to an expert system. *J. Biotechnol.* **2017**, *261*, 194–206.
 192. Qian, Y.; Ding, Q.; Li, Y.; Zou, Z.; Yan, B.; Ou, L. Phosphorylation of uridine and cytidine by uridine-cytidine kinase. *J. Biotechnol.* **2014**, *188*, 81–87.
 193. Kawasaki, H.; Usuda, Y.; Shimaoka, M.; Utagawa, T. Phosphorylation of guanosine using

- guanosine-inosine kinase from *Exiguobacterium acetylicum* coupled with ATP regeneration. *Biosci. Biotechnol. Biochem.* **2000**, *64*, 2259–2261.
194. Zhou, L.; Lacroute, F.; Thornburg, R. Cloning, expression in *Escherichia coli*, and characterization of *Arabidopsis thaliana* UMP/CMP kinase. *Plant Physiol.* **1998**, *117*, 245–254.
 195. Hible, G.; Renault, L.; Schaeffer, F.; Christova, P.; Radulescu, A.Z.; Evrin, C.; Gilles, A.-M.; Cherfils, J. Calorimetric and crystallographic analysis of the oligomeric structure of *Escherichia coli* GMP kinase. *J. Mol. Biol.* **2005**, *352*, 1044–1059.
 196. Nishimoto, M.; Kitaoka, M. Identification of N-acetylhexosamine 1-kinase in the complete lacto-N-biose I/galacto-N-biose metabolic pathway in *Bifidobacterium longum*. *Appl. Environ. Microbiol.* **2007**, *73*, 6444–6449.
 197. Meyer, D.; Schneider-Fresenius, C.; Horlacher, R.; Peist, R.; Boos, W. Molecular characterization of glucokinase from *Escherichia coli* K-12. *J. Bacteriol.* **1997**, *179*, 1298–1306.
 198. Li, L.; Liu, Y.; Wang, W.; Cheng, J.; Zhao, W.; Wang, P. A highly efficient galactokinase from *Bifidobacterium infantis* with broad substrate specificity. *Carbohydr. Res.* **2012**, *355*, 35–39.
 199. Coyne, M.J.; Reinap, B.; Lee, M.M.; Comstock, L.E. Human symbionts use a host-like pathway for surface fucosylation. *Science (80-.)*. **2005**, *307*, 1778–1781.
 200. Thoden, J.B.; Holden, H.M. The molecular architecture of glucose-1-phosphate uridylyltransferase. *Protein Sci.* **2007**, *16*, 432–440.
 201. Chen, Y.; Thon, V.; Li, Y.; Yu, H.; Ding, L.; Lau, K.; Qu, J.; Hie, L.; Chen, X. One-pot three-enzyme synthesis of UDP-GlcNAc derivatives. *Chem. Commun.* **2011**, *47*, 10815–10817.
 202. Koizumi, S.; Endo, T.; Tabata, K.; Nagano, H.; Ohnishi, J.; Ozaki, A. Large-scale production of GDP-fucose and Lewis X by bacterial coupling. *J. Ind. Microbiol. Biotechnol.* **2000**, *25*, 213–217.
 203. Klermund, L.; Groher, A.; Castiglione, K. New N-acyl-D-glucosamine 2-epimerases from cyanobacteria with high activity in the absence of ATP and low inhibition by pyruvate. *J. Biotechnol.* **2013**, *168*, 256–263.
 204. Li, Y.; Yu, H.; Cao, H.; Lau, K.; Muthana, S.; Tiwari, V.K.; Son, B.; Chen, X. *Pasteurella multocida* sialic acid aldolase: a promising biocatalyst. *Appl. Microbiol. Biotechnol.* **2008**, *79*, 963–970.
 205. Yu, H.; Yu, H.; Karpel, R.; Chen, X. Chemoenzymatic synthesis of CMP-sialic acid derivatives by a one-pot two-enzyme system: comparison of substrate flexibility of three microbial CMP-sialic acid synthetases. *Bioorg. Med. Chem.* **2004**, *12*, 6427–6435.
 206. Li, Y.; Xue, M.; Sheng, X.; Yu, H.; Zeng, J.; Thon, V.; Chen, Y.; Muthana, M.M.; Wang, P.G.; Chen, X. Donor substrate promiscuity of bacterial β 1–3-N-acetylglucosaminyltransferases and acceptor substrate flexibility of β 1–4-galactosyltransferases. *Bioorg. Med. Chem.* **2016**, *24*, 1696–1705.
 207. Lau, K.; Thon, V.; Yu, H.; Ding, L.; Chen, Y.; Muthana, M.M.; Wong, D.; Huang, R.; Chen, X. Highly efficient chemoenzymatic synthesis of β 1–4-linked galactosides with promiscuous bacterial β 1–4-galactosyltransferases. *Chem. Commun.* **2010**, *46*, 6066–6068.
 208. Kang, J.-Y.; Lim, S.-J.; Kwon, O.; Lee, S.-G.; Kim, H.H.; Oh, D.-B. Enhanced Bacterial α (2, 6)-Sialyltransferase Reaction through an Inhibition of Its Inherent Sialidase Activity by Dephosphorylation of Cytidine-5'-Monophosphate. *PLoS One* **2015**, *10*.
 209. Yu, H.; Li, Y.; Wu, Z.; Li, L.; Zeng, J.; Zhao, C.; Wu, Y.; Tasnima, N.; Wang, J.; Liu, H. H. pylori α 1–3/4-fucosyltransferase (Hp3/4FT)-catalyzed one-pot multienzyme (OPME) synthesis of Lewis antigens and human milk fucosides. *Chem. Commun.* **2017**, *53*, 11012–11015.
 210. Li, Y.; Li, R.; Yu, H.; Sheng, X.; Wang, J.; Fisher, A.J.; Chen, X. *Enterococcus faecalis* α 1–2-mannosidase (EfMan-I): an efficient catalyst for glycoprotein N-glycan modification. *FEBS Lett.* **2020**, *594*, 439–451.
 211. Chen, R.; Pawlicki, M.A.; Hamilton, B.S.; Tolbert, T.J. Enzyme-catalyzed synthesis of a hybrid N-linked oligosaccharide using N-acetylglucosaminyltransferase I. *Adv. Synth. Catal.* **2008**, *350*, 1689–1695.
 212. Shibatani, S.; Fujiyama, K.; Nishiguchi, S.; Seki, T.; Maekawa, Y. Production and characterization of active soluble human β 1, 4-galactosyltransferase in *Escherichia coli* as a useful catalyst in synthesis of the Gal β 1→4 GlcNAc linkage. *J. Biosci. Bioeng.* **2001**, *91*, 85–87.
 213. Froger, A.; Hall, J.E. Transformation of plasmid DNA into *E. coli* using the heat shock method. *JoVE (Journal Vis. Exp.)* **2007**, e253.
 214. Rohrer, J. Eluent Preparation for High-Performance Anion-Exchange Chromatography with Pulsed Amperometric Detection. *Thermo Fish. Sci. Tech. Note* **2017**, *71*, 1–7.

215. Ritter, J.B.; Genzel, Y.; Reichl, U. High-performance anion-exchange chromatography using on-line electrolytic eluent generation for the determination of more than 25 intermediates from energy metabolism of mammalian cells in culture. *J. Chromatogr. B* **2006**, *843*, 216–226.
216. Thurl, S.; Müller-Werner, B.; Sawatzki, G. Quantification of individual oligosaccharide compounds from human milk using high-pH anion-exchange chromatography. *Anal. Biochem.* **1996**, *235*, 202–206, doi:10.1006/abio.1996.0113.
217. Fischöder, T.; Cajic, S.; Reichl, U.; Rapp, E.; Elling, L. Enzymatic Cascade Synthesis Provides Novel Linear Human Milk Oligosaccharides as Reference Standards for xCGE-LIF Based High-Throughput Analysis. *Biotechnol. J.* **2019**, *14*, 1800305.
218. Selman, M.H.J.; Hemayatkar, M.; Deelder, A.M.; Wuhrer, M. Cotton HILIC SPE microtips for microscale purification and enrichment of glycans and glycopeptides. *Anal. Chem.* **2011**, *83*, 2492–2499, doi:10.1021/ac1027116.
219. Hennig, R.; Rapp, E.; Kottler, R.; Cajic, S.; Borowiak, M.; Reichl, U. N-Glycosylation fingerprinting of viral glycoproteins by xCGE-LIF. In *Methods in Molecular Biology*; Humana Press Inc., 2015; Vol. 1331, pp. 123–143.
220. Mahour, R.; Lee, J.W.; Grimpe, P.; Boecker, S.; Grote, V.; Klamt, S.; Seidel-Morgenstern, A.; Rexer, T.F.T.; Reichl, U. Cell-free multi-enzyme synthesis and purification of uridine diphosphate galactose. *ChemBioChem* **2021**.
221. Mahour, R.; Klapproth, J.; Rexer, T.F.T.; Schildbach, A.; Klamt, S.; Pietzsch, M.; Rapp, E.; Reichl, U. Establishment of a five-enzyme cell-free cascade for the synthesis of uridine diphosphate N-acetylglucosamine. *J. Biotechnol.* **2018**, *283*.
222. Chen, J.-K.; Shen, C.-R.; Liu, C.-L. N-acetylglucosamine: production and applications. *Mar. Drugs* **2010**, *8*, 2493–2516.
223. Mahour, R.; Rexer, T.F.T. Enzymatic method for preparation of UDP-Galactose 2021, International Patent Application Number: PCT/ EP2020/077396.
224. Grimpe, P. Multienzyme systems for synthesis of activated sugars, Otto-von-Guericke Universität Magdeburg, 2020.
225. Nakajima, K.; Kizuka, Y.; Yamaguchi, Y.; Hirabayashi, Y.; Takahashi, K.; Yuzawa, Y.; Taniguchi, N. Identification and characterization of UDP-mannose in human cell lines and mouse organs: Differential distribution across brain regions and organs. *Biochem. Biophys. Res. Commun.* **2018**, *495*, 401–407, doi:10.1016/j.bbrc.2017.10.173.
226. Bento, C.F.D. Advanced Development of Sugar Nucleotide Regeneration Cascade, Universidade de Nova Lisboa, 2018.
227. Mahour, R.; Rexer, Thomas, F.T. Enzymatic method for preparation of GDP-Fucose 2020, International Patent Application Number: PCT/EP2020/059182.
228. Mahour, R.; Marichal-Gallardo, P.A.; Rexer, T.F.T.; Reichl, U. Multi-enzyme Cascades for the In Vitro Synthesis of Guanosine Diphosphate L-Fucose. *ChemCatChem* **2021**, *13*, 1981–1989, doi:10.1002/cctc.202001854.
229. Kornfeld, R.H. Control of synthesis of guanosine 5'-diphosphate D-mannose and guanosine 5'-diphosphate L-fucose in bacteria. *Biochim. Biophys. Acta (BBA)-General Subj.* **1966**, *117*, 79–87.
230. Sturla, L.; Bisso, A.; Zanardi, D.; Benatti, U.; De Flora, A.; Tonetti, M. Expression, purification and characterization of GDP-d-mannose 4, 6-dehydratase from Escherichia coli. *FEBS Lett.* **1997**, *412*, 126–130.
231. Somoza, J.R.; Menon, S.; Schmidt, H.; Joseph-McCarthy, D.; Dessen, A.; Stahl, M.L.; Somers, W.S.; Sullivan, F.X. Structural and kinetic analysis of Escherichia coli GDP-mannose 4, 6 dehydratase provides insights into the enzyme's catalytic mechanism and regulation by GDP-fucose. *Structure* **2000**, *8*, 123–135.
232. Rexer, Thomas, F., T.; Mahour, R. Enzymatic method for preparation of CMP-Neu5Ac 2021, International Patent Application Number: PCT/EP2021/059101.
233. Asahi, S.; Tsunemi, Y.; Doi, M. Improvement of a cytidine-producing mutant of Bacillus subtilis introducing a mutation by homologous recombination. *Biosci. Biotechnol. Biochem.* **1995**, *59*, 2123–2126.
234. Asahi, S.; Tsunemi, Y.; Izawa, M.; Doi, M. A 3-deazauracil-resistant mutant of Bacillus subtilis with increased production of cytidine. *Biosci. Biotechnol. Biochem.* **1995**, *59*, 915–916.
235. Klermund, L.; Poschenrieder, S.T.; Castiglione, K. Biocatalysis in Polymersomes: Improving Multienzyme Cascades with Incompatible Reaction Steps by Compartmentalization. *ACS Catal.* **2017**, *7*, 3900–3904, doi:10.1021/acscatal.7b00776.
236. Lee, Y.-C.; Chien, H.-C.R.; Hsu, W.-H. Production of N-acetyl-D-neuraminic acid by recombinant whole cells expressing Anabaena sp. CH1 N-acetyl-D-glucosamine 2-epimerase

- and Escherichia coli N-acetyl-D-neuraminic acid lyase. *J. Biotechnol.* **2007**, *129*, 453–460.
237. Doi, M.; Tsunemi, Y.; Asahi, S. Optimization of Conditions for Production of Uridine by a Mutant of *Bacillus subtilis*. *Biosci. Biotechnol. Biochem.* **1994**, *58*, 1608–1612, doi:10.1271/BBB.58.1608.
238. Enei, H.; Sato, K.; Hirose, Y. METHOD OF PRODUCING GUANOSINE BY FERMENTATION 1975.
239. Lee, J.-H.; Chung, S.-W.; Lee, H.-J.; Jang, K.-S.; Lee, S.-G.; Kim, B.-G. Optimization of the enzymatic one pot reaction for the synthesis of uridine 5'-diphosphogalactose. *Bioprocess Biosyst. Eng.* **2010**, *33*, 71.
240. Woo, J.S.; Kim, B.-G.; Kim, D.H.; Choi, Y.H.; Song, J.-K.; Kang, S.Y.; Seo, W.M.; Yang, J.Y.; Lee, S.M. Method for preparing sialic acid derivative 2017.
241. Liu, J.L.C.; Shen, G.J.; Ichikawa, Y.; Rutan, J.F.; Zapata, G.; Vann, W.F.; Wong, C.H. Overproduction of CMP-sialic acid synthetase for organic synthesis. *J. Am. Chem. Soc.* **1992**, *114*, 3901–3910.
242. Nahálka, J.; Wu, B.; Shao, J.; Gemeiner, P.; Wang, P.G. Production of cytidine 5'-monophospho-N-acetyl- β -D-neuraminic acid (CMP-sialic acid) using enzymes or whole cells entrapped in calcium pectate–silica-gel beads. *Biotechnol. Appl. Biochem.* **2004**, *40*, 101–106.
243. Kulakovskaya, T. V.; Vagabov, V.M.; Kulaev, I.S. Inorganic polyphosphate in industry, agriculture and medicine: Modern state and outlook. *Process Biochem.* **2012**, *47*, 1–10.
244. Wazer, J.R. Van; Campanella, D.A. Structure and properties of the condensed phosphates. IV. Complex ion formation in polyphosphate solutions. *J. Am. Chem. Soc.* **1950**, *72*, 655–663.
245. Bonting, C.F.C.; Kortstee, G.J.J.; Boekestein, A.; Zehnder, A.J.B. The elemental composition dynamics of large polyphosphate granules in *Acinetobacter* strain 210A. *Arch. Microbiol.* **1993**, *159*, 428–434.
246. Kulaev, I.S.; Vagabov, V.; Kulakovskaya, T. *The biochemistry of inorganic polyphosphates*; John Wiley & Sons, 2005; ISBN 0470858184.
247. Parnell, A.E.; Mordhorst, S.; Kemper, F.; Giurrandino, M.; Prince, J.P.; Schwarzer, N.J.; Hofer, A.; Wohlwend, D.; Jessen, H.J.; Gerhardt, S. Substrate recognition and mechanism revealed by ligand-bound polyphosphate kinase 2 structures. *Proc. Natl. Acad. Sci.* **2018**, *115*, 3350–3355.
248. Ishige, K.; Hamamoto, T.; Shiba, T.; Noguchi, T. Novel method for enzymatic synthesis of CMP-NeuAc. *Biosci. Biotechnol. Biochem.* **2001**, *65*, 1736–1740.
249. Resnick, S.M.; Zehnder, A.J.B. In vitro ATP regeneration from polyphosphate and AMP by polyphosphate:AMP phosphotransferase and adenylate kinase from *Acinetobacter johnsonii* 210A. *Appl. Environ. Microbiol.* **2000**, *66*, 2045–2051, doi:10.1128/AEM.66.5.2045-2051.2000.
250. Li, X.; Qi, C.; Wei, P.; Huang, L.; Cai, J.; Xu, Z. Efficient chemoenzymatic synthesis of uridine 5'-diphosphate N-acetylglucosamine and uridine 5'-diphosphate N-trifluoroacetyl glucosamine with three recombinant enzymes. *Prep. Biochem. Biotechnol.* **2017**, *47*, 852–859.
251. Bayer, R.J.; DeFrees, S.; Ratcliffe, M. Enzymatic synthesis of glycosidic linkages 1998.
252. Hawkes, J.S.; Gibson, R.A.; Robertson, D.; Makrides, M. Effect of dietary nucleotide supplementation on growth and immune function in term infants: a randomized controlled trial. *Eur. J. Clin. Nutr.* **2006**, *60*, 254–264.
253. Lecca, D.; Ceruti, S. Uracil nucleotides: from metabolic intermediates to neuroprotection and neuroinflammation. *Biochem. Pharmacol.* **2008**, *75*, 1869–1881.
254. Kensler, T.W.; Cooney, D.A. Chemotherapeutic inhibitors of the enzymes of the de novo pyrimidine pathway. In *Advances in Pharmacology*; Elsevier, 1981; Vol. 18, pp. 273–352 ISBN 1054-3589.
255. Hadfield, A.F.; Sartorelli, A.C. The pharmacology of prodrugs of 5-fluorouracil and 1- β -D-arabinofuranosylcytosine. In *Advances in Pharmacology*; Elsevier, 1984; Vol. 20, pp. 21–67 ISBN 1054-3589.
256. Lawitz, E.; Mangia, A.; Wyles, D.; Rodriguez-Torres, M.; Hassanein, T.; Gordon, S.C.; Schultz, M.; Davis, M.N.; Kayali, Z.; Reddy, K.R. Sofosbuvir for previously untreated chronic hepatitis C infection. *N. Engl. J. Med.* **2013**, *368*, 1878–1887.
257. Lindsley, C.W. Novel drug approvals in 2015 and thus far in 2016 2016.
258. McIntosh, J.A.; Benkovics, T.; Silverman, S.M.; Huffman, M.A.; Kong, J.; Maligres, P.E.; Itoh, T.; Yang, H.; Verma, D.; Pan, W. Engineered Ribosyl-1-Kinase Enables Concise Synthesis of Molnupiravir, an Antiviral for COVID-19. *ACS Cent. Sci.* **2021**.
259. Doi, M.; Tsunemi, Y.; Asahi, S. Optimization of Conditions for Production of Uridine by a Mutant of *Bacillus subtilis*. *Biosci. Biotechnol. Biochem.* **1994**, *58*, 1608–1612.
260. Wu, H.; Li, Y.; Ma, Q.; Li, Q.; Jia, Z.; Yang, B.; Xu, Q.; Fan, X.; Zhang, C.; Chen, N. Metabolic

- engineering of *Escherichia coli* for high-yield uridine production. *Metab. Eng.* **2018**, *49*, 248–256.
261. Du, T.; Buenbrazo, N.; Kell, L.; Rahmani, S.; Sim, L.; Withers, S.G.; DeFrees, S.; Wakarchuk, W. A bacterial expression platform for production of therapeutic proteins containing human-like O-linked glycans. *Cell Chem. Biol.* **2019**, *26*, 203–212.
 262. Liang, T.; Xu, Z.; Jia, W.; Zhang, H.; Yang, F.; Zou, X.; Zhang, Y. A simple bacterial expression system for human ppGalNAc-T and used for the synthesis of O-GalNAc glycosylated interleukin 2. *Biochem. Biophys. Res. Commun.* **2020**, *529*, 57–63.
 263. Tabata, K.; Koizumi, S.; Endo, T.; Ozaki, A. Production of UDP-N-acetylglucosamine by coupling metabolically engineered bacteria. *Biotechnol. Lett.* **2000**, *22*, 479–483.
 264. Fujio, T.; Maruyama, A. Enzymatic production of pyrimidine nucleotides using *Corynebacterium ammoniagenes* cells and recombinant *Escherichia coli* cells: enzymatic production of CDP-choline from orotic acid and choline chloride (part I). *Biosci. Biotechnol. Biochem.* **1997**, *61*, 956–959.
 265. Wehrst, M.; Tanjore, D.; Eng, T.; Lievense, J.; Pray, T.R.; Mukhopadhyay, A. Engineering robust production microbes for large-scale cultivation. *Trends Microbiol.* **2019**.
 266. Zhou, J.; Fan, L.; Wei, P.; Huang, L.; Cai, J.; Xu, Z. Efficient production of uridine 5'-diphospho-N-acetylglucosamine by the combination of three recombinant enzymes and yeast cells. *Prep. Biochem. Biotechnol.* **2010**, *40*, 294–304.
 267. Zhai, Y.; Liang, M.; Fang, J.; Wang, X.; Guan, W.; Liu, X.; Wang, P.; Wang, F. NahK/GlmU fusion enzyme: characterization and one-step enzymatic synthesis of UDP-N-acetylglucosamine. *Biotechnol. Lett.* **2012**, *34*, 1321–1326.
 268. Bültner, T.; Elling, L. Enzymatic synthesis of UDP-galactose on a gram scale. *J. Mol. Catal. B Enzym.* **2000**, *8*, 281–284.
 269. Hei, C.L.; Lee, S.D.; Jae, K.S.; Liou, K. One-pot enzymatic synthesis of UDP-D-glucose from UMP and glucose-1-phosphate using an ATP regeneration system. *J. Biochem. Mol. Biol.* **2004**, *37*, 503–506, doi:10.5483/bmbrep.2004.37.4.503.
 270. Weyler, C.; Heinzle, E. Multistep synthesis of UDP-glucose using tailored, permeabilized cells of *E. coli*. *Appl. Biochem. Biotechnol.* **2015**, *175*, 3729–3736.
 271. Gutmann, A.; Nidetzky, B. Unlocking the Potential of Leloir Glycosyltransferases for Applied Biocatalysis: Efficient Synthesis of Uridine 5'-Diphosphate-Glucose by Sucrose Synthase. *Adv. Synth. Catal.* **2016**, *358*, 3600–3609, doi:10.1002/adsc.201600754.
 272. Schmölder, K.; Lemmerer, M.; Gutmann, A.; Nidetzky, B. Integrated process design for biocatalytic synthesis by a Leloir Glycosyltransferase: UDP-glucose production with sucrose synthase. *Biotechnol. Bioeng.* **2017**, *114*, 924–928, doi:10.1002/bit.26204.
 273. Feng, Y.; Yao, M.; Wang, Y.; Ding, M.; Zha, J.; Xiao, W.; Yuan, Y. Advances in engineering UDP-sugar supply for recombinant biosynthesis of glycosides in microbes. *Biotechnol. Adv.* **2020**, 107538.
 274. De Bruyn, F.; Maertens, J.; Beauprez, J.; Soetaert, W.; De Mey, M. Biotechnological advances in UDP-sugar based glycosylation of small molecules. *Biotechnol. Adv.* **2015**, *33*, 288–302.
 275. Wendisch, V.F.; Eberhardt, D.; Herbst, M.; Jensen, J.V.K. Biotechnological production of amino acids and nucleotides. In *Biotechnological Production Of Natural Ingredients For Food Industry*; Bicas, J.L., Maróstica, M.R.J., Pastore, G.M., Eds.; Bentham Science, 2016; pp. 60–163.
 276. Bhattacharyya, T.; Saha, P.; Dash, J. Guanosine-derived supramolecular hydrogels: recent developments and future opportunities. *ACS omega* **2018**, *3*, 2230–2241.
 277. Hunter, C.A. Quantifying intermolecular interactions: guidelines for the molecular recognition toolbox. *Angew. Chemie Int. Ed.* **2004**, *43*, 5310–5324.
 278. Sullivan, F.X.; Kumar, R.; Kriz, R.; Stahl, M.; Xu, G.-Y.; Rouse, J.; Chang, X.; Boodhoo, A.; Potvin, B.; Cumming, D.A. Molecular cloning of human GDP-mannose 4, 6-dehydratase and reconstitution of GDP-fucose biosynthesis in vitro. *J. Biol. Chem.* **1998**, *273*, 8193–8202.
 279. Alberty, R.A. Effect of pH on Protein–Ligand Equilibria. *J. Phys. Chem. B* **2000**, *104*, 9929–9934.
 280. Pfeiffer, M.; Bulfon, D.; Weber, H.; Nidetzky, B. A Kinase-Independent One-Pot Multienzyme Cascade for an Expedient Synthesis of Guanosine 5'-Diphospho-d-mannose. *Adv. Synth. Catal.* **2016**, *358*, 3809–3816.
 281. Fey, S.; Elling, L.; Kragl, U. The cofactor Mg²⁺—A key switch for effective continuous enzymatic production of GDP-mannose using recombinant GDP-mannose pyrophosphorylase. *Carbohydr. Res.* **1997**, *305*, 475–481.
 282. Li, L.; Liu, Y.; Wan, Y.; Li, Y.; Chen, X.; Zhao, W.; Wang, P.G. Efficient enzymatic synthesis of

- guanosine 5'-diphosphate-sugars and derivatives. *Org. Lett.* **2013**, *15*, 5528–5530.
283. Albermann, C.; Distler, J.; Piepersberg, W. Preparative synthesis of GDP- β -l-fucose by recombinant enzymes from enterobacterial sources. *Glycobiology* **2000**, *10*, 875–881.
 284. Asahi, S.; Tsunemi, Y.; Izawa, M.; DOI, M. Cytidine production by mutants of *Bacillus subtilis*. *Biosci. Biotechnol. Biochem.* **1994**, *58*, 1399–1402.
 285. Asahi, S.; Doi, M.; Tsunemi, Y.; Akiyama, S. Regulation of pyrimidine nucleotide biosynthesis in cytidine deaminase-negative mutants of *Bacillus subtilis*. *Agric. Biol. Chem.* **1989**, *53*, 97–102.
 286. Mahmoudian, M.; Noble, D.; Drake, C.S.; Middleton, R.F.; Montgomery, D.S.; Piercey, J.E.; Ramlakhan, D.; Todd, M.; Dawson, M.J. An efficient process for production of N-acetylneuraminic acid using N-acetylneuraminic acid aldolase. *Enzyme Microb. Technol.* **1997**, *20*, 393–400.
 287. Zhang, X.; Liu, Y.; Liu, L.; Li, J.; Du, G.; Chen, J. Microbial production of sialic acid and sialylated human milk oligosaccharides: Advances and perspectives. *Biotechnol. Adv.* **2019**.
 288. Kragl, U.; Gygax, D.; Ghisalba, O.; Wandrey, C. Enzymatic two-step synthesis of N-acetylneuraminic acid in the enzyme membrane reactor. *Angew. Chemie Int. Ed. English* **1991**, *30*, 827–828.
 289. Hamamoto, T.; Takeda, S.; Noguchi, T. Enzymatic Synthesis of Cytidine 5'-Monophospho-N-acetylneuraminic Acid. *Biosci. Biotechnol. Biochem.* **2005**, *69*, 1944–1950.
 290. Endo, T.; Koizumi, S.; Tabata, K.; Ozaki, A. Large-scale production of CMP-NeuAc and sialylated oligosaccharides through bacterial coupling. *Appl. Microbiol. Biotechnol.* **2000**, *53*, 257–261, doi:10.1007/s002530050017.
 291. Lee, S.; Lee, J.; Yi, J.; Kim, B. Production of cytidine 5'-monophosphate N-acetylneuraminic acid using recombinant *Escherichia coli* as a biocatalyst. *Biotechnol. Bioeng.* **2002**, *80*, 516–524.
 292. Yu, H.; Lau, K.; Thon, V.; Autran, C.A.; Jantscher-Krenn, E.; Xue, M.; Li, Y.; Sugiarto, G.; Qu, J.; Mu, S. Synthetic disialyl hexasaccharides protect neonatal rats from necrotizing enterocolitis. *Angew. Chemie Int. Ed.* **2014**, *53*, 6687–6691.
 293. Lu, N.; Ye, J.; Cheng, J.; Sasmal, A.; Liu, C.-C.; Yao, W.; Yan, J.; Khan, N.; Yi, W.; Varki, A. Redox-controlled site-specific α 2–6-sialylation. *J. Am. Chem. Soc.* **2019**, *141*, 4547–4552.
 294. Wong, C.H.; Haynie, S.L.; Whitesides, G.M. Enzyme-catalyzed synthesis of N-acetyllactosamine with in situ regeneration of uridine 5'-diphosphate glucose and uridine 5'-diphosphate galactose. *J. Org. Chem.* **1982**, *47*, 5416–5418.
 295. Endo, T.; Koizumi, S.; Tabata, K.; Kakita, S.; Ozaki, A. Large-scale production of N-acetyllactosamine through bacterial coupling. *Carbohydr. Res.* **1999**, *316*, 179–183.
 296. Koizumi, S. Large-scale production of oligosaccharides using bacterial functions. *Trends Glycosci. Glycotechnol.* **2003**, *15*, 65–74.
 297. Yu, H.; Li, Y.; Zeng, J.; Thon, V.; Nguyen, D.M.; Ly, T.; Kuang, H.Y.; Ngo, A.; Chen, X. Sequential one-pot multienzyme chemoenzymatic synthesis of glycosphingolipid glycans. *J. Org. Chem.* **2016**, *81*, 10809–10824.
 298. McGuire, M.K.; Meehan, C.L.; McGuire, M.A.; Williams, J.E.; Foster, J.; Sellen, D.W.; Kamau-Mbuthia, E.W.; Kamundia, E.W.; Mbugua, S.; Moore, S.E. What's normal? Oligosaccharide concentrations and profiles in milk produced by healthy women vary geographically. *Am. J. Clin. Nutr.* **2017**, *105*, 1086–1100.
 299. Choi, Y.H.; Kim, J.H.; Park, B.S.; Kim, B. Solubilization and Iterative Saturation Mutagenesis of α 1, 3-fucosyltransferase from *Helicobacter pylori* to enhance its catalytic efficiency. *Biotechnol. Bioeng.* **2016**, *113*, 1666–1675.
 300. Jung, S.; Park, Y.; Seo, J. Production of 3-Fucosyllactose in Engineered *Escherichia coli* with α -1, 3-Fucosyltransferase from *Helicobacter pylori*. *Biotechnol. J.* **2019**, *14*, 1800498.
 301. Schelch, S.; Eibinger, M.; Gross Belduma, S.; Petschacher, B.; Kuballa, J.; Nidetzky, B. Engineering analysis of multienzyme cascade reactions for 3'-sialyllactose synthesis. *Biotechnol. Bioeng.* **2021**, *118*, 4290–4304.
 302. Gilbert, M.; Bayer, R.; Cunningham, A.-M.; DeFrees, S.; Gao, Y.; Watson, D.C.; Young, N.M.; Wakarchuk, W.W. The synthesis of sialylated oligosaccharides using a CMP-Neu5Ac synthetase/sialyltransferase fusion. *Nat. Biotechnol.* **1998**, *16*, 769–772.
 303. Rech, C.; Rosencrantz, R.R.; Křenek, K.; Pelantová, H.; Bojarová, P.; Römer, C.E.; Hanisch, F.; Křen, V.; Elling, L. Combinatorial one-pot synthesis of poly-N-acetyllactosamine oligosaccharides with Leloir-glycosyltransferases. *Adv. Synth. Catal.* **2011**, *353*, 2492–2500.
 304. Engel, A.M.; Sobek, H.; Greif, M.; Malik, S.; Thomann, M.; Jung, C.; Reusch, D.; Ribitsch, D.; Zitzenbacher, S.; Luley, C. Rec. ST6Gal-I variants to control enzymatic activity in processes of

- in vitro glycoengineering. In Proceedings of the BMC proceedings; BioMed Central, 2013; Vol. 7, p. P110.
305. Lippold, S.; Nicolardi, S.; Domínguez-Vega, E.; Heidenreich, A.-K.; Vidarsson, G.; Reusch, D.; Habegger, M.; Wuhrer, M.; Falck, D. Glycoform-resolved FcγRIIIa affinity chromatography–mass spectrometry. In Proceedings of the MABs; Taylor & Francis, 2019; Vol. 11, pp. 1191–1196.
 306. Kiyoshi, M.; Caaveiro, J.M.M.; Tada, M.; Tamura, H.; Tanaka, T.; Terao, Y.; Morante, K.; Harazono, A.; Hashii, N.; Shibata, H. Assessing the heterogeneity of the Fc-glycan of a therapeutic antibody using an engineered FcγReceptor IIIa-immobilized column. *Sci. Rep.* **2018**, *8*, 1–11.
 307. Umaña, P.; Jean-Mairet, J.; Moudry, R.; Amstutz, H.; Bailey, J.E. Engineered glycoforms of an antineuroblastoma IgG1 with optimized antibody-dependent cellular cytotoxic activity. *Nat. Biotechnol.* **1999**, *17*, 176–180.
 308. Ratner, M. Genentech's glyco-engineered antibody to succeed Rituxan 2014.
 309. Cameron, F.; McCormack, P.L. Obinutuzumab: first global approval. *Drugs* **2014**, *74*, 147–154.
 310. Chung, S.; Quarumby, V.; Gao, X.; Ying, Y.; Lin, L.; Reed, C.; Fong, C.; Lau, W.; Qiu, Z.J.; Shen, A. Quantitative evaluation of fucose reducing effects in a humanized antibody on Fcγ receptor binding and antibody-dependent cell-mediated cytotoxicity activities. *MABs* **2012**, *4*, 326–340.
 311. Shah, N.; Kuntz, D.A.; Rose, D.R. Golgi α-mannosidase II cleaves two sugars sequentially in the same catalytic site. *Proc. Natl. Acad. Sci.* **2008**, *105*, 9570–9575.
 312. Rose, D.R. Structure, mechanism and inhibition of Golgi α-mannosidase II. *Curr. Opin. Struct. Biol.* **2012**, *22*, 558–562.
 313. Foster, J.M.; Yudkin, B.; Lockyer, A.E.; Roberts, D.B. Cloning and sequence analysis of GmII, a Drosophila melanogaster homologue of the cDNA encoding murine Golgi α-mannosidase II. *Gene* **1995**, *154*, 183–186.
 314. Gramer, M.J.; Eckblad, J.J.; Donahue, R.; Brown, J.; Shultz, C.; Vickerman, K.; Priem, P.; van den Bremer, E.T.J.; Gerritsen, J.; van Berkel, P.H.C. Modulation of antibody galactosylation through feeding of uridine, manganese chloride, and galactose. *Biotechnol. Bioeng.* **2011**, *108*, 1591–1602.
 315. Raju, T.S.; Jordan, R.E. Galactosylation variations in marketed therapeutic antibodies. *MABs* **2012**, *4*, 385–391.
 316. Pierpont, T.M.; Limper, C.B.; Richards, K.L. Past, present, and future of rituximab—the world's first oncology monoclonal antibody therapy. *Front. Oncol.* **2018**, *8*, 163.
 317. Hainsworth, J.D.; Litchy, S.; Burriss III, H.A.; Scullin Jr, D.C.; Corso, S.W.; Yardley, D.A.; Morrissey, L.; Greco, F.A. Rituximab as first-line and maintenance therapy for patients with indolent non-Hodgkin's lymphoma. *J. Clin. Oncol.* **2002**, *20*, 4261–4267.
 318. Randall, K.L. Rituximab in autoimmune diseases. *Aust. Prescr.* **2016**, *39*, 131.
 319. Weiner, G.J. Rituximab: mechanism of action. In Proceedings of the Seminars in hematology; Elsevier, 2010; Vol. 47, pp. 115–123.
 320. Freeman, C.L.; Sehn, L.H. A tale of two antibodies: obinutuzumab versus rituximab. *Br. J. Haematol.* **2018**, *182*, 29–45.
 321. Nahta, R. e; Esteva, F.J. Trastuzumab: triumphs and tribulations. *Oncogene* **2007**, *26*, 3637–3643.
 322. Collins, D.M.; O'donovan, N.; McGowan, P.M.; O'sullivan, F.; Duffy, M.J.; Crown, J. Trastuzumab induces antibody-dependent cell-mediated cytotoxicity (ADCC) in HER-2-non-amplified breast cancer cell lines. *Ann. Oncol.* **2012**, *23*, 1788–1795.
 323. Oholendt, A.L.; Zadlo, J.L. Ramucirumab: a new therapy for advanced gastric cancer. *J. Adv. Pract. Oncol.* **2015**, *6*, 71.
 324. Zahavi, D.; AlDeghather, D.; O'Connell, A.; Weiner, L.M. Enhancing antibody-dependent cell-mediated cytotoxicity: a strategy for improving antibody-based immunotherapy. *Antib. Ther.* **2018**, *1*, 7–12.
 325. van der Horst, H.J.; Nijhof, I.S.; Mutis, T.; Chamuleau, M.E.D. Fc-Engineered Antibodies with Enhanced Fc-Effector Function for the Treatment of B-Cell Malignancies. *Cancers (Basel)*. **2020**, *12*, 3041.
 326. Larsen, M.D.; de Graaf, E.L.; Sonneveld, M.E.; Plomp, H.R.; Nouta, J.; Hoepel, W.; Chen, H.-J.; Linty, F.; Visser, R.; Brinkhaus, M. Afucosylated IgG characterizes enveloped viral responses and correlates with COVID-19 severity. *Science (80-)*. **2021**, *371*.
 327. Chakraborty, S.; Gonzalez, J.; Edwards, K.; Mallajosyula, V.; Buzzanco, A.S.; Sherwood, R.; Buffone, C.; Kathale, N.; Providenza, S.; Xie, M.M. Proinflammatory IgG Fc structures in

- patients with severe COVID-19. *Nat. Immunol.* **2021**, *22*, 67–73.
328. Rugo, H.S.; Im, S.-A.; Cardoso, F.; Cortés, J.; Curigliano, G.; Musolino, A.; Pegram, M.D.; Wright, G.S.; Saura, C.; Escrivá-de-Romaní, S. Efficacy of margetuximab vs trastuzumab in patients with pretreated ERBB2-positive advanced breast cancer: a phase 3 randomized clinical trial. *JAMA Oncol.* **2021**, *7*, 573–584.
 329. Osch, T.L.J. van; Nouta, J.; Derksen, N.I.L.; Mierlo, G. van; Schoot, C.E. van der; Wuhrer, M.; Rispens, T.; Vidarsson, G. Fc Galactosylation Promotes Hexamerization of Human IgG1, Leading to Enhanced Classical Complement Activation. *J. Immunol.* **2021**, doi:10.4049/JIMMUNOL.2100399.
 330. Wei, B.; Gao, X.; Cadang, L.; Izadi, S.; Liu, P.; Zhang, H.-M.; Hecht, E.; Shim, J.; Magill, G.; Pabon, J.R.; et al. Fc galactosylation follows consecutive reaction kinetics and enhances immunoglobulin G hexamerization for complement activation. <https://doi.org/10.1080/19420862.2021.1893427> **2021**, *13*, doi:10.1080/19420862.2021.1893427.
 331. Yu, M.; Brown, D.; Reed, C.; Chung, S.; Lutman, J.; Stefanich, E.; Wong, A.; Stephan, J.-P.; Bayer, R. Production, characterization and pharmacokinetic properties of antibodies with N-linked Mannose-5 glycans. *MAbs* **2012**, *4*, 475–487.
 332. Macharoen, K.; Li, Q.; Márquez-Escobar, V.A.; Corbin, J.M.; Lebrilla, C.B.; Nandi, S.; McDonald, K.A. Effects of Kifunensine on Production and N-Glycosylation Modification of Butyrylcholinesterase in a Transgenic Rice Cell Culture Bioreactor. *Int. J. Mol. Sci.* **2020**, *21*, 6896.
 333. Brantley, T.J.; Mitchelson, F.G.; Khattak, S.F. A class of low-cost alternatives to kifunensine for increasing high mannose N-linked glycosylation for monoclonal antibody production in Chinese hamster ovary cells. *Biotechnol. Prog.* **2021**, *37*, e3076.
 334. Kommineni, V.; Markert, M.; Ren, Z.; Palle, S.; Carrillo, B.; Deng, J.; Tejada, A.; Nandi, S.; McDonald, K.A.; Marcel, S. In vivo glycan engineering via the mannosidase I inhibitor (Kifunensine) improves efficacy of rituximab manufactured in *Nicotiana benthamiana* plants. *Int. J. Mol. Sci.* **2019**, *20*, 194.
 335. Shi, X.; Jarvis, D.L. Protein N-glycosylation in the baculovirus-insect cell system. *Curr. Drug Targets* **2007**, *8*, 1116–1125.
 336. Ruhnau, J.; Grote, V.; Juarez-Osorio, M.; Bruder, D.; Mahour, R.; Rapp, E.; Rexer, T.F.T.; Reichl, U. Cell-Free Glycoengineering of the Recombinant SARS-CoV-2 Spike Glycoprotein. *Front. Bioeng. Biotechnol.* **2021**, *0*, 683, doi:10.3389/FBIOE.2021.699025.
 337. De Pourcq, K.; Tiels, P.; Van Hecke, A.; Geysens, S.; Vervecken, W.; Callewaert, N. Engineering *Yarrowia lipolytica* to produce glycoproteins homogeneously modified with the universal Man 3 GlcNAc 2 N-glycan core. *PLoS One* **2012**, *7*, e39976.
 338. Pallister, E.G.; Choo, M.S.F.; Tai, J.-N.; Leong, D.S.Z.; Tang, W.-Q.; Ng, S.-K.; Huang, K.; Marchesi, A.; Both, P.; Gray, C. Exploiting the disialyl galactose activity of $\alpha 2$, 6-sialyltransferase from *Photobacterium damsela* to generate a highly sialylated recombinant α -1-antitrypsin. *Biochemistry* **2019**, *59*, 3123–3128.
 339. Wang, M.; Wang, Y.; Liu, K.; Dou, X.; Liu, Z.; Zhang, L.; Ye, X.-S. Engineering a bacterial sialyltransferase for di-sialylation of a therapeutic antibody. *Org. Biomol. Chem.* **2020**, *18*, 2886–2892.
 340. Klymenko, O. V.; Shah, N.; Kontoravdi, C.; Royle, K.E.; Polizzi, K.M. Designing an Artificial Golgi reactor to achieve targeted glycosylation of monoclonal antibodies. *AIChE J.* **2016**, *62*, 2959–2973.
 341. Hamilton, B.S.; Wilson, J.D.; Shumakovich, M.A.; Fisher, A.C.; Brooks, J.C.; Pontes, A.; Naran, R.; Heiss, C.; Gao, C.; Kardish, R. A library of chemically defined human N-glycans synthesized from microbial oligosaccharide precursors. *Sci. Rep.* **2017**, *7*, 1–12.
 342. Jewett, M.C.; Stark, J.C.; Delisa, M.P.; Jaroentomeechai, T. Method for rapid in vitro synthesis of glycoproteins via recombinant production of N-glycosylated proteins in prokaryotic cell lysates 2020.
 343. Stark, J.C.; Jaroentomeechai, T.; Moeller, T.D.; Hershewe, J.M.; Warfel, K.F.; Moricz, B.S.; Martini, A.M.; Dubner, R.S.; Hsu, K.J.; Stevenson, T.C. On-demand biomanufacturing of protective conjugate vaccines. *Sci. Adv.* **2021**, *7*, eabe9444.
 344. Kokhan, O.; Marzolf, D.R. Detection and quantification of transition metal leaching in metal affinity chromatography with hydroxynaphthol blue. *Anal. Biochem.* **2019**, *582*, 113347.
 345. Mahour, R.; Rexer, T.F.T. Enzymatic method for preparation of UDP-GlcNAc 2021, International Patent Application Number: PCT/EP2020/077383.
 346. Swaim, C.M.; Brittain, T.J.; Marzolf, D.R.; Kokhan, O. Quantification of Metal Leaching in

- Immobilized Metal Affinity Chromatography. *JoVE (Journal Vis. Exp.)* **2020**, e60690.
347. Tamás, M.J.; Sharma, S.K.; Ibstedt, S.; Jacobson, T.; Christen, P. Heavy metals and metalloids as a cause for protein misfolding and aggregation. *Biomolecules* **2014**, *4*, 252–267.
348. Louie, A.Y.; Meade, T.J. Metal complexes as enzyme inhibitors. *Chem. Rev.* **1999**, *99*, 2711–2734.
349. Briffa, J.; Sinagra, E.; Blundell, R. Heavy metal pollution in the environment and their toxicological effects on humans. *Heliyon* **2020**, *6*, e04691.
350. Ghadge, R.S.; Patwardhan, A.W.; Sawant, S.B.; Joshi, J.B. Effect of flow pattern on cellulase deactivation in stirred tank bioreactors. *Chem. Eng. Sci.* **2005**, *60*, 1067–1083.
351. Thomas, C.R.; Geer, D. Effects of shear on proteins in solution. *Biotechnol. Lett.* **2011**, *33*, 443–456.
352. Bustamante, M.C.C.; Cerri, M.O.; Badino, A.C. Comparison between average shear rates in conventional bioreactor with Rushton and Elephant ear impellers. *Chem. Eng. Sci.* **2013**, *90*, 92–100.
353. Woodley, J.M. Scale-Up and Development of Enzyme-Based Processes for Large-Scale Synthesis Applications. In *Science of Synthesis: Biocatalysis in Organic Synthesis*; Faber, K., Fessner, W.D., Turner, N., Ed.; 2015; pp. 515–546.
354. Kohl, A.; Srinivasamurthy, V.; Böttcher, D.; Kabisch, J.; Bornscheuer, U.T. Co-expression of an alcohol dehydrogenase and a cyclohexanone monooxygenase for cascade reactions facilitates the regeneration of the NADPH cofactor. *Enzyme Microb. Technol.* **2018**, *108*, 53–58.
355. Jeon, E.-Y.; Baek, A.-H.; Bornscheuer, U.T.; Park, J.-B. Enzyme fusion for whole-cell biotransformation of long-chain sec-alcohols into esters. *Appl. Microbiol. Biotechnol.* **2015**, *99*, 6267–6275.
356. Chen, H.; Huang, R.; Zhang, Y.-H.P. Systematic comparison of co-expression of multiple recombinant thermophilic enzymes in *Escherichia coli* BL21 (DE3). *Appl. Microbiol. Biotechnol.* **2017**, *101*, 4481–4493.
357. Zhang, J.; Kowal, P.; Chen, X.; Wang, P.G. Large-scale synthesis of globotriose derivatives through recombinant *E. coli*. *Org. Biomol. Chem.* **2003**, *1*, 3048–3053.
358. Jordheim, L.P.; Durantel, D.; Zoulim, F.; Dumontet, C. Advances in the development of nucleoside and nucleotide analogues for cancer and viral diseases. *Nat. Rev. Drug Discov.* **2013**, *12*, 447–464.
359. Di Cosimo, R.; Mc Auliffe, J.; Poulouse, A.J.; Bohlmann, G. Industrial use of immobilized enzymes. *Chem. Soc. Rev.* **2013**, *42*, 6437–6474, doi:10.1039/c3cs35506c.
360. Zucca, P.; Sanjust, E. Inorganic materials as supports for covalent enzyme immobilization: methods and mechanisms. *Molecules* **2014**, *19*, 14139–14194.
361. Cao, L. *Carrier-bound immobilized enzymes: principles, application and design*; John Wiley & Sons, 2006; ISBN 3527607080.
362. Cao, L. Immobilised enzymes: science or art? *Curr. Opin. Chem. Biol.* **2005**, *9*, 217–226.
363. Cvijetinovic, S. Development of a Cascade of Immobilized Enzymes for the Synthesis of Activated Sugars. **2018**.
364. Xiao, C. Enzymatic Synthesis of Common Sugar Nucleotide and Therapeutic Oligosaccharides. **2018**.
365. Booth, W.T.; Schlachter, C.R.; Pote, S.; Ussin, N.; Mank, N.J.; Klapper, V.; Offermann, L.R.; Tang, C.; Hurlburt, B.K.; Chruszcz, M. Impact of an N-terminal polyhistidine tag on protein thermal stability. *ACS omega* **2018**, *3*, 760–768.
366. Mandelboim, O.; Malik, P.; Davis, D.M.; Jo, C.H.; Boyson, J.E.; Strominger, J.L. Human CD16 as a lysis receptor mediating direct natural killer cell cytotoxicity. *Proc. Natl. Acad. Sci.* **1999**, *96*, 5640–5644.

Appendix A: List of Chemicals

Table A. 1: List of chemicals used in this study.

Name	Manufacturer	Article No.
2-(N-Morpholino)-ethane sulphonic acid	Carl Roth	4256.2
3-(N-morpholino) propane sulphonic acid	Carl Roth	6979.5
3-Fucosyllactose	ELICITYL	GLY060-95%
6'-Sialyl-N-acetyllactosamine sodium salt	Merck	37966
6'-Sialyllactose sodium salt	Carbosynth	OS04398
8-Aminopyrene-1,3,6-trisulfonic acid trisodium salt	Merck	9341
96-Well AcroPrep™ Filter Plate	PALL	Pall 5054
9-Aminoacridine	Merck	92817
Acetonitrile	Thermo Scientific	A955
Adenosine 5'-diphosphate sodium salt	Merck	A2754
Adenosine 5'-monophosphate disodium salt	Merck	1930
Adenosine 5'-triphosphate disodium salt hydrate	Carbosynth	NA00135
Ampicillin sodium salt	Carl Roth	K029.1
Bio-Gel P-10	Bio-Rad	1504144
b-Nicotinamide adenine dinucleotide phosphate, reduced form, tetrasodium salt	Carbosynth	NN10871
Chloramphenicol	Carl Roth	3886.1
CMP-Neu5Ac sodium salt	Carbosynth	MC04391
Cytidine	Carbosynth	NC04070
Cytidine 5'-diphosphate sodium salt hydrate	Merck	C9755
Cytidine 5'-monophosphate disodium salt	Carbosynth	NC05637
Cytidine 5'-triphosphate disodium salt	Carbosynth	NC03860
Dimethyl sulfoxide	Merck	D8418
di-Potassium hydrogen phosphate	Carl Roth	P749.1
D-Lactose monohydrate	Merck	61339
D-mannose	Carbosynth	MM06704
Ethanol	Merck	1117270500
Galactose	Carbosynth	MG05201
GeneScan™ 500 LIZ™ dye Size Standard	Thermo Fisher	4322682
Glucose	Merck	G7528
Glycerol	Carl Roth	3783.1
Guanosine	Carbosynth	NG06314
Guanosine 5'-diphospho-a-D-mannose disodium salt	Carbosynth	MG05610
Guanosine 5'-diphospho-b-L-fucose disodium salt	Carbosynth	MG01912
Guanosine 5'-monophosphate disodium salt	Carbosynth	NG02982
Guanosine 5'-triphosphate disodium salt	Carbosynth	NG01208
Hi-Di™ Formamide	Thermo Fisher	4311320
Hydrochloric acid	Carl Roth	4025
IGEPAL® CA-630	Merck	18896
Imidazole	Carl Roth	3899.4

Isopropyl b-D-thiogalactopyranoside	Carbosynth	EI05931
Kanamycin sulfate	Merck	10106801001
Lacto- <i>N</i> -fucopentaose V	ELICITYL	GLY062-80%
Lacto- <i>N</i> -neotetraose	ELICITYL	GLY021-95%
Lacto- <i>N</i> -triose II	ELICITYL	GLY011-95%
L-fucose	Carbosynth	MF06710
L-glutamine	Merck	G6392
Magnesium chloride hexahydrate	Applichem	131396.121
Magnesium sulfate heptahydrate	Carl Roth	261.1
Maltose monohydrate	Carl Roth	8951.1
Man3	Agilent	GKR-002300
Manganese (II) Chloride Dihydrate	Merck	1.05934.0100
N-2-Hydroxyethylpiperazine-N'-2-ethane sulphonic acid	Carl Roth	HN78.3
<i>N</i> -acetyl-D-galactosamine	Carbosynth	MA04390
<i>N</i> -acetyl-D-glucosamine	Carbosynth	MA00834
<i>N</i> -acetyl-D-mannosamin	Carl Roth	5525.2
<i>N</i> -acetylneuraminic acid	Carbosynth	MA00746
Potassium dihydrogen phosphate	Carl Roth	P018.1
Sodium acetate	Thermo Fisher	59326
Sodium chloride	Carl Roth	9265.1
Sodium hydroxide	Fluka	72064H
Sodium polyphosphate	Merck	10652910000
Sodium pyruvate	Merck	P8574
Spectinomycin dihydrochloride pentahydrate	Merck	S4014
TCX6D medium	Xell AG	1070-0001
Trifluoroacetic acid	Merck	302031
Tris hydrochloride	Applichem	A3452,0500
Tryptone	Carl Roth	8952.2
UDP-D-galactose disodium salt	Carbosynth	MU06699
UDP-D-glucose disodium salt	Carbosynth	MU08960
UDP-GlcNAc disodium salt	Carbosynth	MU07955
Uridine	Carbosynth	NU06309
Uridine 5'-diphosphate disodium salt hydrate	Merck	94330
Uridine 5'-monophosphate disodium salt	Carbosynth	NU02983
Uridine 5'-triphosphate trisodium salt	Carbosynth	NU03863
Yeast extract	Carl Roth	2363.2

Appendix B: List of Plasmids

Table B. 1. Information regarding the plasmids used in this study.

Gene	Plasmid	Restriction site	Manufacturer
EF_2217	pET-22b(+)	NdeI-XhoI	BioCat GmbH
EH233_20615	pET-28a(+)	NdeI-BamHI	BioCat GmbH
fkp	pET-100/D-TOPO		GeneArt
fucTa	pET-22b(+)	NdeI-XhoI	BioCat GmbH
galk	pET-100/D-TOPO		GeneArt
glmu	pET-15b	NdeI-XhoI	BioCat GmbH
gmd	pET-28a(+)	BamHI-EcoRI	BioCat GmbH
gmk	pET-28a(+)	NdeI-XhoI	BioCat GmbH
LgtA	pMAL-c4X	SacI-BamHI	BioCat GmbH
LgtB	pET-15b	NdeI-XhoI	BioCat GmbH
MGAT1	pET-28a(+)	NdeI-XhoI	BioCat GmbH
MGAT2	pET-28a(+)	BamHI-EcoRI	BioCat GmbH
nanA	pET-22b(+)	NdeI-XhoI	BioCat GmbH
neuA	pET-100/D-TOPO		GeneArt
plst6	pCold II	NdeI-XhoI	BioCat GmbH
SPO1727	pACYCDuet™-1	NdeI-KpnI	BioCat GmbH
udk	pET-28a(+)	BamHI-SacI	BioCat GmbH
UMK3	pACYCDuet™-1	NcoI-NotI	BioCat GmbH
wcaG	pET-28a(+)	BamHI-EcoRI	BioCat GmbH
β1,4GALT1	pET-28a(+)	BamHI-EcoRI	BioCat GmbH

Appendix C: Validation of HPAEC-UV-PAD measurements

Table C. 1. Validation data of HPAEC-UV-PAD gradients. Limit of detection (LOD), and limit of quantification was 3.3, and 10 times of the standard deviation of the response over the slope of the calibration curve.

Compound	Variance	LOD (μM)	LOQ (μM)	n	Range (μM)		R ²
					Low	High	
GDP-sugars							
ADP	nh	0.4	1.2	7	0.5	25	0.9918
AMP	h	0.1	0.3	7	0.5	25	0.9999
ATP	nh	1.6	5	7	0.5	25	0.9960
GDP	h	0.5	1.6	7	0.9	47.5	0.9999
GDP-Fuc	nh	1.3	3.8	7	0.8	42.5	0.9963
GDP-Man	nh	1.3	4	7	1	48.5	0.9987
GMP	nh	0.6	1.9	7	1	50	0.9997
GTP	nh	0.3	1	7	0.8	42.5	0.9999
Guo	nh	0.8	2.6	7	1	50	0.9972
CMP-Neu5Ac							
ADP	nh	0.1	0.2	7	0.3	22.5	0.9999
AMP	nh	0.1	0.2	7	0.3	22.5	0.9999
ATP	nh	0.1	0.3	7	0.3	22.5	0.9999
CDP	nh	0.2	0.6	7	1	60	0.9999
CMP	nh	0.2	0.7	7	1	60	0.9999
CMP-Neu5Ac	nh	0.2	0.6	7	1	60	0.9999
CTP	nh	0.1	0.4	7	1	60	1.0000
Cyt	nh	0.6	1.8	7	1	100	0.9990
UDP-GlcNAc							
ADP	nh	0.1	0.1	8	0.3	22.5	0.9998
AMP	nh	0.1	0.2	8	0.2	15	0.9993
ATP	nh	0.1	0.1	8	0.3	22.5	0.9996
UDP	nh	0.2	0.7	8	0.5	30	0.9992
UDP-GlcNAc	nh	0.1	0.2	8	1	60	0.9997
UMP	nh	0.2	0.5	8	1	60	0.9998
Uri	nh	0.2	0.5	8	1	60	0.9996
UTP	nh	0.1	0.4	8	1	60	0.9998
UDP-Gal							
ADP	nh	0.1	0.2	8	0.3	37.5	1.0000
AMP	nh	0.1	0.1	8	0.3	37.5	1.0000
ATP	nh	0.1	0.2	8	0.3	37.5	1.0000
UDP	h	0.4	1.2	8	1	100	1.0000
UDP-Gal	nh	0.1	0.3	8	1	100	1.0000
UMP	nh	0.1	0.3	8	1	60	1.0000
Uri	nh	0.1	0.3	8	1	60	1.0000
UTP	nh	0.2	0.6	8	1	60	1.0000
Neutral HMOs							
LNnT	nh	1.1	3.3	12	1	100	0.9958
LacNAc	nh	0.7	2.1	9	1	40	0.9983
LNT II	nh	0.2	0.7	7	1	50	0.9991
3-FL	nh	0.1	0.2	7	1	50	0.9999
Acidic HMOs							
6'-SL	nh	0.2	0.8	7	1	50	0.9999
6'-SLN	nh	0.2	0.7	7	1	50	0.9991

Abbreviations: h, homogeneous variance; nh, non-homogenous variance.

Appendix D: SDS-PAGE of purified enzymes

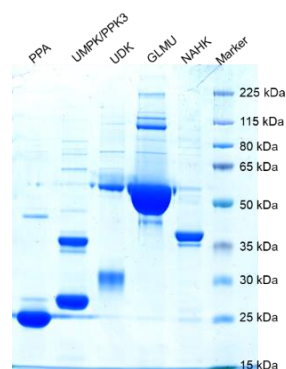


Figure D. 1. SDS-PAGE of one-step His-tagged purified enzymes used for synthesis of UDP-GlcNAc/UDP-GalNAc. Theoretical masses are as follows: PPA, 19 kDa; UMPK, 22 kDa; PPK3, 35 kDa; UDK, 24 kDa; GLMU, 50 kDa; NAHK, 40 kDa. All the enzymes were His-tagged which adds ~2.5 kDa to the theoretical mass [365].

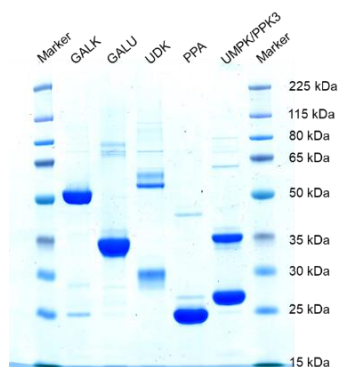


Figure D. 2. SDS-PAGE of purified enzymes for synthesis of UDP-Gal. The theoretical mass of the enzymes are as follows: GALK, 44.3 kDa; GALU, 32.9 kDa; UDK, 24.4 kDa; PPA, 19.3 kDa; UMPK, 22.5 kDa; PPK3, 34.7 kDa. All the enzymes were His-tagged which adds ~2.5 kDa to the theoretical mass [365].

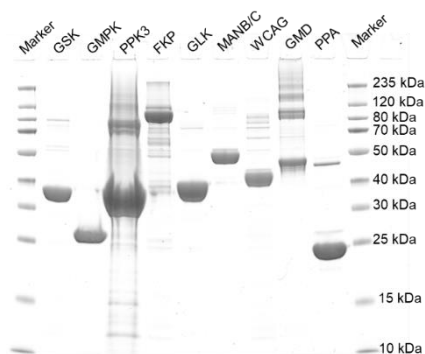


Figure D. 3. SDS-PAGE of purified enzymes for synthesis of UDP-Gal. The theoretical mass of the enzymes are as follows: GALK, 44.3 kDa; GALU, 32.9 kDa; UDK, 24.4 kDa; PPA, 19.3 kDa; UMPK, 22.5 kDa; PPK3, 34.7 kDa. All the enzymes were His-tagged which adds ~2.5 kDa to the theoretical mass [365].

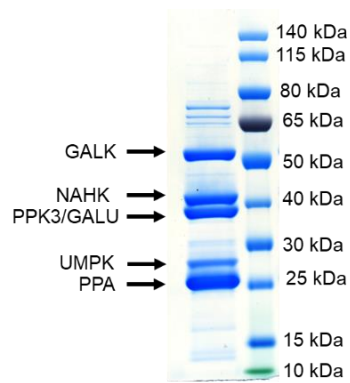


Figure D. 4. SDS-PAGE of purified enzymes for synthesis of UDP-Gal. The theoretical mass of the enzymes are as follows: GALK, 45 kDa; NAHK, 40 kDa; GALU, 33 kDa; UMPK, 23 kDa; PPK3, 35 kDa; PPA, 19.3 kDa. All the enzymes were His-tagged which adds ~2.5 kDa to the theoretical mass [365].

Appendix E: MS of sugar nucleotides

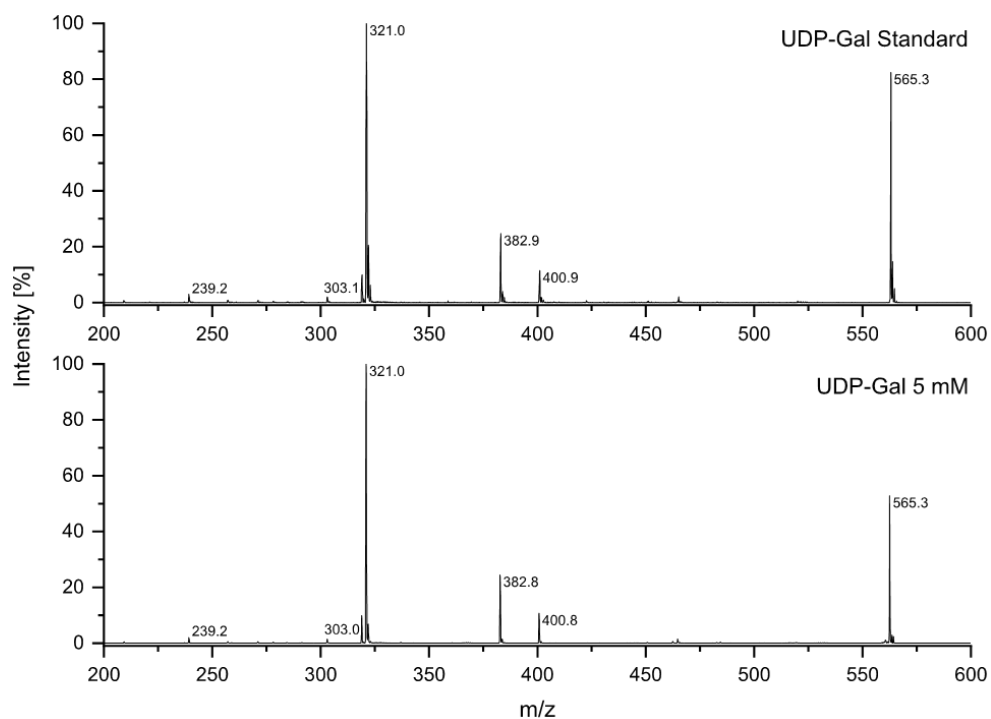


Figure E. 1. MALDI-TOF-MS analysis of a commercial UDP-Gal standard (top) and 5 mM of synthesized UDP-Gal (bottom). The MS measurement was performed by Valerian Grote from the Bioprocess Engineering group at the Max Planck Institute for Dynamics of Complex Technical Systems.

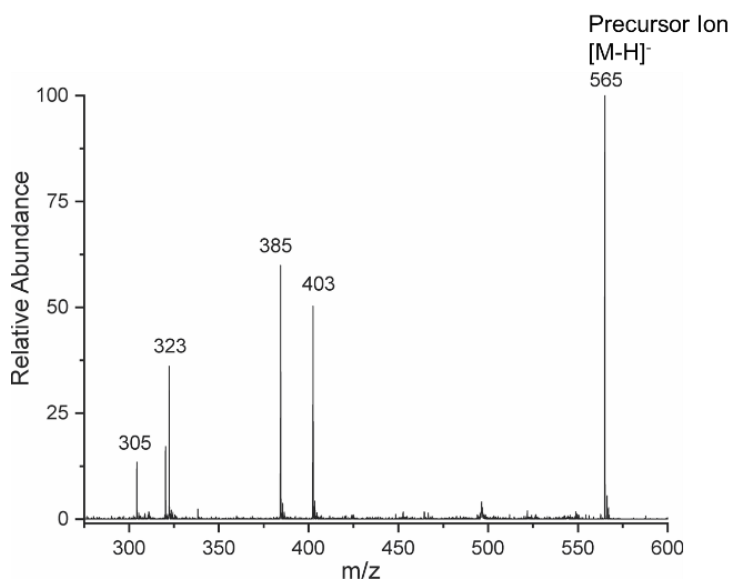


Figure E. 2. Mass spectra of reaction product of the UDP-Man produced from Man, Uri, PolyP_n and a catalytic amount of ATP. Theoretical mass, [M-H]⁻ = 565.0. The MS measurement was performed by Valerian Grote from the Bioprocess Engineering group at the Max Planck Institute for Dynamics of Complex Technical Systems.

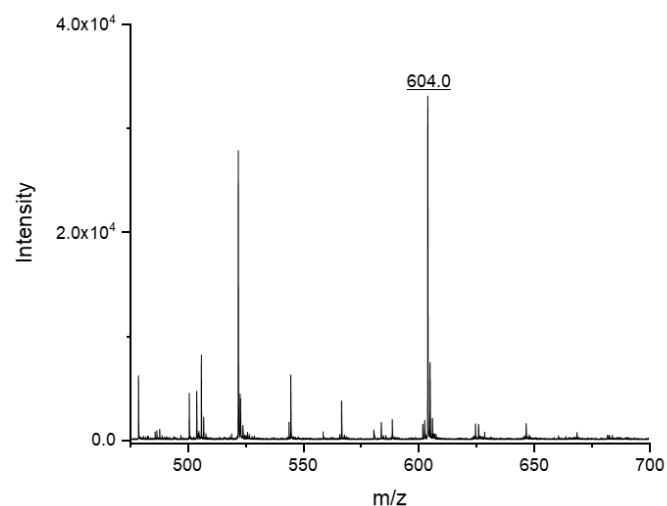


Figure E. 3. Mass spectra of reaction product of the GDP-Man produced from Man, Guo, PolyP_n and a catalytic amount of ATP. Theoretical mass, $[M-H]^- = 604.3$.

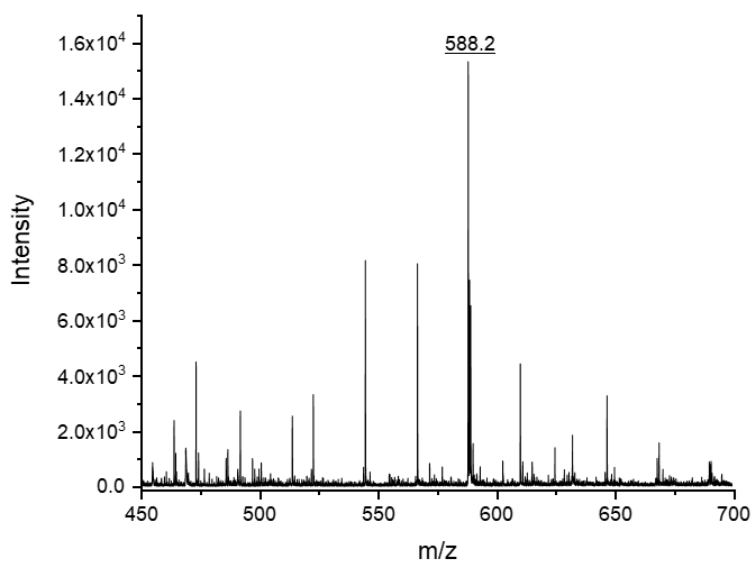


Figure E. 4. Mass spectra of GDP-Fuc produced from Fuc, Guo, PolyP_n and a catalytic amount of ATP. Theoretical mass, $[M-H]^- = 588.2$.

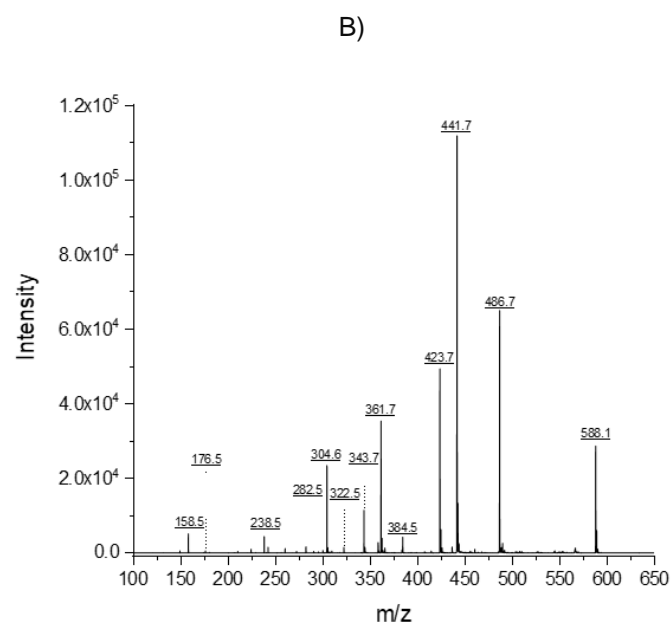
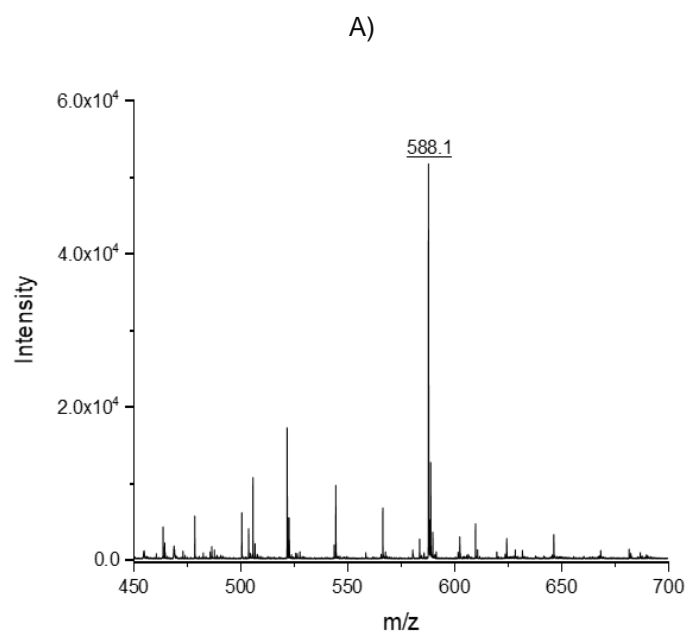


Figure E. 5. (A) Mass spectra of GDP-Fuc produced from Man, Guo, L-Glu, PolyPn and a catalytic amount of ATP and NADPH. Theoretical mass, $[M-H] = 588.3$, (B) MS/MS spectra of the peak at 588.2.

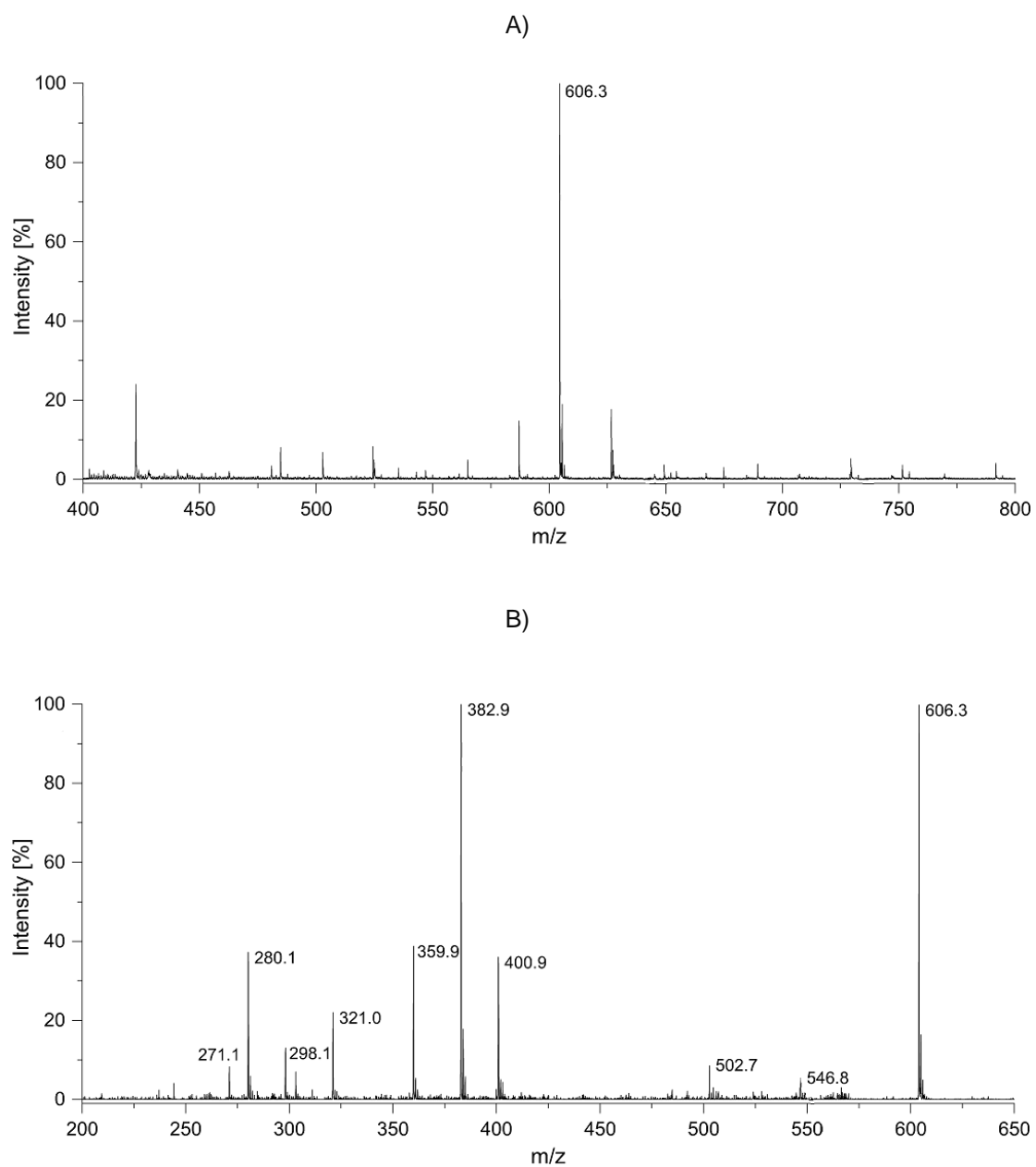


Figure E. 6. (A) MS spectra of reaction product of the UDP-GlcNAc produced from co-expressed enzymes, Theoretical mass, $[M-H] = 606.4$. (B) MS/B spectra of the peak 606.3 Da. The MS measurement was performed by Valerian Grote from the Bioprocess Engineering group at the Max Planck Institute for Dynamics of Complex Technical Systems.

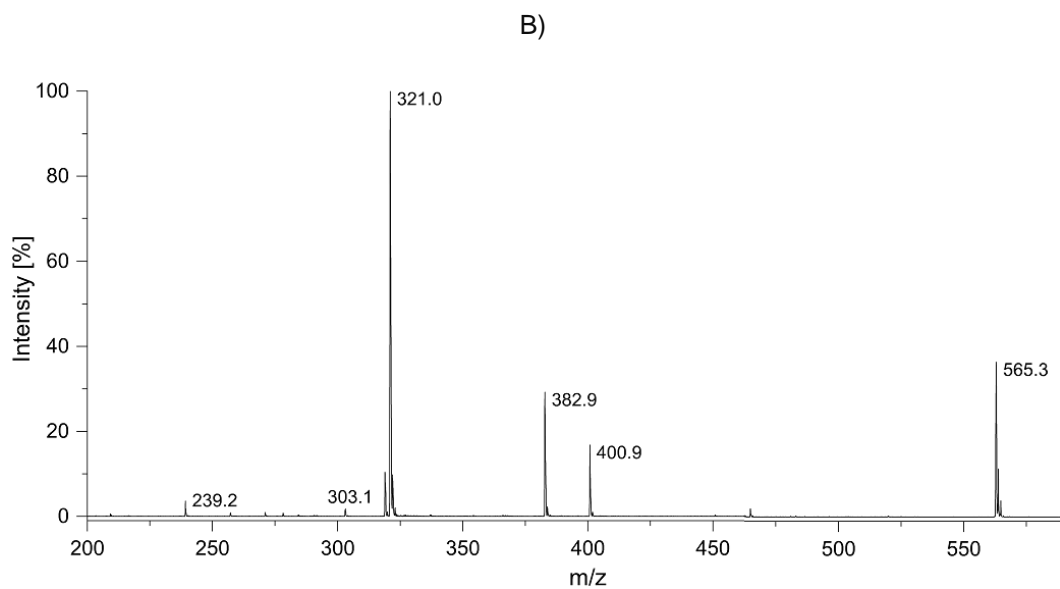
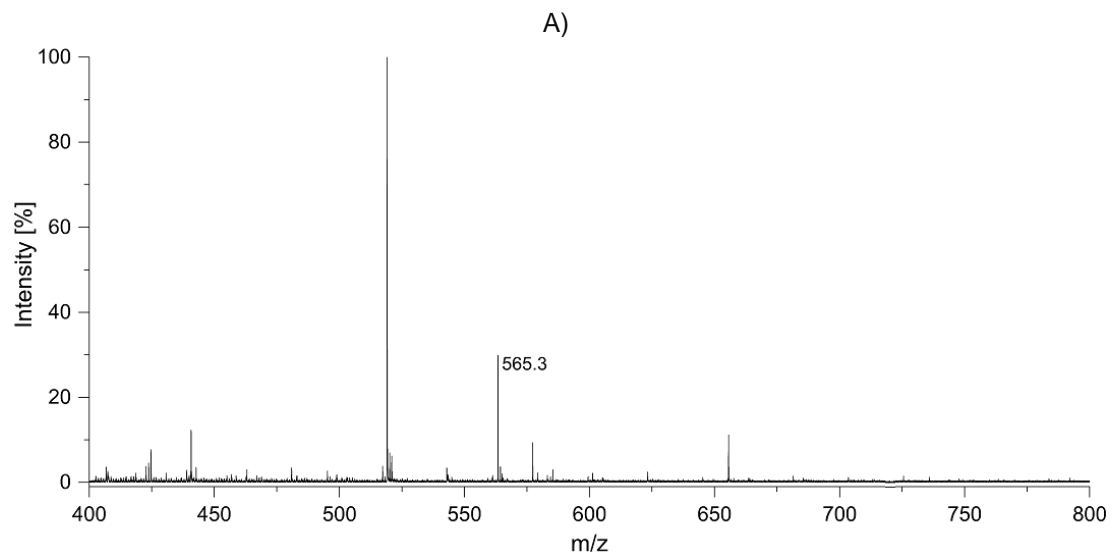


Figure Appendix D. 1. (A) MS spectra of reaction product of the UDP-Gal produced from co-expressed enzymes, Theoretical mass, $[M-H]^- = 565.3$. (B) MS/B spectra of the peak 565.3 Da. The MS measurement was performed by Valerian Grote from the Bioprocess Engineering group at the Max Planck Institute for Dynamics of Complex Technical Systems.

Appendix F: CHO-DP12 cultivation data

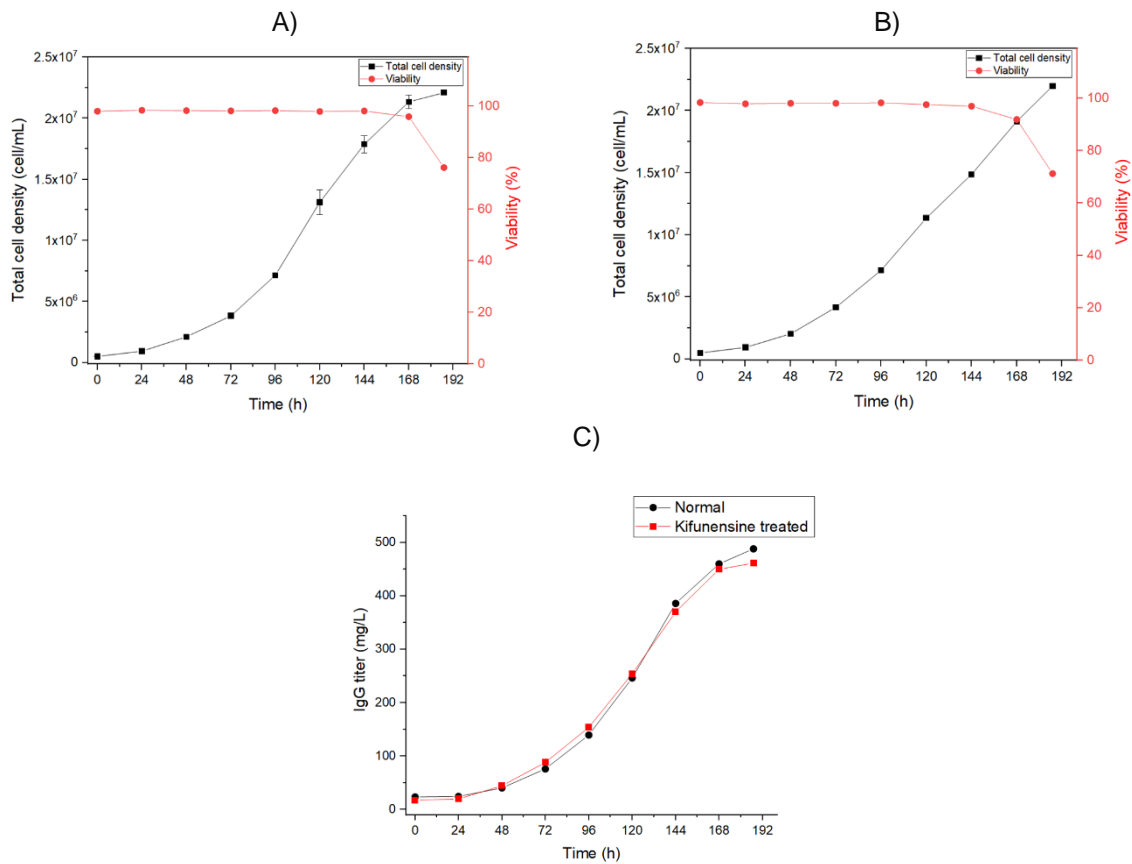


Figure F. 1. Data of CHO-DP12 cells cultivation. A) Cell count and viability of cells under normal condition (no kifunensine treated). B) Cell count and viability of cells under 25 µg/mL kifunensine. C) IgG titer of normal and kifunensine treated cells. The normal cultivation was performed in triplicate and the error bars represent the standard deviation.